Spectroscopic studies of the perturbation of water at organic interfaces

Christopher, David John

Spectroscopic Studies of the Perturbation of Water at Organic Interfaces

by

David John Christopher

A Thesis submitted in partial fulfilment of the requirements for the degree of Doctor of Philosophy of the University of Durham.

Department of Chemistry
University of Durham

1992

Spectroscopic Studies of the Perturbation of Water at Organic Interfaces

David John Christopher

Abstract

Fourier transform infrared spectroscopy (FTIR) has been employed to study the state of water and water-head group interactions in AOT microemulsions in n-heptane. Isotopic dilution of water (4% D_2O in H_2O) has been used to monitor the uncoupled ν(OD) band of HOD as a function of W_o (the number of water molecules per head group). It is found that the ν(OD) band always consists of a single band profile and there is no evidence of co-existing multiple water species in these systems (on the vibrational time scale). By detailed examination of the ν(SO) and ν(CO) bands of the head group it is found that up to $W_o = 6$ (severely perturbed) water molecules are bound closely to the sulphonate and Na^+ ions at the water/organic interface. Beyond this point all the water molecules seem to have a similar vibrational relaxation rate but there are still gradual structural and electronic changes as the water molecules move further away from the first hydration shell. At higher values of W_o than 12 there is some evidence that the water molecules are similar to those in the bulk. However, up to twenty water molecules per head group are probably needed to observe spectra of bulk-like water. A two site model has been developed to predict the frequency of the decoupled ν(OD) band as a function of W_o.

^{17}O NMR spectroscopy and FTIR have been used to investigate the extent of water perturbation in the caesium pentadecafluoro-octanoate (CsPFO)/ water system. This system forms discotic micelles above the CMC across the whole composition range. In the nematic and lamellar phases, these micelles align in a magnetic field. Decoupled water HOD (4% in D_2O) was used to examine the infrared spectrum of water. The water is shown to be perturbed to the extent of $W_o = 15$, which accounts for the surfactant headgroup, the counter-ion and a small amount of water near the micellar surface. ^{17}O NMR quadrupolar splittings were observed due to the anisotropic motion of water at the micellar interface, and the slow motions of the micelles. T_1 relaxation measurements at 298 and 320 K have been made, and a range of correlation times for the water molecule derived on the basis of a two site model.

Acknowledgement

I should like to thank my supervisor Dr. Jack Yarwood for all his ebullient encouragement and advice; also to Drs. Peter Belton and Brian Hills of AFRC, Norwich for valuable discussions. Funding is gratefully acknowledged from the AFRC.

Memorandum

The research presented in this thesis has been carried out in the Department of Chemistry, University of Durham, and in the AFRC Institute of Food Research, Norwich, between September 1989 and September 1992. It is the original work of the author unless stated otherwise. None of this work has been submitted for any other degree.

Preface

The first paper on the properties of oil, water and surfactants was written on clay tablets in cuneiform in about 700 B.C., and was retrieved by George Smith along with the rest of Ashurbanipal's library at Nineveh in the nineteenth century following Layard's initial discoveries[1]. The first known usage is that of the Australian sawfly larva (ca.10^8 B.C.). This primitive and highly successful insect has a caterpillar larval stage that encapsulates poisonous terpenes and other secondary compounds of the eucalyptus leaves on which it feeds in a diverticulum that contains the oils in a microemulsion. The microemulsion is used to great effect in repelling predators. The first human usage is that in Mother Gardner's recipe for washing woollens, still on sale in Melbourne, and reputedly still more effective than products of present-day competitors. It is made of soap, methylated spirits, water, and a dash of eucalyptus oil.

So just what is a microemulsion? James Morris[2] in his marvellous trilogy on the British Empire had this to say on the Jubilee celebration for Queen Victoria.

> *"If to the Queen herself all the myriad peoples of the Empire really did seem one, to the outsider their unity seemed less apparent. Part of the Jubilee celebration was to give the Empire a new sense of cohesion, but it was like wishing reason upon the oceans so enormous was the span of that association, and so unimaginable its contrasts and contradictions."*

Microemulsions really are a lot like the British Empire, elusive, full of contradiction, and yet with an underlying thread of unity[3].

(1) D Tabor, J. Colloid Interface Sci., 75,240,(1980)
(2) James Morris and Pax Britannica, *Heavens Command and Farewell the Trumpets*, Penguin Books, London 1979
(3) After Evans D. F., Mitchell D. J., Ninham B. W., *J. Phys. Chem.*, **90**, 2817, (1986) with apologies.

CONTENTS

LIST OF FIGURES

TABLES

Chapter 4 AOT Experimental

Chapter 5 AOT Results

Chapter 6 Discussion

CHAPTER 1

INTRODUCTION TO SURFACTANTS

1.1. Introduction to surfactants

A surfactant is a molecule that adsorbs to a surface or interface and changes the properties of the surface. The name surfactant derives from contraction of the term surface active agent. Surfactants work by changing the free energy of the surface. This surface (or interfacial) free energy is the minimum amount of energy needed to create the interface. More familiar is the term surface tension. This is a similar quantity, but is actually the interfacial free energy per unit area of surface[1].

Surface properties differ from those of the bulk. In the bulk, a molecule is able to interact strongly with its neighbours, which surround it in every direction. At a surface, some part of the molecule is exposed to another phase (be it a gas, a liquid or a solid). Consequently the molecule at the surface is at a higher potential due to the reduced interactions. Energy must therefore be expended in bringing a molecule from the bulk to the surface; i.e., work has to be done.

A surfactant molecule comprises two distinct parts. The *lyophilic* (solvent-loving) group has strong attraction for the solvent, whereas the *lyophobic* (solvent-hating) group has very little attraction for the solvent.

When a surfactant dissolves, infiltration into the solvent by a lyophobic group is unfavourable. The free energy of the system will be increased as the lyophobic group distorts the structure of the liquid solvent. To reduce the free energy of the system, the solvent and surfactant will tend to separate. It requires less work to bring a lyophobic group to the surface than to bring a solvent molecule to the surface (especially for a solvent that has strong intermolecular interactions such as water). Therefore the surfactant molecule is expelled to an interface. So for the surfactant-solvent system less work is required to bring a molecule to the surface, compared with the solvent only system. Thus the surface tension (surface free energy per unit area) has been lowered.

Also present in the surfactant-solvent system is the lyophilic group. This group interacts strongly with the solvent. Complete removal of the surfactant

from the system as explained above is unfavourable for the lyophilic group. Thus the lyophilic group ensures that once the surfactant molecule is expelled to the surface, it remains at the surface. This may be accomplished by orienting the surfactant molecule such that the lyophilic group is in the solvent, and the lyophobic group is oriented away from the solvent.

The above introduction served as a physical definition of the properties of a surfactant molecule. The interface is created between two immiscible phases, e.g., oil and water. As far as the chemist is concerned, the molecule must be selected so as to be surface active for the particular system required.

For water, the lyophobic (or hydrophobic) group is often a long chain hydrocarbon. A chain less than C_8 is too soluble to be a surfactant; i.e., there is insufficient hydrophobicity of the hydrocarbon chain. A chain longer than C_{20} tends not to dissolve at all in water. Other examples are fluorocarbon chains, siloxane chains or polypropylene oxide polymers. In water, the lyophilic (or hydrophilic) group is often ionic or highly polar. However in a non-polar solvent these hydrophilic groups will be lyophobic, thus causing the surface activity to change.

Figure 1.1 Schematic representation of a surfactant molecule

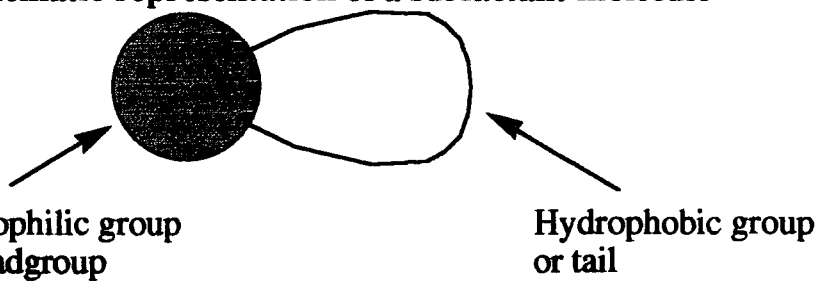

This figure shows schematically the form of a surfactant molecule in an aqueous system.

In this work, two surfactants will be considered in some detail. The emphasis is put on the behaviour of water that is most closely associated with the

surfactant molecule. The two systems are introduced here in the context of their behaviour as typical surfactant molecules.

1.1.1. Succinic esters as surfactants

A class of surfactants that is used extensively as wetting agents for paints, printing inks and textiles is based on sulphosuccinate esters.

Figure 1.2 A sulpho-succinate ester

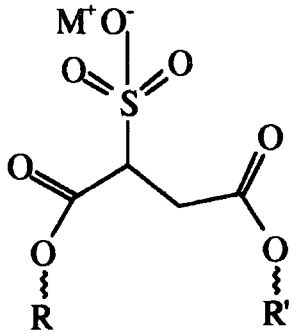

The bis(2-ethylhexyl) ester is soluble in both water and in hydrocarbons and other organic solvents making it particularly suitable for use in dry cleaning. These sulphosuccinate ester surfactants are particularly useful as they may be synthesized without a metal counter-ion. The amide mono-esters happen to be among the least eye irritating of surfactants, and are therefore used in cosmetic applications. The bis(2-ethylhexyl) ester has been extensively studied here and a more complete description of its properties is given later. The molecule is usually called Aerosol Octyl or AOT.

1.1.2. Perfluorinated surfactants

A perfluorinated carboxylic acid is more completely ionized in solution than the corresponding hydrocarbon fatty acid. This is because of the stabilization of the perfluorinated anion by electron withdrawal due to the high electronegativity of the fluorine atom. The chemical structure leads to high thermal stability and resistance to oxidising agents. As far as the surface active properties are concerned, the perfluorinated surfactant is much more effective at

reducing the surface tension than the hydrogenated version, because of the stability of the anion, and the rigidity of the fluorocarbon chain.

The uses of perfluorinated surfactants range from fire retardants and suppression of chromic acid in chromium plating to the rendering of natural surfaces (textiles, paper, leather) resistant to attack by both oil and water. However these surfactants are expensive because precursors do not occur naturally; conversely they are not broken down by micro-organisms.

The surfactant properties of perfluoro chain molecules do not depend critically on the counter ion used, because of the complete ionization. However, in concentrated solutions the phase behaviour does depend on the counter-ion used. The surfactant molecule caesium pentadecafluoro-octanoate (CsPFO) has been investigated here. Caesium was chosen as for the counter-ion as the phase diagram has been well characterized, and a range of phase structures is obtainable. CsPFO molecules form phases with unusual structures, and the behaviour of water in these phases has been investigated.

1.2. Spectroscopic studies of Surfactant systems

An understanding of the perturbation of water by adsorption at a polar organic interface has long been a topic of interest. Real and model systems are well characterized macroscopically[2], but a quantitative understanding of interactions and dynamics at the molecular level is lacking.

The frequency of intra-molecular vibrations covers the frequency range from approximately 6×10^{12} to 1×10^{14} Hz (200-4000 cm^{-1}). This means that the radiation is in the mid-infrared region of the electromagnetic spectrum. The lifetime of the vibrationally excited state is therefore less than 1×10^{-12} s. For a water molecule, the time-scale for diffusional and rotational motion is of the order of 10^{-11} s, so vibrational spectroscopy effectively observes a static molecule[3]. Each absorption band in the spectrum arises from a different environment. Therefore molecules that are in differing locations may be distinguished.

Pure water absorbs strongly in the mid-infrared, but by using isotopic dilution with D_2O, the spectrum of water can be measured accurately. This also decouples the water molecule vibrations. This method has not been applied previously to the quantitative study of water in model systems that are discussed here.

The questions that will be addressed in this work are of the following form:

How many types of water molecule are present in an AOT microemulsion?

In what states are these water molecules?

Is it possible to gain an understanding of the structure of the interface?

The strategy for answering these questions will be to observe the vibrational spectra of AOT microemulsions that contain different amounts of water. The spectra of water are complicated by vibrational coupling. This may be eliminated by using HDO as discussed in the next chapter. To date no work has been published on AOT microemulsions involving the study of the fundamental vibrations of HDO.

Similarly when considering the caesium perfluoro-octanoate / water system, the behaviour of the water molecules dictates the phase structure observed. In addition to vibrational spectroscopy of this system, nuclear magnetic resonance of the ^{17}O nucleus of water will also be investigated. NMR observes species with lifetimes much longer than vibrational spectroscopy and is very sensitive to chemical and diffusive exchange. By comparing the results from NMR and infrared spectroscopy, information of the state of water at the interface will be available.

1.3. References

(1) Rosen M. J. *Surfactants and interfacial phenomena;* 2nd ed.; Wiley: New York, **1989**.
(2) Tanford C. *The Hydrophobic Effect: Formation of Micelles and Biological Membranes*; Wiley: New York, **1980**.
(3) Eisenberg D., Kauzmann W. *The Structure and Properties of Water*; OUP: Oxford, **1969**.

CHAPTER 2

VIBRATIONAL SPECTROSCOPY

2.1. Vibrational spectroscopy

The motions or vibrations of polyatomic molecules may, at first sight, appear disorderly. However, it is possible to reduce the motions to a set of normal or fundamental modes, equal in number to the number of degrees of vibrational freedom of the molecule. During a normal mode of vibration, the nuclei move in phase in a straight line, thus passing through the mean position simultaneously and reaching the turning point simultaneously.

The displacement of nuclei from their mean positions is caused by thermal excitation or by interaction of an electric field with an electric dipole. If the displacements are small, then to a first approximation, the restoring force is proportional to the displacement, i.e., harmonic motion. The forces that oppose the displacement are the resistance of the chemical bond to compression or extension.

Thus far molecular vibrations have been presented from the classical view point. It is necessary to solve the Schrödinger equation to obtain the wavefunctions and energy eigenvalues. The Hamiltonian has both kinetic and potential parts[1]:

$$H_v \psi_v = E_v \psi_v$$

$$H_v = \frac{1}{2}\left(-\hbar^2 \sum_k^{3N-6} \frac{\partial^2}{\partial Q_k^2} + \sum_k^{3N-6} \lambda_k Q_k \right) \quad \text{..... (2.1)}$$

where

H_v = Hamiltonian operator
ψ_v = vibrational wavefunction
E_v = energy of the wavefunction ψ_v
Q_k = normal co-ordinate Q_k
λ_k = root of the secular equation and represents frequency of normal mode Q_k

The advantage of using normal co-ordinates is that it allows the Schrödinger equation to be factorised into a set of 3N-6 equations. The energy levels of the k-th normal mode of vibration are the eigenvalues belonging to the wavefunction ψ_k such that:

$$E_v = \left(v+\frac{1}{2}\right)h\nu_k \quad \text{..... (2.2)}$$

where

v = vibrational quantum number

ν_k = frequency of the k^{-th} mode

2.1.1. Selection rules

In a polyatomic molecule, the dipole moment μ and the transition moment **M** are both vectors. The dipole moment is a function of the normal coordinates:

$$\mu = \mu^o + \sum_k \left(\frac{\partial\mu}{\partial Qk}\right)_o Qk \quad \text{..... (2.3)}$$

This gives the transition moment as:

$$\mathbf{M} = \left\langle \psi^*_{v'_k} \middle| \mu \middle| \psi_{v''_k} \right\rangle \quad \text{..... (2.4)}$$

where the primes indicate the vibrational energy level.

It may be shown that for the integral to be non-vanishing, that:

$$v'_k = v''_k \pm 1 \quad \text{..... (2.5)}$$

Therefore for polyatomic molecules, the harmonic selection rule dictates that transitions occurring with absorption or emission of radiation do so with a vibrational quantum number change of one unit only. However, if either ψ_v is not a harmonic oscillator wavefunction, or the dipole moment is not of the form given in equation (2.3) then the harmonic oscillator selection rule (equation 2.5) breaks down.

The symmetry of the vibrational wavefunctions is also important in predicting whether a transition has intensity or not. If **M** as in equation (2.4) is not to vanish then **M** must be totally symmetric. Otherwise there is at least one symmetry operation that changes its sign, giving a zero integral. The ground state wavefunction is totally symmetric, so for **M** to be symmetric, the excited state and the transition dipole moment must belong to the same symmetry class. It may be shown that the components of μ have the same symmetry species as the co-ordinate axes x,y,z, of the molecule. Therefore the symmetry selection rule

allows transitions from the ground state to any excited state whose wavefunction has the same symmetry as at least one of the axes x,y,z, of the molecule.

2.1.2. Anharmonicity

The harmonic oscillator selection rule is only an approximation, and will therefore break down, either through large displacements or non-quadratic restoring forces. This is termed mechanical anharmonicity. Another type of anharmonicity is electrical anharmonicity, which occurs when the dipole moment does not change linearly with Q. Little is known about the variation of μ with Q, but it is presumed that its value is low for both very small and very large internuclear distances (See figure 2.1)[1].

Figure 2.1 Relation between the dipole moment of a diatomic molecule and the bond extension r.

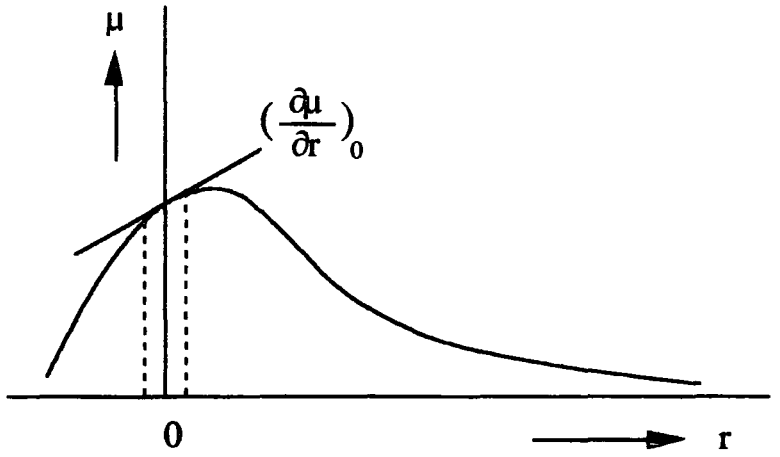

The dashed vertical lines represent the amplitude of the vibration. The tangent drawn at r=0 represents $\frac{\partial \mu}{\partial Q}$ at r=0, which is constant for small displacements. The tangent i.e. $\frac{\partial \mu}{\partial Q}$ must have a non-zero value for the vibration to be active.

2.1.3. Fermi Resonance

When an overtone or combination of energy levels coincides with another vibrational energy level, then resonance can occur. The resonance splits these degenerate energy levels and mixes the wavefunctions, allowing transfer of

intensity from one mode to another. The modes must be of the same symmetry otherwise the interaction integral will be zero.

2.2. Integrated intensities

The absolute intensity of an infrared absorption band relates the spectrum to the number of molecules being observed. For a pure liquid the absorption is only pathlength dependent. For a solution the concentration also influences the absorption[2].

If infrared radiation of intensity I_0 is incident on a cell of path length l/cm then the transmitted radiation I is given by $I=I_0\exp(-\varepsilon l)$, where ε is the extinction coefficient. For solutions the concentration (c/moles.dm^{-3}) is also accounted for: $I=I_0\exp(-\varepsilon c l)$. The extinction coefficient is the reciprocal value of the path length through which the light must pass to be reduced to the 1/eth part. This is Beer's law, and applies to monochromatic radiation.

In a dispersive infra-red spectrometer, radiation is passed through a monochromator to the detector. However, the entrance and exit slits are of a finite size. This together with angular dispersion of the radiation means that the radiation reaching the detector is not truly monochromatic. An interval of wavelengths is detected, the distribution being assumed to be triangular about ν_0. This effect serves to broaden absorption bands, although only narrow bands (< 5 cm^{-1}) will be severely distorted. In a Fourier transform instrument the resolution is essentially governed by the delay, or maximum optical path difference between the two beams (see chapter 4)

Another cause of broadening in solution is intermolecular collision. The energy levels of the molecules are perturbed by the approach of solvent or solute molecules giving a larger distribution of energy levels hence a broader absorption band.

As the radiation reaching the detector is not monochromatic, this means that Beer's law can never be exactly obeyed. Beer's law may also not be obeyed when solutions are highly concentrated or when there are strong intermolecular

interactions. In these cases, molecular aggregates may be formed thus effectively reducing the number of solute species and hence the absorption.

As every absorption in the infra-red is a band rather than a δ-function, it is useful to discuss the total integrated absorption of the band. Quoting only the peak height gives no information on width or shape, whereas the integrated absorption intensity, if obtainable, includes this information by definition.

If it is assumed that an isolated absorption band is being described, then ε starts from zero, goes through a maximum and returns to zero. A band may be described by the Lorentzian function:

$$\varepsilon = \frac{a}{b^2+(\nu-\nu_0)2} \text{ where } 2b = \text{half-width, } \frac{a}{b^2} = \text{maximum intensity}$$

This function only reaches zero at ±infinity, so the limits of integration must be chosen such that the error in the wings is small. Were the exact form of the band shape truly Lorentzian then the integrated intensity (A) would be found easily :

$$\underline{A} = \frac{1}{cl}\int \log\left(\frac{I_0}{I}\right) d\nu = \frac{a\pi}{bcl}$$

A problem arises due to convolution of the band shape with the slit function in dispersive spectroscopy; or convolution of the apodization function with the true spectrum in the case of Fourier transform spectroscopy (The apodization function is necessary to reduce the interferogram to zero at its extremities, as only a finite-sized discrete Fourier transform is possible) Instead of the true transmission ratio being measured $\left(\frac{I_0}{I}\right)$, an apparent transmission ratio is observed $\left(\frac{T_0}{T}\right)$ where

$$\left(\frac{T_0}{T}\right) = \frac{\int f(\nu_0,\nu_i).\left(\frac{I}{I_0}\right) d\nu_i}{\int f(\nu_0,\nu_i)\, d\nu_i}$$

in which $\int f(\nu_0,\nu_i)d\nu_i$ is the slit function (usually a triangular function) or apodization function with ν_o being the band centre and ν_i the wavenumber

Hence an apparent integrated intensity is defined as

$$\underline{B} = \frac{1}{cl}\int \log\left(\frac{T_o}{T}\right) dv$$

$\underline{A}$ and $\underline{B}$ have similar definitions and it can be shown that

$$\underline{A} = \text{Limit}\{\underline{B}\}_{cl \to 0}$$

As was explained above, only narrow bands are severely distorted by convolution with another function. Hence it would be reasonable to expect that for broader bands (>10 cm^{-1}) that $\underline{A}$ and $\underline{B}$ would be of similar value. This is indeed the case. If the parameters of the band are evaluated, it can be shown that, as a consequence of convolution with a function that:

(i) The apparent intensity is always less than the true intensity ($\underline{B} < \underline{A}$)

(ii) The apparent bandwidth is always greater than the true bandwidth.

$\underline{A}$ may be obtained from $\underline{B}$ by extrapolation to zero path length or zero concentration, as long as the following conditions are satisfied:

(i) The incident intensity is constant over the whole bandwidth,

(ii) The convolution function does not change over the width of the band (i.e. the resolution does not change over the bandwidth). $\underline{A}$ is thus found by plotting a series of values for $\underline{B}$ that have been obtained with a different path length (or concentration) and extrapolating the line to zero path length (or concentration).

The background chosen from which to calculate the integral is important in obtaining an accurate numerical value for the integral. One method is to draw a tangent from the next absorption minimum, although quite a significant error will be introduced by this method as bands often overlap. A curved baseline may be constructed using a Lorentzian or power type equation, although this produces a significant error. A significant proportion of the integrated area contributing to the intensity of a Lorentzian band is in the wings of the band, beyond 5 half-widths from the centre of the band. So error is introduced if the band is overlapped, or if the integral limits chosen are insufficiently displaced from the band centre. The noise level is also important for obtaining an accurate baseline.

2.3. Vibrational spectroscopy of water

2.3.1. The HDO molecule

The fundamental vibrations of OH and OD groups take place on a time-scale[3] of 10^{-13} to 10^{-14} s. The diffusion time-scale is of the order of 10^{-11} s for a water molecule. Rotation is also on a pico-second time-scale, the same as vibrational relaxation. So observation of the vibrations by IR/Raman spectroscopy effectively occurs for a molecule in a static environment where there is no translation. Thus the particular frequency of vibration observed is dependent upon the local environment of the water molecule, and may therefore be used to distinguish environments.

A useful way to study the vibration of water is by using HDO for the following reasons :

(1) The vibrations $\nu_1+\nu_3$ are only very weakly coupled, as they are very different in frequency. This leads to a band shape that is simpler than for the situation where the vibrations are coupled.

(2) Fermi resonance of $\nu_1+2\nu_2$ does not occur as the energy levels are not degenerate. This allows clear observation of the ν(OD) band.

(3) The ν(OD) vibration of HDO in H_2O occurs in a relatively transparent window in the mid-infrared, i.e. a region where there are few other bands.

(4) The concentration of HDO is always suppressed as its mole fraction can never exceed 0.5. This is important because intermolecular coupling of ν(OD) vibrations is unlikely to occur if the concentration of HDO is low.

One further complication is that in a H_2O (or D_2O) molecule, the two OH (or OD) bonds may not be identical due to structural disorder. In this case the ν_3 vibration is not necessarily antisymmetric and can therefore undergo Fermi resonance with $2\nu_2$.

2.3.2. Bandwidths

The bandwidths in decoupled water are typically 160 cm^{-1} for ν(OD) of HDO in bulk D_2O.

The reasons for the large bandwidths are many:

(1) Coupling of vibrations to nearest neighbours - although this does not occur for HDO as it is an inherently dilute species.

(2) Hydrogen bonding to other molecules.

(3) Structural disorder. There is a distribution of O - O separations between water molecules. This gives a range of perturbing potentials for the electrons in the OH bond to experience, so a range of frequencies exists. The converse indicates that ice is an ordered structure since it has narrower bandwidths (50 cm^{-1})[3].

2.3.3. Vibrational spectroscopy of water in organic materials

Some infra-red studies of AOT/oil/liquid water systems have been carried out[4,5]. Deconvolution of the coupled ν(OH) band into its component bands apparently reveals the number of types of water in the system[4]. If there were an absence of band structure, then a continuous distribution of local environments would be indicated. A structured band may comprise two or more separate bands indicating both hydrogen bonded and non-hydrogen bonded types of water. Therefore a question to be answered is whether distinct environments or a continuous distribution of environments can be detected on the time-scale of the infra-red experiment.

Hydrogen bonding decreases the frequency of vibration of an OH (or OD) group. The intensity may be affected also. Non hydrogen bonded bands are less intense than hydrogen bonded bands, the intensity of the latter increasing by an order of magnitude on formation. As the temperature of the system is increased, the hydrogen bonds are more easily broken[3,6]. Thus the intensity of the band decreases, at the expense of the non-hydrogen bonded band. That is, an isosbestic point occurs in the spectrum as two species are in equilibrium.[7]

Studies of carbon tetrachloride saturated with water apparently showed several peaks when the bands were resolved[6]. These were assigned to oligomers and a monomer. At 353 K in the gas phase and 77 K in a matrix an open dimer is favoured, whose frequency is between that of a monomer and a cyclic dimer. In the liquid phase it was postulated that the cyclic dimer would be favoured[6]. However two distinctly strong peaks were observed over a broad background. The peak at 3592 cm^{-1} being assigned to the O-H...O vibration of the linear dimer; the peak at 3693 cm^{-1} to the antisymmetric OH_2 vibration. This experiment was repeated and gave spectra of similar appearance. Slightly higher frequency positions were observed: 3708 and 3618 cm^{-1}. The higher frequencies indicate a smaller degree of perturbation or less extensive hydrogen bonding; possibly the carbon tetrachloride was not saturated with water so that the water molecules were more dilute and more vapour like leading to higher frequencies. The primary source for frequency shift from vapour phase for water in carbon tetrachloride is the interaction with the lone pair electrons on chlorine.

Studies of water in various liquid alkanes[8] show similar results for a varying hydrocarbon chain length. A broad band at 3715 cm^{-1} and a side band at 3810 cm^{-1}. These systems were studied in order to ascertain whether water clusters exist. It appears that they do not as the frequencies of the OH stretching bands are very high and monomeric like. The ν_3 band is very broad, indicative of free rotation.

Extensive studies of water dissolved in various oxygen bases (e.g. ketones, ethers) have been carried out[9,10]. The shifts and integrated intensities have been used to give a guide to the strength of the hydrogen bonds. It is found that the integrated intensity actually gives a better guide than frequency position. Factor analysis on the band profile shows that there are two component bands. A maximum of six bands might be expected from three water types[9]:

(1) Water molecules isolated but hydrogen bonded to two solvent molecules giving local symmetry,

(2) OH groups bonded to solvent oxygen and van der Waals forces between OH and alkyl chain of another solvent molecule,

(3) Both OH groups experience van der Waals type interactions to the alkyl chains of two molecules.

For ketones with longer or branched alkyl chains, four bands exist in the OH stretching region indicative of two distinct water types:

(1) vibrations from hydrogen bonded molecules, bonding to the carbonyl group,

(2) vibrations from water molecules hydrogen bonded to the carbonyl group and experiencing van der Waals attraction to another alkyl group on a different ketone molecule.

The greater alkyl bulk of di-n-propyl, di-iso-propyl and di-n-butyl ketones reduce the probability that a water molecule may intersperse between two ketone molecules, as the carbonyl groups cannot approach near enough due to the alkyl bulk. Thus the OH bonds in water form van der Waals type bonds between water molecules and alkyl chains. If the temperature is increased the labile hydrogen bonds are broken so the concentration of 2:1 solvent:water complexes decreases whilst the concentration of the 1:1 complexes increases.

With ethers[10] the results are similar. Conclusions from the work with ethers and ketones are:

(1) The OH intensity decreases with increasing alkyl chain length due to steric interactions

(2) The pK_a of the solvent correlates with the total integrated intensity of the OH stretching region[8-10].

The pK_a is thus a measure of the tendency of a solvent to form hydrogen bonds with water. The ν_1 frequency of 1,4-dioxan is low when compared with other members of the series. This vibrational mode is due to a 1:1 solvent:water-complex vibration. 1,4-Dioxan, being a diether, is able to form chains between

itself and water molecules. Thus there may be a large number of water molecules that are severely perturbed by forming two hydrogen bonds each.

2.3.4. Water in surfactant aggregates.

In Raman studies of n-dodecane/hexanol/water microemulsions[11] results have been analysed in terms of two water types:

(1) bulk water within the microemulsion particle of radius 25-100 Å

(2) boundary water interacting with the surfactant.

Using the concentration of water in several systems and the intensities of the OH (or OD) bands, the depth of the boundary layer has been calculated, on the basis of a change in intensity on interaction. Detailed studies of some systems can actually reveal the number of water molecules bound to each surfactant head group[12]. In the water/benzene/egg lecithin system, infrared spectroscopy is able to show the presence of three water types, whereas NMR can only show two types due to its slower time-scale. Reverse micelles of egg lecithin were studied with increasing water content and the extinction coefficient for each water type calculated to aid characterization of the water types.

Direct or non-reverse micelles do not contain a central core of water. Individual water molecules may penetrate into the middle of the micelle, as shown by studies on sodium octanoate micelles. Using a control molecule of sodium 7-oxo-octanoate[13], the carbonyl stretching band was monitored. The carbonyl band is sensitive to water interactions[9]. Monitoring the carbonyl band frequency position shows that although water can penetrate into the micelle core, its lifetime there is short.

A substantial amount of work on AOT systems has been undertaken, some of it to determine the state of water. AOT/carbon tetrachloride/water microemulsions are thought to exhibit two types of water environments[5]. Interfacial water is attached to the polar headgroups of AOT and bulk-like water is in the core of the microemulsion particles. The frequencies of OH stretching in each case are:

(1) 3580 cm^{-1} ν_3(O-H) of water in the surfactant layer

(2) 3480 cm^{-1} ν_1(O-H) stretch of water in the surfactant layer

(3) 3280 cm^{-1} Hydrogen bonded water (this corresponds to the pure liquid frequency)

AOT is a very bulky molecule, and does not pack easily to form liquid crystalline type phases, the alkyl chains remaining liquid like. This is shown by the fact that no matter how much water penetrated into the microemulsion core, the methylene CH_2 stretches remained liquid like.

Thus the vibrational spectra of water contained within organic compounds are affected by the nature of the interface, and the extent of hydrogen bonding. Monomeric water can occur in solvents such as liquid alkanes, but in more polar solvents, the water tends to aggregate together. Nevertheless, this environment for water still shows the water to be perturbed; the nature and extent of this perturbation will be investigated in this work.

2.4. References

(1) Wilson E. B., Decius J. C., Cross P. C. *Molecular Vibrations*; McGraw-Hill: New York, **1955**.
(2) Potts W. J. *Chemical Infrared Spectroscopy*; Wiley: New York, **1963**.
(3) Eisenberg D., Kauzmann W. *The Structure and Properties of Water*; OUP: Oxford, **1969**.
(4) Jain T. K., Varshney M., Maitra A. *J. Phys. Chem.* **1989**, *93*, 7409.
(5) MacDonald H., Bedwell B., Gulari E. *Langmuir* **1986**, *2*, 704.
(6) Shippey T. A., Symons M. C. R., Brivati J. A. *Mol. Phys.* **1979**, *38*, 1693.
(7) Balay A., Karstu O., Stevens T. *Infrared Physics* **1963**, *3*, 211.
(8) Strauss H., Conrad *Biophysical Journal* **1985**, *48*, 117.
(9) Ford T. A., Paul S. O. *J. Chem. Soc. Faraday Trans. II* **1981**, *77*, 33.
(10) Ford T. A., Paul S. O. *Spectrochimica Acta A* **1981**, *37A*, 415.
(11) Mallamace F., Migliardo P., Vasi C., Wanderlingh F. *Phys. Chem. Liq.* **1981**, *11*, 47.
(12) Boicelli C. A., Giomini M., Giuliani A. M. *App. Spec.* **1984**, *38*, 537.
(13) Casal H. L. *J. Am. Chem. Soc.* **1988**, *110*, 5203.

Chapter 3

AOT Background

3.1. AOT

Oil and water do not mix, but can be made to by the addition of a third molecule, which is able to bridge the interface between the oil and the water. Such a molecule is termed a surface active agent or surfactant.

With sufficient surfactant, a large enough area may be covered such that the oil and water appear to be homogeneous on a macroscopic scale. On the molecular scale however, many arrangements of the oil, water and surfactant are possible. Structures range from micelles, hexagonal phases, cubic phases, bicontinuous phases and lamellar phases. These are well documented for a variety of surfactants and numerous studies by many techniques have been carried out.

On an even smaller scale, the molecular interactions at the interface have been subject to less investigation. The principal aim of this work is to investigate the behaviour of the water molecule when it is associated with a surfactant interface. The interface comprises the head group of the surfactant as well as some of the tail of the surfactant.

An understanding of the interactions that occur at an interface is crucial if the processes occurring are to be controlled. For example the activity of a bound enzyme depends dramatically on the interfacial environment.

The most commonly used picture of a reverse micelle is of a spherical aggregate of surfactant molecules, containing water. The water is usually described using a two state model: viscous or structured bound water close to the interface, which is in equilibrium with water in the centre of the pool that is more like bulk water. Many properties of the water show discontinuities when about 8-12 water molecules for each surfactant molecule have been added[1-19].

The actual number depends on the technique used to measure the property. However the data are consistent with hydration of the AOT head group and counter-ions when there is only a small amount of water present. This water is highly structured or perturbed; the perturbation decreases as the amount of

water increases and the reverse micelles swell, such that bulk-like water is present.

3.1.1. Uses of reverse micelles and microemulsions

- They can be used as a micro-reactor — reactions can take place in a constrained space e.g. synthesis of micro-colloids of the semiconductor CdS.
- Enzymes retain their activity in a microemulsion as they only require surface wetting by water to maintain their conformation.
- Universal solvent for hydrophobic and hydrophilic molecules - useful for the formation of oligopeptides from amino acids.

3.2. Description of the system and a literature review.

Figure 3.1 The AOT molecule Sodium bis{2-ethyl-hexyl}sulpho-succinate

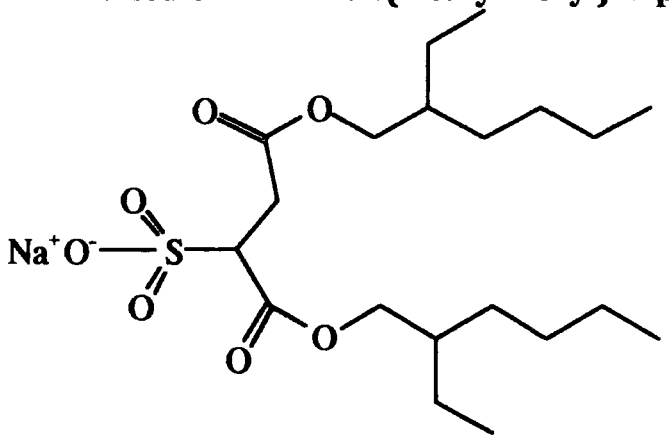

AOT (which stands for Aerosol Octyl) is a frequently studied molecule, and its mesophases appear to be well characterised. Many studies and several extensive reviews concerned with AOT exist[20-23]. A wealth of experiments has been carried out to elucidate the structure and properties of the AOT aggregates in non-aqueous and apolar media. Chemists have exploited the ability to control the size of the AOT aggregate. This has led to the application of AOT aggregates

to the synthesis and study of molecules entrapped within the core of the aggregate[23].

AOT is not a difficult molecule to synthesize, and is therefore readily available commercially. One route to AOT is the condensation of maleic anhydride with 2-ethyl-hexan-1-ol followed by reaction with sodium bisulphite[24].

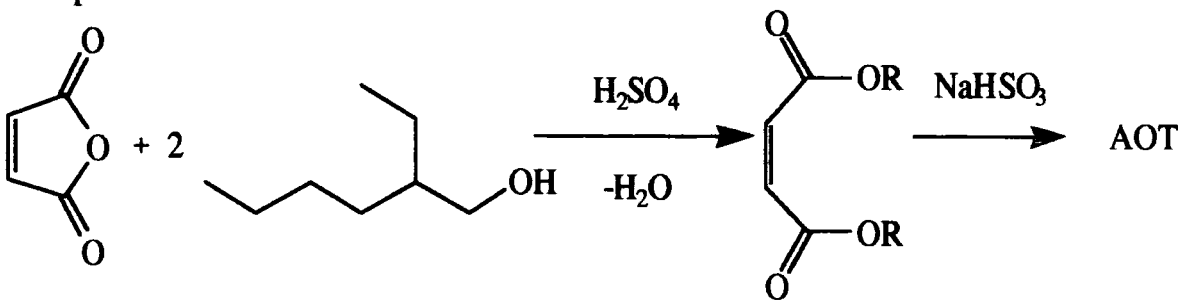

None of the above reactions is stereospecific so a mixture of isomers is produced.

The most commonly studied phase of AOT is that which comprises reverse micelles. A reverse micelle is a thermodynamically stable self assembled aggregate of surfactant molecules in an apolar solvent. Where the core of the reverse micelle also contains water, the system is often called a microemulsion; although the division is arbitrary. Within one phase, the particles are of the same type but may vary in size and are surrounded by oil. The size of an AOT microemulsion particle is independent of the concentration of aggregates and depends on the amount of water in the water pool. This phase is a thermodynamically stable solution of aggregates of surfactants, ions and polar molecules (water) in a hydrophobic solvent. On a phase diagram they are referred to as the L_2 phase (as distinct from the L_1 phase that refers to direct (non-reverse) micelles). Although the aggregates are of finite size and have well defined shapes, usually spherical or spheroidal, they are polydisperse. Below is shown a schematic diagram of a reverse micelle.

Figure 3.2 Schematic diagram of the cross section through a reverse micelle, showing the various regions envisaged by workers in this area.

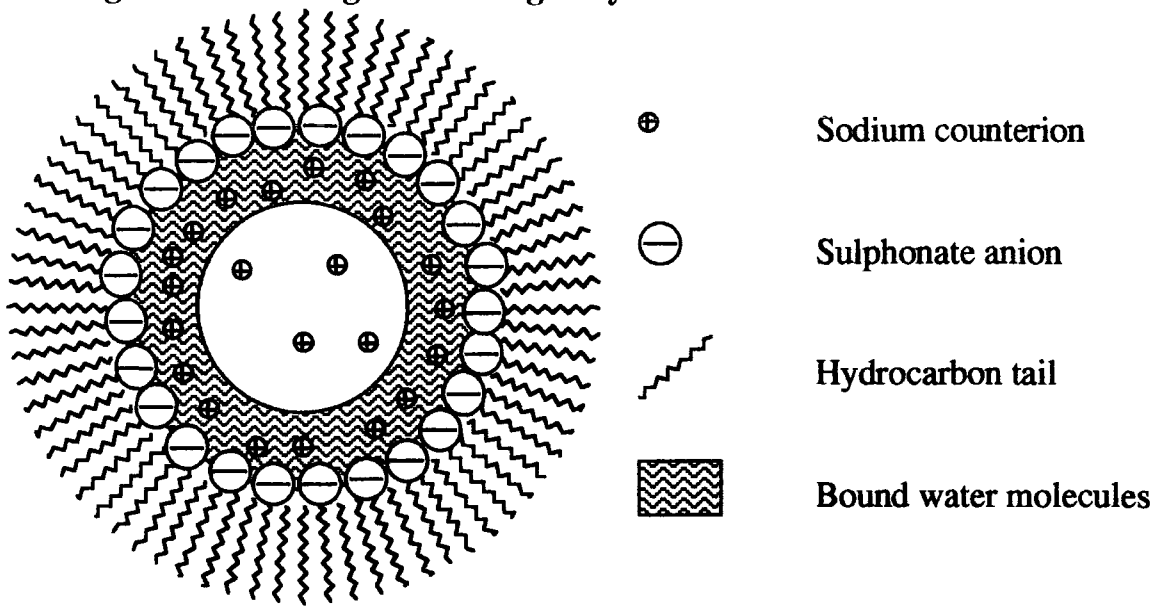

The driving force for aggregation is the enthalpy of hydration of the ionic headgroup and counterion. There is also a favourable enthalpy contribution from the formation of hydrogen bonded networks of water when water forms a pool at the centre of the reverse micelle. This is the hydrophobic effect. The affinity of water for itself is the driving force for the formation of water-containing aggregates.

The entropy contribution favours the formation of reverse micelles, as the entropy of the water will be higher in a water pool than at an interface with a hydrophobic material. For a monomeric AOT molecule in oil without water in the system, AOT will only dissolve in the oil if the ionic headgroup can be shielded from the apolar oil. This can occur if the headgroup is positioned so as to shield the ionic moiety, but this is an unfavourable entropy contribution. If however reverse micelles form, then the ionic headgroups cluster together (a favourable enthalpy contribution) and the hydrocarbon tails are free to move (a favourable entropy contribution).

3.2.1. Why is this system so extensively studied?

The merits of AOT as a system to study are:

1) Reproducible and controllable properties: the size of the reverse micelles is controlled by the water to surfactant ratio W_0. In most papers, the characteristic parameter used to describe the system is the molar ratio of water to surfactant. This is denoted by various symbols (such as R), but throughout this work the quantity will be termed W_0. To a first approximation, the value of W_0 may be interpreted as the number of water molecules associated with each surfactant molecule.
2) The one phase AOT/water/oil system forms over a wide range of surfactant, water and oil concentrations.
3) No co-surfactant is necessary. With some surfactants such as sodium dodecylsulphate, hexanol or similar must be added to form a one phase system.
4) Perceived ability to mimic naturally occurring membranes. The AOT molecule has properties similar to natural membrane forming molecules such as phosphatidylcholines, in that the head group can take up different conformations, and the two hydrocarbon tails affect the packing of the surfactant. Hence water in AOT reverse micelles is thought to be bound in a similar way to water found *in vivo*.

3.2.2. What remains unknown about the AOT system?

Much of the literature has concentrated on trying to define the amount of water that is needed to hydrate an AOT molecule. It is then assumed that any extra water added beyond this minimum hydrating amount will behave like ordinary or bulk water. However it must be remembered that the AOT reverse micelle is a dynamic entity, and so inter-particle exchange will occur. Studies of the exchange of water, or other solubilized molecules, between reverse micelles have been made[7,25]. The actual process of exchange involves diffusion, and therefore has a rate constant of the order of $k_D = 10^{10}$ $dm^3mol^{-1}s^{-1}$. However, for exchange to occur, the reverse micelles must have sufficient kinetic energy such that a collision can be successful. Only of the order of 1 in 1000 reverse

micellar encounters result in exchange of material[26], so that the rate constant that describes the exhcange of material is $k_{ex} = 10^{-3} \times k_D = 10^7$ $dm^3 mol^{-1} s^{-1}$. This is a second order rate constant. Therefore the lifetime of a reverse micelle depends on the concentration of droplets in solution.

For example, a system comprisiong 0.1 $mol.dm^{-3}$AOT, at $W_o = 10$, will typically have droplets of aggregation number of the order of 100. This means that the droplet concentration ($C_{droplet}$) is 10^{-3} $mol.dm^{-3}$. Therefore the lifetime of an individual droplet is:

$$\tau_{1/2} = \frac{1}{k_{ex} C_{droplet}} = 10^{-4} s$$

It is known that the aggregation number increases as a function of W_o (see later in this chapter). Therefore as W_o increases, the droplet concentration decreases, and the lifetime increases.

As the amount of water within a reverse micelle increases, so the properties of ordinary or bulk water come to dominate the water, as the core of the reverse micelle contains mostly ordinary or bulk water. However it must be remembered that the reverse micelles are small and so the water molecules are never far from an interface. Also the concentration of counter-ions in the reverse micelle is high, which also affects the properties of the water.

It has been known for many years that AOT formed aggregates in apolar media[27] that were able to swell and accommodate large amounts of water. Early work on the system tended to be rather ambitious and therefore somewhat unsystematic[28,29], in attempting to characterise the behaviour of AOT in many different non-aqueous and apolar solvents. These experiments were hampered by the lack of a model for the size or shape of AOT aggregates. However, since then, many structural investigations have been carried out[14-16,19,26,30-36].

Much effort has been devoted to the determination of aggregate size, structure and life-time as well as intra- and inter-aggregate interactions. This has been achieved with various scattering techniques such as light scattering[8,9,19,29,37,38], and small angle neutron scattering[14,34,39-43]. To a first

approximation, scattering experiments (where the wavelength used is of the order of the intermolecular distance) provide information on intermolecular distances and diffusion[44]. Scattering experiments can be complicated to interpret as the effects of inter-aggregate interactions and polydispersity must be separated from the effects due to size and structure. This means that an unambiguous interpretation is not possible. The spectra from longer wavelength techniques, such as IR and NMR, (see below) are able to supply the details of longer range effects such as molecular conformation[44].

Where most contention seems to have been[11,16,18], is in the area of the aggregates' microstructure within a particular phase; even the conformation of each individual AOT molecule within an aggregate has been determined[11,16,45-47]. This is a subject about which infrared spectroscopy can provide useful information. In this respect, infrared spectroscopy differs from NMR spectroscopy in that the infrared experiment effectively observes species with much shorter lifetimes[44] $\tau = \frac{1}{\omega_{obs}} = 10^{-14}$ s.

Another issue that has been discussed is whether water is a prerequisite for the formation of reverse micelles. It was thought that without any water whatsoever, reverse micelles would not form[9]; the water acts as a binding agent for the ionic headgroup. However, the existence of dry micelles as observed by small angle X-ray scattering has been reported[48]. It is thought that dry AOT molecules are close packed around an icosahedron, to leave a space of radius 4.4 Å for water[14]. The existence of dry reverse micelles has been rationalized in terms of the transient nature of the reverse micelles, with polydispersity allowing some of the reverse micelles to be devoid of water. This seems to make more chemical sense. If water is present, then for thermodynamic reasons, the sodium and sulphonate ions will be hydrated before the carbonyl or ester groups. If water is not present then reverse micelles must form in order to protect the sodium ions. The process of micellization is dynamic. Most studies consider reverse micelles to be thermodynamically stable entities, which indeed they are.

However, the reverse micelle is not kinetically stable. Once an aggregate is formed, it may break down and re-form in another way. Although only 1 in 1000 inter-micellar collisions result in dimerization and exchange of material in the core[49], this does mean that the lifetime of a micelle, once it is formed, is short.

3.2.3. Percolation

The above points are tied in with the phenomenon of percolation. Percolation of electric charge through a microemulsion may be characterized by the onset of a large increase in the electrical conductivity of the system. Debate has occurred as to the reason why - at the molecular level - percolation should occur. For a given water/surfactant/oil system, percolation does not occur below certain values of volume fraction of microemulsion droplet or temperature. These values define the percolation threshold[36].

The onset of percolation has been attributed to the formation of a bicontinuous phase that allows the charge carriers to transport current through the water continuous phase. Alternatively the percolation threshold occurs at low volume fractions because of the nature of inter-aggregate interactions. To resolve the problem, the results of electrical conductivity experiments have been compared with self-diffusion coefficient measurements of water by pulsed field gradient NMR experiments[36]. Whilst a large change in the electrical conductivity was clearly observed for a microemulsion with $W_0 = 30$ at 30 °C, the self diffusion coefficient of water remained almost invariant across the whole temperature range of the experiment (20—70 °C). When the volume fraction of water (ϕ_W) within the microemulsion droplets was varied, similar results were obtained. The electrical conductivity showed that the percolation threshold is at $\phi_W = 0.05$, whereas the self diffusion coefficient showed no change until the bicontinuous phase was reached i.e. when $\phi_W > 0.3$. Variation of W_0 gave similar results, with a percolation threshold at $W_0 \approx 40$–45, which is the point on the phase diagram where the water/oil phase becomes the bicontinuous water/oil + water phase.

These results suggest that at the percolation threshold, there is electrical connectivity in the system, although translation of water molecules is still restricted to be within the micelle. Small angle neutron scattering measurements have shown that the microemulsion maintains its discrete reverse micelle structure beyond the percolation threshold[14]. This shows that the percolation threshold is not the same as the transition to a bicontinuous phase. In fact percolation is unlikely to occur in the bicontinuous phase as the electric charge may then be carried in the same way as in bulk aqueous solution. Mechanisms of percolation or percolative conduction therefore invoke ideas of hopping of charge carriers between reverse micelles, across the surfactant monolayers when they approach each other.

3.2.4. Studies of the AOT system by particular techniques

Very few papers however have actually applied infrared spectroscopy to the AOT system[1,15,35,50,51].

The work of MacDonald *et al*[15] was limited to a few concentration values of AOT, although spectra were recorded in different solvents and with added sodium chloride. Useful band assignments were collected in this work, mainly from work on water[52] and lipid bilayers[53], which AOT is thought to model. However, assessment of this work reveals that the analysis of the results relies on the existence of bulk-like water even at W_0 values as low as 4. This seems questionable and will be revisited in the discussion in chapter 6.

Experiments performed by Kise *et al*[50] on the AOT/ water/ benzene system did not draw firm conclusions from the spectral behaviour. The trends observed in the band positions etc. have also been observed in this work but in much more detail.

An interesting paper by Jain *et al*[35], argues for three types of water in the reverse micelle, based on Gaussian curve fitting to the coupled ν(OH) band. As will be extensively discussed in chapter 6, the basis for the assignment of the

vibrational bands seems questionable owing to effects such as intermolecular coupling.

3.2.5. AOT Aggregates - What shape is predicted?

As the molecular structure shows, the AOT molecule possesses two branched hydrocarbon tails, and an extended headgroup. The packing of AOT in a mesophase may be described using the packing parameter as follows[54,55]:

If the following terms are defined

V The molecular volume of the surfactant including the amount of oil and water that penetrates into the surfactant layer ($Å^3$).

Σ The area per polar head group ($Å^2$)

L The length of the hydrophobic hydrocarbon chain (Å). This does not allow for any folding of the chains if the surfactant is loosely packed.

A number called the surfactant parameter may then be defined $P = \frac{V}{\Sigma L}$

The value of the surfactant parameter indicates the type of aggregate structure formed when surfactant and water, or when surfactant, oil and water are mixed.

$P<\frac{1}{3}$	spherical micelles in water
$\frac{1}{3}<P<\frac{1}{2}$	rod micelles in water
$\frac{1}{2}<P<2$	lamellar phases in water or oil
$2<P<3$	rod micelles in oil
$3<P$	spherical micelles in oil

For AOT[56]

V	600 $Å^3$
Σ	55 $Å^2$
L	8 Å

This gives P=1.36 i.e. >1. Because of the branched chain in the AOT tail, AOT molecules will form aggregates that are able to swell to accommodate large amounts of water. However it must be remembered that this model involves many approximations. No allowance has been made for interactions between

aggregates so the model can only apply to dilute dispersions of aggregates. The model does however emphasise that the space filling properties of the surfactant tail are an important factor in the stability of the reverse micelle[57].

If the aggregates are spherical then it is particularly simple to establish a relationship between the radius of the particle and its composition[58]. By considering the geometry of a sphere, $v=\frac{4}{3}\pi r^3$ and $s=4\pi r^2$, then if v is the volume of the water in the centre, s is the total surface area of the core then the radius of the water core is given by:

$$r_w = \frac{3v}{s} = \frac{3}{\Sigma}\frac{v_{water}\, n_{water}}{n_{aot}}$$

where n_{water} and n_{aot} are the numbers of molecules of each of these species in the reverse micelle, and v_{water} is the average volume of a water molecule (30Å^3).

Now for AOT, Σ, the surface area per head group is constant and equal to 55 Å^2. This gives an expression for the radius of the water core at the centre of the reverse micelle in terms of the molar ratio of water to surfactant:

$$r_w \approx 1.5\, W_o \qquad \text{(in Å)}$$

$$W_o = \frac{n_{water}}{n_{aot}} = \text{mole ratio of water to surfactant}$$

The important point to notice about this equation is that there is a linear relationship between radius and the mole ratio. This implies that the size of the particle can be controlled accurately, thereby providing one of the main reasons for the applications of AOT reverse micelles. This is an oversimplification as Σ is not constant. At very low values of W_o (<6) then, apparently Σ falls[59] to 38 Å^2. This however may be due to the AOT molecules becoming interdigited at low W_o values[17].

3.2.6. Inter-aggregate interactions

For a dilute dispersion, reverse micelles experience van der Waals forces and short range repulsive forces. However the van der Waals forces are often insignificant so the interactions approximate to a hard sphere type repulsion[60]. In

more concentrated dispersions, then attractive forces become important and indeed cause phase separation[61,62] although this is not fully understood.

3.2.7. Methods to determine the structure of reverse micelles

A method often applied to the study of biological structures is electron microscopy. Only solid samples can be examined so freezing of the reverse micelles would be necessary. However cooling rates are insufficiently fast to prevent phase separation or changes of structure. This is especially the case for ionic surfactants where structural changes occur quickly. Non-ionic surfactants[63], which have lower exchange rates, are in fact amenable to investigation by electron microscopy.

3.2.8. Scattering techniques

Scattering of sub-atomic particles or electromagnetic radiation by an object, such as a reverse micelle aggregate, will produce the Fourier transform of the image of the object. Information on the sample may then be obtained by applying an inverse Fourier transform. Noise, finite resolution, and the wave vector range mean that the analysis is not simple. For solutions, the fluid is in constant motion which means that the spatial coherence is lost, i.e. an average over space and time is obtained. Consequently a model must be used to fit to the scattering data, and information is obtained indirectly. The wave vector of the particular type of radiation or particle used for the scattering experiment governs the spatial resolution of the experiment. This explains why many different scattering experiments are performed (e.g. with light, neutrons or x-rays).

The size of the reverse micelle can be found if the effects of inter-particle interactions are removed from the scattering data. Dilution or knowing the interaction potential[56] are two methods. It may also be necessary to account for the effects of polydispersity[39].

The figure 3.3 below shows the radius of the water core R_W as a function of W_O. The data are taken from various sources[17,56,59]. The size is important because this controls the properties of molecules dispersed within the water core.

For example, CdS micro-paritcles may be formed within the aqueous core, the size of which depends on the R_w[64].

The figure 3.3 also shows the aggregation number N of AOT molecules per reverse micelle as determined by dynamic light scattering[65]. When the aggregation number and the radius of the water core are both known, then the effective area per head group (Σ) may be found.

Figure 3.3 AOT reverse micelles. Water core radius (Rw) and aggregation number (N) versus W_o.

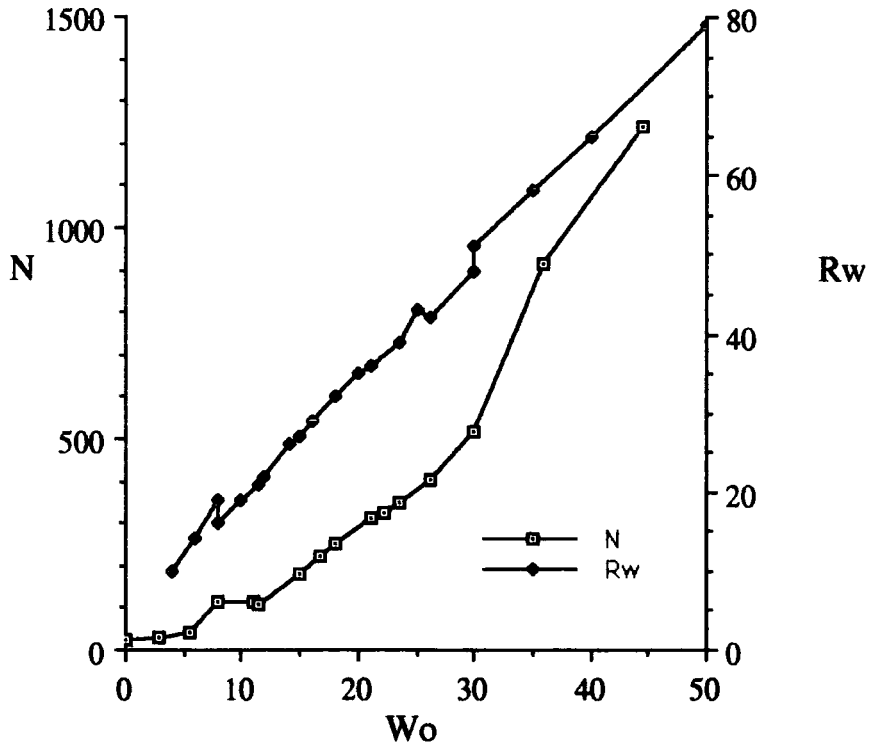

3.2.9. Fluorescence methods

This method relies on monitoring the fluorescence decay of a probe molecule that penetrates into some part of the reverse micelle[7,26,66-70]. It is a dynamic method and can give information on exchange between micellar aggregates. However for $W_o < 20$, a probe molecule can change the size of the reverse micelle, so it is not simple to interpret the fluorescence profiles.

Nevertheless some studies using the fluorescence technique[26] have yielded useful information about the behaviour of the surfactant interface as the temperature is varied between 10 and 40 °C. As the temperature rises, the penetration of solvent molecules in between AOT tails decreases because of the thermal energy. Hence the AOT tails are able to pack more effectively, increasing the aggregation number, lowering the curvature and causing the reverse micelles to swell.

3.2.10. NMR

Nuclear magnetic resonance has been used extensively to investigate the AOT system.[2,11,12,16-18,31,46,71-78]

By adding ^{17}O enriched H_3O^+ to an AOT/iso-octane/water system, the ^{17}O linewidth can be used to deduce various dynamic parameters. For $W_0 = 30$, it was found[2] that the coalescence rate was $8\times10^6\ M^{-1}s^{-1}$. The benefits of using H_3O^+ are several. H_3O^+ hardly perturbs the system compared with a fluorescence probe. Also as the species added is H_3O^+, the inter-micellar exchange rate is the same as water. Furthermore the linewidth of the ^{17}O line is strongly pH dependent. The scalar coupling of ^{17}O with protons in a molecule is modulated by the H_3O^+ and OH^- catalysed proton exchange with the surrounding molecules. At the extremes of pH, proton exchange is so fast that it does not contribute to the linewidth.

The behaviour of water is quantified[2]: for $W_0>15$, the reorientational correlation times for water are 3 to 5 times longer for the water bound at the interface than for bulk water. Moreover, the correlation times were found to be independent of W_0, providing $W_0 > 15$. The NMR data support the pseudo-phase or two site model that describes the water as being either bound or free.

A unique feature of NMR is the ability to determine unambiguously the headgroup conformations [11,16]. The three protons in the succinic acid part of the headgroup form an ABX-type system. The coupling constants between the protons have been measured, and the way in which they vary with W_0 can be explained by changes of conformation of the headgroup as W_0 changes. It was

concluded that conformation changes to minimise steric interactions, while maximising the separation of hydrophobic and hydrophilic parts of the molecule. This information is used later (chapter 6) to aid the assignment of the infrared spectra.

The ^{13}C relaxation times[18] have been used to obtain local reorientation times for each carbon in the hydrocarbon tail. Times are short near the tail end(10 ps) and longer near the polar headgroup(200 ps). This gives a crude measure of the mobility, and indicates that the interfacial film is fluid-like. However, the analysis of the data is more complicated[79]. Local anisotropy means that the ^{13}C-^{1}H dipolar interactions are not averaged. So relaxation is also influenced by slower motions such as surfactant reorientation and micelle rotation.

The sizes of micelles may be inferred from chemical shift data using a two site model[17]. This approach will be used in chapter 6 to investigate the infra-red data. NMR thus provides many useful ways to analyse the AOT reverse micelle system.

3.2.11. Motions of molecules in surfactant phases

There are several processes relevant to water and surfactant motion that occur in reverse micellar (and micellar) systems.

Monomer - micelle exchange is well known for direct (non-reverse) micelles in aqueous solutions. It is an important mechanism for the transfer of surfactant molecules between micelles. In solution micelles themselves do not approach near enough to exchange material due to double layer repulsions at the micelle surface. Kato *et al* have recently determined monomer-micelle exchange rates for the CsPFO/water system (investigated later in this thesis)[80] They found that the mean (first order) dissociation rate constant was $0.76\times10^{6}\ s^{-1}$.

For reverse micelles, monomer micelle exchange is much less common, there is little data available on the concentrations of AOT monomers in solution, because the values are very low. Reverse micelles interact via collision processes

as discussed above in section 3.2.2. The translational diffusion coefficients depend inversely on the radius of AOT reverse micelles, are of the order of 10^{-10} m^2s^{-1} as found by neutron scattering[32].

The segmental motions of individual AOT molecules may be studied. From NMR as mentioned above, reorientation times for the CH_2 groups in the molecule are short near the tail end(10 ps) and longer near the polar headgroup(200 ps).

3.3. References

(1) Christopher D. J., Yarwood J., Belton P. S., Hills B. P. *J. Coll. Interf. Sci.* **1992**, *152*, 465.
(2) Carlström G., Halle B. *Langmuir* **1988**, *4*, 1346.
(3) D'Aprano A., Lizzio A., Turco Liveri V. *J. Phys. Chem.* **1987**, *91*, 4749.
(4) D'Aprano A., Lizzio A., Liveri V. T. *J. Phys. Chem.* **1988**, *92*, 1985.
(5) D'Aprano A., Donato I. D., Goffredi M., Turco Liveri V. *Journal of Solution Chemistry* **1992**, *21*, 323.
(6) D'Aprano A., D'Arrigo G., Goffredi M., Paparelli A., Turco Liveri V. *J. Chem. Phys.* **1991**, *95*, 1304.
(7) Eicke H. F., Shepherd J. C. W., Steinemann A. *J. Coll. Interf. Sci.* **1975**, *56*, 168.
(8) Eicke H. F., Rehak J. *Helv. Chim. Acta* **1976**, *59*, 2883.
(9) Eicke H. F., Christen H. *Helv. Chim. Acta* **1978**, *61*, 2259.
(10) Goffredi F., Turco Liveri V., Vassallo G. *J. Coll. Interf. Sci.* **1992**, *151*, 396.
(11) Heatley F. *J. Chem. Soc. Faraday Trans. I* **1987**, *83*, 517.
(12) Heatley F. *J. Chem. Soc. Faraday Trans. I* **1988**, *84*, 343.
(13) Heatley F. *J. Chem. Soc. Faraday Trans. I* **1989**, *85*, 917.
(14) Kotlarchyk M., Huang J. S., Chen S. H. *J. Phys. Chem.* **1985**, *89*, 4382.
(15) MacDonald H., Bedwell B., Gulari E. *Langmuir* **1986**, *2*, 704.
(16) Maitra A. N., Eicke H. *J. Phys. Chem.* **1981**, *85*, 2687.
(17) Maitra A. *J. Phys. Chem.* **1984**, *88*, 5122.
(18) Ueno M., Kishimoto H., Kyogoku Y. *Bull. Chem. Soc. Jpn.* **1976**, *49*, 1776.
(19) Zulauf M., Eicke H. F. *J. Phys. Chem.* **1979**, *83*, 480.
(20) *Interfacial phenomena in Apolar Media*; Eicke H.-F., Parfitt G. D., Ed.; Marcel Dekker: New York, **1987**.
(21) Luisi P. L. In *Structure and reactivity in reverse micelles*; Eds. M. P. Pileni; Elsevier: Amsterdam, **1989**; Vol. 65; pp 262.
(22) *Reverse Micelles*; Luisi P. L., Straub B. E., Ed.; Plenum: New York, **1989**.
(23) Pileni M. P. *Structure and reactivity in reverse micelles*; Elsevier: Amsterdam, **1989**; Studies in Physical and Theoretical Chemistry; .
(24) Luisi P. L., Magid L. J. *CRC Critical Reviews in Biochemistry* **1986**, *20*, 409.
(25) Fletcher P. D. I., Howe A. M., Robinson B. H. *J. Chem. Soc. Faraday Trans. I* **1987**, *93*, 985.
(26) Lang J., Jada A., Malliaris A. *J. Phys. Chem.* **1988**, *92*, 1946.
(27) Mattoon R. W., Mathews M. B. *J. Chem. Phys.* **1949**, *17*, 496.
(28) Kitahara A., Kobyashi T., Tachibana T. *J. Phys. Chem.* **1962**, *363*, 66.
(29) Peri J. B. *J. Coll. Interf. Sci.* **1968**, *29*, 6.
(30) Fontell K. *J. Coll. Interf. Sci.* **1973**, *44*, 318.
(31) Wong M., Thomas J. K., Nowak T. *J. Am. Chem. Soc.* **1977**, *99*, 4730.
(32) Day R. A., Robinson B. H., Clarke J. H. R., Doherty J. V. *J. Chem. Soc. Faraday Trans. I* **1978**, *74*, 132.

(33) Howe A., Toprakcioglu C., Dore J. C., Robinson B. H. *J. Chem. Soc. Faraday Trans. I* **1986**, *82*, 2411.
(34) Sheu E. Y., Chen S., Huang J. S. *J. Phys. Chem.* **1987**, *91*, 3306.
(35) Jain T. K., Varshney M., Maitra A. *J. Phys. Chem.* **1989**, *93*, 7409.
(36) Maitra A., Mathew C., Varshney M. *J. Phys. Chem.* **1990**, *94*, 5290.
(37) Yan Y. D., Clarke J. H. R. *J. Chem. Phys.* **1990**, *93*, 4501.
(38) Bakale G., Beck G., Thomas J. K. *J. Phys. Chem.* **1992**, *96*, 2328.
(39) Robinson B. H., Toprakcioglu C., Dore J. C., Chieux P. *J. Chem. Soc. Faraday Trans. I* **1984**, *80*, 13.
(40) Toprakcioglu C., Dore J. C., Robinson B. H., Howe A., Chieux P. *J. Chem. Soc. Faraday Trans. I* **1984**, *80*, 413.
(41) Chen S. *Physica B* **1986**, *137*, 183.
(42) Chen S. H., Chang S. L., Strey R., Samseth J., Mortensen K. *J. Phys. Chem.* **1991**, *95*, 7427.
(43) Wu X., Tong P., Huang J. S. *J. Coll. Interf. Sci.* **1992**, *148*, 104.
(44) Yarwood J., Döge G. In *Spectroscopy and Relaxation in Molecular Liquids*; Eds. D. Steele and J. Yarwood; Elsevier: Amsterdam, **1991**; .
(45) Ueno M., Kishimoto H., Kyogoku Y. *Chemistry Letters* **1977**, 599.
(46) Thompson K. F., Gierasch L. M. *J. Am. Chem. Soc.* **1984**, *106*, 3648.
(47) Jain T. K., Maitra A. *Colloid. Surf.* **1989**, *36*, 87.
(48) North A. N., Dore J. C., Mc Donald J. A., Robinson B. H., Heenan R. H., Howe A. M. *Colloid. Surf.* **1986**, *19*, 21.
(49) Robinson B. H. *Chem. Brit.* **1990**, *26*, 342.
(50) Kise H., Iwamoto K., Seno M. *Bull. Chem. Soc. Jpn.* **1982**, *55*, 3856.
(51) Giammona G., Goffredi F., Turco Liveri V., Vassallo G. *J. Coll. Interf. Sci.* **1992**, *submitted*, preprint available.
(52) Walrafen G. E. In *hydrogen bonded solvent systems*; Eds. A. K. Covington and P. Jones; Taylor and Francis: London, **1968**; .
(53) Tso T. L., Lee E. K. C. *J. Phys. Chem.* **1985**, *89*, 1612.
(54) Israelachivili J. N., Mitchell D. J., Ninham B. *J. Chem. Soc. Faraday Trans. II* **1976**, *72*, 1525.
(55) Mitchell D. J., Ninham B. W. *J. Chem. Soc. Faraday Trans. II* **1981**, *77*, 601.
(56) Langevin D. In *Structure and reactivity in reverse micelles*; Eds. M. P. Pileni; Elsevier: Amsterdam, **1989**; Vol. 65; pp 13.
(57) Brown D., Clarke J. H. R. *J. Phys. Chem.* **1988**, *92*, 2881.
(58) Pileni M. P. In *Structure and reactivity in reverse micelles*; Eds. M. P. Pileni; Elsevier: Amsterdam, **1989**; Vol. 65; pp 44.
(59) Cabos C., Delord P. *Journal of Physics Letters* **1980**, *41*, 455.
(60) Caljé A. A., Agterof W. G. M., Vrij A. In *Micellization, Solubilization and Microemulsions*; Eds. K. L. Mittal; plenum: New York, **1977**; Vol. 2.
(61) Lemaire B., Bothorel P., Roux D. *J. Phys. Chem.* **1983**, *87*, 1023.
(62) Pincus P. A., Safran S. A. *J. Phys. Chem.* **1987**, *86*, 1644.
(63) Jahn W., Strey R. *J. Phys. Chem.* **1988**, *92*, 2294.
(64) Meyer M., Walberg C., Kurihara K., Fendler J. H. *Journal of the Chemical Society. Chemical Communications* **1984**, 90.
(65) Day R. A., Robinson B. H., Clark J. H. R., Doherty J. V. *J. Chem. Soc.* **1979**, *75*, 132.
(66) Howe A. M., McDonald J. A., Robinson B. H. *J. Chem. Soc. Faraday Trans. I* **1987**, *83*, 1007.
(67) van der Auweraer M., de Schryver F. C. In *Structure and reactivity in reverse micelles*; Eds. M. P. Pileni; Elsevier: Amsterdam, **1989**; Vol. 65; pp 70.
(68) Belletete M., Lachapelle M., Durocher G. *J. Phys. Chem.* **1990**, *94*, 5337.
(69) Johannsson R., Almgren M., Alsins J. *J. Phys. Chem.* **1991**, *95*, 3819.
(70) Zhang J., Bright F. V. *J. Phys. Chem.* **1991**, *95*, 7900.
(71) Hauser H., Haering G., Pande A., Luisi P. L. *J. Phys. Chem.* **1989**, *93*, 7869.
(72) Carlström G., Halle B. *J. Phys. Chem.* **1989**, *93*, 3287.
(73) Leser M. E., Kooijman M., Pollitte J., Magid L. J. *J. Phys. Chem.* **1991**, *95*, 9013.
(74) Callaghan P. T., Soderman O. *J. Phys. Chem.* **1983**, *87*, 1737.
(75) De Marco A., Menegatti E., Luisi P. L. *Journal of Biochemical and Biohysical Methods* **1986**, *12*, 325.

(76) Geiger S., Eicke H. F. *J. Coll. Interf. Sci.* **1986**, *110*, 181.
(77) Llor A., Rigny P. *J. Am. Chem. Soc.* **1986**, *108*, 7533.
(78) Quist P. O., Halle B. *J. Chem. Soc. Faraday Trans. I* **1988**, *84*, 1033.
(79) Söderman O., Walderhaug H. *Langmuir* **1986**, *2*, 51.
(80) Kato S., Harada S., Nakashima H., Nomura H. *J. Coll. Interf. Sci.* **1992**, *150*, 305.

CHAPTER 4

AOT EXPERIMENTAL

4. AOT Experimental

This chapter is divided into two sections. Firstly the sample preparation, and methods of measuring the spectra are presented, then the details of the instrumental parameters are considered.

4.1. Materials

For the purposes of measuring the infrared spectra of AOT microemulsions some workers have shown that it is feasible to use AOT as supplied without further purification[1-3]. Other workers have purified it[4]. Various methods exist[5], although it seems to make little difference to the results obtained by these workers. It is thought that 99+% purity is sufficient for spectroscopic purposes[6] but it is more critical to purify the AOT if kinetic measurements are to be made within the microemulsion[7,8].

AOT (Aldrich, 99%) was used as supplied. Initially a stock solution was made by dissolving AOT in heptane(Aldrich, 99% spectral grade gold label) in a volumetric flask (to produce a stock solution). This was stored over fresh molecular sieve (Aldrich, 8-12 mesh) to remove as much water as possible. This stock solution would then be diluted with water to make up the microemulsion.

The AOT purchased contains a small amount of water. To simply determine the quantity of water contained within the sample, the following procedure was followed. An infrared transmission spectrum of a 0.1 mol.dm^{-3} solution of AOT in heptane was obtained. From this, the spectrum of heptane was subtracted, after correcting for the amount of heptane present. The resulting spectrum shows the AOT and the water that it contains (Figure 4.1 below). If the integrated area of this ν(OH) stretch is measured and compared with spectrum of a sample that contains a known amount of added water then the integrated area corresponds to approximately 0.5 equivalents of water per AOT molecule.

Figure 4.1 FTIR spectrum of 0.1 mol.dm^{-3} AOT/heptane as supplied – spectrum of heptane. Pathlength = 14.0 μm, CaF_2 plates. Ambient temperature

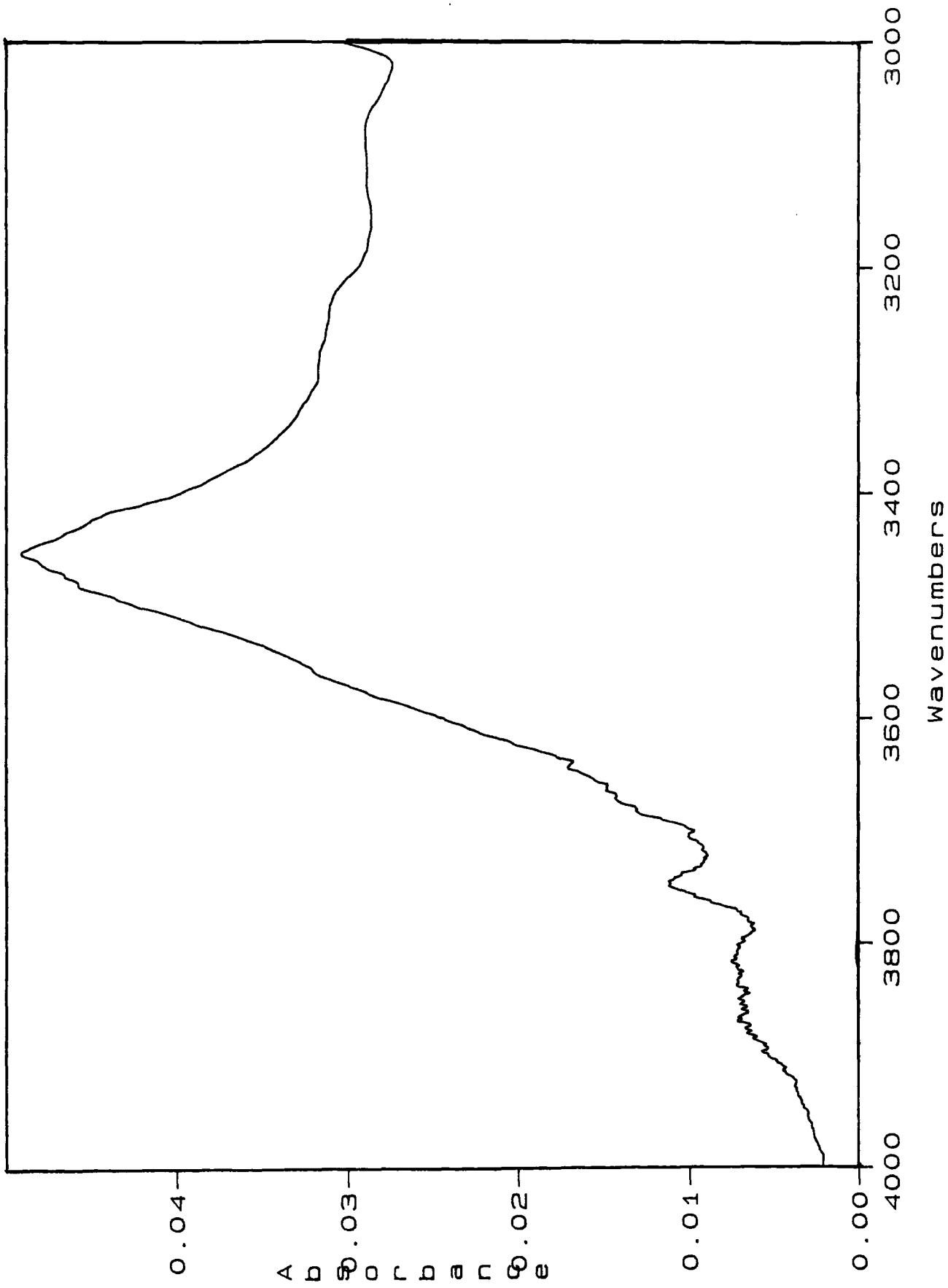

Therefore the W_0 values refers to the amount of water added. To improve the accuracy, 0.5 should be added to W_0 to give the total amount of water present. However the amount of water included with the AOT will vary with time depending of storage conditions.

The water used to make up each microemulsion sample was either D_2O (Aldrich 99.8 atom %D) or distilled H_2O (see table 4.1).

4.2. Experimental procedure to make the microemulsions

2 ml of stock solution was measured, using a micrometer driven 0.5 ml syringe (±5 µl), into a sample bottle and the required quantity of water was added using a microsyringe (±0.1 µl). The volume of water was calculated so that the system would be hydrated to a known extent: i.e. the W_o value would be accurately known. The mixture of heptane, water and AOT was then shaken, became cloudy and cleared after a few seconds. All of the samples that were made up were clear and one phase, and were used within a few days. However when W_o exceeded 50 then the solutions often remained cloudy or separated after some days. This indicates that approximately 50 water molecules per head group is the largest microemulsion obtainable with heptane as the solvent.

4.3. Infrared Spectroscopic measurements

The cell which holds the sample of AOT microemulsion was constructed with teflon spacers of various thickness. Both AgCl and CaF_2 are suitable for holding samples which contain water as these salts are insoluble in aqueous solutions. CaF_2 was used initially. Subsequent experiments used AgCl plates, which have some advantages over CaF_2. The merits of each are set out below:

(a) CaF_2 will easily crack if it is subjected to a thermal shock, whereas AgCl is a more plastic crystal so does not crack. This ability of AgCl to deform slightly means that cells assembled with AgCl plates seal better.

(b) AgCl darkens on prolonged exposure to light

(c) AgCl reacts with metals to deposit silver. This is a disadvantage if one wishes to use very thin cell spacers as these are usually made from aluminium which dissolves into the AgCl plate.

(d) AgCl has a wider transmission range in the mid infra-red. Whereas CaF_2 absorbs radiation below 1200 cm^{-1}, AgCl is transparent down to 700 cm^{-1}.

Transmission spectra were recorded on a Mattson Sirius instrument by coadding 256 spectra at 2 cm^{-1} resolution, using a liquid nitrogen cooled mercury cadmium telluride detector (see below).

The pathlength of the empty cell was calculated from the observed interference fringes[9] (see below for a description of this method).

The temperature of the cell was held constant above room temperature at 20°C by means of a circulating water system.

The general procedure in these experiments was:

(a) To make a solution of AOT in heptane of a specific concentration. This is the stock solution from which all other samples were made.

(b) Measure the pathlength of the empty cell.

(c) Record the spectrum of the stock solution.

(d) Record the background single beam spectrum.

(e) Fill the cell and record the microemulsion single beam spectrum.

(f) Empty and clean the cell. Hydrate a sample of stock solution to the required W_o value then repeat from (d)

In this way a series of spectra each with a different W_o value were obtained. The spectrum of heptane was also recorded during each set of experiments so that the solvent absorption could be subtracted form the spectra.

Table 4.1 Values of W_o, water isotope, pathlength, temperature and cell plate material for AOT microemulsions made in these experiments.

	Filenames	Wo values used	Water isotope	path-length /μm	Temp /°C±0.5	Plates
A	hpt001-023	0,0.5,1,1.5,2,2.5,3,3.5, 4,4.5,5,10,15,20,25, 30,35,40,45	H_2O	14.0	Room Temp	CaF_2
B	had01-10	0,0.5,1,1.5,2,2.5, 3,3.5,4,4.5,5	4% D_2O +H_2O	14.1	25±0.5	CaF_2
C	had30-41	0,1,2,3,4,5,6, 10,15,20	4% D_2O +H_2O	104	20±0.5	CaF_2
D	had54-60	0,1,5,10,15,20	4% D_2O +H_2O	521	20±0.5	CaF_2
E	d001-20	0,1,2,4,3,5,6,7,8,9,10, 11,12,13,14,15,16, 17,18,19,20	4% D_2O +H_2O	57	20±0.5	AgCl
F	h001-5	0,1,2,3,4,5	4% H_2O +D_2O	114	20±0.5	AgCl
G	d001-20	0,1,2,4,4,5,6,7,8,9,10, 11,12,13,14,15,16, 17,18,19,20	D_2O	114	25±0.5	AgCl
H	wo02-20	0,2,4,6,8,10,12,15,20	8% H_2O +D_2O	207	25±0.5	AgCl
J	wo20-45	20,25,30,35,40,45	4% H_2O +D_2O	30	25±0.5	AgCl

Experiment A was a set of solutions made up using only H_2O. The coupled water band can be seen clearly increasing in intensity as W_o is increased. W_o was increased in steps of 0.5 and the differences in the spectra can be seen at this level of increase in W_o. This set of experiments (A) has the largest range of W_o values, extending up to 45 water molecules per surfactant.

The next set of experiments (B) was carried out using water which consisted of H_2O and 4% D_2O(v/v). At 4% enrichment of D_2O, the intensity of the ν(OD) band is low. To enable the band profile to be recorded accurately the experiment (B) was repeated using samples with longer pathlengths

(Experiments C and D). A set of experiments with large W_o values using decoupled water was also carried out.

AgCl plates were then obtained which enabled the symmetric S=O band to be observed $\nu \approx 1050\ cm^{-1}$. In these experiments the water used for forming the microemulsion was only D_2O. This allows the coupled ν(OD) band to be examined. In addition the carbonyl band ν(C=O) can be observed without interference from the overlap of the water bending vibration $\delta(H_2O)$.

Experiment (H) was performed using 8% D_2O (v/v) instead of 4%. This was done in order to show that the results obtained were not merely an artefact of using 4% isotopic dilution.

To conclude, data for each vibration in the AOT/heptane/water system have been obtained as a function of W_o. The water isotopic dilution was always 4%, except for experiment H.

4.4 Measurement of cell pathlength

When light passes through an interface where a change of refractive index occurs, then a proportion of the light will be reflected, and a proportion transmitted. In an infrared transmission cell, there are two plates (usually made of a salt e.g. KBr, CaF_2 or AgCl) separated by an air gap. The gap is formed by a spacer that may be as thin as 6 μm, if made of aluminium foil.

Figure 4.2 Schematic diagram of interference fringes.

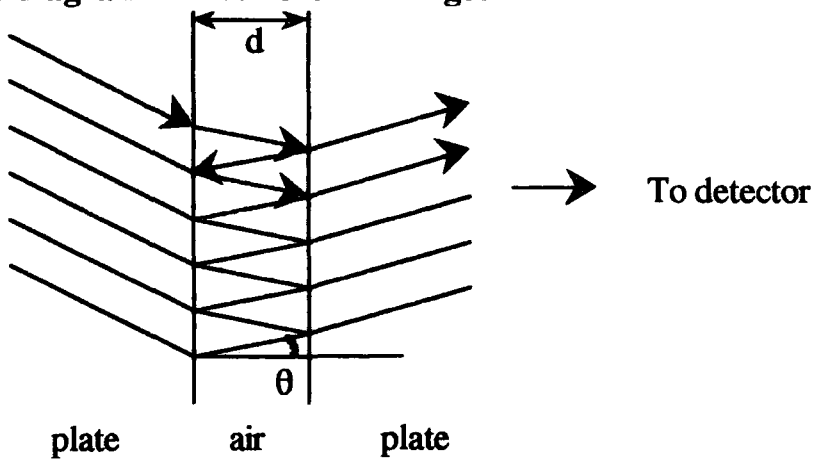

The angles on the above diagram are greatly exaggerated in order to show the path of the beam of light. The figure 4.2 shows how interference occurs. Multiple internal reflections occur within the cell, but the path of one incident beam only is shown to indicate how the process occurs.

Reflections will occur when there is a large refractive index difference between the plate and the medium within the cell, i.e. when the cell is empty. Whether the interference is constructive or destructive depends on the optical path difference between the paths of light. The intensity of the interference pattern varies sinusoidally with the wavelength of the light. A position of maximum transmission, i.e. constructive interference, occurs[9] when $2d=n.\lambda$ where n is an integer, and λ is the wavelength of the light.

It can be shown that $d = \frac{n}{2\Delta\bar{\nu}}$ where d is the pathlength, n is the number of interference fringes and $\Delta\bar{\nu}$ is the wavenumber difference between n successive maxima in the spectrum. Thus the pathlength of a transmission cell may be accurately found by averaging several values of d for different interference fringes in the spectrum.

4.5 Instrumental Considerations

The theory behind molecular vibrations has been outlined in chapter 2. Here, the method used to measure these vibrations is described.

A spectrometer is a device that records a spectrum. The spectrum is the intensity of absorption or emission of energy as a function of frequency or wavelength absorbed or emitted from a sample. Spectrometers generally comprise a radiation source, a sample, a detector and some means to separate the radiation in some dimension such as time, frequency or space. Fourier transform infrared (FTIR) instruments conform to this simplified model, the radiation being separated in the time dimension by the spectrometer.

Sources for the infrared region of the spectrum are black body radiators, which are incoherent and polychromatic. The infrared beam is emitted from the

source and passes through an iris of variable size, the purpose of which is to minimize beam divergence. The optical path then takes the beam through the interferometer, the operation of which is well described in the literature[10]. The beam-splitter is made from alkali-metal/halide coated with semiconductor (Ge or Si) with no parallel surfaces to avoid interference. In a FTIR instrument the only moving part is one of the mirrors, which is driven by electro-magnets. The detector is a mercury-cadmium-telluride semiconductor device that operates at 78 K. It has a very fast response time to infrared radiation, and is therefore ideal for use in rapid scanning instruments. The size of the detector element is only a few millimetres across, as the device is difficult to manufacture. This incidentally is the reason why large photo-diode type detectors or charge coupled devices have not been developed yet for infrared radiation. Nevertheless, the detector is very sensitive and is able to detect single monolayers of material. The spectrometer layout is shown in figure 4.3 overleaf.

If the distance from the point of zero path difference of the moving mirror travel is represented by x, then the for monochromatic radiation of wavenumber (frequency) $\bar{\nu}_0$ intensity at the detector is given by[11]:

$$I(x) = S(\bar{\nu}_0)(1+\cos 2\pi \bar{\nu}_0 x) = S(\lambda_0)(1+\cos \frac{2\pi x}{\lambda_0})$$

where $S(\bar{\nu}_0)$ is the spectral amplitude at wavenumber $\bar{\nu}_0$. λ_0 is $\bar{\nu}_0$ expressed as a wavelength. I(x) will reach a maximum when

$$2\pi \bar{\nu}_0 x = 2n\pi : n = 0,1,2,3\ldots \text{ or when } x = \frac{n}{\bar{\nu}_0}$$

I(x) is therefore the interferogram, the form of which for monochromatic radiation is a cosine wave. Such a pattern is observed when a laser is used, indeed this is the reference within the spectrometer. A low power He/Ne laser emitting light of wavelength 652 nm is introduced into the optical path of the spectrometer.

Figure 4.3 Layout of Mattson Sirius spectrometer.

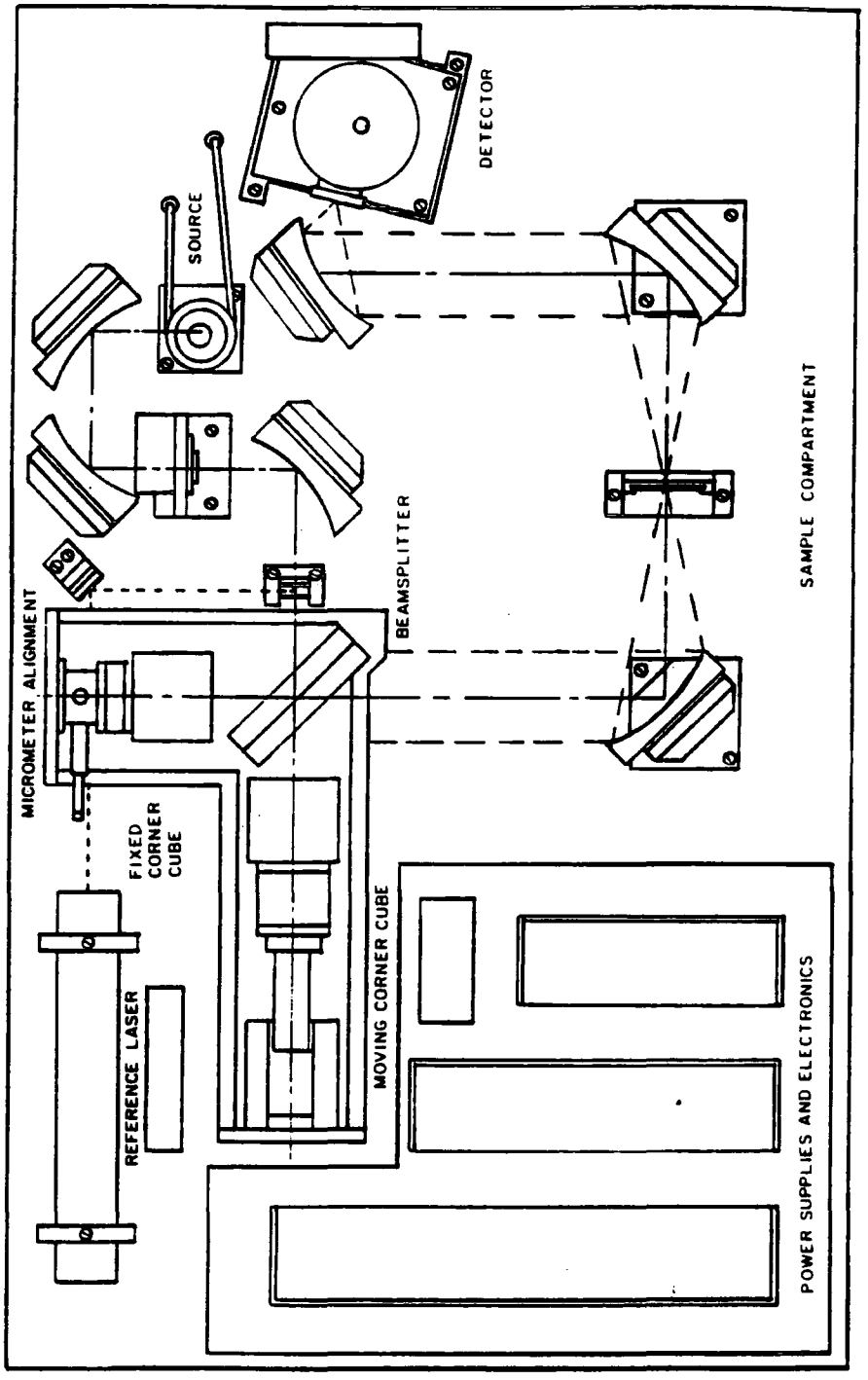

When the optical path difference between the recombined beams is zero, then a maximum in intensity is observed. This signifies that there is zero optical path difference between the two paths, and the maximum in intensity is used to trigger the detector to commence measurements.

If the interferometer is illuminated by frequencies between $\bar{\nu}_L$ and $\bar{\nu}_H$ then:

$$I(x) = \int_{\bar{\nu}_L}^{\bar{\nu}_H} S(\bar{\nu})[1 + cos\, 2\pi\bar{\nu}x]\,d\bar{\nu}$$

For a rapid scanning instrument this may be approximated to the following equation:

$$I'(x) = \int_{\bar{\nu}_L}^{\bar{\nu}_H} S(\bar{\nu})[cos\, 2\pi\bar{\nu}x]\,d\bar{\nu}$$

$S(\bar{\nu})$ is obtained by Fourier transformation of I' (x), to yield:

$$S(\bar{\nu}) = \int_0^{x_{max}} I'(x)[cos\, 2\pi\bar{\nu}x]\,dx = \int_0^{x_{max}} I'(x)\, exp(-2\pi i\bar{\nu}x)\,dx$$

However, there is no standard form for this function so numerical integration is required, and the interferogram is represented by a summation. If the interferogram is an even function (which theoretically it should be, but in practice is not because of digitisation) then I(x) = I(-x) and

$$S(\bar{\nu}) = \sum_{x=0}^{x_{max}} I'(x)[cos\, 2\pi\bar{\nu}x]$$

In this case, x is actually represented by $x = n\Delta x$, where Δx is the sampling interval, and n is the number of the sampling interval (i.e. $1,2,3,\ldots x_{max}$). Typically Δx is of the order of a few microns, and n may have values up to several thousands. Therefore x_{max} is the maximum mirror travel, which gives rise to a maximum optical path difference of $D = 2x_{max}$. The spectral resolution depends on the maximum delay between the two beams:

$$\delta\bar{\nu} = \frac{1}{D}$$

If Δx is too large then the spectrum is incompletely described. Sampling must occur at least every half wavelength so (i.e. at the Nyquist frequency):

$$\Delta x \leq \frac{1}{2}\lambda_{min} \text{ or } \Delta x \leq \frac{1}{2\bar{\nu}_{min}}$$

Therefore if energy is present up to 4000 cm^{-1} then sampling is required every 1.25 μm

There are advantages to using a FTIR instrument over a dispersive instrument.

(1) The multiplex advantage.

All of the spectral elements are observed at all times. This is an essential procedure to use when the system has limited source power (such as astronomical interferometry), but is still advantageous even when the system is detector noise limited, as in this instance.

For a dispersive instrument the signal to noise ratio is given by:

$$\frac{S}{N}(\text{dispersive}) = \sqrt{\frac{\text{observation time}}{\text{number of spectral elements}}}$$

whereas for a FT instrument, the signal to noise ratio is:

$$\frac{S}{N}(\text{FT}) = \sqrt{\text{observation time}}$$

Therefore, the gain in the signal to noise ratio is:

$$\frac{\frac{S}{N}(\text{FT})}{\frac{S}{N}(\text{dispersive})} = \sqrt{\text{number of spectral elements}}$$

For an FT instrument, the number of spectral elements is the number of scans made by the interferometer.

(2) The throughput advantage.

In a dispersive instrument, the frequencies are sorted by the monochromator, which will contain gratings and slits, deliberately to discard unwanted radiation. In a FT instrument, the image of the source at the detector is only attenuated by the sample, so more radiation reaches the detector.

The above advantages, the lack of many moving parts in the spectrometer, the ever decreasing costs and reliability of electronic systems together with the very high sensitivity, mean that the FT instrument has become an effective instrument for measuring infrared spectra.

4.6 References

(1) Robinson B. H., Steytler D. C., Tack R. D. *J. Chem. Soc. Faraday Trans. I* **1977**, *73*, 481.
(2) Kise H., Iwamoto K., Seno M. *Bull. Chem. Soc. Jpn.* **1982**, *55*, 3856.
(3) Quist P., Halle B., Furó I. *J. Chem. Phys.* **1991**, *95*, 6945.
(4) Jain T. K., Varshney M., Maitra A. *J. Phys. Chem.* **1989**, *93*, 7409.
(5) Thompson K. F., Gierasch L. M. *J. Am. Chem. Soc.* **1984**, *106*, 3648.
(6) Howe A. M., McDonald J. A., Robinson B. H. *J. Chem. Soc. Faraday Trans. I* **1987**, *83*, 1007.
(7) Peri J. B. *J. Coll. Interf. Sci.* **1968**, *29*, 6.
(8) Fletcher P. D. I., Perrins N. M., Robinson B. H., Toprakcioglu C. In *Reverse Micelles*; Eds. P. L. L. a. B. E. Straub; Plenum: New York, **1989**; ; pp 69.
(9) Potts W. J. *Chemical Infrared Spectroscopy*; Wiley: New York, **1963**.
(10) Banwell C. N. *Fundamentals of Molecular Spectroscopy*; McGraw-Hill: London, **1983**.
(11) Griffiths P. R. *Transform Techniques in Chemistry*; Plenum: New York, **1978**.

CHAPTER 5

AOT RESULTS

5.1 Water Vibrations

5.1.1 Measurement of the parameters of the infrared absorption bands.

The band parameters were measured directly from the digitised spectra. The peak frequency quoted is the position of maximum absorption. Full widths at half height (FWHH) were measured after linear baseline correction had been applied to the spectrum over as wide a range as possible. This method was found to give the most consistent results when measuring the band width.

When the data from experiment (H) was analysed, which used 8% D_2O enrichment instead of 4%, then except for the integrated intensities, all of the spectral parameters that were measured were found to be independent of the proportion of D_2O in the mixture.

This band envelope (figure 5.2) is very broad as the vibrations of the water molecules from which it arises are coupled. It has an asymmetric shape, comprising at least three bands. The shape changes on hydration with the lower frequency band becoming more intense. A Beer's law plot is strictly valid only for a single absorption band. The coupled water band has a complex shape so quantitative information cannot be deduced from a Beer's law type plot.

However figure 5.3 shows that the data, although giving a reasonably good fit to a single straight line, do show a gradual curvature so may be better considered as either:

(i) a curve, representing a gradual change in water environment, or

(ii) two straight lines each with a correlation coefficient of r=0.99. This implies a break point at some value of $W_o \approx$ 10-15 where the existing types of water change.

The whole of the mid-infrared range is shown in figure 5.1 below. The integrated band areas have been obtained and the data are given in table 5.1.

5.1.2 Coupled OH stretching band

Table 5.1 The integrated band area of the coupled ν(OH) stretching band as a function of W_0 : H_2O only, ambient temperature CaF_2 plates, pathlength = 14 μm (Expt A).

W_0	Integrated area cm^{-1}
0	2.1
0.5	9.2
1	19.3
1.5	29.8
2	32.3
2.5	65.3
3.5	82.7
4.5	96.0
5	110.5
10	244.6
15	336.1
20	433.9
25	483.9
30	578.9
35	634.8
40	730.4
45	786.2

Figure 5.1 The whole mid-IR spectrum of AOT/heptane/H_2O microemulsions as a function of W_0. W_0 values are 0, 10, 45. H_2O only, ambient temperature, CaF_2 plates, pathlength = 14 μm (Expt A).

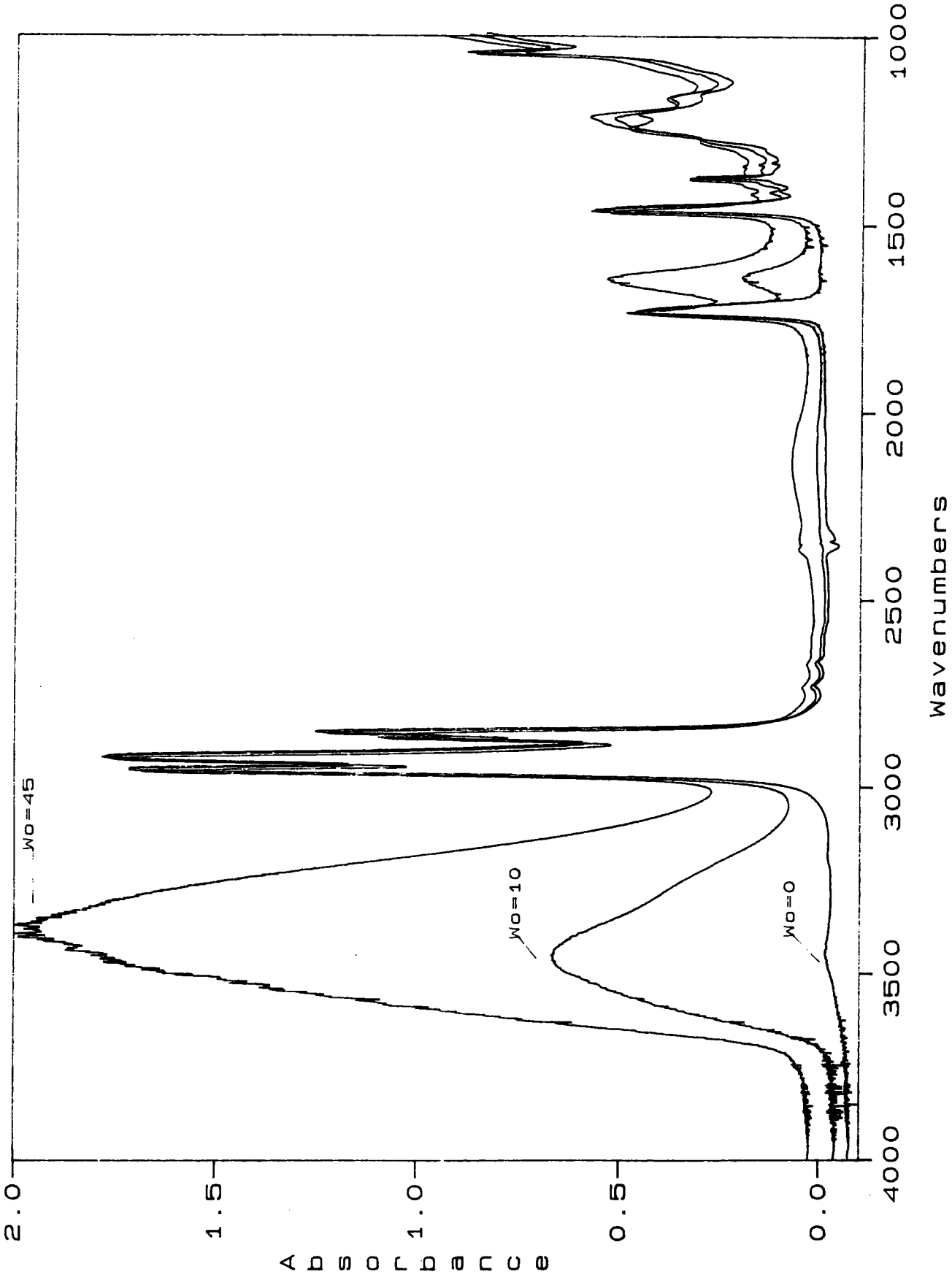

Figure 5.2 Coupled ν(OH) vibration and CH stretching vibrations in AOT/heptane/H_2O microemulsions as a function of W_o. W_o values are 0.5, 1, 1.5, 2, 2.5, 3, 3.5, 4, 4, 5.5, 10, 15, 20, 25, 30, 35, 40, 45. Ambient temperature, pathlength = 14 μm

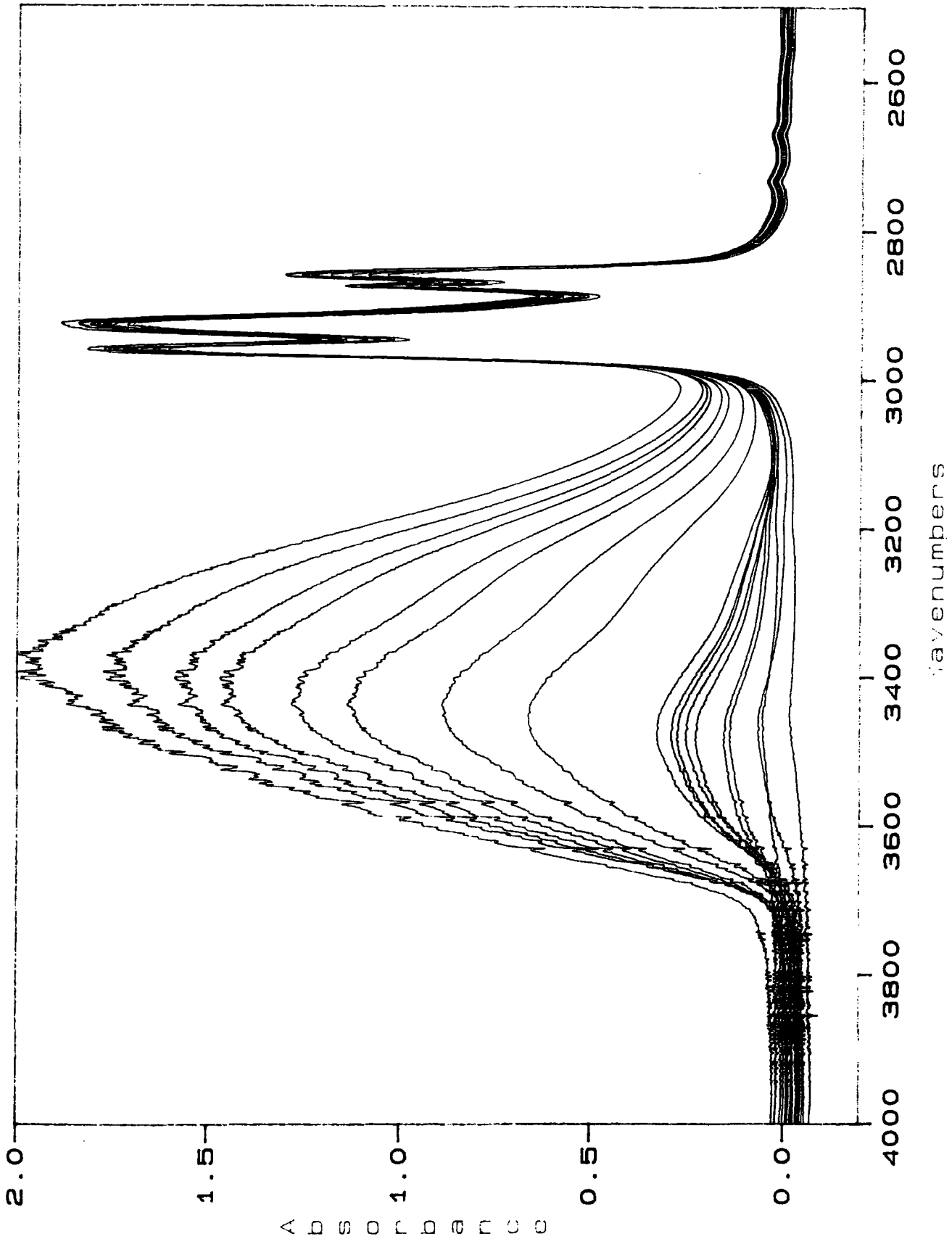

Figure 5.3 Integrated area of coupled ν(OH) band in AOT/heptane/H_2O microemulsions: Ambient temperature, pathlength = 14 μm, CaF_2 plates(experiment A). Integration range 3000-3800 cm^{-1}.

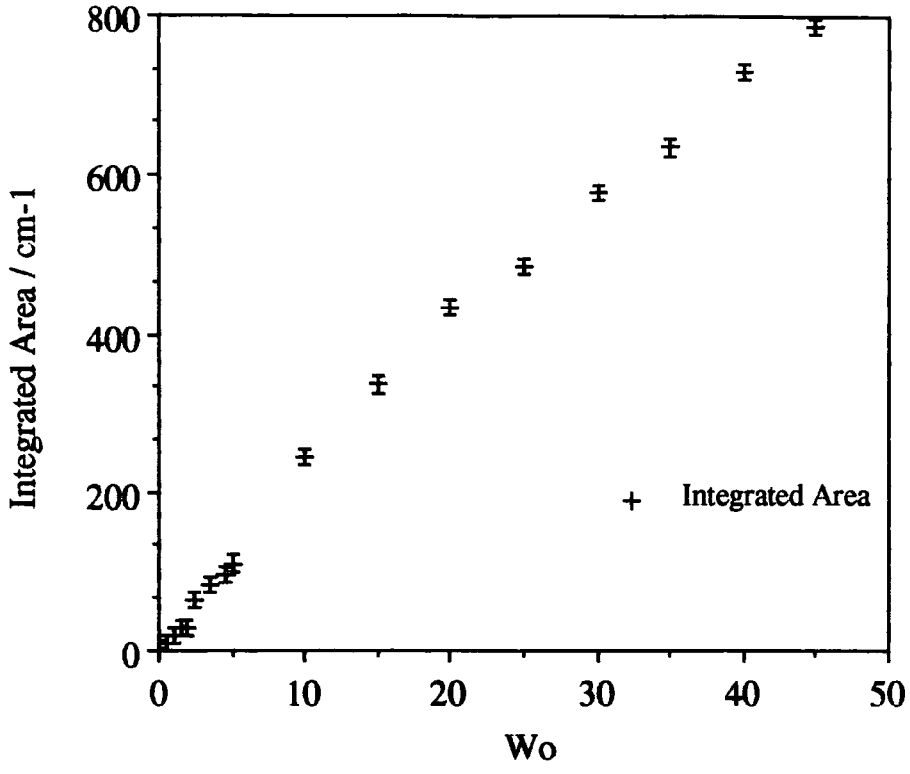

5.1.3 Decoupled ν(OD) stretching vibration

The next band in the spectrum of water to be examined is the ν(OD) stretching band of decoupled water HDO. In water (H_2O + 4%D_2O) at 298 K this band occurs at 2500 cm^{-1}. To observe this band it is first necessary to subtract the spectrum of heptane from that of the microemulsion, as weak overtones of the CH bending modes occur in the region of the ν(OD) band.

So that the band has sufficient intensity to be observed and has a high signal to noise ratio, pathlengths greater than 100 μm were generally used. The temperature of these experiments was accurately controlled to within ±0.5°C so that the band positions were reliable. (See table 4.1)

To observe this band (and the ν_a band) it is necessary to subtract from each microemulsion spectrum the spectrum of the solvent heptane, as various

weak overtone bands mask the true profile of the OD band even though the decoupled OD band is usually thought to be in a transparent region in the spectrum. A subtraction factor of the order of 1.0 is effective in reducing the contribution of weak overtone bands. The spectra are shown in figure 5.4

Figure 5.4 Decoupled ν(OD) vibration in AOT/heptane/D_2O microemulsions as a function of W_o. W_o=1,5,10,15,20. Temperature = 20 °C, pathlength = 521 μm

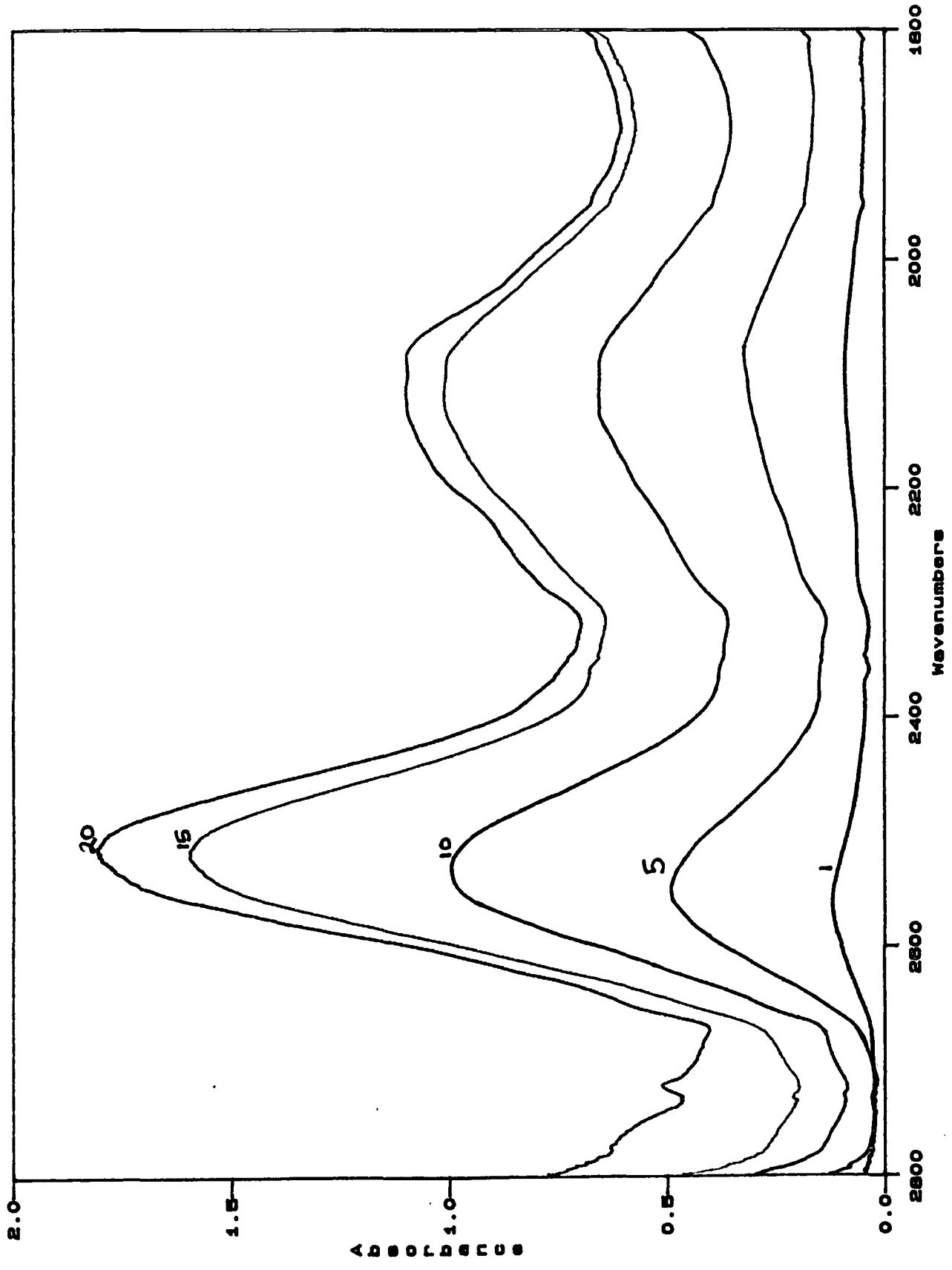

5.1.3.1 Integrated area

The integrated intensity (area) of the decoupled ν(OD) band has been obtained and the data are presented below in table 5.2. The relevant experimental conditions are given in table 4.1.

Table 5.2 Integrated intensities of decoupled ν(OD) band between 2700 and 2300 cm^{-1} after base line correction.

W_0	C	D	E	H	J
0.5					
1	2.4	11.4	1.0		
1.5					
2	3.9		2.4	15.8	
2.5					
3	7.6		3.8		
3.5					
4	11.2		5.5	34.4	
4.5					
5	13.5	70.3	7.4		
6	16.5			56.1	
7			10.3		
8			10.7	75.1	
9			12.0		
10	27.4	132	12.5	95.3	
11			14.9		
12			17.7	113	
13			17.5		
14			17.5		
15	37.7	190	20.7	134	
16			21.6		
20	40.2			185	15.2
25					22.1
30					26.8
35					28.6
40					31.0
45					36.1

The units of the integrated areas are cm^{-1}.

For definitions of the labels C, D, E, H, J see table 4.1

The data given in table 5.2 need to be normalized with respect to the pathlength and the % deuterium enrichment, to make meaningful comparisons. This has been done and the data are given in table 5.3

Table 5.3 Integrated intensities of decoupled ν(OD) band, normalized to pathlengths and normalized to % deuterium enrichment. The factor of 2 in experiment H accounts for the 8% D_2O enrichment in this experiment.

For definitions of the labels C, D, E, H, J see table 4.1

W_o	C 104μm	D 521μm	E 57μm	H* 2×207μm	J 30μm
0.5					
1	23	22	18		
1.5					
2	37		42	38	
2.5					
3	72		67		
3.5					
4	108		97	83	
4.5					
5	129	135	130		
6	158			135	
7			180		
8			192	181	
9			211		
10	264	254	219	230	
11			262		
12			310	272	
13			307		
14			307		
15	362	365	364	323	
16			378		
20	386			446	505
25					737
30					891
35					951
40					1032
45					1203

The data given above in table 5.3 are plotted below (figure 5.5) as a function of W_0 for all the data sets as given. The data are therefore normalized to pathlength and % deuterium enrichment.

Figure 5.5 Integrated area of decoupled ν(OD) band as a function of Wo.

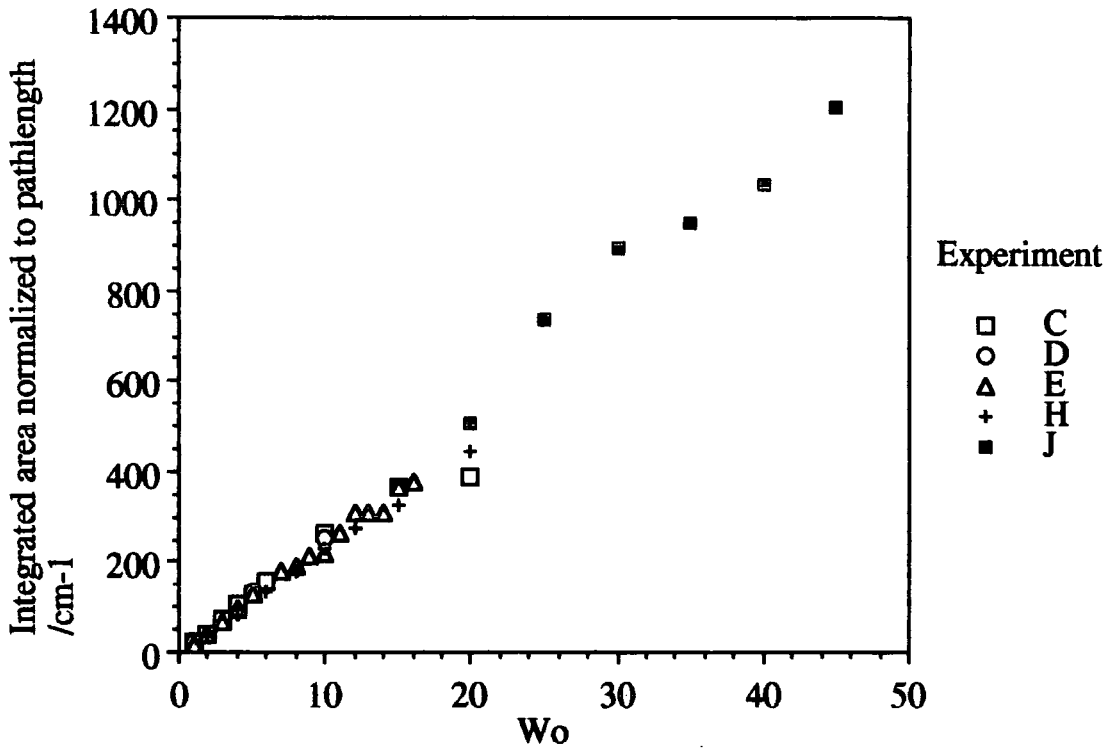

The intensity of this band increases on hydration as would be expected from adding water. A Beer's law plot is valid for this band as there appears to be only one band in this region unlike the coupled ν(OH) stretching band (see 5.1.1).

The plot is probably best described by two straight lines. One from $W_o = 1$ to 10, corresponding to water being taken up by the surfactant head group; the second line for $W_o > 10$ where bulk water starts to appear in the core of the micelle.

5.1.3.2 Frequency maximum

Table 5.4 Frequency position of decoupled ν(OD) band as a function of W_o under the experimental conditions as defined in table 4.1

Wo	C	D	E	H	J
0.5					
1	2570	2568	2565		
1.5					
2	2568		2564	2562	
2.5					
3	2561		2562		
3.5					
4	2557		2554	2557	
4.5					
5	2555	2554	2551		
6	2550			2552	
7			2542		
8			2539	2545	
9			2537		
10	2533	2538	2536	2538	
11			2529		
12			2529	2534	
13			2529		
14			2529		
15	2526	2524	2527	2527	
16			2526		
20	2522	2521		2521	2519
25					2516
30					2512
35					2511
40					2511
45					2510

All the frequencies are in units of cm^{-1} measured to ± 1
For definitions of the labels C, D, E, H, J see table 4.1

The data given in table 5.4 above are plotted here (figure 5.6) as a function of W_o for all the data sets as given. The conditions under which the experiments were carried out are defined in table 4.1.

Figure 5.6 Frequency position of ν(OD) band as a function of W_o

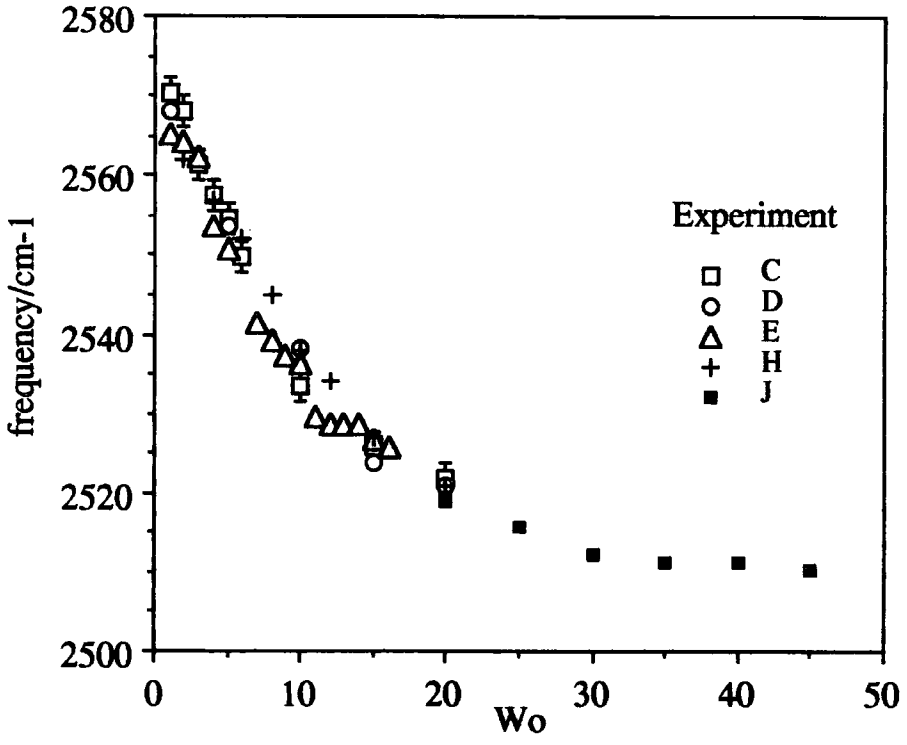

The error in the frequency measurement is ±1 cm^{-1}

The frequency maximum of the ν(OD) band decreases on hydration. This is an indication of the increasing strength of hydrogen bonding between HOD...X, or HDO...Y on adding water.

The actual frequency may represent some average strength as there is a range of environments of water molecules. This will be discussed further in chapter 6.

5.1.3.3 Band Width

The band width of the decoupled ν(OD) band has been measured and the data are presented here in table 5.5. The measurement of the bandwidth is subject to the error of the choice of baseline as discussed above.

Table 5.5 The full width at half height of the decoupled ν(OD) band

Wo	C	D	E	H	J
0.5					
1	136	132	129		
1.5					
2	134		145	152	
2.5					
3	148		149		
3.5					
4	156		156	165	
4.5					
5	162	157	164		
6	162			172	
7			161		
8			163	176	
9			162		
10	165	163	159	179	
11			161		
12			162	182	
13			164		
14			166		
15	161	161	165	179	
16			158		
20	157	155		180	
25					165
30					165
35					164
40					172
45					165

All the widths are in units of cm^{-1} measured to ± 2
For definitions of the labels C, D, E, H, J see table 4.1

The data as given in table 5.5 are plotted below in figure 5.7.

Figure 5.7 The full widths at half height of ν(OD) band as a function of W_o

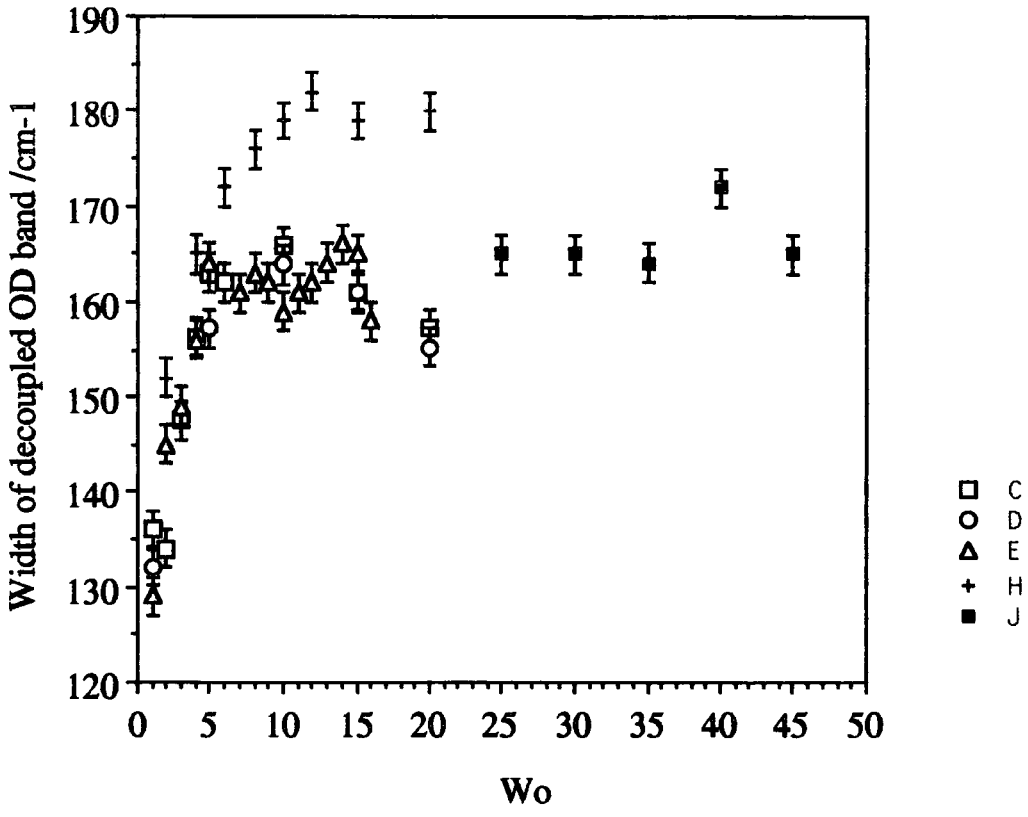

The experimental conditions are defined in table 4.1

The bandwidth of ν(OD) in bulk water is 160±5 cm^{-1} for water[1]. The results presented here show that there is a significant increase in band width on hydration and that a maximum difference of about 50 cm^{-1} in widths is observed. Experiment H does not agree with the other data. This experiment was performed using 8% enriched water as opposed to 4% for all the other experiments. There will therefore be increased coupling of the vibrations which increases the bandwidths. At 8% enrichment of D_2O in H_2O, approximately 1 in 12 water molecules will contain a deuterium atom. If each water molecule is surrounded by 6 other water molecules in the first hydration shell, then there is a high probability of there being another deuterium atom in the second hydration shell.

The width ceases to increase rapidly after about $W_0 = 6$. The bandwidth arises from the distribution in water environments. On adding water, the sulphonate headgroup and sodium counter-ion are the first sites for the water to be bound to. These headgroups are ionic so the interactions with the water will be stronger than subsequent interactions of water with ester groups. On reaching $W_0 = 6$, the head group may well be fully hydrated (See discussion under sulphonate group, chapter 6) and the water molecules are situated in the maximum range of environments. This means that the water is bound to each type of site that exists. The width of the OD band then remains constant within experimental error.

5.1.4 Coupled ν(OD) stretching vibration

The coupled ν(OD) band was also examined in experiment G. The spectra are shown if figure 5.8. The integrated area of the band has been found and the data are presented in table 5.6 and plotted in figure 5.9.

Table 5.6 Integrated band area of coupled ν(OD) stretching band as a function of W_0. Temp = 25°C, pathlength = 114μm,

W_0	Integrated area cm^{-1}
1	6.1
2	18.7
3	29.3
4	39.5
5	50.9
6	64.1
7	73.3
8	84.5
9	97.6
10	108.0
11	123.0
12	135.9
13	144.6
14	155.5
15	171.8
16	175.4
17	186.2
18	204.1
19	207.1
20	225.0

Figure 5.8 Coupled ν(OD) vibration in AOT/heptane/D_2O microemulsion as a function of W_o. W_o = 1...20. Temp = 25°C, pathlength = 114μm, (Experiment G).

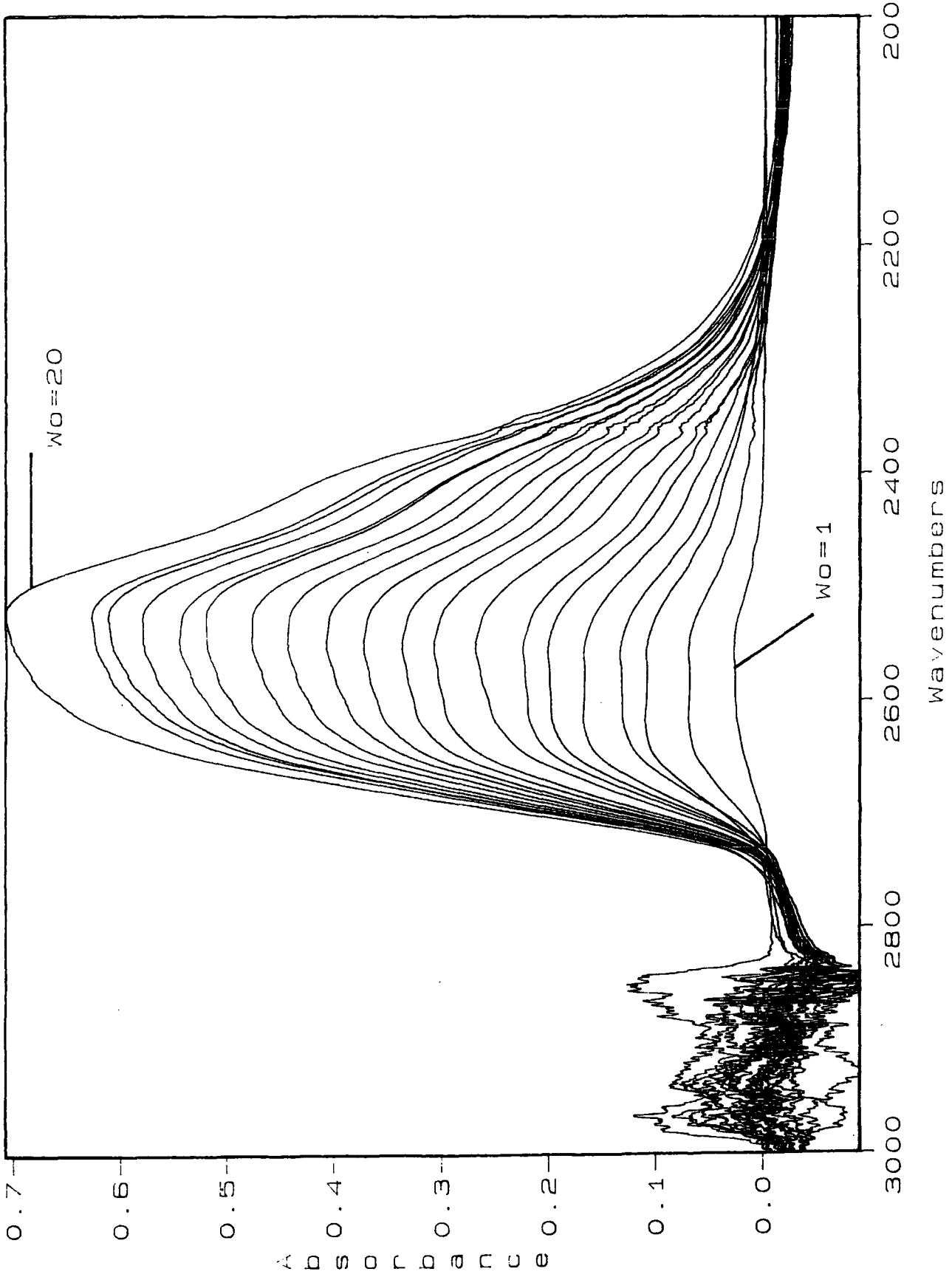

Figure 5.9 Integrated area of coupled OD band, between 2750 and 2190 cm^{-1}

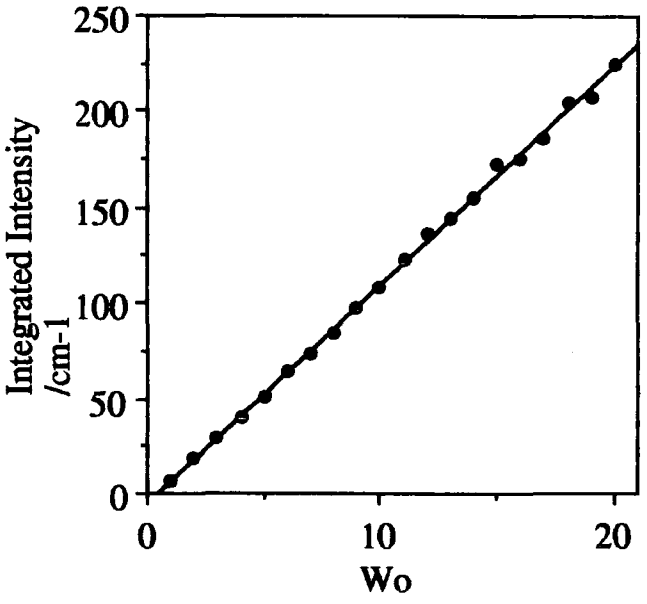

The straight line in figure 5.9 indicates that there is little perturbation of the water as W_O is increases

5.1.5 Water Association band ν_a 2120 cm^{-1}

The next band to be examined is the association band, (figure 5.10) which is a combination band of $\nu_2+\nu_{libration}$ and occurs in the region of 2120 cm^{-1}. Decoupled water complicates the analysis of this band for two reasons. Firstly the OD stretching band overlaps the association band, and secondly the presence of HOD species changes the frequencies of the bands that make up the association band, which therefore leads to a complex envelope of bands in this region.

Figure 5.10 Association band ν_a of H_2O where W_o= 1, 5, 10, 45. These spectra are of reverse micelles containing H_2O only.

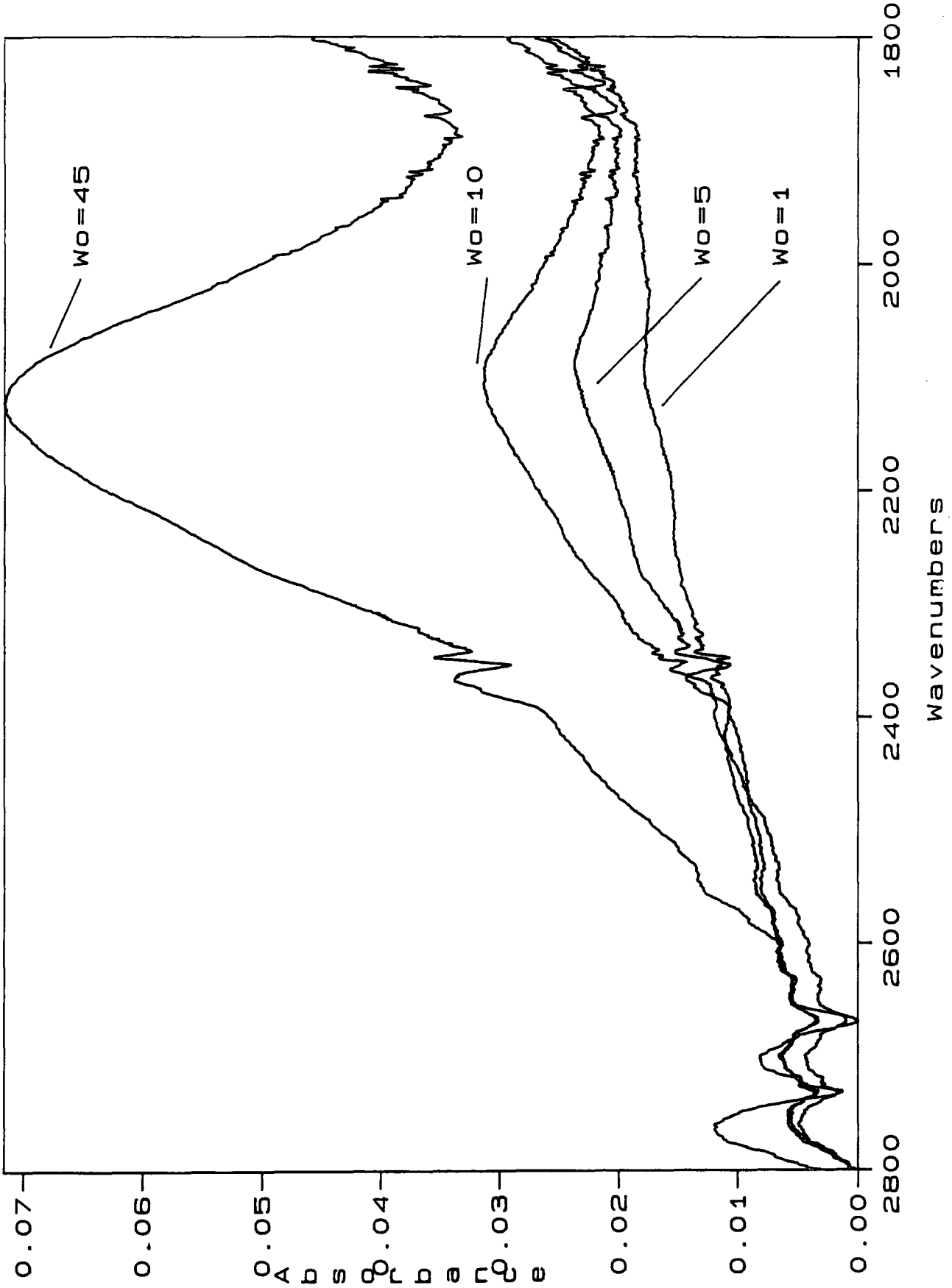

5.2 Surfactant Vibrations

5.2.1 Sulphonate symmetric stretch $\nu(SO_3^-)$

The band at 1051 cm^{-1} has been assigned to the symmetric stretching mode of the sulphonate group[2]. It shows significant changes (Figure 5.11) on hydration in the position of the frequency maximum, and width. A graph of ν_{max} versus W_o clearly shows two steps, one at $W_o = 3$ and another at $W_o = 10$. The validity of these steps is discussed under section 6.1.2

The step at $W_o = 3$ may be explained as the bonding of 3 water molecules to sulphonate which bridge to Na^+; and the step at $W_o = 10$ interpreted as the full hydration of the head group and counter ion. The sodium ions will bind to six water molecules in total[3]. On further hydration the sulphonate group might no longer necessarily bridge to sodium ions so the second step is observed.

Figure 5.11 showing position of symmetric sulphonate stretch as a function of W_o

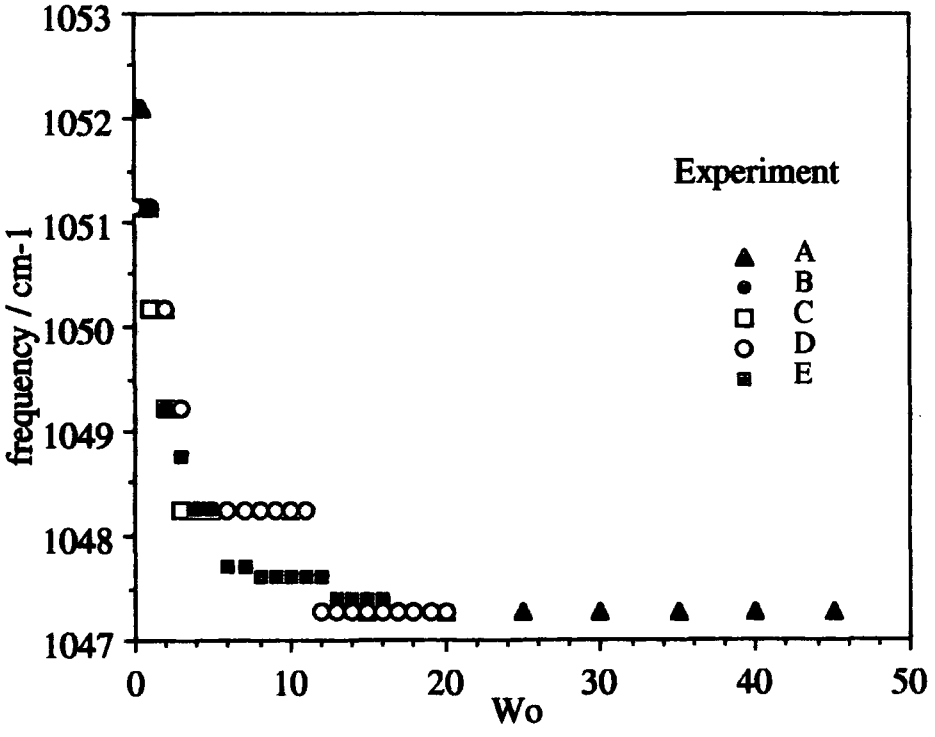

The accuracy with which the frequencies are measured is ±1 cm^{-1}.

5.2.1.1 Frequency

The frequency position of the symmetric sulphonate stretch has been measured from the spectra and the data are presented here in table 5.7.

Table 5.7 Frequency position /cm^{-1} of symmetric sulphonate stretching band as a function of W_0. See table 4.1 for definitions of A,G,E,G.

W_0	A	B	E	G
0	1052	1052	1051	1052
0.5	1052	1051		
1	1051	1051	1051	1051
1.5	1050	1050		
2	1050	1049	1050	1049
2.5	1049	1049		
3	1048	1049	1049	1048
3.5	1048	1048		
4	1048	1048	1048	1048
4.5	1048	1048		
5	1048	1047	1048	1048
6			1048	1047
7			1048	1047
8			1048	1047
9			1048	1047
10	1048		1048	1047
11			1048	1047
12			1047	1047
13			1047	1047
14			1047	1047
15	1047		1047	1047
16			1047	1047
17			1047	
18			1047	
19			1047	
20	1047		1047	
25	1047			
30	1047			
35	1047			
40	1047			
45	1047			

5.2.1.2 Band Width

The band width of the symmetric sulphonate stretch has been determined for experiments and the data are presented in table 5.8 and plotted in figure 5.12.

Table 5.8 Full width at half height of symmetric sulphonate stretching band as a function of W_0. For experimental conditions A,G,J see table 4.1

W_0	A	G	J
0	18	18	
0.5	18		
1	19	18	
1.5	18		
2	18	17	
2.5	16		
3	16	16	
3.5	16		
4	15	15	
4.5	16		
5	15	15	
6		14	
7		14	
8		15	
9		15	
10	14	14	
11		14	
12		14	
13		14	
14		14	
15	14	14	
16		14	
17		14	
18		14	
19		14	
20	14	14	13
25	13		13
30	13		13
35	13		13
40	13		13
45	13		13

Figure 5.12 showing full width at half height of symmetric sulphonate stretching band as a function of W_o

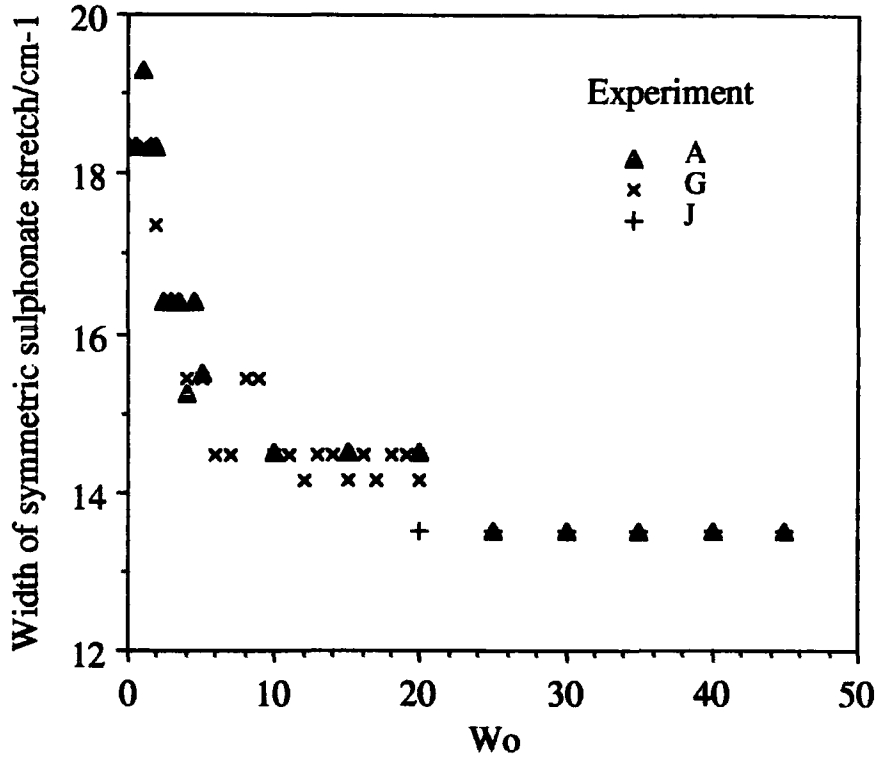

The width is subject to larger error than the frequency position measurement because the baseline is less well defined at the lower frequencies as the salt plates are beginning to absorb radiation . Nevertheless, the three sets of data shows that the bandwidth decreases as a function of W_o.

5.2.2 Carbonyl stretching band ν(CO)

The analysis of the carbonyl band requires a set of data which has been obtained using D_2O only for hydrating the system (experiment G). This is necessary as the broad ν_2 bending mode of H_2O at 1650 cm^{-1} (FWHH≈80 cm^{-1}), overlaps the carbonyl stretching mode (see figure 5.13). On hydration, the lower frequency band at 1722 cm^{-1} increases in intensity. The data set which has been obtained with D_2O alone is discussed in chapter 6.

Figure 5.13 ν(CO) vibration and $\delta(H_2O)$ at $W_o = 0, 3, 15, 45$. The water used is 4% D_2O in H_2O, and shows the overlap between the ν(CO) and $\delta(H_2O)$ vibrations. Experiment (A) ambient temperature, pathlength 14μm

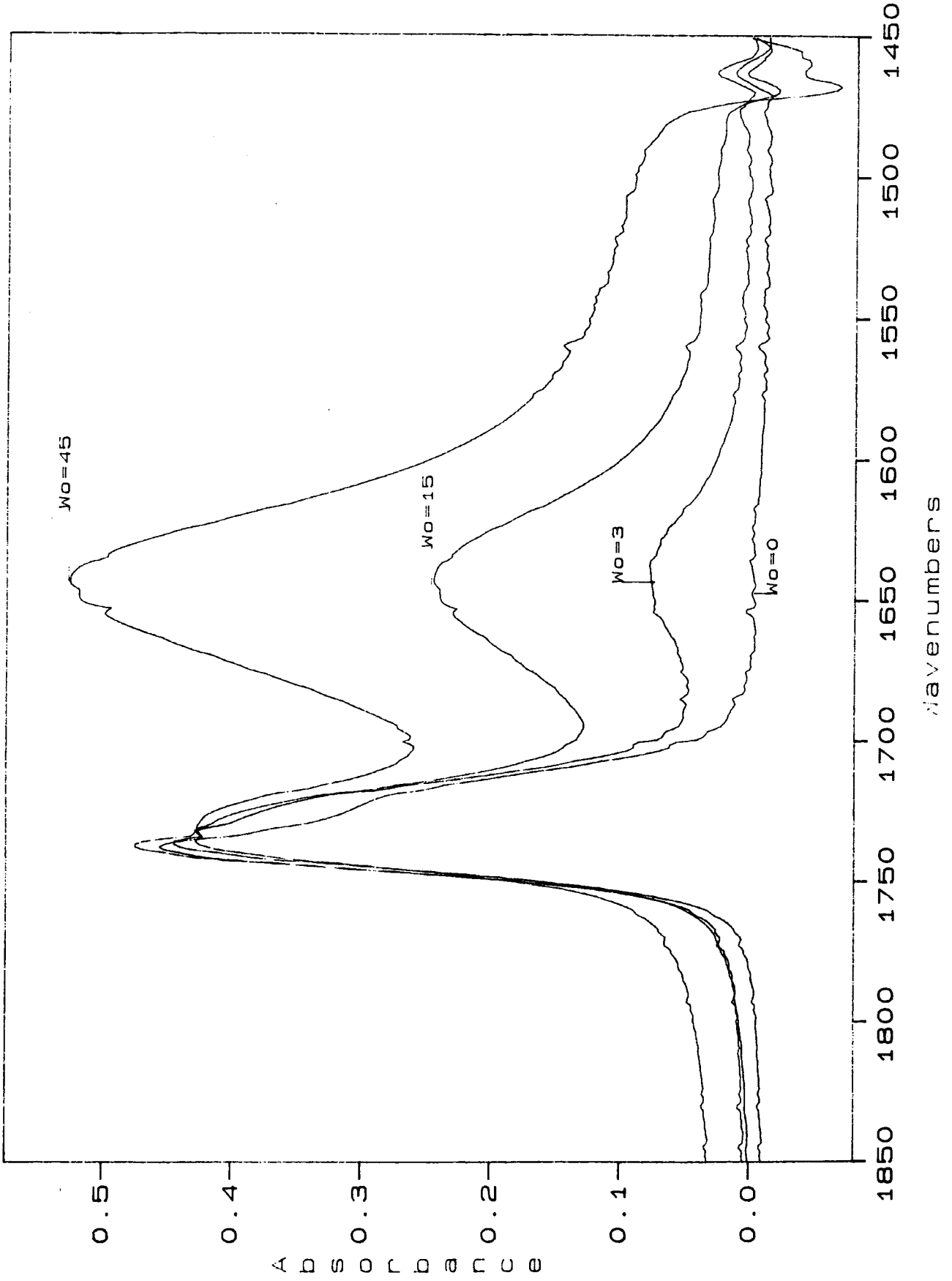

5.2.3 CH stretching vibrations

The spectra of pure heptane and AOT in heptane differ very little in this region. The bands have been assigned as follows:

ν cm^{-1}	ν cm^{-1}	assignment[4]
2958	$\nu_{as}(CH_3)$	antisymmetric methyl stretch
2926	$\nu_{as}(CH_2)$	antisymmetric methylene stretch
2873	$\nu_S(CH_3)$	symmetric methyl stretch
2859	$\nu_S(CH_2)$	symmetric methylene stretch

5.2.3.1 $\nu_{as}(CH_3)$

In the stock solution ($W_o = 0$) this band resembles that of pure heptane. So does the band for $W_o = 1$. On hydration the band gradually becomes narrower by 4 cm^{-1} with $W_o = 45$.

5.2.3.2 $\nu_{as}(CH_2)$

This follows a similar trend to the $\nu_{as}(CH_3)$ band, becoming narrower by 6 cm^{-1} at $W_o = 45$.

No narrowing is observed with either of the symmetric stretching bands. Narrowing of the bands is interpreted as a narrowing in the distribution of different types of CH environments, that is the system becomes somewhat more ordered on hydration.

There is possibly a weak shoulder at 2900 cm^{-1} which corresponds to a tertiary CH stretching vibration.

No frequency shifts were observed in this region (spectrometer resolution = 2 cm^{-1}).

5.2.4 CH bending mode

No changes in the CH bending modes of AOT were observed on hydration. The bands resemble those of pure heptane so it would seem that the surfactant hydrocarbon chains remain liquid like. This is in accordance with the observations of Casal[5].

5.3 References

(1) Eisenberg D., Kauzmann W. *The Structure and Properties of Water*; OUP: Oxford, **1969**.
(2) MacDonald H., Bedwell B., Gulari E. *Langmuir* **1986**, *2*, 704.
(3) Hauser H., Haering G., Pande A., Luisi P. L. *J. Phys. Chem.* **1989**, *93*, 7869.
(4) Silverstein R. M., Bassler G. C., Morril T. C. *Spectrometric identification of organic compounds;* 4th ed.; Wiley: New York, **1981**.
(5) Casal H. L. *J. Am. Chem. Soc.* **1988**, *110*, 5203.

CHAPTER 6

AOT DISCUSSION

6. Detailed examination of spectral behaviour as a function of Wo

In this chapter each band in the infrared spectrum of the AOT/ water/ heptane system as a function of W_o will be examined in turn.

6.1. Decoupled OD vibration.

As was discussed in chapter 2, the HDO molecule is a most useful molecule to study the mid-infrared spectra of systems containing water for the following reasons:

(1) Weak coupling of the vibrations $\nu_1+\nu_3$ owing to the difference in frequency. Simpler band shapes therefore result

(2) Non-degeneracy of the energy levels means that Fermi resonance of $\nu_1+2\nu_2$ cannot occur.

(3) The frequency position of the ν(OD) vibration of HDO in H_2O is in a region where there are few other bands.

(4) The mole fraction of HDO can never exceed 0.5. This decreases the possibility of intermolecular coupling of ν(OD) vibrations.

A further complication is that in the isotopically pure species (H_2O or D_2O), the two OH (or OD) bonds are not necessarily identical due to structural disorder. In this case the ν_3 vibration is not totally antisymmetric and can therefore undergo Fermi resonance with $2\nu_2$.

6.1.1.Band Width

The band width of ν(OD) in H_2O enriched with a few percent D_2O is 160 ±5 cm^{-1} at 25 °C[1]. This is the band width in water only. The band width in the AOT /water /heptane system depends on W_o (Figure 5.7). The figure reveals that for very small values of W_o ($W_o \leq 6$) the width of ν(OD) is greatly reduced compared with bulk water. At $W_o=1$ the band width is 130±4 cm^{-1}, which indicates a significant perturbation of the water. Therefore these first 6 water molecules are in an environment that is very different from bulk water.

These first six water molecules are bonded to the sodium and sulphonate group ions (see sections 6.4 and 6.5). The origin of the band widths in decoupled water is the structural disorder of the liquid[1]. Structural disorder leads to a range of distances and hence a range of intermolecular potentials. These potentials will have various energies so a range of frequencies will exist. In the AOT system where there is a small amount of water ($W_O \leq 6$) then these water molecules are in a well defined environment around the headgroup ions. Consequently the potential is more similar for each of these first 6 water molecules than for those in bulk water. This leads to a well defined frequency and a narrow band at low W_O.

As W_O increases, then the water not only binds to the sodium and sulphonate ions, but is also expected to bond to the carbonyl and ester groups (see section 6.6). When sufficient water has been added to hydrate the ionic parts of the headgroup, the ν(OD) band width increases, thereby indicating the presence of bulk water. This is inferred from the band width, which reaches the bulk water value of 160 cm^{-1} when $W_O > 6$. This will be further discussed when the behaviour of the sodium counter-ion is considered (see below).

6.1.2. Frequency

To a first approximation the position of an infrared absorption band depends on the force constant for the bond of the atoms involved. This in turn depends on the bond strength. Hydrogen bonding by one species to an OH (or OD) group reduces the electron density in the OH bond, thereby decreasing the frequency of the vibration. Figure 5.6 (the graph of position of ν(OD) versus W_O) therefore shows that hydrogen bonding increases as W_O increases. The actual behaviour of the band position may be interpreted in more than one way. Either a distribution of water environments exists, each being slightly different, thus leading to a gradual change of frequency as the system is hydrated; or the observed position of ν(OD) is the weighted average of the frequency position of

the bound water and the frequency position of the bulk water. These two approaches are the well known continuum and mixture models for water[1].

A quantitative analysis of the frequency position based on the two site model is presented in chapter 7.

6.1.3. Integrated Intensity

The integrated intensity of the ν(OD) band shows a linear increase with respect to W_o (figure 6.1).

Figure 6.1 Average of integrated area of decoupled ν(OD) at each W_o value band versus Wo

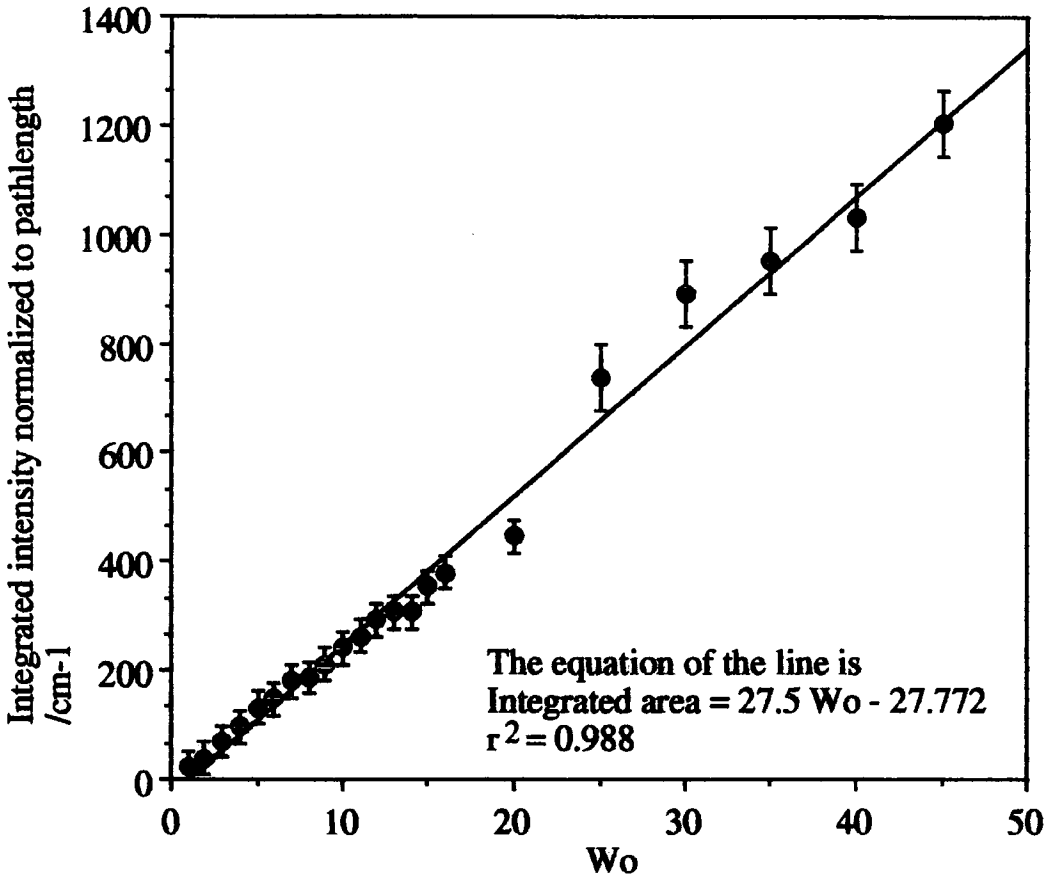

The above figure 6.1 is similar to 5.3 except that the data have been averaged at each W_o value and a linear least-squares fit to the data is shown.

The apparent linear behaviour of the integrated area of the ν(OD) with respect to W_o might initially suggest that the behaviour of the water is unchanged as W_o increases; i.e. that the water is unperturbed. However the band width changes as W_o increases, and the band width is a contributing factor to the

integrated intensity. For a purely Gaussian or Lorentzian band the integrated intensity is proportional to the product of the band width and the height (the absorbance). Therefore it is possible to predict the shape of the graph of integrated intensity by multiplying the band width by the absorbance. When this is done, a graph with two straight lines is predicted as shown schematically in figure 6.2.

Figure 6.2 Schematic prediction of the form of the integrated intensity.

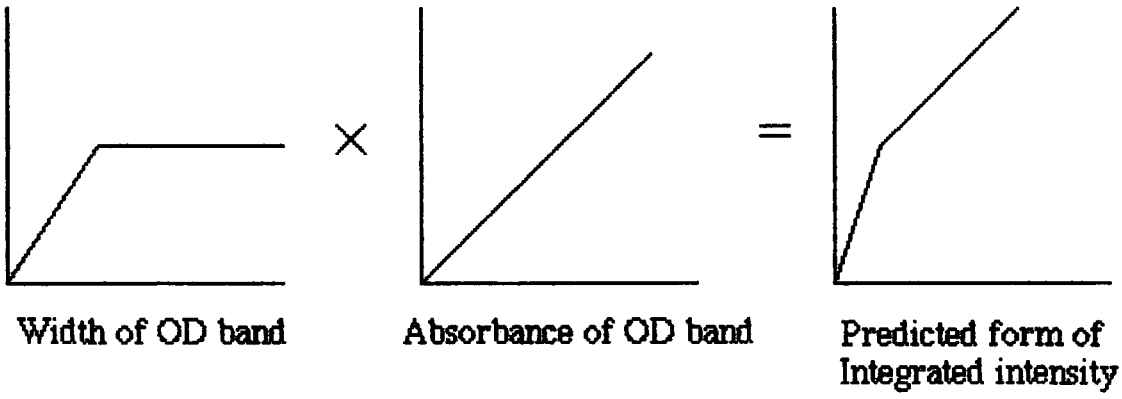

The predicted form of the integrated intensity (figure 6.2) is not actually observed (figure 6.1). The reasons for this could be :

1) Experimental error. The random error in the measurement is likely to be small as the experiment was performed several times (see table 4.1)
2) The water is perturbed up to $W_0 = 6$. Effectively the extinction coefficient of the water when $W_0<6$ is different from that of water present when $W_0>6$. The band width of ν(OD) shows a break in the behaviour of the water at $W_0 = 6$, and is discussed later in this chapter.

It is unlikely that there is such a distinct change in the extinction coefficient at exactly $W_0 = 6$. Instead the extinction coefficient is more likely to vary gradually across the W_0 range. This would lead to the graph as shown in figure 6.1. It is known that the bandwidth, and hence the vibrational relaxation rate change when $W_0 <6$. It is therefore quite likely that the extinction coefficient

will be different at low values of W_0 from its value at high W_0. This is important when trying to describe the behaviour of the coupled spectra of water.

6.2. Coupled vibrations - separation into component bands

In principle, those changes observed in the behaviour of the decoupled ν(OD) band should be reflected in changes seen in the OH band. However the analysis of the ν(OH) absorption band is complicated by vibrational coupling and Fermi resonance as mentioned in chapter 2. It is of course possible to use water that contains a few percent H_2O in D_2O to make the AOT reversed micelles. This would allow the decoupled ν(OH) band to be analysed. However when this was attempted, problems with the water vapour within the spectrometer and ice collecting on the liquid nitrogen cooled detector were experienced, and could not be entirely removed by purging with dry nitrogen gas. Hence the coupled band of ν(OH), which does not suffer from the same experimental problems due to its high intensity, will be examined.

Examination of the coupled ν(OH) band in pure water[1] suggests that if the separate bands can be resolved, then at least three bands are present in the band profile. The question remains as to what these separate bands may be attributed.

In the AOT/water/oil system the band shape of the coupled ν(OH) band has been examined by MacDonald[2] and Jain[3]. Their analyses are based on the premise that each band in the profile of the ν(OH) absorption arises from a separate water species; i.e. a water molecule in a particular environment either free, or bound to an ion or polar group. If separate absorption bands can be resolved, then it follows that the amount of bound water or free water may be calculated. However in this work, examination of the decoupled ν(OD) vibration shows only one band in the spectrum at all W_0 values. This means that the analysis of the coupled bands by MacDonald[2] and Jain[3] is erroneous in attributing the separate bands to identifiable water species.

However, there is no reason why the spectrum, which obviously comprises more than one band, should not be deconvoluted in order to find out how each

component contributes to the total spectrum. The coupled ν(OH) and coupled ν(OD) spectra will now be examined. The results will be compared with the decoupled (OD) spectra to show why separate bands arise in the spectrum.

Procedure for the deconvolution of coupled bands of ν(OH)

It is first necessary to deconvolute the bands. This has been done with the software 'Curvefit' within the data analysis package as supplied by Mattson Instruments. It works in the following way:

1) An initial estimate of the band parameters is supplied. The frequency position, full width at half height (FWHH) and absorbance is defined for each separate band in the profile.
2) The band shape is defined as either Gaussian, Lorentzian or some linear combination of the two. The bands were best described using the Gaussian band shape.

This does not necessarily indicate that the bands are genuinely Gaussian in shape. A Lorentzian band has significant intensity at a position of 5×FWHH from the band centre, whereas at the same position the intensity of a Gaussian band is negligible. In order to analyse the coupled ν(OH) band it is necessary to perform a base-line correction on some spectra. This inevitably results in a cut-off in intensity so the band loses its Lorentzian character. Hence Gaussian bands better describe the spectrum.

3) The band parameters are optimised by trial and error. Using a χ^2 distribution to minimise the error between the calculated band profile and the spectrum tended to produce erratic results, if the trial estimate were not sufficiently precise. This was a limitation of the computer software available.

According to the literature[2,3], three bands are necessary to describe the band profile of the coupled ν(OH) vibration in AOT microemulsion. The frequencies and widths of these band were used as initial estimates in fitting to the data obtained in this work.

Table 6.1 showing band parameters of coupled ν(OH) band in AOT/water/oil systems

Data from reference[3]. All numbers are in cm^{-1}	
Frequency position	FWHH
3610	90
3490	180
3290	240

Table 6.2 showing band parameters of coupled ν(OH) band in AOT/water/oil systems as found in this work

Band parameters obtained in this work	
Frequency position	FWHH
3608	107
3491	186
3334	187
3083	233

As can be seen from the tables 6.1 and 6.2, it was necessary to use four bands in order to describe the spectra completely. However the fourth band (see table 6.3) is of very low intensity and has a very large FWHH. This fourth band is most likely to arise from the Lorentzian character of the other bands in the spectrum.

When analysing the computer-fitted absorption bands it was found that the positions and widths of the bands did not vary with W_o. Only the absorbance values varied, as shown in table 6.3. This illustrates the problem of finding multiple solutions in the curve fitting procedure, as the analysis of the decoupled ν(OD) vibration showed that the position and width do vary as a function of W_o.

The absorption band at 3083 cm^{-1} is very low in intensity. It is usually an order of magnitude lower in intensity than the other bands, and on this basis alone it may be neglected from the analysis. In addition the frequency of this band 3083 cm^{-1} is very low for an OH vibration and is not easily assigned.

Table 6.3 showing absorbance values of ν(OH) bands (Conditions as in Experiment A table 4.1)

W_o	Absorption of band at 3608 cm^{-1} width 107 cm^{-1}	Absorption of band at 3491 cm^{-1} width 186 cm^{-1}	Absorption of band at 3334 cm^{-1} width 287 cm^{-1}	Absorption of band at 3083 cm^{-1} width 233 cm^{-1}
0.5	0.013	0.045	0.011	0.001
1	0.022	0.086	0.030	0.003
1.5	0.038	0.116	0.038	0.001
2	0.038	0.116	0.038	0.001
2.5	0.061	0.186	0.092	0.013
3	0.066	0.197	0.090	0.003
3.5	0.077	0.228	0.120	0.008
4	0.081	0.232	0.122	0.006
4.5	0.086	0.251	0.140	0.009
5	0.093	0.278	0.172	0.017
10	0.153	0.481	0.425	0.047
15	0.183	0.575	0.627	0.059
20	0.225	0.678	0.825	0.078
25	0.251	0.725	0.950	0.094
30	0.330	0.861	1.266	0.145
35	0.325	0.846	1.321	0.153
40	0.372	0.878	1.580	0.187
45	0.396	0.861	1.688	0.162

The next four pages show exampled of the spectra of coupled ν(OH) vibrations together with the components that make up the synthetic spectra.

Figure 6.3 Coupled ν(OH) vibration at W_0 = 2, 15, 40. The bands are superimposed to have the same height, thus showing the shapes more effectively.

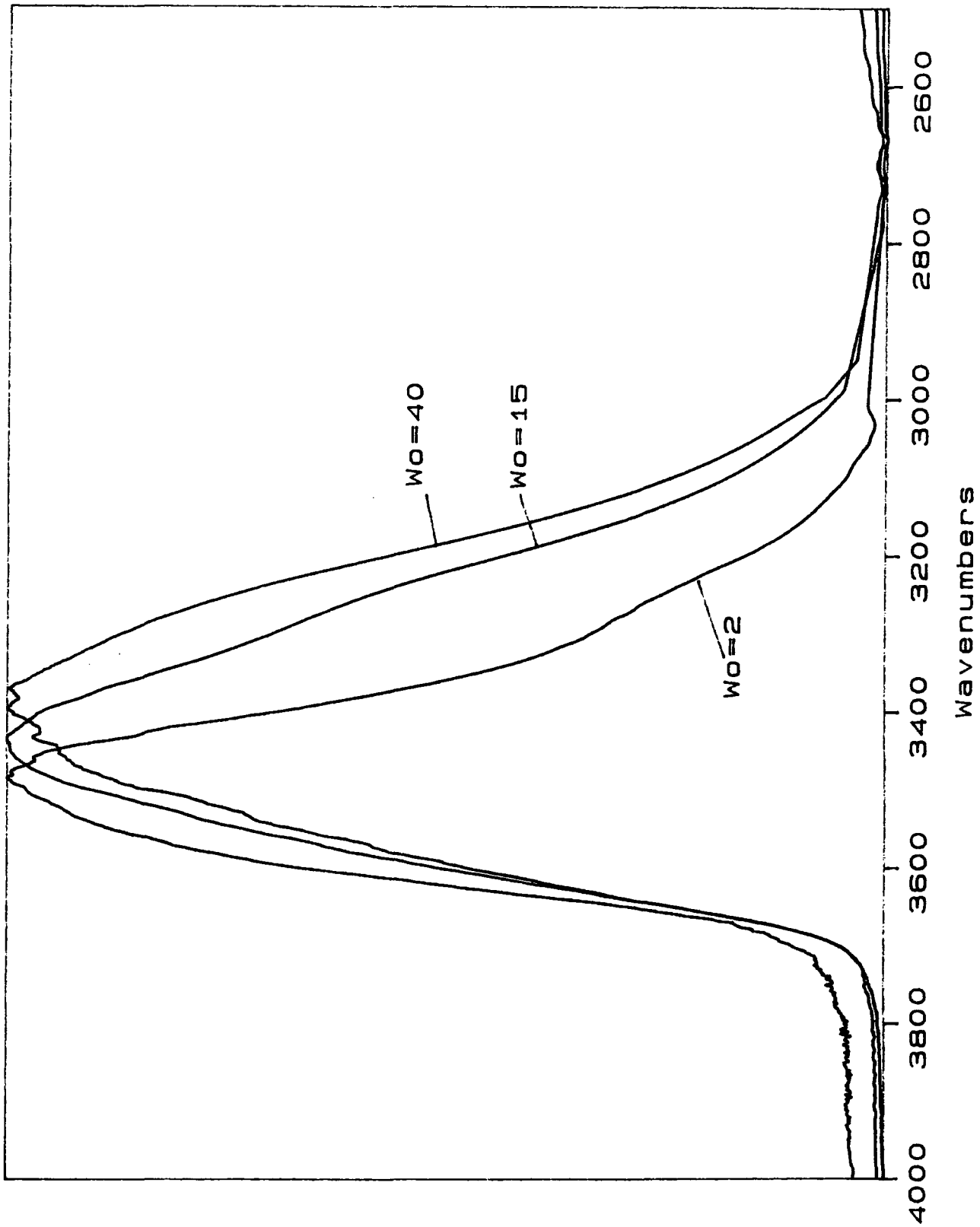

Figure 6.4 Coupled ν(OH) vibration in AOT/heptane/H_2O microemulsions where $W_0 = 2$ (solid line). The synthetic spectrum and its components are shown with dotted lines. The difference between the experimental and the synthetic spectra is also shown.

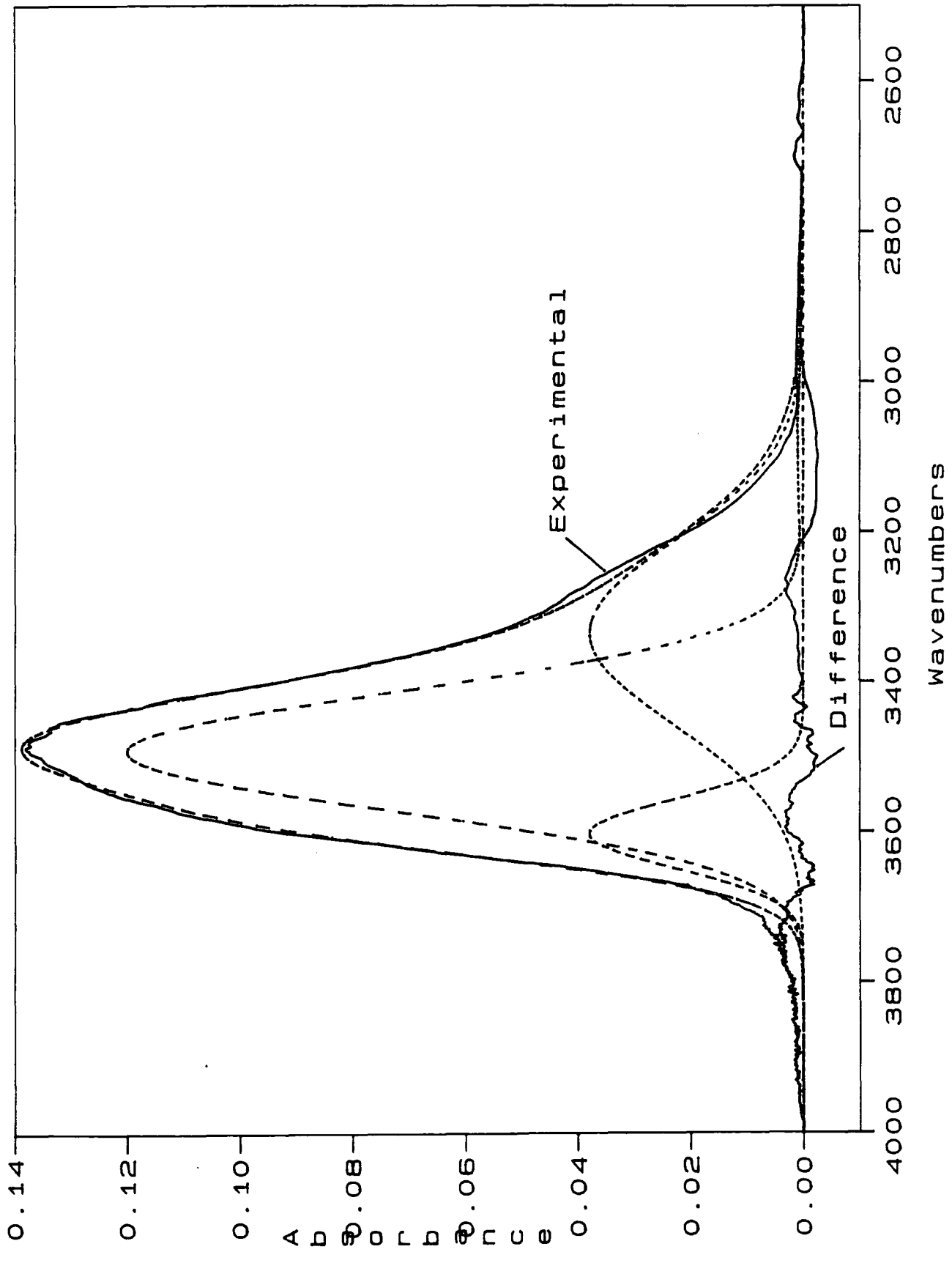

Figure 6.5 Coupled ν(OH) vibration in AOT/heptane/H_2O microemulsions where $W_o = 15$ (solid line). The synthetic spectrum and its components are shown with dotted lines. The difference between the experimental and the synthetic spectra is also shown.

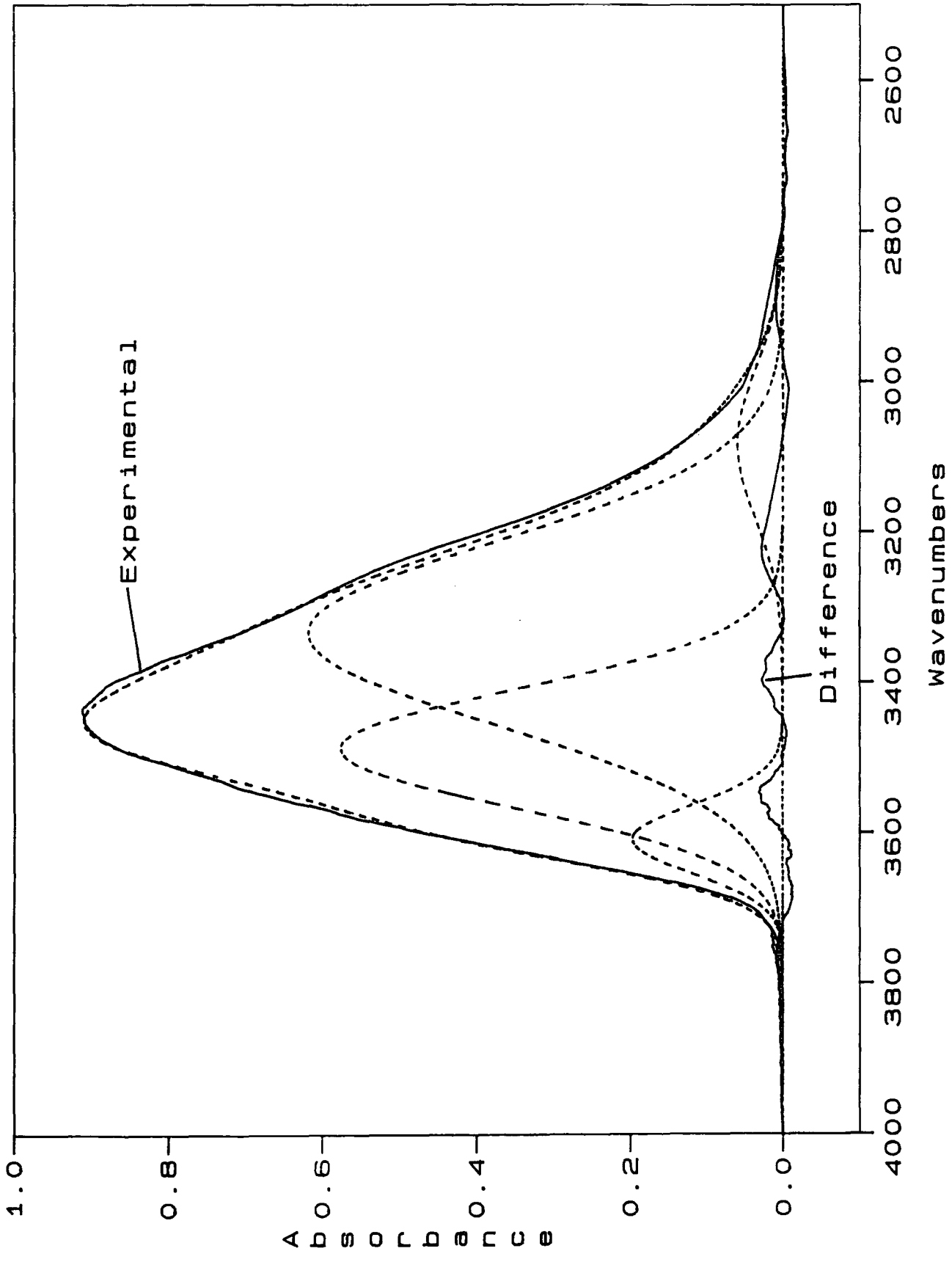

Figure 6.6 Coupled ν(OH) vibration in AOT/heptane/H_2O microemulsions where $W_0 = 45$ (solid line). The synthetic spectrum and its components are shown with dotted lines. The difference between the experimental and the synthetic spectra is also shown.

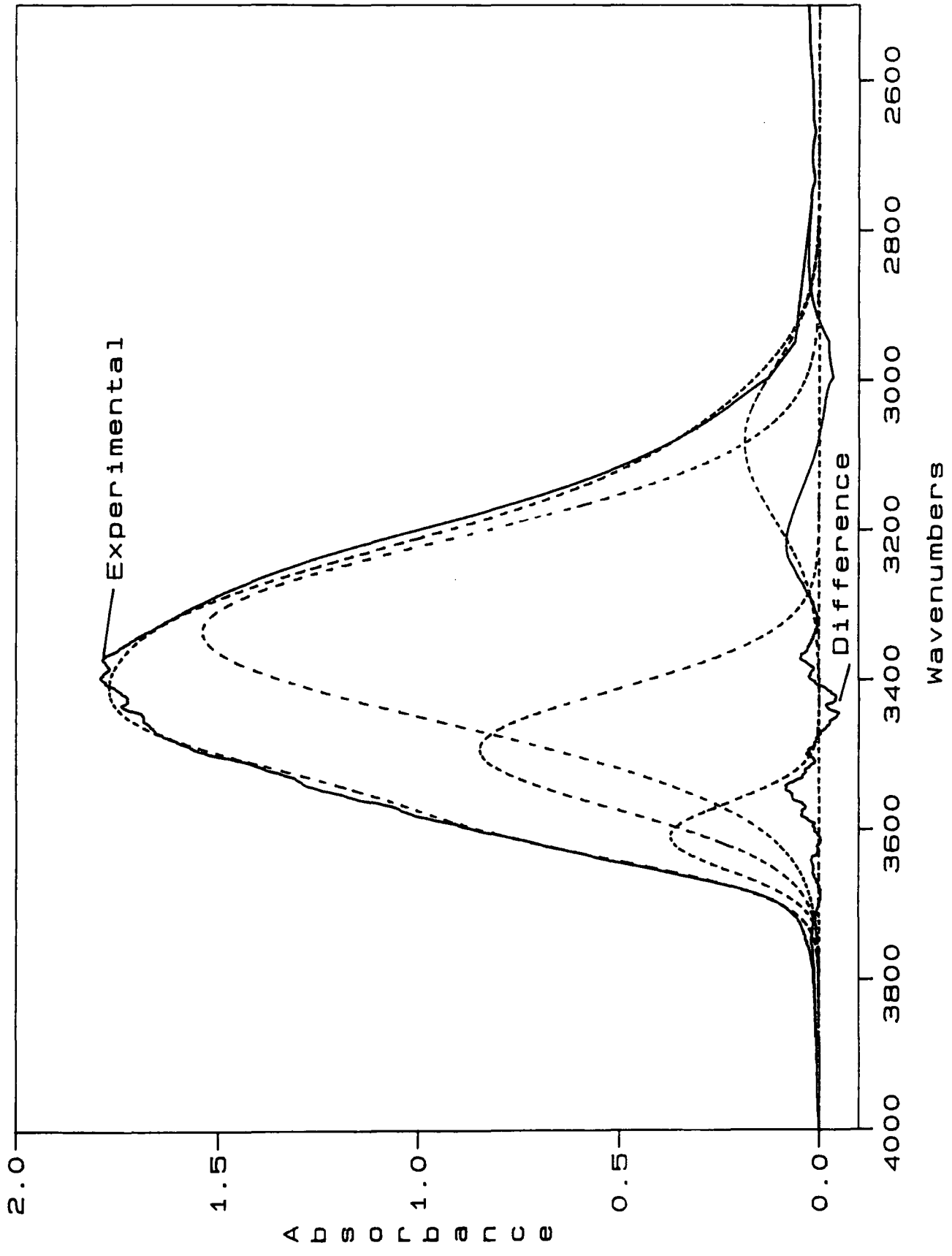

The integrated area of the ν(OH) vibration increases with W_o (figure 5.3), as expected due to the increasing quantity of water present. The absorbance of each band will contribute to the overall integrated area for the ν(OH) vibration (It is at this point that Jain *et al* [3] assign each band to a separate water species.).

To investigate the spectra further, some nomenclature will be defined: Let the integrated area of the ν(OH) absorption band be A_o (at some value of W_o). Let the three component bands at 3334, 3491 and 3608 cm^{-1} be denoted by the subscripts b, r and i respectively. (These letters were chosen so as to conform to the assignment of Jain *et al* [3] in that b refers to bulk water, r refers to restricted water and i refers to interfacial water. Although it must be remembered that no significance is being attached to this nomenclature)

The areas of each separate band are thus A_b,A_r,A_i. It follows that $A_o = A_b+A_r+A_i$. The plot of A_o versus W_o will be identical to figure 5.3 in the previous chapter. When the separate components of A_o are plotted as a function of W_o, then figure 6.7 is obtained.

Figure 6.7 Integrated Intensity for each peak in the ν(OH) band profile.

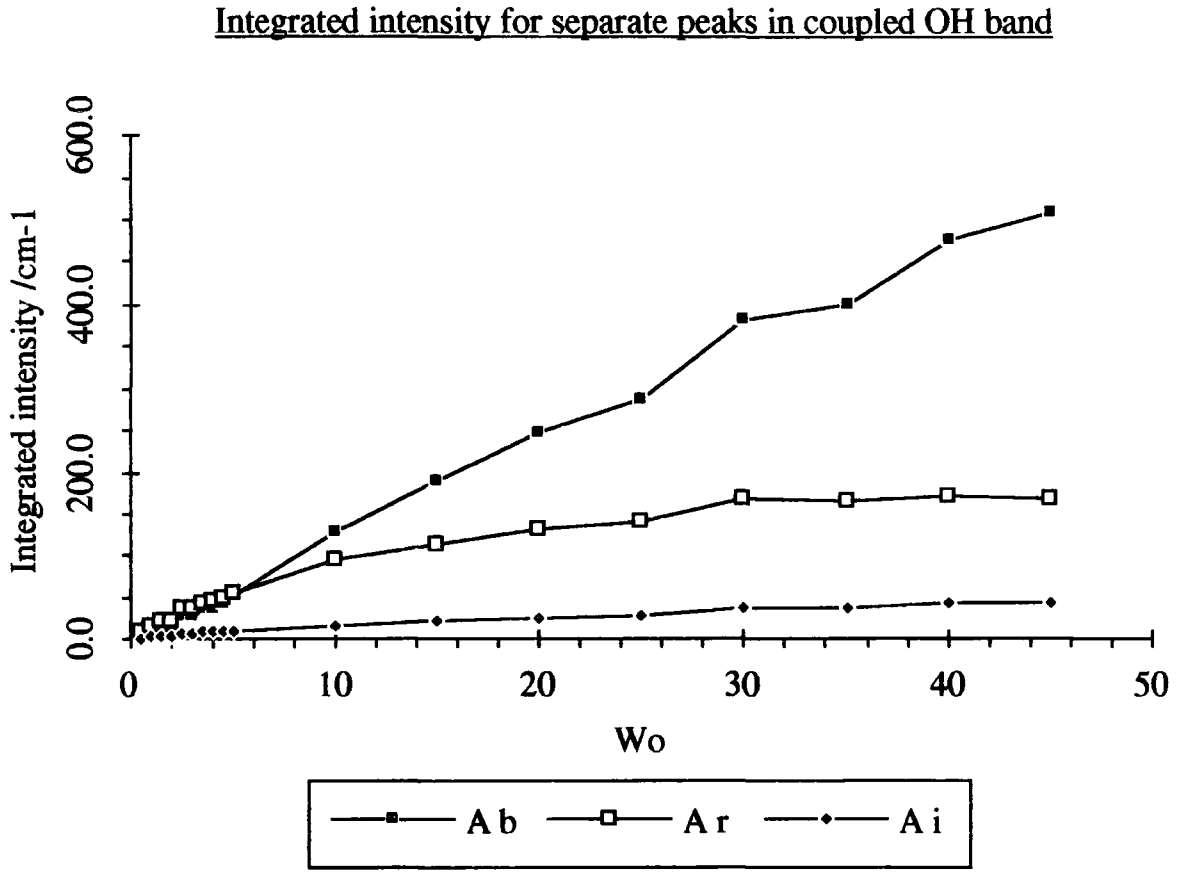

(The lines serve as a guide to the eye).

This graph shows how the intensity of the three separate component bands of the spectrum of water change as a function of W_o. To consider this relationship further, the fractions that each component contributes to the total may be calculated.

The fractions that each band component contributes to the total intensity are:

$$p_b = \frac{A_b}{A_o} \qquad p_r = \frac{A_r}{A_o} \qquad p_i = \frac{A_i}{A_o}$$

Table 6.4 Fractions of the 3 component bands in the coupled ν(OH) spectrum.

Wo	p_b band at 3334 cm^{-1}	p_r band at 3491 cm^{-1}	p_i band at 3608 cm^{-1}
0.5	0.244	0.648	0.108
1.0	0.319	0.593	0.087
1.5	0.298	0.590	0.111
2.0	0.298	0.590	0.111
2.5	0.391	0.512	0.097
3.0	0.371	0.527	0.102
3.5	0.405	0.498	0.097
4.0	0.403	0.497	0.100
4.5	0.418	0.486	0.096
5.0	0.445	0.466	0.090
10	0.535	0.393	0.072
15	0.587	0.349	0.064
20	0.612	0.326	0.062
25	0.628	0.310	0.062
30	0.650	0.287	0.063
35	0.664	0.275	0.061
40	0.691	0.249	0.061
45	0.705	0.233	0.062

Figure 6.8 shows how the fractions of each component band vary as a function of W_o

Figure 6.8 Fractions of the component bands the coupled ν(OH) spectrum that contribute to the whole spectrum.

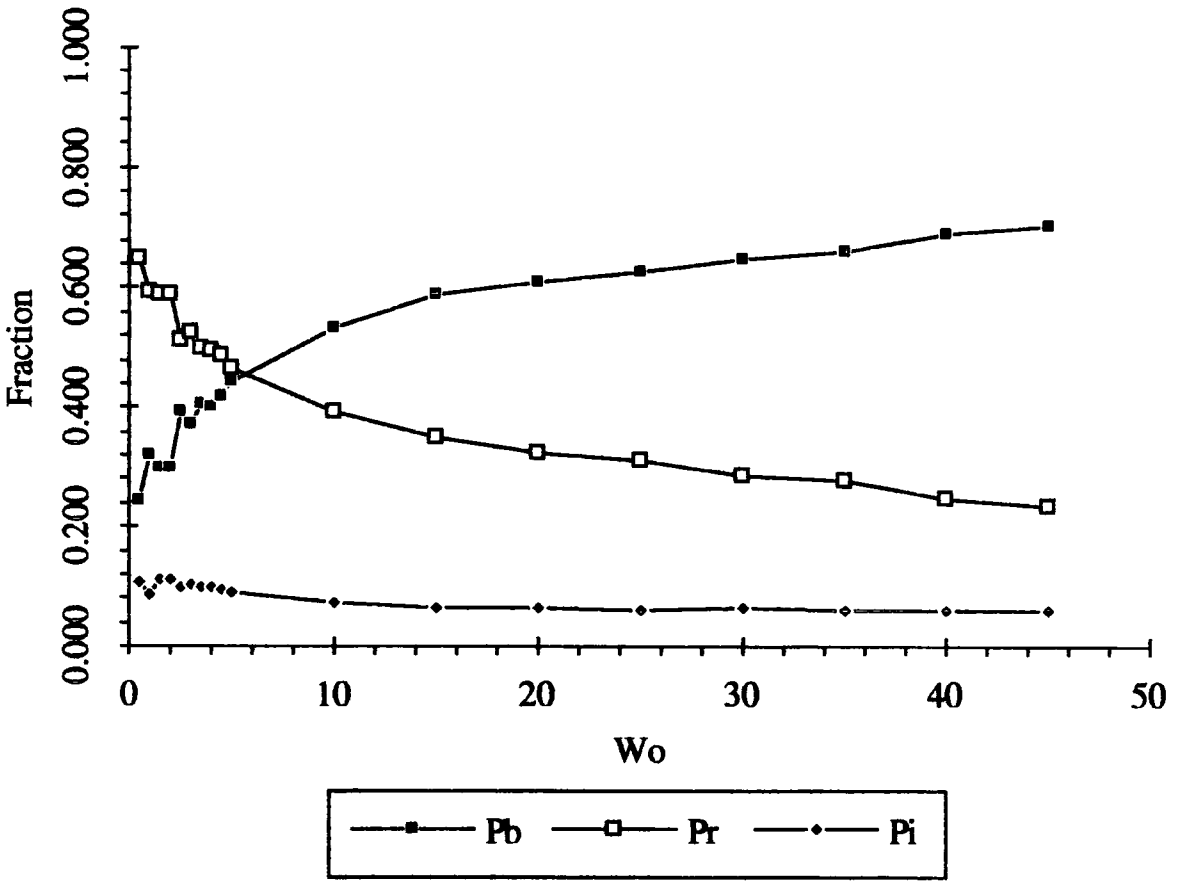

It can be seen from the graph that p_i (the highest frequency component) remains low between 0.06 and 0.1 across the whole of the W_o range. At low values of W_o the value of p_r is high, but decreases as more water is added. The point where p_b becomes greater than p_r appears to be at $W_o = 6$. This is also the same W_o value at which the band width of the decoupled ν(OD) band indicates the existence of bulk water, i.e. there is a distinct change in the spectrum of the water. This is most likely due to changes in the water molecule environments that cause a change in the extent of intermolecular coupling.

At this point, the spectrum of the coupled ν(OD) vibration should be examined. This will provide more information as to whether the component

bands arise from separate water species, or from the mechanism of coupling of vibrations.

6.3. Coupled OD vibration

Examination of the coupled bands of the ν(OD) vibration ought to yield similar information about the system. Just as the coupled ν(OH) band may be separated into its component bands, so may the ν(OD) band. Three bands were necessary to simulate each spectrum at a particular W_o value.

The replacement of H_2O with D_2O in the reverse micelle will make no difference to the information available from the spectra as the structure of the reverse micelle is unchanged. (As mentioned in chapter 3 the only effect of substitution is to decrease the overall size of the micelle as D_2O favours a more curved interface[4].)

However it is apparent that the spectra of H_2O and D_2O in the AOT reverse micelles are somewhat different. Comparison of figures 6.9, which shows the coupled D_2O band, with figure 6.10, which shows the coupled H_2O band, reveals the differences.

Figure 6.9 Coupled ν(OD) vibration in AOT/heptane/D_2O microemulsions where Wo = 10 (solid line). The synthetic spectrum and its components are shown with dotted lined. The difference between the experimental and the synthetic spectra is also shown.

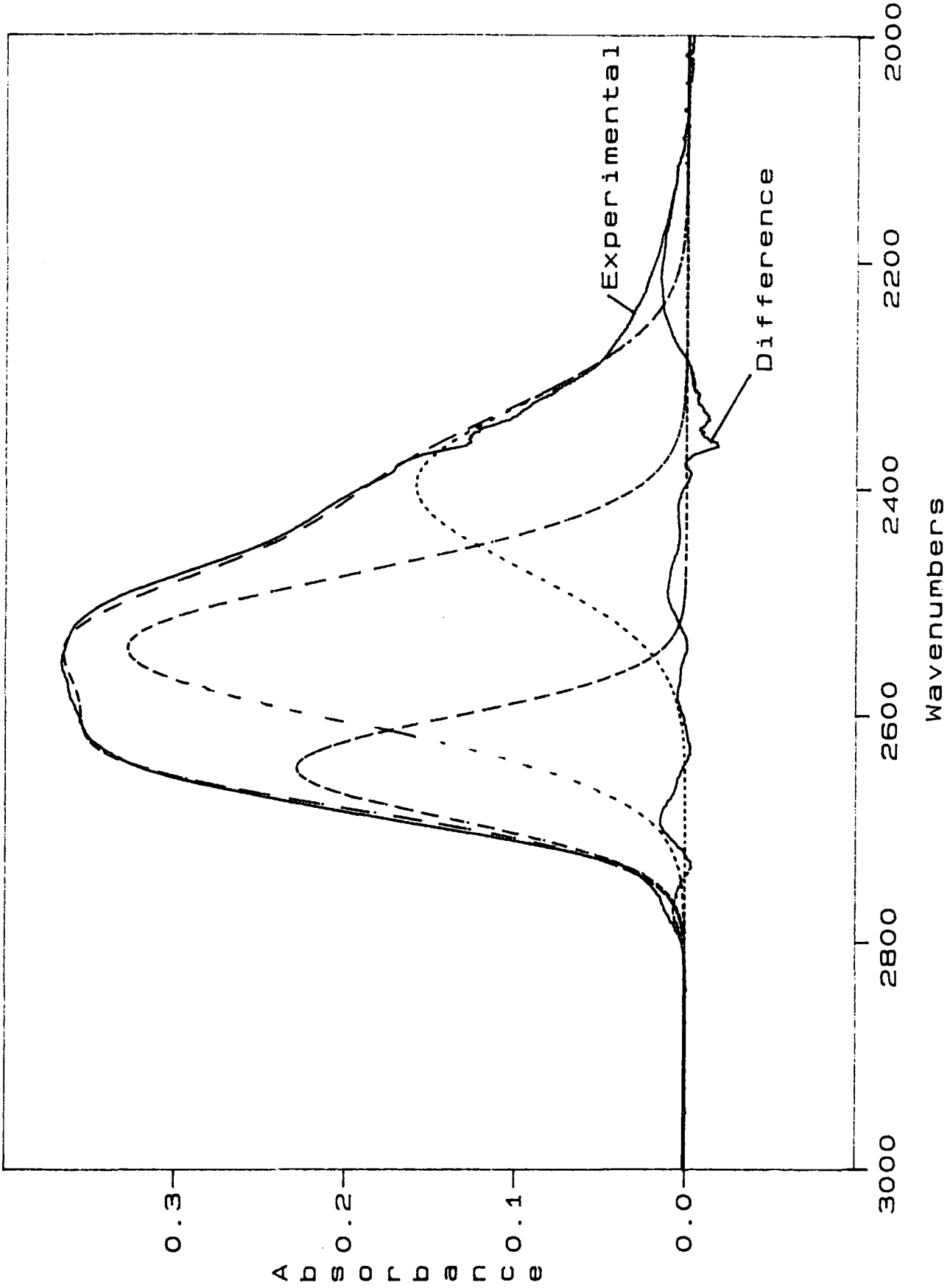

Figure 6.10 Coupled ν(OH) vibration in AOT/heptane/H_2O microemulsions where $W_0 = 20$ (solid line). The synthetic spectrum and its components are shown with dotted lined. The difference between the experimental and the synthetic spectra is also shown.

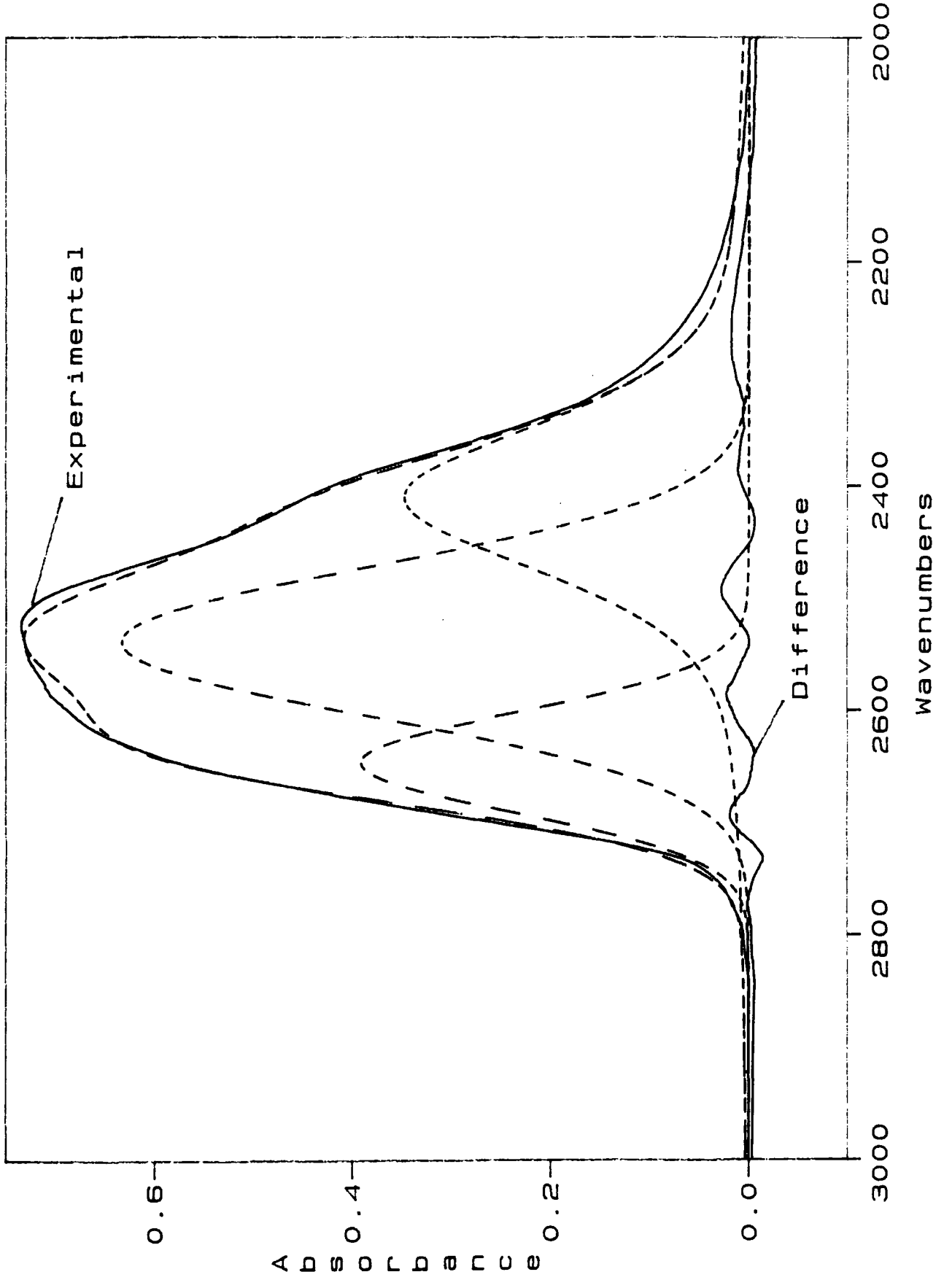

In order to make a trial solution easier to obtain, the frequencies of the component bands in the spectrum of coupled ν(OD) vibrations may be predicted. For an harmonic oscillator, the replacement of an H atom with a D atom should decrease the frequency of the vibration by the square root of the ratio of the masses concerned; i.e. $1:\sqrt{2} = 1:1.414$. Now as deuterium is more massive than hydrogen, the zero point energy (ZPE) of ν(OD) will be lower than that of ν(OH)[5]. Therefore in an anharmonic potential, ν(OH) will be affected more by the anharmonicity than will ν(OD), because of the difference in ZPE. In practice the ratio 1:1.41 is found to fall to less than 1:1.37 [5].

Using the empirical ratio 1:1.37 it is possible to predict the frequencies of the component bands of the coupled ν(OD) vibration, as table 6.6 shows.

Table 6.6 ν(OD) frequencies predicted from ν(OH) frequencies and mass ratio.

ν(OH) frequency positions as used above. All numbers are in cm^{-1}	Predicted position of ν(OD) bands- obtained by dividing ν(OH) position by 1.37 Frequency position
3610	2635
3490	2547
3290	2401

An analysis similar to that applied to the coupled ν(OH) data has been performed for the coupled ν(OD) data, i.e. the spectra are deconvoluted, each component is integrated and information on how the components change with W_0 is obtained. The results are presented in table 6.7 . Note the close correspondance between the predicted frequencies (table 6.6 column 2) and the frequencies suggested by the trial solutions (table 6.7).

Table 6.7 Coupled ν(OD) absorption values (Experiment G)

W_o	Absorption of band at 2409 cm^{-1} Width 160 cm^{-1} A_b	Absorption of band at 2540 cm^{-1} Width 153 cm^{-1} A_r	Absorption of band at 2645 cm^{-1} Width 105 cm^{-1} A_i
1	2.66	3.29	0.53
2	7.44	9.08	1.92
3	10.55	13.20	4.20
4	13.49	17.19	7.04
5	17.01	20.87	10.44
6	20.19	25.33	14.71
7	22.00	28.22	17.13
8	23.59	34.80	20.85
9	27.14	39.55	25.39
10	28.44	44.98	27.63
11	31.41	49.48	29.56
12	34.25	55.17	34.06
13	35.61	59.11	36.63
14	36.97	68.83	38.88
15	42.83	71.56	41.93
16	41.84	83.47	32.54
17	42.31	94.16	31.87
18	44.61	104.91	32.29
19	46.15	106.82	33.86
20	53.51	108.76	38.98

These data may now be plotted as a function of W_o. Also included on figure 6.11 is the total integrated intensity, to show the linear nature of the increase in the integrated intensity of the coupled ν(OD) band as a function of W_o.

Figure 6.11 Integrated intensity for each peak in the coupled ν(OD) band profile.

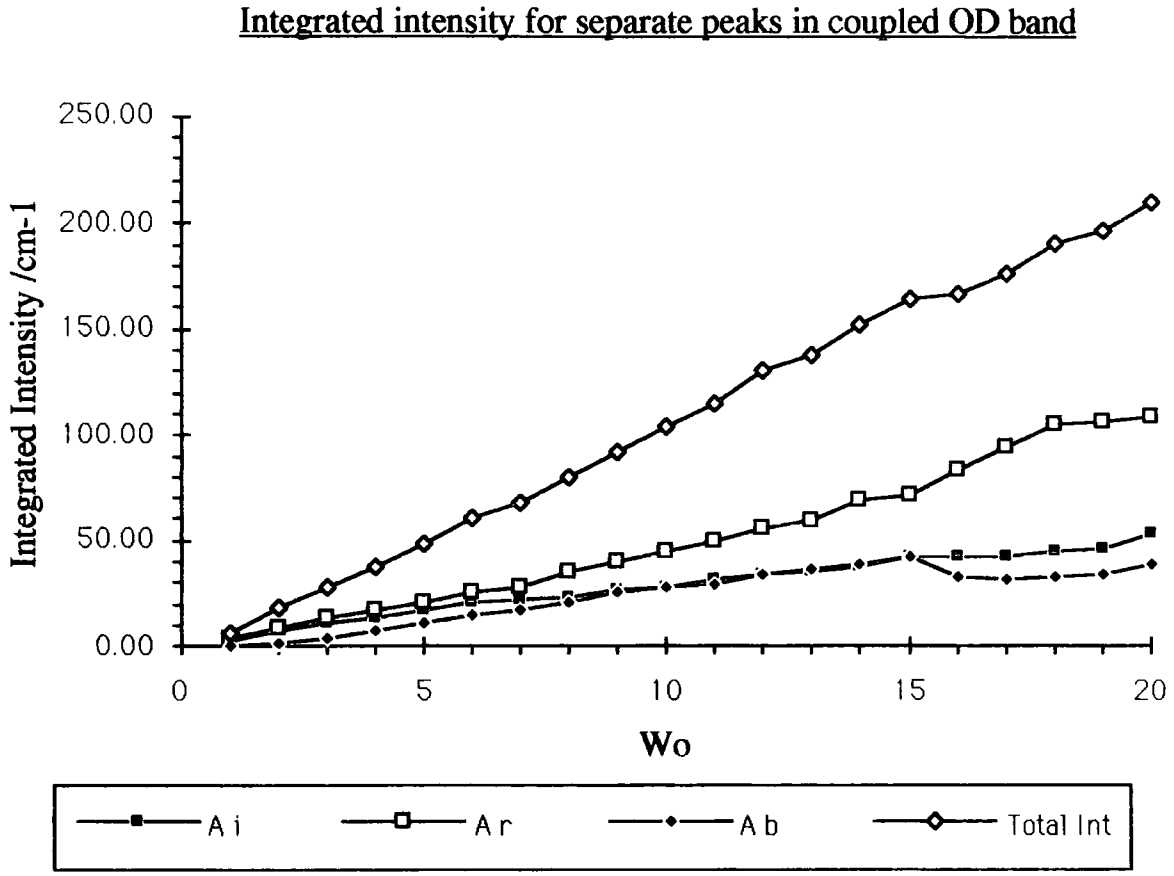

As with the coupled ν(OH) band the fraction each band component contributes to the total intensity may be determined, according to $p_b = A_b/A_o$, $p_r = A_r/A_o$, $p_i = A_i/A_o$. These results are presented in table 6.8.

Table 6.8 Fractions of the 3 component bands in the coupled ν(OD) spectrum.

Wo	p_b	p_r	p_i
1	0.082	0.508	0.410
2	0.104	0.492	0.404
3	0.150	0.472	0.377
4	0.187	0.456	0.358
5	0.216	0.432	0.352
6	0.244	0.421	0.335
7	0.254	0.419	0.327
8	0.263	0.439	0.298
9	0.276	0.430	0.295
10	0.265	0.432	0.273
11	0.258	0.432	0.274
12	0.262	0.425	0.264
13	0.266	0.429	0.259
14	0.256	0.453	0.243
15	0.256	0.437	0.262
16	0.196	0.502	0.252
17	0.181	0.534	0.240
18	0.169	0.549	0.234
19	0.172	0.542	0.234
20	0.185	0.517	0.254

The graph of these data as a function of W_o may be compared to the similar one for the coupled ν(OH) data (figure 6.8).

Figure 6.12 Fractions of the component bands in the coupled ν(OD) spectrum.

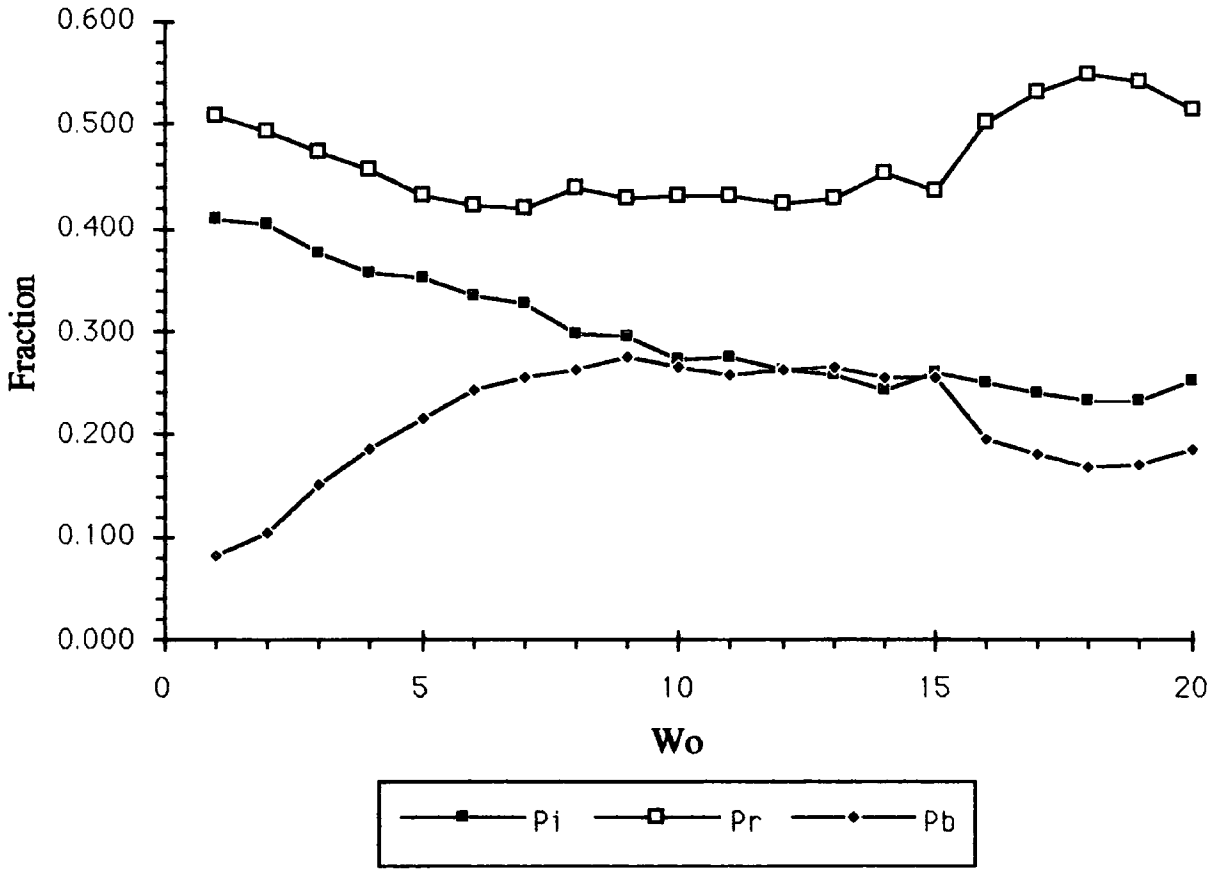

Figures 6.8 and 6.12 are rather different. Figure 6.12 suggests that p_r is always the largest component present. Also the figure implies that the p_b does not increase when $W_o > 10$. The differences between the graphs suggest that the nature and extents of the coupling of ν(OH) to itself and ν(OD) to itself is different. This is discussed below.

The treatment of the coupled ν(OH) and ν(OD) spectra yield different results. If the bands had been assigned to particular water species then the only conclusion that could have been drawn would have been that H_2O and D_2O behave very differently in microemulsions, which is not so.

These discrepancies between figures 6.8 and 6.12 show that component bands cannot be assigned to types of water or particular environments. So the model is not valid in calculating site distributions for the ν(OD) bands as done by Jain *et al* [3]. It may simply be a problem of finding multiple solutions to spectra when answers are sought by computer. However, this would only resolve the difference between the coupled ν(OD) spectra and the coupled ν(OH) spectra.

The coupling of the vibrations of neighbouring water molecules influences the overall shape of the ν(OH) bands. Also Fermi resonance between ν(OH) and 2×δ(OH) leads to a transfer of intensity. Fermi resonance between the first overtone of the bending mode of the water molecule and the symmetric stretch allows a transfer of intensity to the overtone of the bending mode. For H_2O, δ(OH) is at 1645 cm^{-1}, so its overtone will be somewhat less than 3290 cm^{-1}. The frequency is less than double due to anharmonicity[1]. For D_2O, the position of δ(OD) is 1215 cm^{-1}, leading to a first overtone position of less than 2430 cm^{-1}. Now as was discussed above, the ν(OH) vibration has a larger anharmonicity than the ν(OD) vibration. Therefore the difference in energy between the first overtone of δ(OH) and ν(OH) will be larger than the difference between the overtone of δ(OD) and ν(OD). For H_2O the difference is 200 cm^{-1}, whereas for D_2O the difference is 150 cm^{-1}. Consequently the amount of intensity transferred between modes of vibration is different for D_2O than for H_2O. Hence different shape bands are seen.

The extinction coefficient of ν(OD) is not the same as ν(OH)[1] so it may be expected that it will not change in the same way as for ν(OH). Therefore the profile of the coupled ν(OD) vibration differs from that of the ν(OH) vibration. This has previously been neglected, yet is very important if one is assigning bands in a spectrum to a particular species. Unless values for ε are known, then quantitative information on different states of water cannot be obtained. The

probable variation in the extinction coefficients means that the analysis by Jain *et al*[3] is not a complete explanation.

It is the effects of intermolecular coupling of vibrations that is actually being observed. Jain *et al*[3] neglect to account for the intermolecular coupling of vibrations, and this problem has been addressed here. Having examined the coupled vibrations in detail, it seems that the coupled band profile arises from overlap of the symmetric stretch (ν_1), the antisymmetric stretch (ν_3) and overtone of the bending vibration ($2\nu_2$) of a water molecule. The analysis of the decoupled ν(OD) vibration showed that the frequency position varies with W_0. Therefore the variation in the shape of the coupled band may be accounted for by the frequency shift on change in hydrogen bonding, and a change in coupling as the amount of water present changes. In addition the changes in shape of the coupled bands may be due to a change in the extinction as coefficient W_0 is varied.

How then may this explanation be rationalised with respect to the decoupled ν(OD) band? The decoupled band showed no multiple band structure. This does not necessarily mean that multiple sites with differing properties are not present. It may be that the proton exchange between these sites is fast compared with the time-scale of the experiment so that only a single band is observed. The structure of the coupled band would then arise from the coupling of the vibrations. Alternatively if there were a continuous distribution of water molecule environments, then a single band in the decoupled spectrum would arise, its position varying as the range of environments varied. This would still mean however that the structure of the coupled band (ν(OH) or ν(OD)) arose purely from vibrational coupling and Fermi resonance.

Either way, it has been shown here that the structure of the coupled ν(OH) and ν(OD) bands arises from vibrational coupling and Fermi resonance. The cause of the change in shape of the band profile for the coupled bands most probably arises from a change in coupling as the bands move owing to changes

in hydrogen bonding. However, the position of the bending vibration ν_2 is invariant. Therefore, the amount of Fermi resonance will change as W_o is varied. This will lead to a change in the shape of the coupled band of water.

By way of showing that vibrational coupling is important, a very simple experiment may be performed. A drop of pure D_2O is held by capillary action between two CaF_2 plates and the FTIR spectrum is recorded. After 30 minutes another spectrum is recorded, when sufficient H_2O has been able to diffuse into the D_2O to cause a change in the spectrum of the D_2O (figure 6.13). The later spectrum shows a single ν(OH) absorption band. When the two spectra are then subtracted, the difference reveals a decrease in intensity and shape change in the coupled ν(OD) absorption band. The two negative peaks correspond to the ν_3 and $2\nu_2$ vibrations of D_2O. Therefore the coupled ν(OD) absorption at 2500 appears therefore to comprise 3 bands. By isotopically diluting some of the D_2O with H_2O, the coupling of the ν(OD) vibrations become less. This serves to indicate that the spectrum of bulk water arises from intermolecular interactions.

Figure 6.13 Spectrum of D_2O (solid line) held by capillary action between two CaF_2 plates and the same sample 30 minutes later (dashed line) when H_2O has diffused in. The difference (dotted line) is also shown. The positions of the two negative bands in the difference spectrum are 2639 and 2360 cm^{-1}.

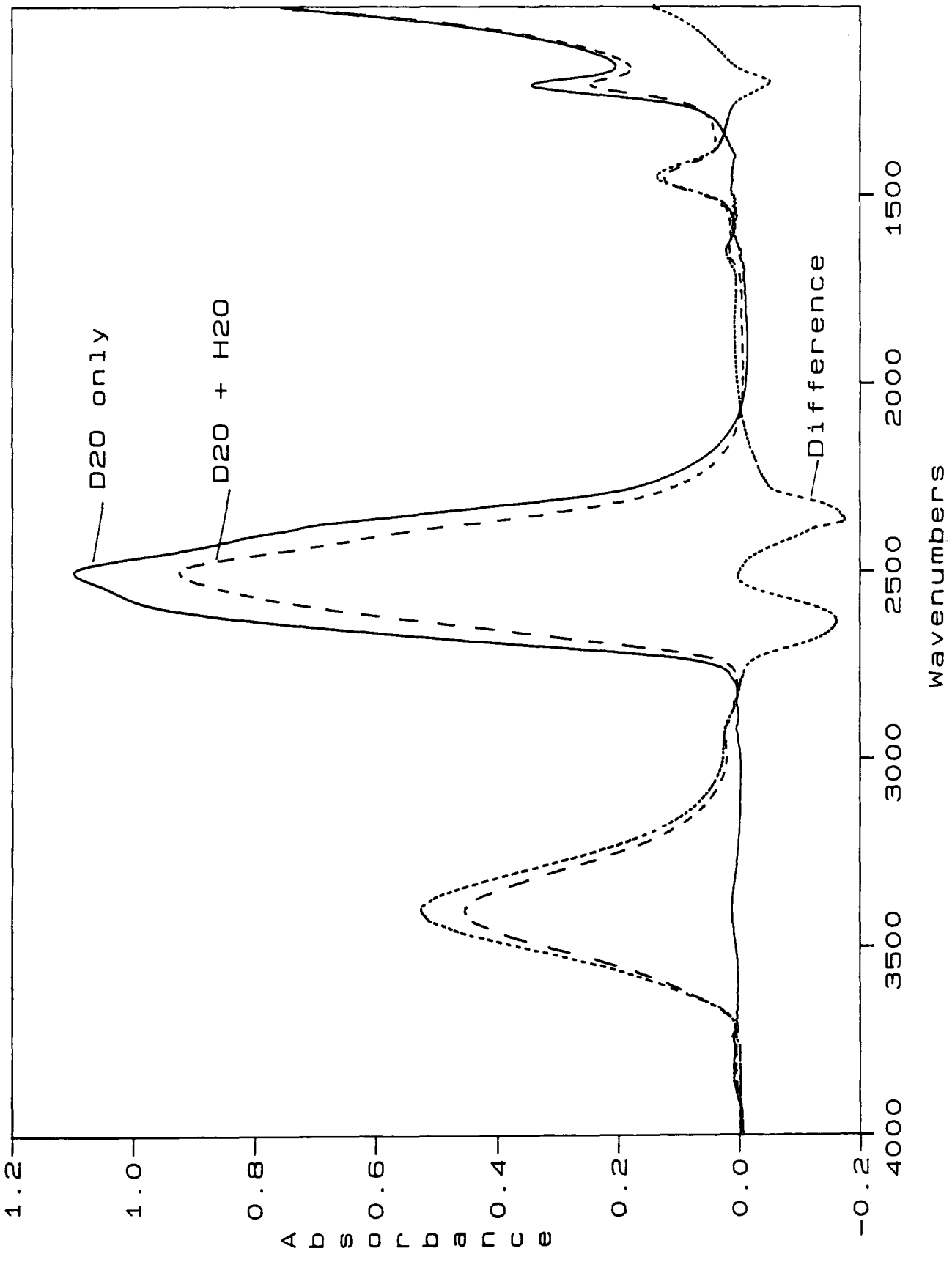

In conclusion, to understand accurately the behaviour of the water in the reverse micelles, account must be taken of the coupling possible between the vibrations and also of the variation in extinction coefficient as W_0 is varied.

6.4. Sulphonate $\nu(SO_3)$ vibration

The sulphonate group plays a most important role in the formation of reverse micelle particles in the AOT system. It is an ionic group and will therefore bind strongly to water. Being in the midst of the molecule the sulphonate group is close to the interface between the polar and apolar regions in the reverse micelle.

The symmetric stretch of the sulphonate band shifts to lower frequency and narrows as W_0 is increased. Hydration of the headgroup is expected and changes in the spectra indicate that hydration is occurring.

Examination of the position of the sulphonate band as a function of W_0 suggests that three water molecules are bound to the sulphonate group. This is because at $W_0 = 3$, the frequency ceases to decrease (see figure 5.10). However the frequency as measured is digitised to within ± 1 cm^{-1}, so changes more gradual than the spectrometer can resolve may be occurring. Nevertheless there is a distinct drop in frequency between $W_0 = 0$ and 3.

Within experimental error, no further change in the ν(SO) band position occurs after $W_0 = 3$. This may be due to full hydration of the sulphonate group. The addition of more than three water molecules does not cause any further shift in frequency so there is no change in the electronic environment of the sulphonate group when $W_0 > 3$.

The full width at half height of the symmetric sulphonate stretch follows the same trend as the frequency (figure 5.10). Here, a more gradual decrease in the width exists, as opposed to the stepped decrease in the frequency. However the error in measuring the width is much larger (at least ± 2 cm^{-1}).

From a statistical argument the width of an infrared absorption band may arise from a large number of environments for that particular molecule. However

for large molecules the width of an infrared absorption band[6] is directly dependent on the rate of vibrational dephasing. These two approaches can be used to explain the data obtained here. Either the range of environments that surrounds the sulphonate group decreases as the headgroup is hydrated, or the rate of environmental fluctuation decreases. Consequently this implies that as the AOT molecule is hydrated, the sulphonate group becomes saturated at a value of $W_O = 3$.

The exact location of the water molecules surrounding the sulphonate group can be discussed only after the effect of the sodium ion has been considered.

6.5. Sodium counter-ion

The coordination number of sodium in water is six[7]. The data from the AOT system studied here agree with this.

Before any further conclusions can be drawn about the behaviour of the water surrounding the headgroup of the AOT molecule, it is essential to consider the sodium counter-ion in some detail. When there is very little water present in an AOT reversed micelle, then because opposite ionic charges attract each other, the sodium ion must be bound to the sulphonate group. Two questions arise. What happens as water is added? What is the behaviour (or location) of the sodium ion when sufficient water has been added to hydrate completely all the AOT headgroup?

Vibrational spectroscopy is obviously unsuitable for examining the sodium ion itself, although the effect of the sodium ion on the water is readily measured. NMR experiments on the ^{23}Na nucleus allow direct observation of the counter-ion.

From ^{23}Na NMR studies[7] six water molecules per head group will interact strongly with the sodium ions. This confirms the known hydration number of sodium as six. The first 6 water molecules to be added to the system will therefore bind to the sodium ion. Simultaneously however, the sulphonate group

is also being hydrated. This suggests that from $W_0 = 0$ to 3 the water molecules bind to both the sodium and the sulphonate group. The only way that this is possible is if there is a bridging structure between the cation and anion as suggested by figure 6.14.

Figure 6.14 AOT with 3 bridging water molecules between the sulphonate head group and the sodium counter-ion.

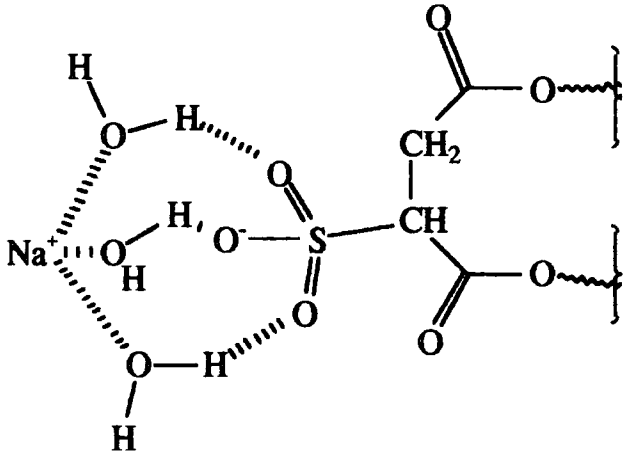

As the sulphonate group is hydrated by $W_0 = 3$, then the next three water molecules to be added to the system will not be associated with the sulphonate group and will instead bind to the sodium ion.

Once there is sufficient water within the reverse micelle for all the polar groups to be hydrated, then the sodium ion with its 6 surrounding water molecules will be able to move within the core of the reverse micelle. Sodium counter-ions may therefore be located either at the interface or free within the core of the micelle. The distribution between the two sites for the sodium ion, has been measured[7]. It was established that at least 3/4 of the ions were bound to the inner surface of the reversed micelle.

Now the sulphonate groups, which are part of the surfactant headgroup, are constrained to be at the interface between the aqueous part and the non-aqueous part of the reverse micelle. Since 3/4 of the sodium ions are bound and suffer restricted motion, they must be located at the interface. Ionic attraction between ions of opposite charge is responsible for the degree of binding to the micellar surface.

Consequently for large W_0 values, the bulk water within the core of the micelle will have a depleted sodium concentration, compared with the case where all the sodium ions are free to move throughout the micelle. This implies that a third type of water exists and the explanation has been invoked to clarify the behaviour of water in AOT reverse micelles[3,8]. The three types are: the interfacial water bound to the inner surface of the reverse micelle, the bulk water within the core of the reverse micelle and the third type is water that is bound to the sodium ions but free to move throughout the water core.

6.6. Carbonyl ν(CO) vibration

The carbonyl band clearly has two components at all W_0 values (see figure 6.16). It has been suggested previously[9,10] that these two bands arise from a mixture of rotational isomers; in particular the gauche (ν(CO) ≈ 1722 cm^{-1}) and trans (ν(CO) ≈ 1739 cm^{-1}) conformers drawn in figure 6.15.

Figure 6.15 The gauche-like and trans-like isomers of AOT at an interface

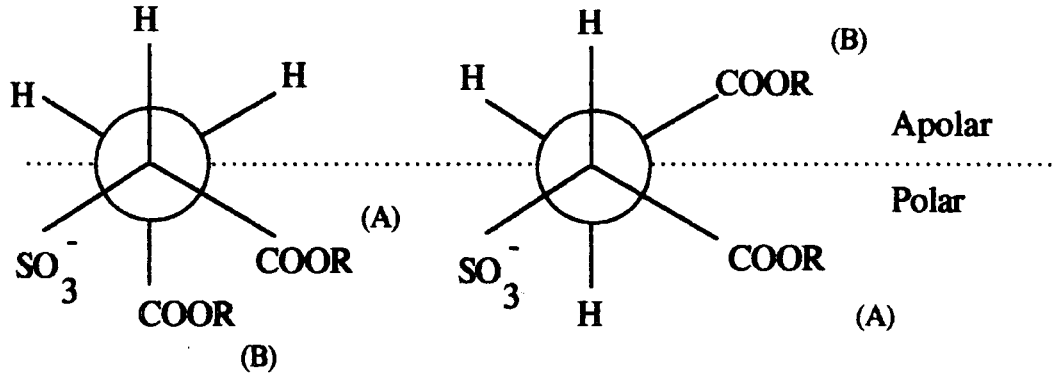

gauche (1722 cm^{-1}) trans (1739 cm^{-1})

It has also been demonstrated[9] that the proportion of the conformers varies with temperature and with the nature of the solvent environment. In an apolar medium (at low water concentrations) the trans-like rotamer is expected to be favoured because, in this conformation, the molecule is extended with the head group at the centre. Also this conformation allows the hydrocarbon chains to shield the headgroup from the apolar solvent. Thus at low W_0 values the

intensity ratio of the two absorption bands I_r (= I_{1722}/I_{1737}) is expected to be relatively low. The gauche conformation is wedge shaped and is therefore expected to be the most amphiphilic. Therefore when W_o is increased the population of gauche conformations will increase, causing I_r to rise.

The spectrum (figure 6.16) may be resolved into two bands by curve-fitting synthetic spectra to the absorption band. One absorption band is at 1739 cm^{-1}, and the second is at 1722 cm^{-1}. The band widths of each component band do not change as W_o is varied.

Figure 6.16 ν(CO) vibration in AOT/heptane/D_2O microemulsions as a function of W_o at W_o = 0, 1, 2, 3, 4, 5, 6, 10, 15, 20.

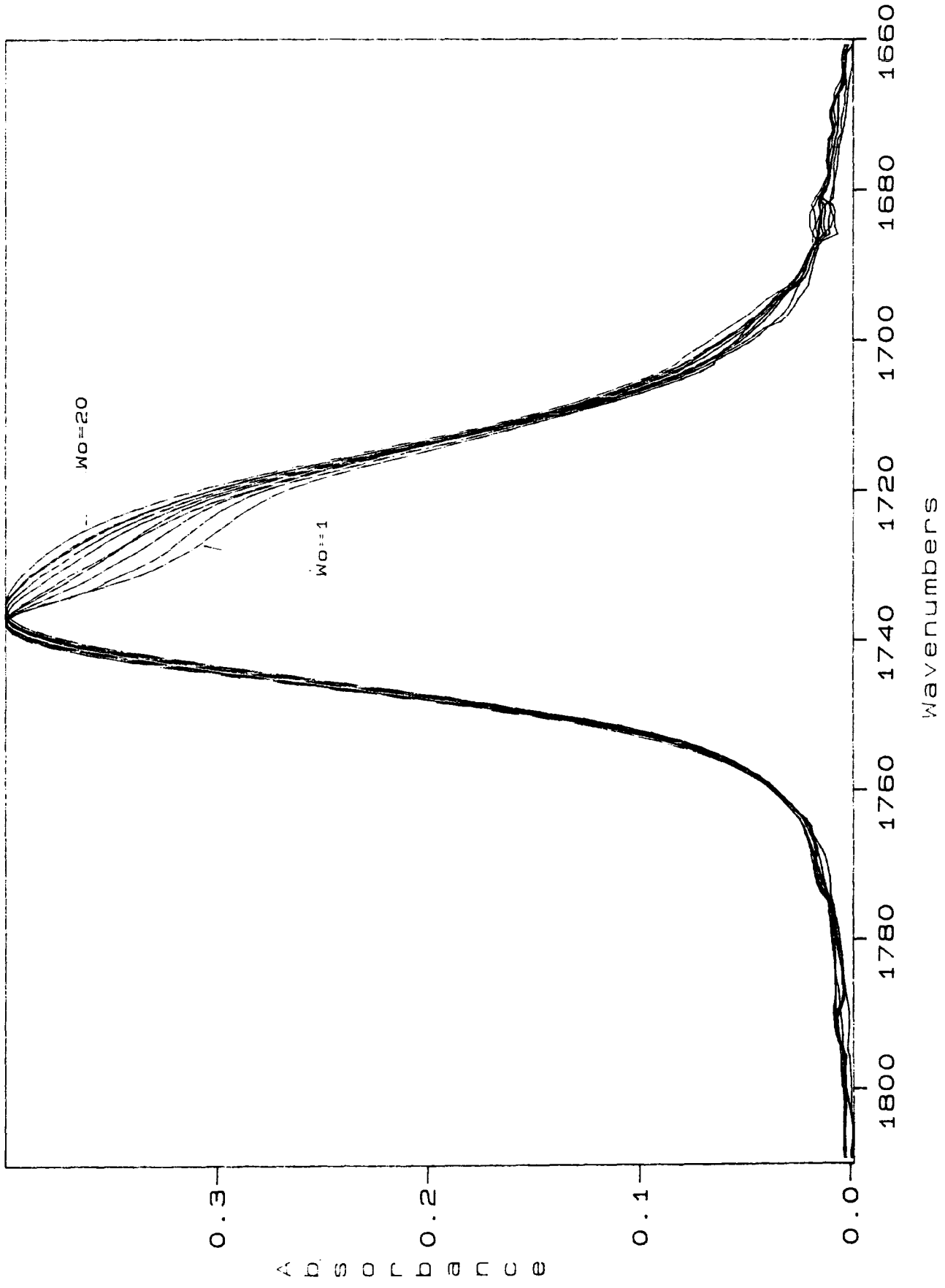

The table 6.9 shows the integrated intensity of each absorption band in the carbonyl group.

Table 6.9 Absorption intensity of carbonyl bands at 1739 and 1722 cm^{-1}

W_o	Intensity of band at 1739 cm^{-1} trans	Intensity of band at 1722 cm^{-1} gauche	Intensity ratio
0	0.315	0.220	0.69
1	0.317	0.220	0.69
2	0.300	0.228	0.76
3	0.298	0.231	0.77
4	0.299	0.244	0.81
5	0.291	0.239	0.82
6	0.303	0.253	0.83
7	0.287	0.250	0.87
8	0.287	0.270	0.94
9	0.297	0.280	0.94
10	0.297	0.259	0.87
11	0.287	0.264	0.92
12	0.285	0.269	0.94
14	0.280	0.273	0.97
15	0.279	0.275	0.98
16	0.330	0.330	1.00
17	0.300	0.300	1.00
18	0.295	0.295	1.00
19	0.294	0.295	1.00
20	0.295	0.297	1.00

When the values of the intensity ratio versus W_o are plotted then the following figure 6.17 results. The form of the curve suggests that as W_o increases, then the intensity ratio reaches 1.0. The intensity of the high frequency peak (trans conformation) hardly changes as W_o is increased, whereas the intensity of the gauche peak rises, as is evident from both the spectrum and figure 6.17.

Figure 6.17 showing intensity ratio of 1739 absorption band to 1722 absorption band

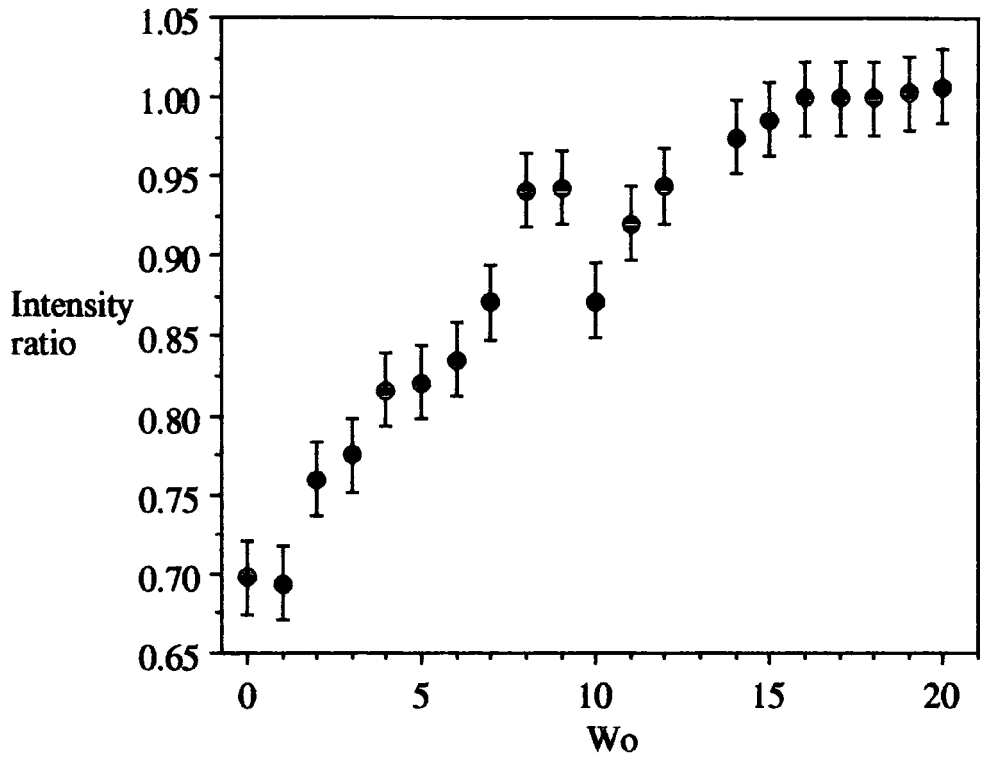

This graph has been produced by taking the ratio of the peak intensity at 1739 cm^{-1} to the intensity at 1722 cm^{-1}.

It might be expected that the trans conformers will decrease in population as W_o is increased and larger reverse micelle aggregates requiring wedge shaped surfactant molecules are formed. However this does not appear to occur. Instead the intensity of the 1739 cm^{-1} band (attributed to the trans conformation[9]) remains constant within error. This may be due to the equilibrium between AOT monomers and aggregates. If monomers are always present, then the monomeric AOT molecule will be in the trans conformation whereby the polar headgroup and the water molecules bonded to it will be shielded from the apolar solvent (heptane) by the hydrophobic tail of the surfactant. The increase in intensity of the band at 1722 cm^{-1} with increasing W_o indicates an increase in the population of gauche conformers. This in turn implies that the number of AOT molecules that are part of an AOT aggregate increases as W_o increases.

The above interpretation is similar to that of Maitra *et al*[9]. However an important point seems to have been neglected from their interpretation. It is most important to remember that the two C=O groups in AOT are not symmetrically equivalent. This will itself give rise to two bands, even in the absence of rotational isomerism. Consequently relative intensity changes of the two different ν(C=O) vibrations leads to a more complicated intensity distribution than can be predicted on the basis of conformational changes alone.

The intensity of one ν(C=O) vibration increases as W_O increases. The intensity of the other is constant for all W_O. If the two carbonyl groups have distinct frequencies, then there will be two overlapping bands at all values of W_O. Assume that the frequency positions of the vibrations are 1739 cm^{-1} for carbonyl group (A) and 1722 cm^{-1} for carbonyl group (B). At low values of W_O (say W_O = 0-2), the molecule will be in a conformation such that the ionic headgroups are protected from the apolar hydrocarbon. As W_O is increased, so the wedge shaped gauche conformer is more able to form a curved surface, as the increased amount of water will tend to collect together to solvate the headgroup ions. On changing conformation, the second carbonyl group therefore moves to a more polar environment, and the intensity of this band increases.

Possibly then group B is the one increasing in intensity and group A remains constant, being fixed by H-bonding to the SO_3^- group. The frequency of hydrogen bonded C=O groups is ≈ 1740 cm^{-1}, and if group B is moving to a polar environment, its frequency will fall. No frequency shifts are observed, so it seems that one carbonyl group is changing its environment.

A further point, which hardly seems to have been discussed in the literature is the fact that isomers of AOT molecules will exist. One study[11] notes that the different isomers will cause differences in the NMR quadrupolar splitting patterns for selectively deuterated AOT molecules. However it is noted that the amphiphilic character of the molecule is not altered by the existence of isomers. As mentioned in chapter 3, none of the reactions used in the common

route to AOT is stereospecific, so a mixture of isomers will be produced. In the figure 6.14 above, the positions of the sulphonate and the -COOR group may be reversed. This means that the conformations of the each molecule in the reverse micelle will depend on which isomer of AOT is present.

6.7. Conclusions

When water is added to a non-aqueous solution of AOT the initial interactions are associated with the hydration of the $RSO_3^-Na^+$ head group. The first three water molecules are strongly hydrogen-bonded to the anion. The HOD ν(OD) vibrational band is shifted to high frequency (compared with liquid water) showing that this interaction also involves the cation Na^+. Addition of three more water molecules per head group results in a fully solvated cation. The frequency shift towards the value for bulk water continues at the same rate up to $W_o \sim 12$ showing that the environment surrounding each water molecule is highly perturbed up to the point where the second solvation shell around the head group is completed at $W_o \approx 12$. However, the vibrational relaxation rate of the water molecule as indicated by the band width of the ν(OD) vibration appears to show a break at $W_o = 6$. This implies that during hydration by up to six water molecules per head group, the distribution of environments increases and/or that the environmental fluctuations become faster. Between $W_o \approx 6$ and 12 (in the second solvation shell) the ν(OD) band-width shows that the water molecules are more similar to those in bulk water. This emphasises the fact that no evidence exists for distinct types of water molecules, other than those that are bound to the ions. It is suggested that the spectroscopic data are best interpreted in terms of a continuum of water molecule interactions in rapid equilibrium with each other. However, the water core in AOT microemulsions even at $W_o > 40$ is not identical with that of pure liquid water. This will be due to the high Na^+ concentration in the core.

The type of AOT/H_2O aggregate formed in these solutions at low water concentrations is not completely clear. There is some evidence of a shift in the

AOT conformational equilibrium as a function of W_0 (at low W_0). This implies that more than 12 and perhaps up to 20 water molecules per headgroup may be needed to form well-defined reversed micelles. Certainly, the spectra of the CO group are still somewhat sensitive to the addition of water above W_0=20.

It seems that to form a coherent picture of the reverse micelles, the possibility of their lifetime must be accounted for. Effects such as polydispersity lead to a loss of resolution in the measurement of certain properties. The equilibrium between monomers and aggregates must also be borne in mind as this will influence the species present. Finally, in quantitatively interpreting the vibrational spectra, care must be taken that the assignment of the band is certain; also that changes in the band can be attributed to a definite chemical effect (such as a change in environment), rather than a physical effect such as a change in extinction coefficient.

6.8 References

(1) Eisenberg D., Kauzmann W. *The Structure and Properties of Water*; OUP: Oxford, **1969**.
(2) MacDonald H., Bedwell B., Gulari E. *Langmuir* **1986**, *2*, 704.
(3) Jain T. K., Varshney M., Maitra A. *J. Phys. Chem.* **1989**, *93*, 7409.
(4) Fletcher P. D. I., Howe A. M., Robinson B. H. *J. Chem. Soc. Faraday Trans. I* **1987**, *93*, 985.
(5) Bellamy L. J. *The Infrared Spectra of Complex Molecules*; Chapman and Hall: London, **1980**Vol. 2.
(6) Yarwood J., Döge G. In *Spectroscopy and Relaxation in Molecular Liquids*; Eds. D. Steele and J. Yarwood; Elsevier: Amsterdam, **1991**; .
(7) Wong M., Thomas J. K., Nowak T. *J. Am. Chem. Soc.* **1977**, *99*, 4730.
(8) Hauser H., Haering G., Pande A., Luisi P. L. *J. Phys. Chem.* **1989**, *93*, 7869.
(9) Maitra A. N., Eicke H. *J. Phys. Chem.* **1981**, *85*, 2687.
(10) Martin C. A., Magid L. J. *J. Phys. Chem.* **1981**, *85*, 3938.
(11) Olsson U., Wong T. C., Söderman O. *J. Phys. Chem.* **1990**, *94*, 5356.

CHAPTER 7

AOT MODEL CALCULATIONS

7. Two Site Equilibrium Mixture Model

A model originally based on the analysis of NMR data[1] has been further developed to provide information on thermodynamic parameters[2]. This approach is extended here to analyse the findings of the infrared data.

In this model the water is categorized into types according to its environment and consequent spectroscopic behaviour. However the division is arbitrary relying on a knowledge of the number of environments present. The model depends only on the ability of a particular technique to distinguish between environments based on their separation in time and space. In this respect it is worth remembering that infrared spectroscopy can distinguish between short lived species ($\tau=10^{-14}$ s).

Several assumptions need to be made to use this model[1,2]:

1. The system comprises monodisperse spheres.
2. There are just two sites for the water molecules: one in which the water is free(in the sense that it is bulk-like), the other where water is bound in some way. An equilibrium between the two sites exists, hence the name of this model.
3. All the water that is bound in some way is bound to the inner surface of the reverse micelle. The remainder of the water is free or bulk-like at the centre of the reverse micelle.

The frequency of the decoupled ν(OD) band observed is the weighted average as defined by equation 7.1

$$\nu_{obs}=p_{bound}\,\nu_{bound} + p_{free}\,\nu_{free} \quad \text{..... 7.1}$$

ν_{obs} = the experimentally observed frequency / cm^{-1}
p_{bound} = the mole fraction of water molecules that are bound
ν_{bound} = the frequency of a bound water molecule / cm^{-1}
p_{free} = the mole fraction of water molecules that are free
ν_{free} = the frequency of a free water molecule / cm^{-1}

If it is remembered that the sum of mole fractions must equal unity

$$p_{bound} + p_{free} = 1 \quad \text{..... 7.2}$$

then equation 7.1 can be rearranged to give an expression for p_{bound}:

$$p_{bound} = \frac{(\nu_{obs}-\nu_{free})}{(\nu_{bound}-\nu_{free})} \quad \text{.....7.3}$$

A linear relationship has been found to exist between the radius of the water pool (r_w) at the centre of the reverse micelle and the amount of water present[3]. Here r_w includes the head group volume.

$$r_w = A + B\,W_o \quad \text{..... 7.4}$$

where W_o is the molar ratio of water to surfactant. A and B are constants.

$A=r_k$, $B = \frac{3\alpha_s}{\rho_w}$: r_k is the length of the headgroup which projects into the aqueous core , α_s = moles per unit area at the surfactant interface, ρ_w is the density in moles/unit volume of water in the droplet. Both of these quantities α_s and ρ_w are known and will be discussed later.

Consider the surface area of the water pool ($s_{micelle}$) within the reverse micelle

$$s_{micelle} = 4\pi r_w^2 \quad \text{.....7.5}$$

Similarly the volume of the water ($v_{micelle}$) is given by:

$$v_{micelle} = n_{water}\ \bar{v}_{water} = \frac{4}{3}\pi r_w^3 \quad \text{.....7.6}$$

n_{water} = the number of water molecules in the water pool
$\bar{v}_{water}$ = the average volume of a water molecule

According to proposition 3 above, all the bound water is at the interface. This implies that the fraction of bound water is proportional to the surface area of the micelle,

$$p_{bound} \propto s_{micelle}$$

or that the number of water molecules bound is proportional to the surface area of the micelle

$$n_{bound} = k\, s_{micelle} \quad \text{..... 7.7}$$

where k is an arbitrary constant.

Now by definition:

$$p_{bound} = \frac{n_{bound}}{n_{water}} \quad \text{.....7.8}$$

hence combining 7.5 and 7.6 we obtain

$$p_{bound} = \frac{k\, s_{micelle}}{n_{water}} = k\, 4\pi r_w^2 \frac{3\,\bar{v}_{water}}{4\pi r_w^3} = \frac{3k\bar{v}_{water}}{r_{water}}$$

In conjunction with 7.4

$$p_{bound} = \frac{3k\bar{v}_{water}}{A+BW_o} = \frac{3k\bar{v}_{water}/A}{1+\left(\frac{B}{A}\right)W_o} \quad \text{.....7.9}$$

As the amount of water in the micelle is reduced to zero, an approximation can be made:

As $W_o \rightarrow 0$ so $p_{bound} \rightarrow 1$ hence equation 7.9 implies $\frac{3k\bar{v}_{water}}{A} = 1$ which substituting into 7.9 gives

$$p_{bound} = \frac{1}{1+\left(\frac{B}{A}\right)W_o} \quad \text{.....7.10}$$

Remembering the definition of W_o:

$$W_o = \frac{n_{water}}{n_{aot}} \quad \text{.....7.11}$$

where n_{aot} is the number of surfactant molecules in the reverse micelle.

7.8, 7.10 and 7.11 can be combined to give:

$$\frac{n_{bound}}{n_{aot}} = \frac{W_o}{1+\left(\frac{B}{A}\right)W_o} \quad \text{.....7.12}$$

which when inverted gives:

$$\frac{n_{aot}}{n_{bound}} = \frac{1}{W_o} + \frac{B}{A} \quad \text{.....7.13}$$

As the amount of water in the micelle is increased the fraction of bound water becomes very small:

As $W_o \rightarrow \infty$ so $\frac{1}{W_o} \rightarrow 0$ hence

$$\frac{n_{bound}}{n_{aot}} \rightarrow \frac{A}{B} \quad \text{.....7.14}$$

This relationship 7.14 is very significant. It indicates the number of water molecules that are bound to a surfactant molecule in the reverse micelle. This is exactly the information that can be obtained from infrared spectroscopy. The next stage is therefore to develop the model to account for the behaviour of infrared spectra observed.

Combining equations 7.1 and 7.2 to eliminate p_{free}

$$\nu_{obs} = \nu_{free} + p_{bound}(\nu_{bound} - \nu_{free}) \quad \text{7.15}$$

Substitution of 7.10 for p_{bound} gives

$$\nu_{obs} = \frac{\nu_{bound} + \nu_{free}\left(\frac{B}{A}\right)W_o}{1+\left(\frac{B}{A}\right)W_o} \quad \text{7.16}$$

7.1. Comparison with experimental data of the decoupled ν(OD) band

The quantity W_o is known accurately from experiment and can therefore be substituted directly into equation 7.16. Values for ν_{free} and ν_{bound} can be obtained from figure 5.6, which shows the frequency of ν(OD) band as a function of W_o. A value for ν_{free} of 2495 cm^{-1} was selected. This is in good agreement with the value of 2500 cm^{-1} in the literature[4]. Similarly a value for ν_{bound} of 2585 cm^{-1} was selected by extrapolating back to W_o=0 on the graph shown in figure 5.6. These quantities were then substituted into equation 7.16. A value of A/B = 8 gives the best fit to the experimental data. (Figure 7.1)

Table 7.1 showing the observed and calculated frequency of ν(OD)and the difference

Wo	calculated cm^{-1}	experimental cm^{-1}	error cm^{-1}
1	2575	2568	7
2	2567	2565	2
3	2560	2562	-1
4	2555	2556	-1
5	2550	2553	-3
6	2546	2551	-4
7	2543	2542	1
8	2540	2542	-2
9	2537	2537	0
10	2535	2536	-1
11	2533	2529	3
12	2531	2531	0
13	2529	2529	1
14	2528	2529	-1
15	2526	2526	1
16	2525	2526	-1
20	2521	2521	0
25	2517	2516	1
30	2514	2512	2
35	2512	2511	1
40	2510	2511	-1
45	2509	2510	-2

The experimental values quoted are the averages at each W_o value as given in table 5.4

Figure 7.1 showing the observed and calculated frequency of ν(OD) as a function of W_0.

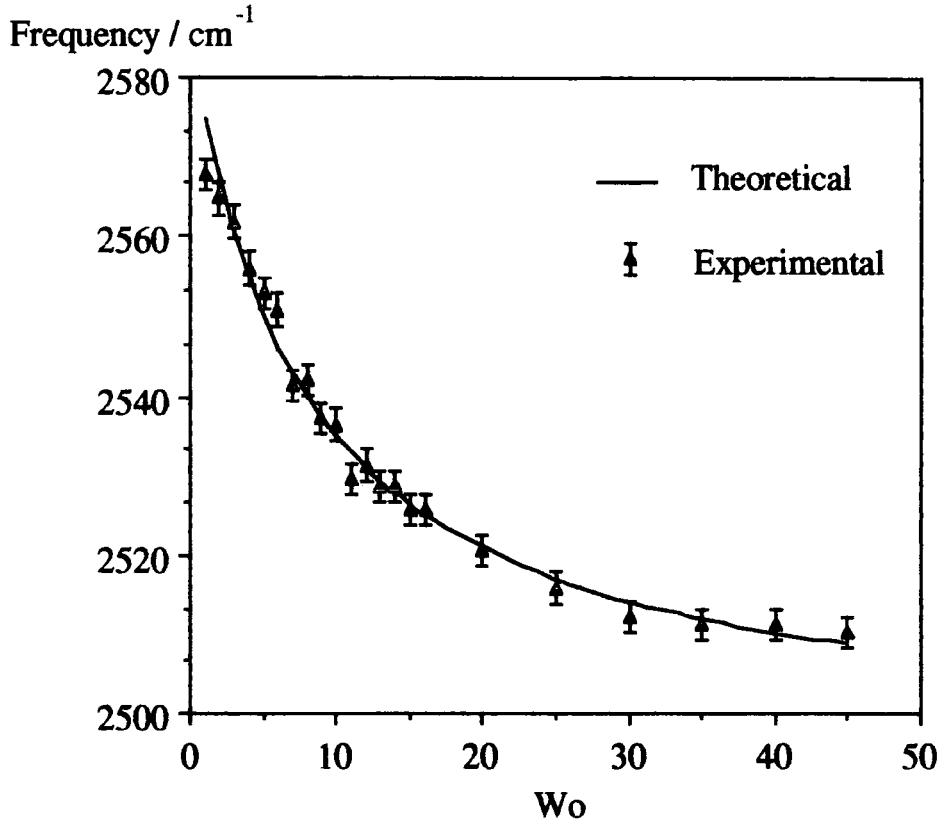

N.B.The experimental data points are averaged at each W_0 value for clarity. See figure 5.6 for a fuller representation.

As can be seen from the above figure 7.1, the model used gives a very good prediction of the observed frequency. The only parameter in the equation 7.16 that is completely unknown from the infra-red data is the ratio A/B. The behaviour of equation 7.16 is such that A/B represents the curvature whereas ν_{bound} and ν_{free} serve mostly to scale the curve to fit to the data. It was shown above (equation 7.14) that A/B represents the number of water molecules bound to an AOT surfactant molecule. It seems reasonable to assume that this number A/B should be an integer or rational number as it describes the number of water molecules that are bound to an AOT headgroup. The value that gives the best fit in the calculation is 8±1. This implies that the first 8 water molecules that are

closely bound to the AOT headgroup in some way suffer the largest degree of perturbation. Whether the ratio A/B is equal to 8 or not is not possible to confirm until the other bands in the spectra of the micelles have been examined.

It is now appropriate to estimate the values of A and B explicitly from the literature values and then to compare with the parameter A/B found in this work. If the estimate is of the same order of magnitude as the parameter A/B used to calculate the frequency shift, then the estimate would seem reasonable.

The quantity A is associated with the amount of penetration of the surfactant headgroup into the water pool. This is likely to be of the order of a few Ångstrom, and an estimate of $r_k \approx 5$ Å [5] does not seem unreasonable.

$$B = \frac{3\alpha_s}{\rho_w}$$

To calculate the value of B, the values for bulk water are used to give an order of magnitude of B. α_s is the number of moles of surfactant per unit area. If the surface area covered by one molecule of AOT[6] is 55 Å^2 then $\alpha_s = 3.02\times10^{-26}$ moles/Å^2. The value of ρ_w may be calculated from the density and molecular weight of water so that $\rho_w = 5.55\times10^{-26}$ moles/Å^3. Therefore $\frac{3\alpha_s}{\rho_w} = 0.61$ Å, which gives a value of A/B = 8. This is the correct order of magnitude. However it must be remembered that these values were calculated from bulk phase values, and that the α_s is known to increase to a plateau value of 55 Å^2 when $W_o > 15$[6].

Here it is the water that is being examined, so it follows that more information can be gained if the surfactant bands are examined.

7.2. Sulphonate symmetric stretching band $\nu(SO_3^-)$

The frequency of the symmetric stretching band of the sulphonate group decreases as a function of W_o (figure 5.10) in a similar way to the ν(OD) band considered above. So the equilibrium model may also be applied to the data sulphonate data.

Figure 7.2 showing the observed and calculated frequency of the symmetric sulphonate stretch.

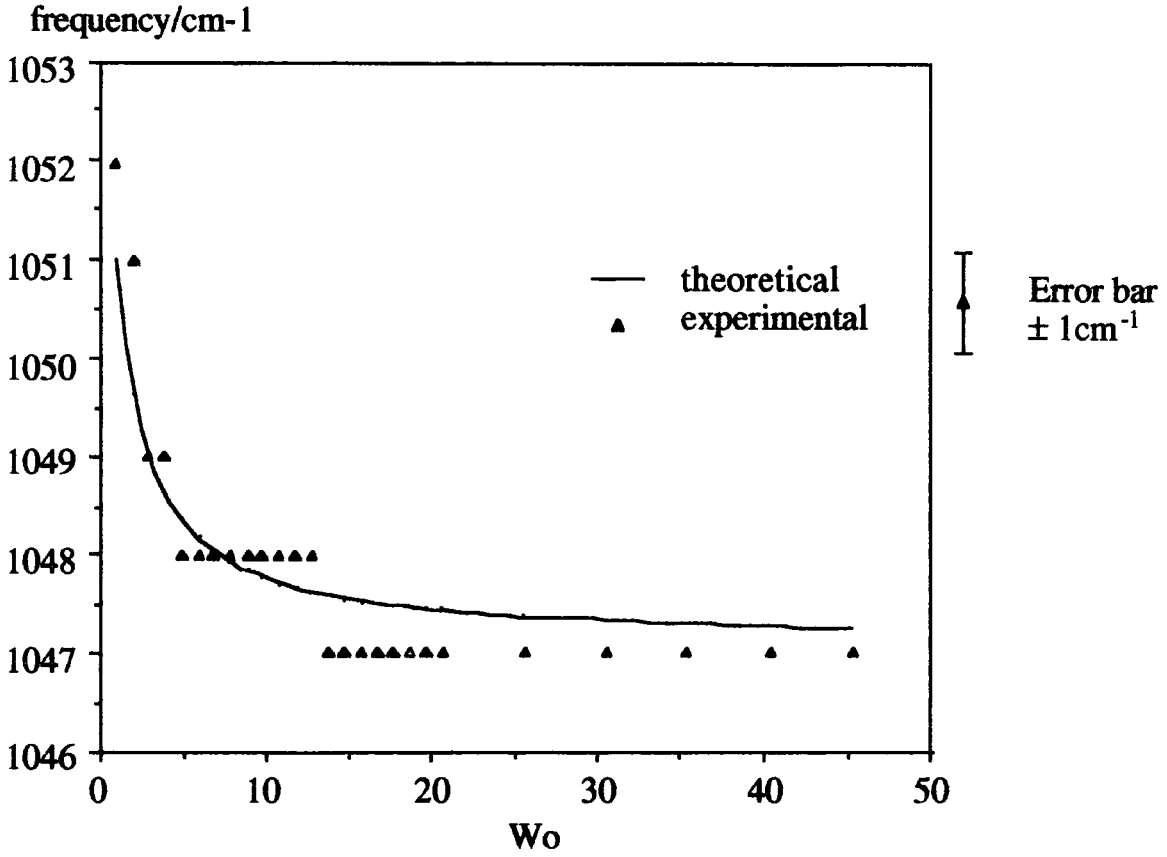

The parameters that give the best fit to the experimental data are:

$\nu_{free} = 1047\ cm^{-1}$, $\nu_{bound} = 1051\ cm^{-1}$, A/B = 2

Table 7.2 showing the observed and calculated frequency of the symmetric sulphonate stretch.

Wo	calculated cm^{-1}	experimental cm^{-1}	error cm^{-1}
0	1051.0	1052	-1.1
1	1049.7	1051	-1.5
2	1049.0	1049	-0.2
3	1048.6	1049	-0.1
4	1048.4	1048	0.1
5	1048.2	1048	-0.1
6	1048.0	1048	0.3
7	1047.9	1048	0.2
8	1047.9	1048	0.3
9	1047.8	1048	0.2
10	1047.7	1048	0.1
11	1047.7	1048	0.1
12	1047.6	1048	0.0
13	1047.6	1047	0.2
14	1047.6	1047	0.2
15	1047.5	1047	0.1
16	1047.5	1047	0.1
17	1047.5	1047	0.2
18	1047.5	1047	0.2
19	1047.5	1047	0.2
20	1047.4	1047	0.2
25	1047.4	1047	0.1
30	1047.3	1047	0.1
35	1047.3	1047	0.0
40	1047.3	1047	0.0
45	1047.3	1047	0.0

7.3. Discussion

The values used for ν_{free} and ν_{bound} have been taken directly from the experimental data measured (chapter 5). ν_{free} was chosen to be equal to the frequency at a high W_o value, and ν_{bound} equal to the frequency at W_o= 1.

The parameter A/B is 2, which according to the model implies that there are two water molecules bound to the sulphonate head-group. This accords with the evidence of Zundel[7] whose work on polystyrene-sulphonate membranes showed that there are two water molecules tightly bound to the sulphonate group.

However before considering the meaning of this value for A/B any further, it is important to remember the source from where it is derived. Equation 7.4 as used in the development of the model contained two empirical parameters A and B (the values of which have since been estimated)

$$r_w = A + B\,W_o \quad \text{..... 7.4}$$

When the sulphonate data is analysed A/B was found to be equal to 2. This may be rationalized as follows. The frequency position of the sulphonate group is only sensitive to the first hydration layer of water. For this large but polarizable ion bonded to the rest of the AOT molecule the hydration number will be small, as suggested by Zundel[7]. Therefore the A/B parameter is regarded as the number of water molecules bound to the sulphonate group.

It was found that when the ν(OD) data was analysed that A/B was equal to 8. In this case, the water bonding to the sodium ions must also be considered. It is known that in the AOT/ water/ alkane system the hydration number of sodium is 6[8]. Therefore this suggests that the first 8 water molecules (i.e. 6+2) added to the system are bound to the ionic parts of the AOT molecule. At W_o values greater than about 8, the frequency position of the ν(OD) vibration still exceeds the bulk water value, but water molecules added in excess of $W_o = 8$ will bind to the carbonyl and ester groups.

It must, however, be borne in mind that these numbers were derived using a two state (or pseudo-phase) model for the behaviour of water. This model assumes that the exchange of water between sites is faster than the time-scale of the experiment, which is why a weighted average is seen. On the NMR time-scale, ($\tau_{obs} > 10^{-6}$ s) the reverse micelles are long lived and the NMR spectra duly show the average between bound and free stated (The lifetime of a reverse

micelle is $\approx 10^{-7}$ s). The infrared observation time is much shorter ($\tau_{obs} \approx 10^{-12}$ s). On this time-scale the reverse micelle is short lived; so it is unclear whether only discrete micelles are influencing the vibrational spectra.

The information obtained just by examining the frequency as a function of W_0 gives a useful indication that the water is bound to some extent. To conclude this discussion, although the model can be very useful in obtaining information, care must be taken that it is not extended to cover data for which it is not valid. The assumptions made at the beginning may be called in to question. There is certainly evidence for a degree of polydispersity in the size distribution of the reverse micelles as measured by SANS[3]. In fact even the shape has been shown to display polydispersity although the equilibrium shape is spherical[9]. There are almost certainly more than two sites for water to bind. Apart from the sodium and sulphonate ions, the binding to the ester groups in the surfactant headgroup may also be important. The model of the system that describes the reverse micelles as discrete particles is not strictly accurate. Droplets will collide and coalesce[10]. Therefore the model of an inner surface to which the water binds breaks down when the particles collide.

It is known that the mean droplet size actually decreases as the critical temperature (where the system is no longer one phase) is approached[11]. Therefore there must be more reverse micelles present, and the total surface area of the phase increases. This in turn means that the simple $r_w=A+BW_0$ relationship is not strictly valid as it does not take account of effects such as polydispersity.

However the reason why the model correctly predicts the behaviour of ν(OD) may more to do with the fast time-scale of the experiment[12]. The lifetime of a species observable with vibrational spectroscopy is of the order of 10^{-14} s The results seem to indicate that an average environment is being observed. The decoupled ν(OD) band does not separate into components, and the frequency changes gradually (but significantly) with W_0.

When the equilibrium model was applied to the ν(OD) data above (section 7.1), then two frequencies were chosen to represent the two environments of water in an AOT microemulsion system. These frequencies were used to represent the extremes of environment (ionicly bound water and free water). However, if a range of environments exists, then the two site approximation used in the equilibrium model is inappropriate.

7.4 References

(1) Maitra A. *J. Phys. Chem.* **1984**, *88*, 5122.
(2) D'Aprano A., Lizzio A., Turco Liveri V. *J. Phys. Chem.* **1987**, *91*, 4749.
(3) Robinson B. H., Toprakcioglu C., Dore J. C., Chieux P. *J. Chem. Soc. Faraday Trans. I* **1984**, *80*, 13.
(4) Wyss H. R., Falk M. *Can. J. Chem* **1970**, *48*, 607.
(5) Sheu E. Y., Chen S., Huang J. S. *J. Phys. Chem.* **1987**, *91*, 3306.
(6) Eicke H. F., Rehak J. *Helv. Chim. Acta* **1976**, *59*, 2883.
(7) Zundel G. *Hydration and intermolecular interaction*; Academic Press: New York, **1969**.
(8) Wong M., Thomas J. K., Nowak T. *J. Am. Chem. Soc.* **1977**, *99*, 4730.
(9) Carlström G., Halle B. *Langmuir* **1988**, *4*, 1346.
(10) Eicke H. F., Shepherd J. C. W., Steinemann A. *J. Coll. Interf. Sci.* **1975**, *56*, 168.
(11) Toprakcioglu C., Dore J. C., Robinson B. H., Howe A., Chieux P. *J. Chem. Soc. Faraday Trans. I* **1984**, *80*, 413.
(12) Yarwood J., Döge G. In *Spectroscopy and Relaxation in Molecular Liquids*; Eds. D. Steele and J. Yarwood; Elsevier: Amsterdam, **1991**; .

CHAPTER 8

CsPFO INTRODUCTION

8. Introduction to Caesium Perfluoro-Octanoate

8.1. Liquid crystals

In dilute aqueous solution, surfactant molecules aggregate together to form micellar aggregates. As the solutions are made more concentrated, phase changes occur, such that liquid crystalline mesophases are formed (e.g. lamellar phases). The main structural feature that distinguishes these liquid crystalline phases from the more dilute micellar phases is the translational ordering of the molecules in the liquid crystalline phase.

Certain surfactant systems exist however, that display orientational order when the aggregate structure is micellar. Examples of these are the decyl-ammonium chloride / ammonium chloride / water[1] and caesium pentadecafluoro-octanoate(CsPFO)/water systems. In this work, the CsPFO system will be examined. It forms mesophases across a wide composition range with just two components.

A micellar phase that exhibits long range orientational order is termed a nematic phase. In general there are several types of nematic phase. Rod shaped micelles form so called calmitic phases (N_C), disc shape micelles form discotic phases (N_D), and lath-like micelle form biaxial nematic phases (N_B), which have two degrees of orientational ordering[2].

In dilute solution above the critical micelle concentration, small angle x-ray scattering (SAXS) measurements show that CsPFO forms disc shaped micelles[3]. At higher concentrations (weight fraction of CsPFO between 0.225 and 0.632) the discotic micelles become orientationally ordered to form a nematic phase. At still higher concentrations a lamellar phase is formed. A schematic representation of the mesophases is shown overleaf.

Figure 8.1 Schematic representation of the mesophases of CsPFO micelles in water.

Isotropic I

Nematic N_D^+

Lamellar L_D

The structure of the lamellar phase is still somewhat uncertain. Measurements made by SAXS, electrical conductivity and NMR suggest that there is no change in shape of the discotic micelles at the phases change between the nematic phase and the lamellar phase. Thus the lamellar phase comprises discotic micelles arranged in planes (a lamellar-discotic phase L_D). However, there is also some evidence from density studies and electrical conductivity, that the lamellar phase comprises the more familiar bilayer structure (L_α); but these observations may also be explained on the basis of fluctuations in the L_D structure. More recently the structure of the L_D phase has been suggested as L_α-type layers with water filled holes, as the SAXS measurements are unable to distinguish between this structure and pockets of water between closely spaced micelles in the L_D phase[4].

The size of the CsPFO micelles as a function of concentration and temperature has been determined by small angle x-ray scattering (SAXS) measurements[5]. The variation of the mean aggregation number versus the weight fraction of CsPFO at 293 and 350 K is shown in figure 8.2 below.

Figure 8.2 Average aggregation number ñ as a function of weight fraction of CsPFO at 293 and 350 K.

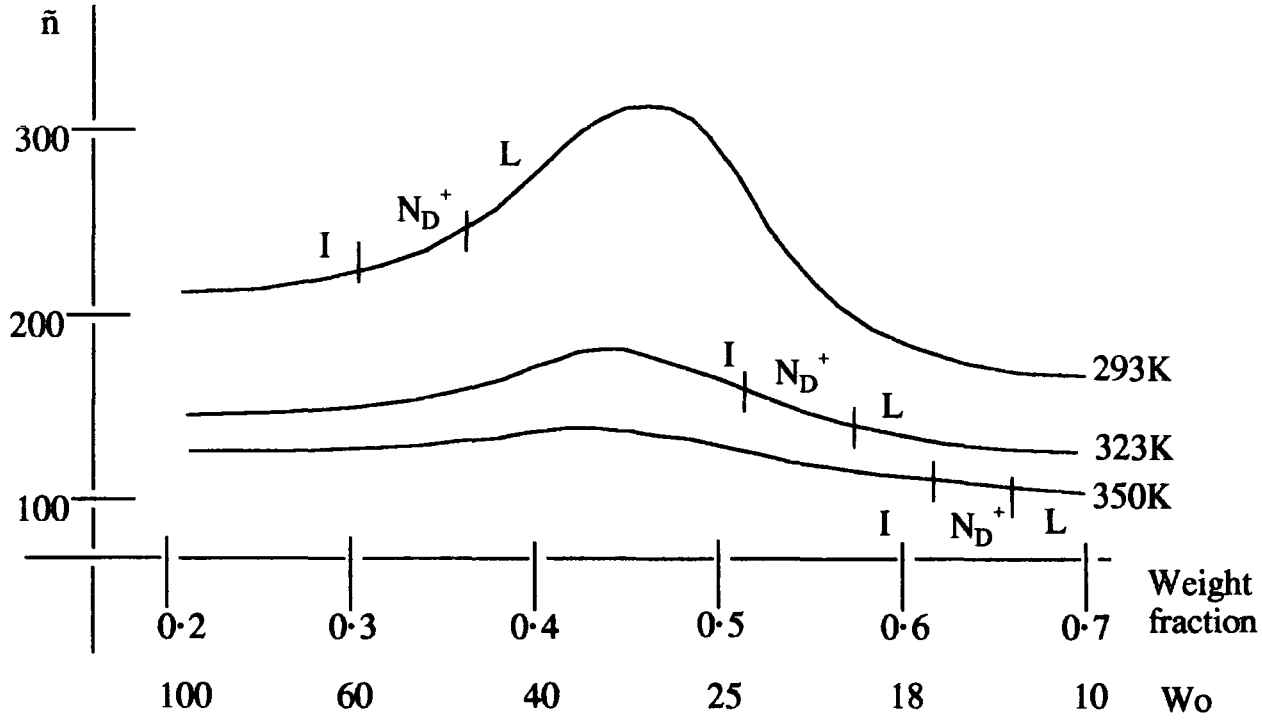

(The nomenclature is explained below.)

The SAXS measurements have shown that the axial ratio of the discotic micelles in all phases ranges from 0.23 to 0.55 with the thickness of the micelle equal to 22 Å. This is in accordance with the extended length of the chain of a perfluoro-octanoate anion[3] being 12.4 Å. The size of the micelle reaches a maximum when the weight fraction is approximately 0.45 at all temperatures, and then decreases. As expected, the size of the micelle increases as the concentration of the surfactant increases. However, the entropy associated with the mixing of the micelles and the degrees of motional freedom oppose growth to infinite L_α-type bi-layers. Nevertheless, it has been calculated[6] that discotic micelles are thermodynamically unstable with respect to L_α bi-layers. The CsPFO/water system contradicts this and Boden *et al*[3,5,7-11] have made extensive investigations as to the reasons why this system displays such behaviour.

For most micelles, intra-micellar interactions determine the shape of the micelle, and these are the dominant interactions at low micellar concentrations. At higher concentrations inter-micellar interactions become important in

controlling the phase behaviour. These interactions are usually repulsive, and are due to interactions in the electrical double layer, or hydration forces of water at the micelle surface. For CsPFO, as figure 8.1 indicates, the discotic micelles remain discrete as the concentration increases. The micelles also shrink. It has been demonstrated that there is an inter-micellar net attractive force between CsPFO micelles at high concentrations[8] that opposes growth to L_α structures. The origin of this force is clearly important in determining the phase structure, but is not fully understood. It has been postulated that at large distances (i.e. inter-micellar distances), the Coulombic force may become attractive in a system that contains very large ions[12]. If the CsPFO micelle is considered to be a large ion, then this is a possible explanation for the attractive force that causes the micelles to contract rather than to grow to form infinite bilayer structures. The details of the behaviour of the counter-ions and the water at the micelle surface are not known, but an understanding of their behaviour at the micelle surface would lead to a greater understanding of the inter-micellar interactions.

8.1.1. Phase diagram of the CsPFO / water system

A complete phase diagram for the CsPFO/D_2O system has been determined[8], principally from analysis of the deuterium NMR spectra. The main features of the phase diagram are shown below.

Figure 8.3 Phase diagram for the CsPFO/D_2O system

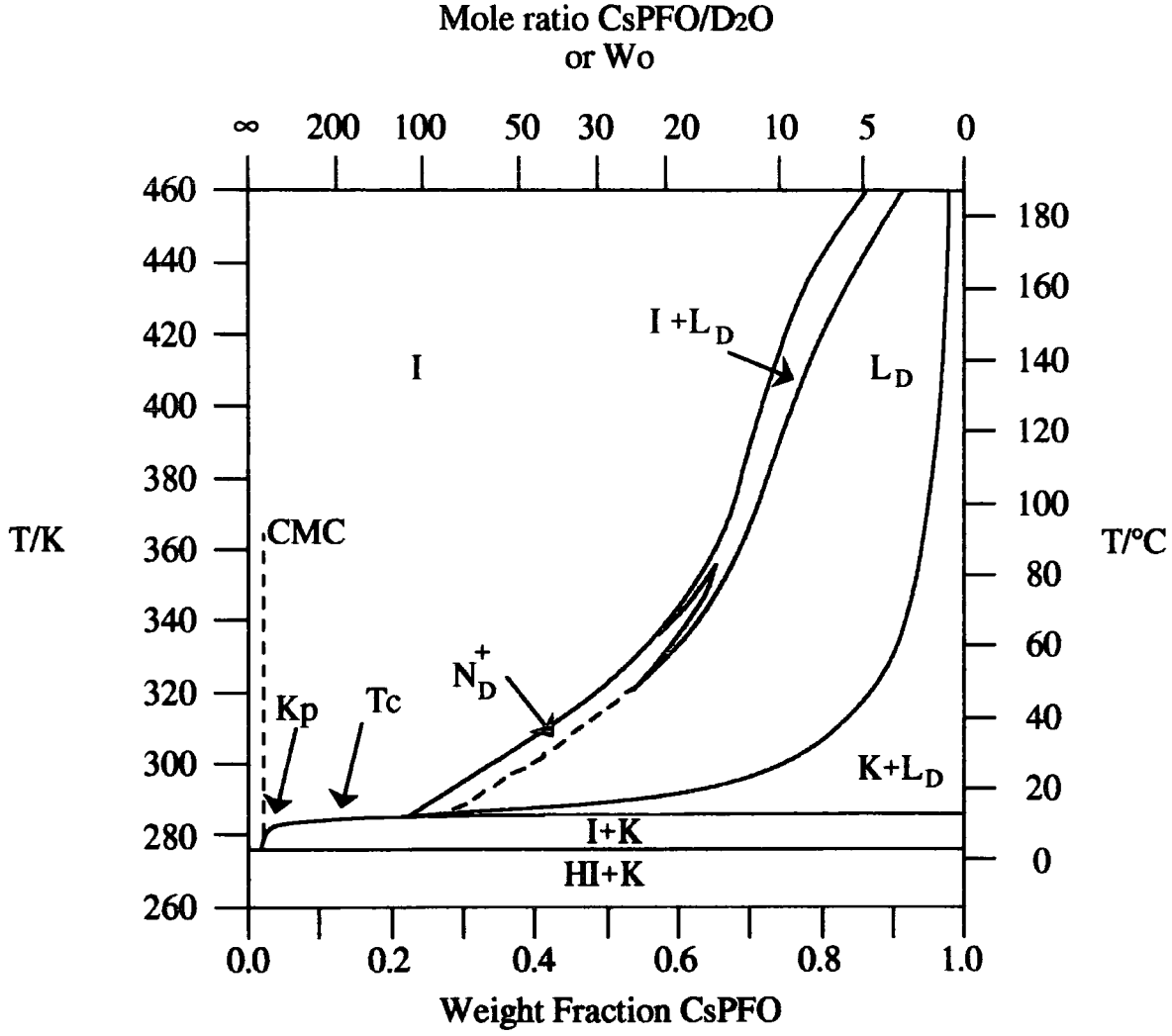

Nomenclature:

K	Crystal
L_D	Lamellar phase
N_D^+	Nematic phase with positive diamagnetic susceptibility
I	Isotropic micellar solution
HI	Heavy ice (D_2O)
CMC	Critical micelle concentration
Tc	Solubility curve for CsPFO in D_2O
Kp	Krafft point

The phase diagram for the CsPFO/H_2O system is essentially the same[13] as the CsPFO/D_2O system. The nematic phase (N_D^+) has a positive diamagnetic susceptibility. This means that a macroscopically aligned sample of the nematic or lamellar phase may be prepared in a magnetic field with a strength greater

than 0.2 T. The phase diagram shows that apart from the pure compounds, there are only three homogeneous single-phase regions: namely the isotropic (I), nematic (N_D^+) and Lamellar (L_D) phases. The other regions are phase co-existence regions which only phase-separate over extended periods of time (>1 day). The solid phase of CsPFO (K) and heavy ice (H) do not mix. The solubility curve is labelled T_C, and meets the CMC at the Krafft point. The Krafft point is the temperature below which micelles will not form: for CsPFO/D_2O this is at 280.0 K. Between 287.0 K and 320.5 K, the boundary between L_D and N_D^+ is shown as a dotted line, which represent a second order phase transition. (A second order phase transition is characterised by a continuous change of chemical potential at the phase transition temperature[14].)

It would seem then that the overall picture to be borne in mind is of the existence of discotic micelles for all phases of CsPFO in water. The amount of water present in the system determines the relative arrangement of the micelles with respect to each other, which in turn determines the phase of the system at that temperature.

8.2. Quadrupolar effects in NMR spectra

In order to gain an understanding of the behaviour of water in the mesophases of CsPFO, NMR spectroscopy of the water has been undertaken. There are three nuclei of water suitable for NMR spectroscopy: namely ^1H, ^2H, and ^{17}O.

Extensive dipolar interactions inhibit the study of the ^1H nucleus in a water rich sample, as both inter- and intramolecular interactions affect the ^1H T_1 relaxation. Proton exchange can average the dipolar interaction if they occur on the same timescale.

^2H NMR of water has been used to investigate and determine the phase diagram[8], as the quadrupolar splittings enable assignment of the phases. However the ^2H nucleus is affected only by intramolecular interactions and by rapid deuteron exchange[15].

In bulk water at pH = 7, the ^{17}O linewidth is broader than at pH = 3, because of the residual scalar interaction between the ^{1}H and ^{17}O nuclei that is modulated by proton exchange. In an anisotropic system such as a liquid crystal, then the ^{17}O nucleus is not affected by rapid proton exchange between solvent and solute, only by slower diffusive exchange between different sites. This makes the ^{17}O nucleus suitable to study the state of water in anisotropic systems[16,17].

This nucleus (^{17}O) nucleus has not been investigated previously in the CsPFO/water system.

8.2.1. Quadrupolar energy levels

Several texts exist describing the effects of a quadrupolar nucleus on an NMR spectrum[18-21]. A brief outline will be given here.

If a nucleus has a spin of $I > \frac{1}{2}$, then it will possess a nuclear electric quadrupole moment. This arises from an asymmetry of the distribution of electrical charges in the nucleus, and as such will respond to an electric field gradient (EFG). A static EFG exists for a nucleus that is in an environment that does not possess cubic symmetry. A dynamic EFG results from time dependent changes in the electric field.

The nuclear electric quadrupole moment is actually a tensor quantity, whose axis system is conveniently chosen to be collinear with the nuclear spin axis. The effective cylindrical symmetry of a rapidly spinning nucleus means that the components of the quadrupole tensor may be represented by a scalar quantity Q and by the nuclear spin vector $\underline{I}$. The electric field gradient at a quadrupolar nucleus is also a tensor quantity, which may be represented by two quantities, eq_{zz} (where e is the unit electric charge and q_{zz} is the maximum component of the field gradient) and η the asymmetry parameter. The electric field gradient at a nucleus is caused by intramolecular effects alone and is affected by the configuration of the electrons near to the nucleus. All filled electronic energy

levels are symmetric and so do not contribute to the EFG. Thus only partly filled energy levels are able to contribute to electric field gradient.

The energy of interaction between a nuclear electric quadrupole moment and a field gradient is quantized as a function of the nuclear spin (I) and the component of the spin m_I. For an axially symmetric field gradient, ($\eta = 0$), the quadrupolar energy levels are given by :

$$E_{EFG} = \frac{eQ\,eq_{zz}}{h} \frac{3m_I^2 - I(I+1)}{4I(2I-1)} \quad \text{..... 10.1}$$

where h is the Planck constant

The quantity $\frac{eQ\,eq_{zz}}{h}$ is termed the quadrupole coupling constant(χ) having units of Hz; it describes the magnitude of the interaction between the nuclear electric quadrupole moment Q, and the field gradient q_{zz}. (Transitions between the energy levels given by E_{EFG} form the basis of nuclear quadrupole resonance spectroscopy or NQR.) For cases where $\eta \neq 0$, q_{zz} will contain an angle dependent term describing the angle between q_{zz} and the electric field gradient.

8.2.2. Splitting of NMR spectra

As is well documented[19,21], nuclear magnetic moments will tend to align in a static magnetic field ($\mathbf{B_0}$). The resulting energy levels are given by:

$$E_{Zeeman} = -\gamma\, \bar{h}\, \mathbf{B_0}\, m_I = -h\, \nu_0\, m_I$$

where γ is the magnetogyric ratio for the nucleus, and ν_0 is the Larmor frequency ($\nu_0 = -\mathbf{B_0}\,\gamma/2\pi$). This is the Zeeman term of the nuclear spin Hamiltonian.

In the presence of a strong magnetic field and a weak EFG, the interaction of the nuclear electric quadrupole moment with the EFG can be considered as a perturbation of the Zeeman interaction (perturbations by electronic shielding, scalar and dipolar coupling will not be considered here). The quadrupolar interaction energy will be different for Zeeman states that correspond to different values of m_I. Hence the nucleus has quantized energy levels:

$$E_{Zeeman,\,EFG}\,h^{-1} = -\nu_0 m_I + \chi \frac{3m_I^2 - I(I+1)}{4I(2I-1)} \frac{1}{2}(3\cos^2\theta - 1)$$

where θ is the angle between the $\mathbf{B_0}$ and q_{zz} (effectively between the magnetic field and the electric field gradient in the molecule).

The usual selection rule for transitions between energy levels is $\Delta m_I = \pm 1$, which implies that the transition frequencies are given by:

$$\nu = \nu_0 - \frac{3\chi(2m_I-1)}{4I(2I-1)} \frac{1}{2}(3\cos^2\theta - 1)$$

where m_I for the above equation ranges from $-I+1$ to I.

Hence the NMR spectrum will consist of 2I lines corresponding to transitions between the different values of m_I. The lines of the spectrum are equidistant (to first order) with a quadrupolar splitting of $\Delta\nu$:

$$\Delta\nu = \frac{3\chi}{2I(2I-1)} \frac{1}{2}(3\cos^2\theta - 1)$$

8.2.3. Intensities

The intensities of the lines in the spectrum are controlled by the magnetic dipole transition matrix element, which is proportional to $A^2 = I(I+1)-m_I(m_I+1)$. For the case of a nucleus of spin $I = \frac{5}{2}$ then A^2 has the following values:

Change of m_I where $\Delta m_I = \pm 1$	A^2
$\pm\frac{5}{2} \Leftrightarrow \pm\frac{3}{2}$	5
$\pm\frac{3}{2} \Leftrightarrow \pm\frac{1}{2}$	8
$-\frac{1}{2} \Leftrightarrow \frac{1}{2}$	9

Therefore for a spin $I = \frac{5}{2}$ nucleus, a quintuplet with components of relative intensity 5:8:9:8:5 is predicted. The figure 8.4 below shows the energy levels for a quadrupolar nucleus of spin $I = \frac{5}{2}$, perturbed by a static electric field gradient, and the resulting NMR spectra.

Figure 8.4 Energy levels and schematic NMR spectra for $I = \frac{5}{2}$ nuclei in the absence and presence of static quadrupolar effects.

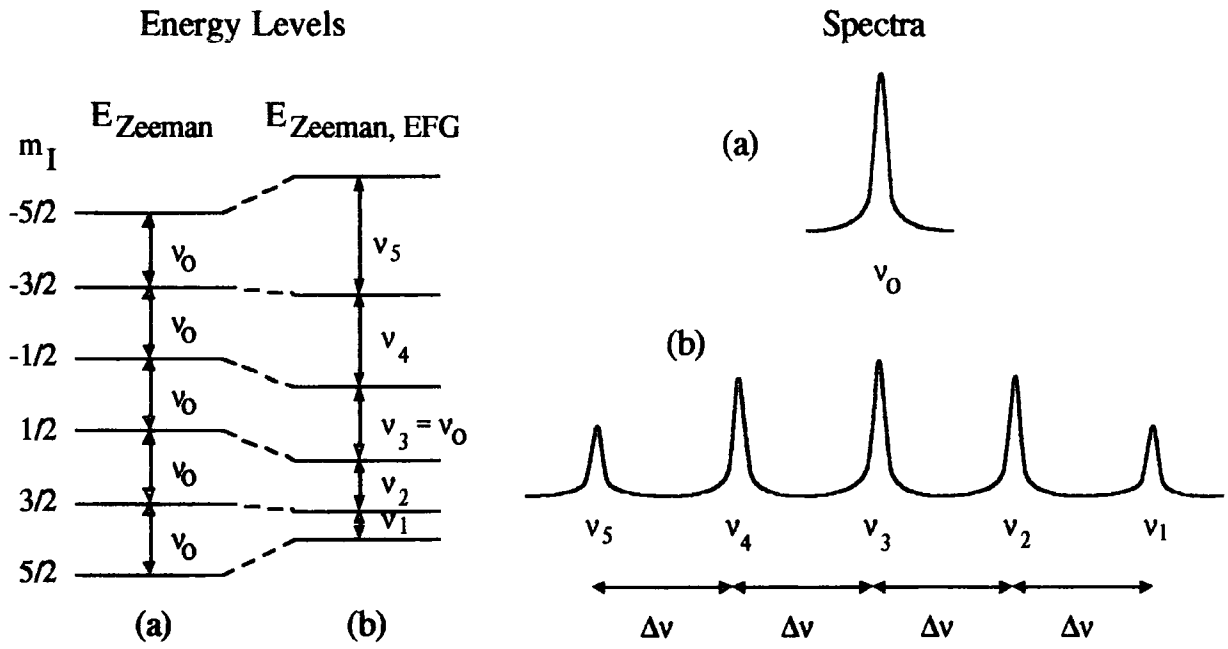

(a) no static quadrupolar effects and (b) first order quadrupolar effects. (Second order quadrupolar effects are only observed when the quadrupolar interaction is strong.)

8.2.4. Effects of molecular orientation.

The above outline applies only for a single crystal oriented such that the angle between the magnetic field and the EFG is θ. The EFG is fixed within the framework of the molecule, so if a molecule moves in some way, then the interaction with the magnetic field $\mathbf{B_0}$ will change. Other molecular orientations will now be considered.

The orientation dependent part of the quadrupolar Hamiltonian is controlled by the factor $(3\cos^2\theta\text{-}1)$. It may be shown that $\langle 3\cos^2\theta\text{-}1 \rangle = 1$. Therefore, for a poly-crystalline or powder sample, where all orientations of the molecule and hence the field gradient, are equally probable, a powder pattern results with peak separation of:

$$\Delta\nu = \frac{3\chi}{4I(2I-1)}$$

For an isotropic liquid, molecular tumbling on a fast time scale (molecular reorientation occurs on a nanosecond time-scale or faster) means that the quadrupolar interaction is averaged to zero. Hence the quadrupolar interaction does not cause splitting of the Zeeman transitions for an isotropic liquid (although the quadrupolar coupling is still a route for relaxation).

For anisotropic mesophases, there is a degree of ordering of the molecules. Thus molecular motion does not cause complete averaging of the quadrupolar splitting. The residual quadrupolar interaction causes splitting of the Zeeman term. However, the quadrupolar splittings are commonly much smaller than for single crystals, due to the molecular motion that causes partial averaging. The degree of ordering of the mesophase may be described by the orientational order parameter S, which represents the average of the orientational fluctuations of the axes of the micelle with respect to the magnetic field $\mathbf{B_0}$.

As was mentioned above, the nematic phase of the CsPFO/water system has a positive diamagnetic susceptibility. Therefore the director n (a vector that represents the average orientation of the mesophase) will align with $\mathbf{B_0}$ in the spectrometer, to produce a macroscopically aligned mesophase. It has been shown[8], that the discotic micelles align with the director n parallel to the magnetic field $\mathbf{B_0}$, rather than perpendicular to the field that would correspond to negative diamagnetic susceptibility.

The situation is further complicated by the existence of multiple sites for molecules in the CsPFO/water system. The surfactant molecules aggregate to form micelles, to the surface of which bind the water molecules. These bound water molecules suffer restricted anisotropic motion, whereas those water molecules that are not bound to the micelle behave much more like bulk water. The water molecules will exchange between the sites, and the life-time at each site will govern whether or not the that site shows quadrupolar splitting. Therefore the quadrupolar interaction must also take account of the fraction of

water molecules that are bound. To proceed further it is necessary to account for the local ordering of the water molecules on the micelle surface, the ordering of the micelles within the mesophase, and the ordering of the mesophase itself. These terms are well described in the literature[13].

8.3 References

(1) Rizzatti M. R., Gault J. D. *J. Coll. Interf. Sci.* **1986**, *110*, 258.
(2) Boden N. *Chem. Brit.* **1990**, *26*, 345.
(3) Boden N., Corne S. A., Holmes M. C., Jackson P. H., Parker D., Jolley K. W. *Journal de Physique (Paris)* **1986**, *47*, 2135.
(4) Tiddy G. J. T., 1992, Personal communication re the structure of the lamellar phase of the CsPFO water system.
(5) Holmes M. C., Reynolds D. J., Boden N. *J. Phys. Chem.* **1987**, *91*, 5257.
(6) Israelachivili J. N., Mitchell D. J., Ninham B. *J. Chem. Soc. Faraday Trans. II* **1976**, *72*, 1525.
(7) Boden N., Jackson P. H., McMullen K., Holmes M. C. *Chem. Phys. Lett* **1979**, *65*, 476.
(8) Boden N., Corne S. A., Jolley K. W. *J. Phys. Chem.* **1987**, *91*, 4092.
(9) Jolley K. W., Smith M. H., Boden N. *Chem. Phys. Lett* **1989**, *162*, 152.
(10) Boden N., Clements J., Jolley K. W., Parker D., Smith M. H. *J. Chem. Phys.* **1990**, *93*, 9096.
(11) Boden N., Clements J., Dawson K. A., Jolley K. W., Parker D. *Phys. Rev. Lett.* **1991**, *66*, 2883.
(12) Sogami I., Ise N. *J. Chem. Phys.* **1984**, *81*, 6320.
(13) Boden N., Jolley K. W., Smith M. H. *Liquid Crystals* **1989**, *6*, 481.
(14) Atkins P. W. *Physical Chemistry*; OUP: Oxford, **1982**.
(15) Woessner D. E. *J. Mag. Res.* **1979**, *39*, 297.
(16) Belton P. S. *Comments Agric. & Food Chemistry* **1990**, *2*, 179.
(17) Belton P. S., Wright K. M. *J. Chem. Soc. Faraday Trans. I* **1986**, *82*, 451.
(18) Lindman B., Forsén S. *Chlorine, Bromine and Iodine NMR. Physico-Chemical and biological applications*; Springer-Verlag: Berlin, **1976**; NMR Basic principles and progress; Vol. 12.
(19) Slichter C. P. *Principles of Magnetic Resonance*; Springer-Verlag: Berlin, **1978**.
(20) Fukushima E., Roeder S. B. W. *Experimental Pulse NMR*; Addison- Wesley: Reading, Massachusetts, **1981**.
(21) Harris R. K. *Nuclear magnetic resonance spectroscopy*; Pitman: London, **1983**.

CHAPTER 9

EXPERIMENTAL NMR OF CsPFO

9.1. Preparation and properties of the CsPFO/water liquid crystalline mesophases.

9.1.1. Preparation of CsPFO

The reagents used in the preparation of the caesium pentadecafluoro-octanoate were Cs_2CO_3 (Aldrich, stated purity: 99.9%) and $CF_3(CF_2)_6COOH$ (Aldrich, stated purity: 98%+). The method used is similar to that published elsewhere[1,2], and is outlined here. The method relies on using stochiometric quantities of reactants. A solution of 18.963 g of $CF_3(CF_2)_6COOH$ in 200 ml of deionised water was warmed to about 60 °C. The raised temperature was used to aid solvation of the pentadecafluoro-octanoic acid. This solution has a pH of about 4. To this, an aqueous solution of Cs_2CO_3, (7.460 g in 50 ml water) was added. Evolution of carbon dioxide causes a foam to form very rapidly on the top of the solution, so it was found best to add the Cs_2CO_3 very slowly with stirring. The stirring was continued until all effervescence had ceased and the reaction is complete. The solution of CsPFO was then evaporated to dryness to yield large, but soft, crystals of CsPFO, (approximately 25 g of CsPFO is obtainable which is a 100% yield). The CsPFO is then recrystallised from ethanol, which leads to a reduction in overall yield. The CsPFO was then stored in a vacuum desiccator, containing phosphorus pentoxide, in an oven at 60 °C.

9.1.2. Characterisation by fluorine NMR

A ^{19}F NMR spectrum (figure 9.1) of a solution of CsPFO in D_2O was acquired using a Bruker AC250 spectrometer (Spectrometer frequency = 235.342 MHz for the ^{19}F nucleus). The spectrum shows seven single peaks. No scalar coupling between fluorine atoms is observed. Typical values for vicinal fluorine-fluorine coupling constants lie in the range 0-5 Hz. At this spectrometer frequency 0-5 Hz is equivalent to 0-0.02 ppm, which is at the limit of the spectrometer resolution.

Figure 9.1. ^{19}F NMR spectrum of CsPFO in dilute solution of D_2O

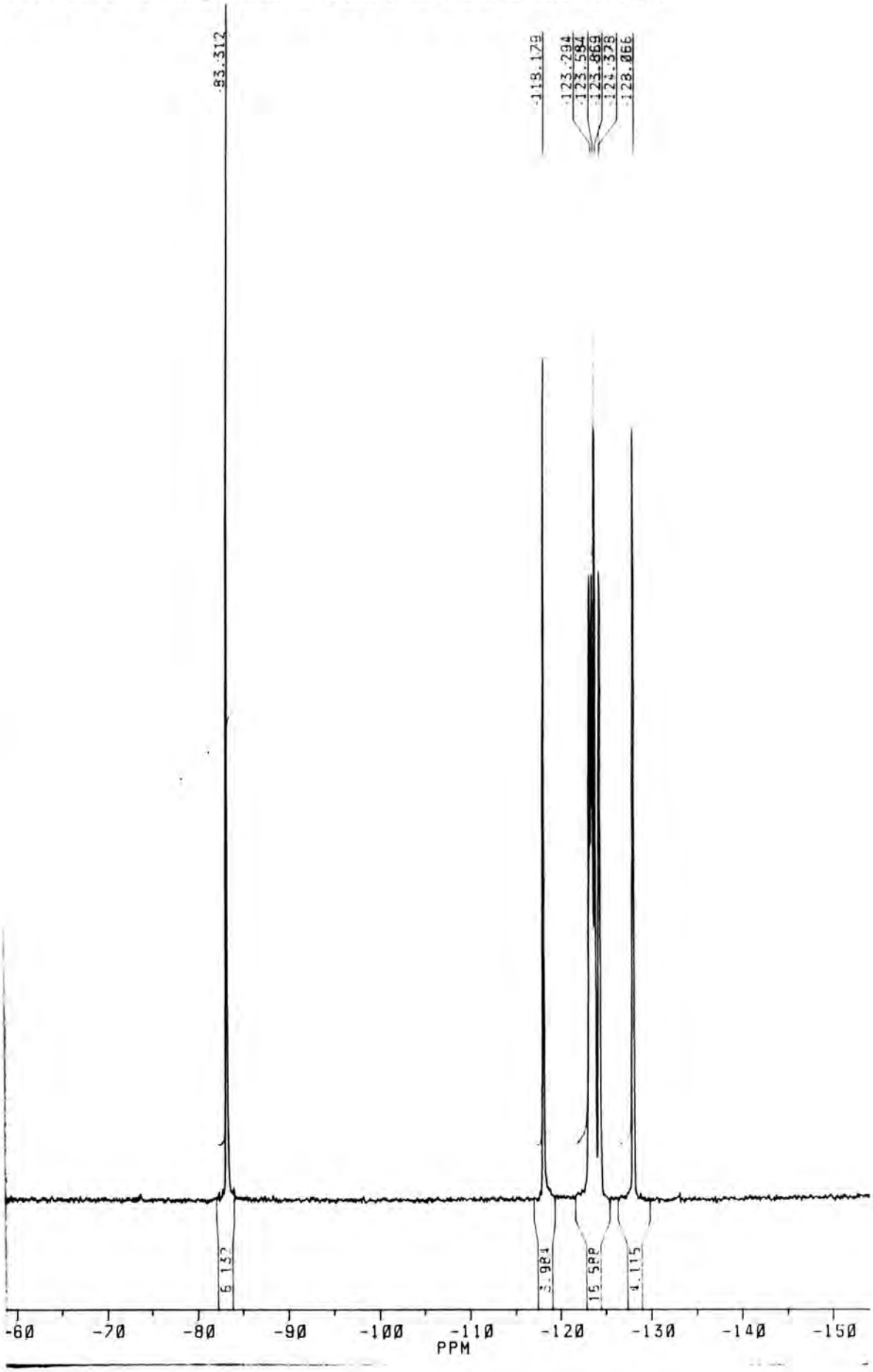

So no clear coupling could be expected to be seen[3]. The seven lines observed correspond to the seven different fluorine atoms positions along the tail of the $C_7F_{15}COO^-$ ion.

The integrals of the peaks indicate that the peak at δ = -83.3 ppm is due to the terminal CF_3 group. The other peaks are then due to CF_2 groups. The peak at δ = -118.2-ppm is due to the CF_2 group next to the CF_3 group. The cluster of four peaks between δ = -123.3-ppm and δ = -124.4-ppm is due to the four CF_2 groups that are between other CF_2 groups. The final peak at δ = -128.1-ppm is due to the CF_2 group next to the carboxylate group. The chemical shift of this peak indicates that these fluorine atoms are the most shielded, as they are able to withdraw electron density from the carboxylate head group. The conclusion from this spectrum is that the spectrum is consistent with a saturated C_7F_{15} chain with no chain branching, and a terminal carboxylate group.

9.1.3. Characterisation by FTIR

It is now necessary to confirm whether the caesium salt or the acid has been produced. Analysis by FTIR will confirm whether the headgroup is protonated or not.

Several spectra were recorded for this purpose. The most informative part of the spectrum to examine is the C=O stretching region around 1700 cm^{-1}. The spectrum of pentadecafluoro-octanoic acid (HPFO) was obtained by casting a film of HPFO onto a calcium fluoride plate from chloroform solution. The spectrum (figure 9.2) shows a maximum absorbance at 1715 cm^{-1}. The band shows a broad subsidiary maximum, indicative of disordered hydrogen bonding in the cast film. This spectrum should be compared with the spectrum of CsPFO on the silicon attenuated total reflection (ATR) crystal. The spectrum of CsPFO on silicon-ATR shows a maximum absorbance at a lower frequency position of 1660 cm^{-1}. The lower frequency position for the salt indicates that the carboxylate group is present[4].

Figure 9.2 FTIR spectra of C=O region of HPFO and CsPFO.

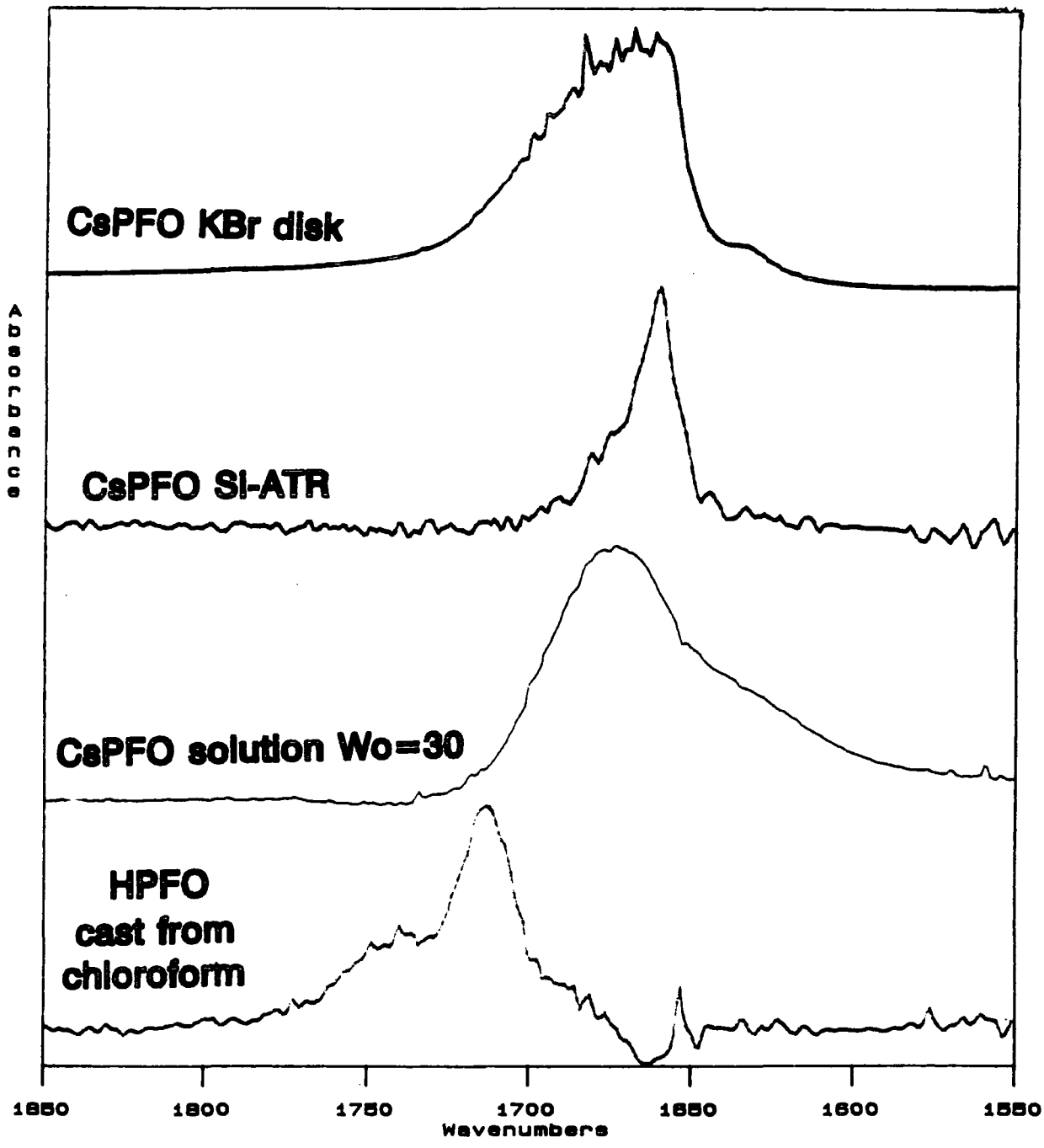

Bellamy[4] quotes a high frequency shift of up to 100 cm^{-1} for the $\nu_{as}(CO_2^-)$ mode, when an α-halogen atom is present. (Usually $\nu_{as}(CO_2^-)$ is at 1550-1610 cm^{-1}.) The shift in the symmetric band is much less reliable. For $Na^+CF_3COO^-$ the bands are at ν_{as} = 1680 cm^{-1} and ν_s = 1457 cm^{-1}. The splitting between ν_{as} and ν_s increases as the delocalised anion becomes more stable, so the perfluorinated species is expected to have a very large splitting. In the spectrum of solid CsPFO on Si-ATR, the band at 1660 cm^{-1} is due to the $\nu_{as}(CO)$ mode of the delocalised carboxylate group. The ν_s mode ought to be visible also, but the splitting is large for metal salts of perfluoro-octanoate anions[1]. Consequently $\nu_s(CO_2^-)$ is obscured by the extensive C-F vibrations in the region of 1200 cm^{-1}.

The spectrum of the solid CsPFO in the KBr disk shows the same frequency maximum as the CsPFO on Si-ATR, which indicates the presence of the carboxylate group. The band shape to high frequency may be due to scattering of the infrared radiation by particles in the sample that are larger than a few microns.

A spectrum of aqueous CsPFO, typical of liquid crystalline mesophase samples to be examined later, is also shown. The sample has a water/surfactant ratio of W_o = 30 and is in the lamellar phase. The frequency position of the ν(C=O) band maximum is 1673 cm^{-1}. This frequency is higher than for the solid CsPFO on Si-ATR and represents the frequency of the hydrated carboxylate group in solution with nearby water and Cs^+ ions. The overlapping peak at 1650 cm^{-1} is the bending mode δ(OH) of water.

Spectra available in the literature[1,5] (figure 9.3) show the spectra of HPFO and sodium-PFO. The main difference that can be seen is in the C=O region where the salt is at a much lower frequency position than the acid.

Thus it is confirmed that the sample made is the caesium salt of pentadecafluoro-octanoic acid - CsPFO.

Figure 9.3 IR spectra of HPFO and NaPFO reproduced from the literature[5].

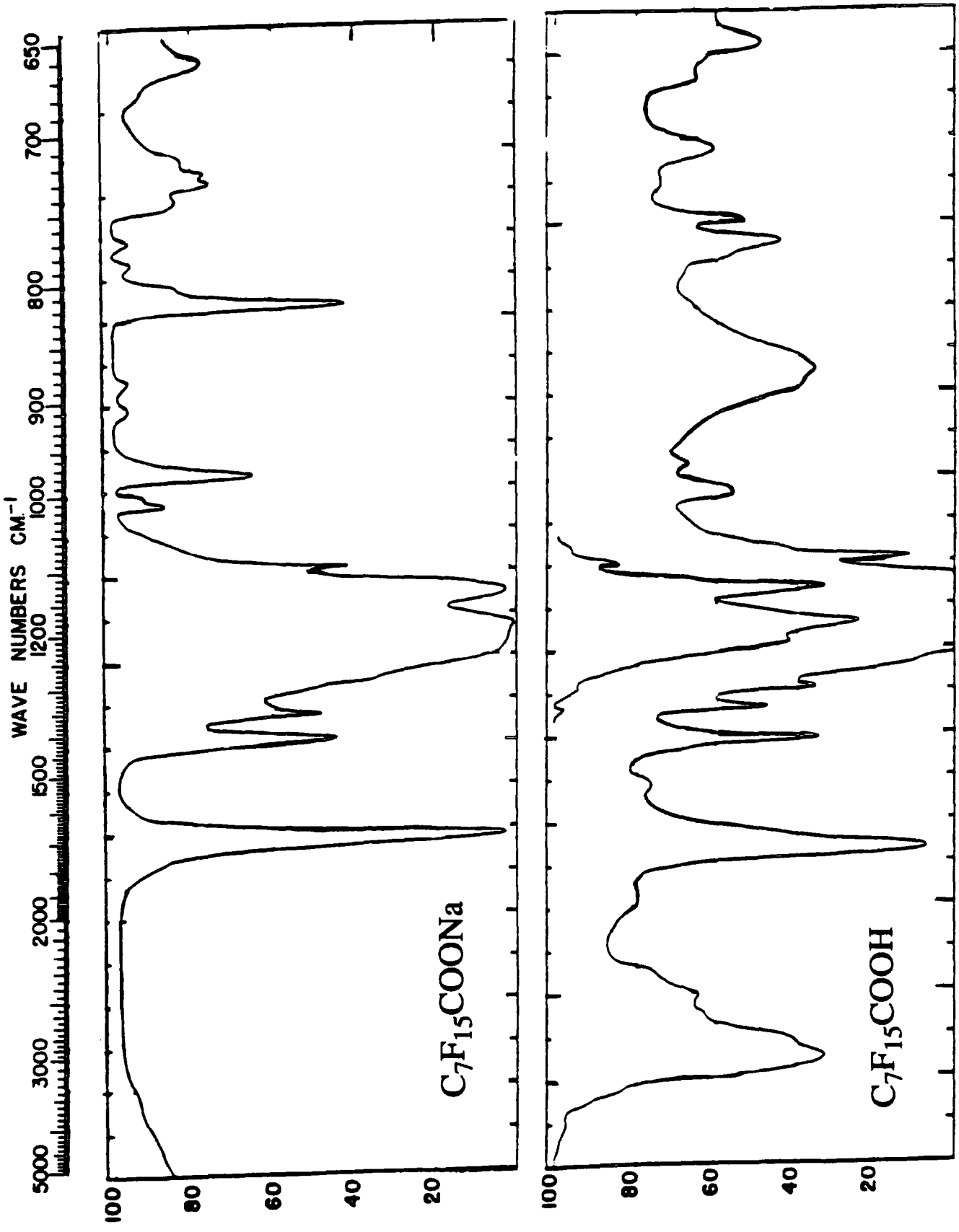

9.2 Measurement of NMR spectra

9.2.1. Sample preparation

The natural abundance of the ^{17}O nucleus is 0.037 %[6]. In order to obtain NMR spectra with good signal to noise within a reasonable time, a large enrichment of the ^{17}O nucleus was used. 1 g of water enriched to 41.2 % with ^{17}O was available (Merck Sharp and Dohme). In order to allow for repetition of experiments, the ^{17}O-enriched water was divided into two portions.

The sample for the NMR experiments was made up as follows: 0.4909 g of the ^{17}O-enriched water was weighed into a 10 mm NMR tube. The CsPFO was made as described in section 9.1.1. CsPFO was weighed then added to the water to achieve the desired mole ratio. The actual amount of CsPFO added to the sample was found by weight difference. Initially the most dilute sample was made. Further samples were made by the addition of CsPFO to the previous sample to make a more concentrated sample. Mixing was effected by heating to about 70 °C in a water bath, taking care that the cap of the NMR tube was not removed by the expansion of air in the sample tube. Shaking the sample made the CsPFO solution appear homogeneous, but also produced bubbles, which were eliminated by the use of a centrifuge. For the most concentrated samples, which were extremely viscous, the most effective method of producing a homogeneous sample was to add very finely ground CsPFO in small batches with warming and centrifuging of the sample between additions of CsPFO.

All the samples from Wo = 204 to 12 contained 0.4909 g of water (41.2 % ^{17}O enriched). The remainder of the samples contained 0.3677 g of water. The average molecular weight of the water is taken as the weighted average of the molecular weight of the two types of water molecule present: i.e. 41.2% × 19.02 + (100-41.2)% × 18.02 = 18.4 g/mol. The molecular weight of CsPFO is 545.972 g/mol.

Table 9.1 Water and CsPFO composition of samples used in the NMR experiments

weight of CsPFO in sample /g	weight of water in sample /g	weight fraction CsPFO	W_o	1/Wo
0.0712	0.4909	0.1267	204	0.00489
0.1460	0.4909	0.2292	100	0.0100
0.1949	0.4909	0.2842	75	0.0134
0.2421	0.4909	0.3303	60	0.0166
0.2796	0.4909	0.3629	52	0.0192
0.3630	0.4909	0.4251	40	0.0249
0.4411	0.4909	0.4737	33	0.0303
0.4831	0.4909	0.4960	30	0.0332
0.7298	0.4909	0.5979	20	0.0501
0.9754	0.4909	0.6652	15	0.0670
1.2071	0.4909	0.7109	12	0.0829
1.0966	0.3677	0.7489	10	0.101
1.3560	0.3677	0.7867	8	0.124
1.5586	0.3677	0.8091	7	0.143
1.8171	0.3677	0.8317	6	0.167
2.1801	0.3677	0.8557	5	0.200
2.7007	0.3677	0.8802	4	0.248

(The column $1/W_o$ has been added here as this quantity is useful when plotting the relaxation times)

Figure 9.4 Location of samples on the phase diagram

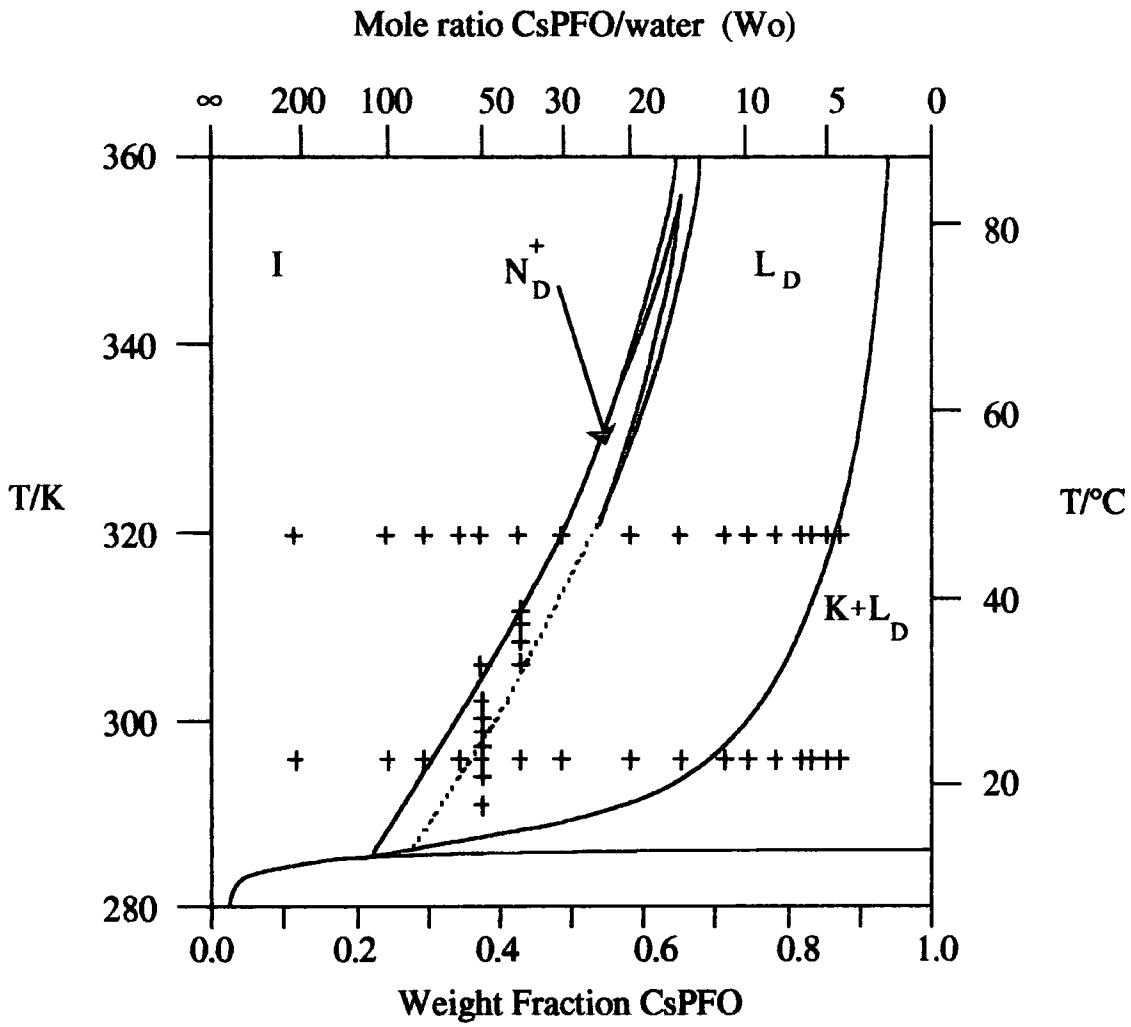

The sample composition and the temperature at which the spectra were recorded are reported on the above phase diagram (for a complete phase diagram see figure 8.3). The samples were made so that the whole range of phase structures could be investigated, at two different temperatures (25 °C and 47 °C).

9.2.2. Recording of Spectra

The spectrometer used was a Bruker MSL 300 with a 7 Tesla superconducting magnet. The spectrometer was tuned to 40.6886 MHz, which is the Larmor frequency of the ^{17}O nucleus, with a sample of pure water (41.2% ^{17}O enriched) in the probe. The power, gain, and sensitivity were each adjusted until the signal intensity from a 90° pulse was such that just less than saturation occurred. The phase of the receiver coils was adjusted such that all the signal is

in the x direction. The probe has to be removed to change the sample and so needs to be reoptimised as the position within the field will change with sample replacement.

To obtain a spectrum the pulse program ONEPULSE is used. This is a single pulse experiment that detects the decay of the magnetization in quadrature (±x and ±y directions), thereby allowing the spectrum to be obtained. The following program parameters need to be set: D1 = duration of 90° pulse, RG = receiver gain, RCPH = receiver phase. In general the pulse durations used were rather longer (20-30 μs for a 90° pulse) than would have been expected from a high power probe. However with this particular probe an instability of signal was observed, caused by probe arcing with the high power. Thus a lower power gain had to be used so a longer pulse time was needed to cause a 90° pulse. A 180° pulse inverts the M_z magnetization such that there is no signal in the x-direction where the detector is. Halving this time value gives the duration of a 90° pulse. For all samples a spectrum was recorded using this ONEPULSE program.

Two different probe-heads were used. One probe-head used a saddle coil as receiver and transmitter, which allowed the sample to be mounted vertically within the magnetic field. The second probe-head was a solenoid coil, in which the sample is horizontally mounted. However, sample handling was found to be difficult with this probe, and would have meant extracting and replacing the sample from the sample tube for each different sample. As the properties being measured depend critically on the water content of the sample, this probe was not used other than for some initial measurements. Typical dead times used were 10 μs.

9.2.3. Sample Temperature.

Temperature control was effected by passing thermostated air through the probe-head, the temperature of which was measured by a thermocouple. The tip of the thermocouple was only a few millimetres away from the sample. The

desired temperature and the rate of heating for the system could both be set. It was found that low to medium rates of heating and a degree of patience were more effective in achieving the desired temperature at the probe head than was a fast rate of heating. This is probably because of the heat capacity of the probe head, which is covered with an aluminium cap in the spectrometer, means that not only the sample is heated by the thermostated air. Discussion with the frequent users of the system as to the accuracy of the temperature at the probe head, suggested that although the temperature was only accurate to ±0.5 K, the temperature of the sample would be precise, providing sufficient time (15-20 minutes) was allowed for the probe head to reach thermal equilibrium[7].

9.2.4. Measurement of spin-lattice relaxation time

The basis of the measurement of spin-lattice relaxation used here is by the inversion-recovery method based on the $\{180°\text{-}\tau\text{-}90°\text{-}T_d\}_n$ pulse sequence. T_d is the delay time, which is set to be at least $5\times T_1$ to allow for Boltzmann populations to be re-established. Typically T_d was set to 100 ms, as the longest T_1 value was found to be 10 ms.

There are several factors that affect the accuracy of the measurement of T_1. Sample inhomogeneities that cause differences in viscosity and hence differences in molecular motions, give rise to different relaxations times. This effect can be reduced by efficient mixing of the sample before insertion into the magnet, and allowing sufficient time (15-20 minutes) for the sample to reach thermal equilibrium.

There are several merits of the inversion-recovery sequence. The method is insensitive to the accuracy of the pulse durations. Since, in this case, the system is always on resonance there are no offset effects[8]. Fast spin-lattice relaxation for the ^{17}O nucleus means that inversion-recovery is an efficient and effective way to measure T_1.

The data were analysed using the program SIMFIT that can handle up to 128 data points. An initial estimate of T_1 is supplied, and an iterative procedure is used to obtain an accurate measure of T_1.

In the case where quadrupolar splitting is observed, the measurement of T_1 is only made on the central line. This is not the true value of T_1, as both single and double quantum transitions between energy levels other than $m_I=\pm\frac{1}{2}$ contribute to the true value of T_1.

9.2.5. Measurement of spin-spin relaxation time

Spin-spin relaxation processes are sensitive to the component of magnetization in the z direction, unlike spin-lattice relaxation. This component M_Z is the same for both the laboratory frame of reference and the rotating frame of reference. Thus a static field in the z direction can act as a source of spin-spin or transverse relaxation. Such fields may typically arise due to magnetic field inhomogeneities. Hence T_2 may be shorter than T_1, but never longer.

The usual method used to measure spin-spin relaxation times is the Carr-Purcell-Meiboom-Gill (CPMG) pulse sequence. For the CPMG[9] with phase cycling, pulse sequence to work, both 90° and 180° pulse durations need to be set. These times are the same as for the single pulse experiment. The whole echo envelope is observed following from one 90° pulse. As the spectrum is just a single line, then the echo is rather narrow. The pulse program stores the heights of the echos in a memory block, the data being analysed later. It is important that sufficient time is allowed for the echos to decay to zero and that the last echo height is zero. The net magnetization in the x-y plane decays to zero, after sufficient time, and the program QUICKFIT takes this last data point as the net magnetization in the x-y plane after infinite time. The program also handles the phase cycling of the 180° x-y pulses, i.e. any mismatch between the field and the receiver that would cause a baseline offset in the decay of the echo heights. QUICKFIT produces a plot of the log of the echo height versus time, the gradient of which is the relaxation time.

Some of the values of T_2 were found to be small (of the order of 1 ms), which is not unexpected for a high viscosity system where correlation times are long. However, this can cause problems with the measurement of the relaxation as the echos decay very rapidly to zero. This problem was compounded by the need to use long pulse durations (20-30 μs for a 180° pulse), and a short time between echos. The relaxation of the spin echos did not appear to behave as expected, probably because selective irradiation of parts of the spectrum was occurring so that pure echos were not being measured. Hence the values of T_2 as measured by the CPMG pulse sequence are not reliable. Instead the spin-spin relaxation data were obtained from line width measurements.

9.3. Results and Discussion

9.3.1. Measurement of the quadrupolar splitting

The single pulse experiments give the spectrum of the ^{17}O nucleus. With reference to figure 8.4, the quadrupolar splitting is quoted here as:

$$\Delta\nu = \frac{1}{2}(\nu_4-\nu_2)$$

i.e. $\Delta\nu$ is the average of the quadrupolar splitting of the first two peaks removed from the central peak. The frequency splitting of the two outer-most peaks is double that of the inner two peaks in nearly all cases. Deviations only occur for large values of the quadrupolar splitting, whenever the excitation band-width is not sufficiently large to excite all the transitions equally. Second order quadrupolar splittings were not observed[10]. The results are given in table 9.2., and are plotted in figure 9.5.

Table 9.2 Quadrupolar splittings of the ^{17}O spectrum for the CsPFO/water system at 298 and 320 K as a function of W_o.

W_o	$\frac{1}{W_o}$	$\Delta\nu$ at 298 K	$\Delta\nu$ at 320 K
204	0.005	0	0
100	0.010	0	0
75	0.013	0	0
60	0.017	1064	0
52	0.019	1204	0
40	0.025	2570	0
33	0.030	3725	0
30	0.033	4537	1343
20	0.050	7165	3020
15	0.067	5119	4379
12	0.083	5975	5518
10	0.100	7718	6650
8	0.125	9277	8112
7	0.143	11306	10314
6	0.167	10366	13349
5	0.200	11521	16753
4	0.250	11500	19103

Figure 9.5 Quadrupolar splittings of the ^{17}O nucleus at 298 and 320 K as a function of $1/W_o$

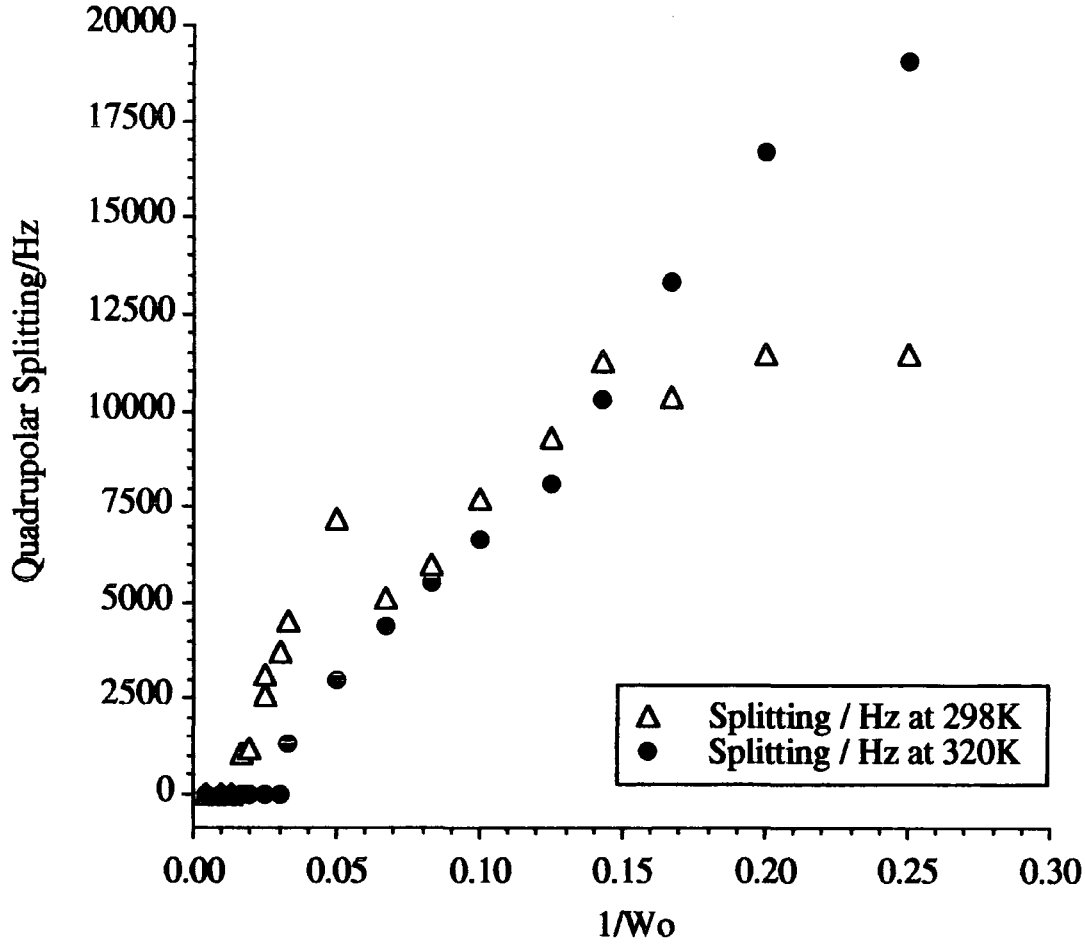

The point at $1/W_o = 0.05$ ($W_o = 40$) seems to have a large random error associated with it, which is evident in other graphs later in this chapter. The data have been plotted in this way according to the method of Tiddy[11]. As may be seen from the above graph, the quadrupolar splitting appears to be a linear function of $1/W_o$ for low values of $1/W_o$ i.e. high values of W_o. At 320 K the quadrupolar splitting is first observed when $W_o = 30$, below which the splitting increases monotonically. At 298 K, there is some scatter in the data, but the quadrupolar splitting ceases to change after $W_o = 7$. This is the point on the phase diagram where there are two phases L_d + K; so the quadrupolar splitting is not reliable here.

The behaviour of the quadrupolar splitting may be described by the following equation[11]:

$$\Delta\nu = \frac{3}{40} p_b E_{Qb} S_b$$

where

p_b = the fraction of ^{17}O nuclei bound to the micelle surface

E_{Qb} = the quadrupole coupling constant of the bound nuclei

S_b = the order parameter describing the time average angle between the electric field gradient and the liquid crystal director axis

Halle has shown[12], that for a two state system (bound water and free water) that the quadrupolar coupling constant for the ^{17}O nucleus is 6.67 MHz, which is very similar to the value found in ice 6.52 MHz. This serves to emphasise that the electric field gradient arises from intramolecular effects. Also, the quadrupolar coupling constant does not vary significantly with temperature. The linear relationship indicates the value of the product of p_b and S_b is a constant.

9.3.2. Quadrupolar splitting as a function of temperature

Figure 9.6 Variation of quadrupolar splitting with temperature for W_o = 40 and 52

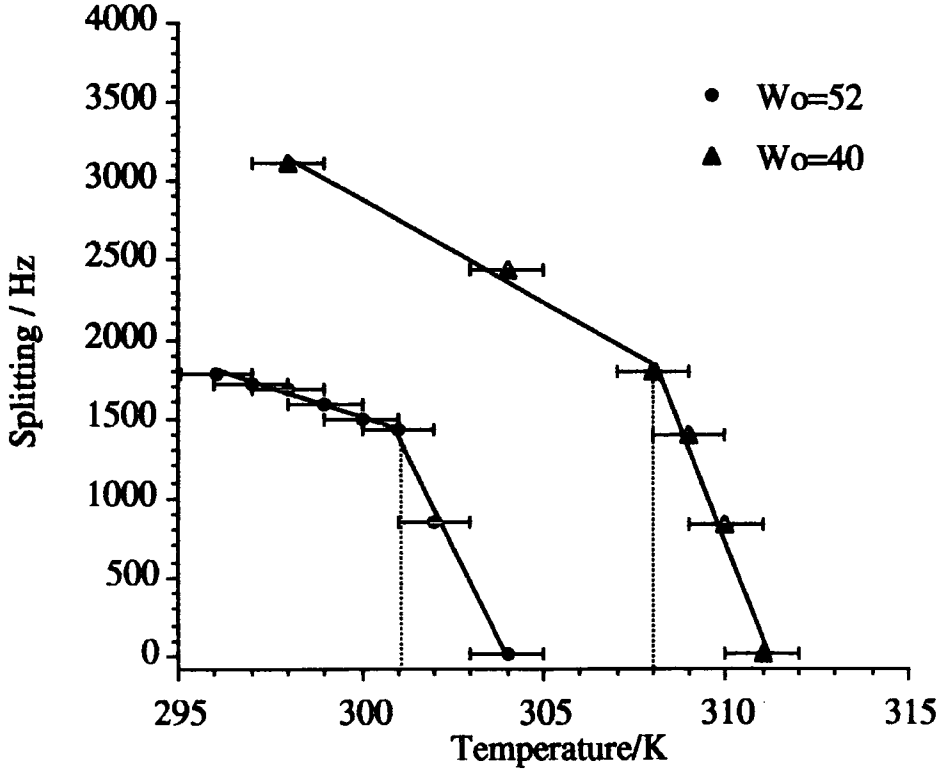

Figure 9.6 shows how the quadrupolar splitting varies with temperature for two samples with W_0= 40 and 52. The initial slow decrease in the splitting is attributed to the effect of the decrease in the order parameter as the temperature is increased. The vertical dashed lines mark the position of the phase transition as on the phase diagram (figure 8.2). The sharp decrease in the quadrupolar splitting after that occurs at the boundary of the nematic/isotropic phase transition. Boden has shown[13] that if the temperature of the system can be controlled to ±0.05 K, then the phase transitions have finite widths in temperature of the order of 0.5 K. i.e. there is a phase co-existence region. So the effect seen here is due to the averaging of the quadrupolar splitting of the ordered nematic phase and the zero splitting of the isotropic phase. Similar results have been seen for the related ammonium perfluoro-nonanoate system[14].

Comparison of the two sets of data on the graph, shows that the phase transition occurs at a lower temperature for the more concentrated samples, as expected. The data also serve to indicate that the correct phases have been prepared.

9.3.3. Line Width Measurements

The width of the absorption line at half-height is equal to $(\pi T_2)^{-1}$. As described above, inhomogeneities in the magnetic field contribute to spin-spin relaxation so the linewidth at half height has a contribution from the magnetic field inhomogeneities. In this case, the relaxation time is termed T_2^*, i.e. T_2 has a contribution from magnetic field inhomogeneities. The measurements of the linewidths are accurate to ±14 Hz, which is the digitisation of the spectra.

Table 9.3 Linewidths and spin-spin relaxation times of the ^{17}O spectrum for the CsPFO/water system at 298 and 320 K as a function of W_o.

Wo	298 K Width at half height / Hz	298 K T_2^* / ms	320 K Width at half height / Hz	320 K T_2^* / ms
pure water	106	3.0	80	4.0
204	118	2.7	95	3.3
100	133	2.4	80	4.0
75	129	2.5	88	3.6
60	130	2.5	79	4.0
52	160	2.0	92	3.5
40	144	2.2	87	3.7
30	182	1.8	122	2.6
20	176	1.8	129	2.5
15	289	1.1	100	3.2
12	282	1.1	145	2.2
10	264	1.2	235	1.4
8	282	1.1	220	1.4
7	275	1.2	213	1.5
6	258	1.2	220	1.4
5	259	1.2	228	1.4
4	227	1.4	206	1.5

Figure 9.7 Linewidth at half height of central peak as a function of W_o

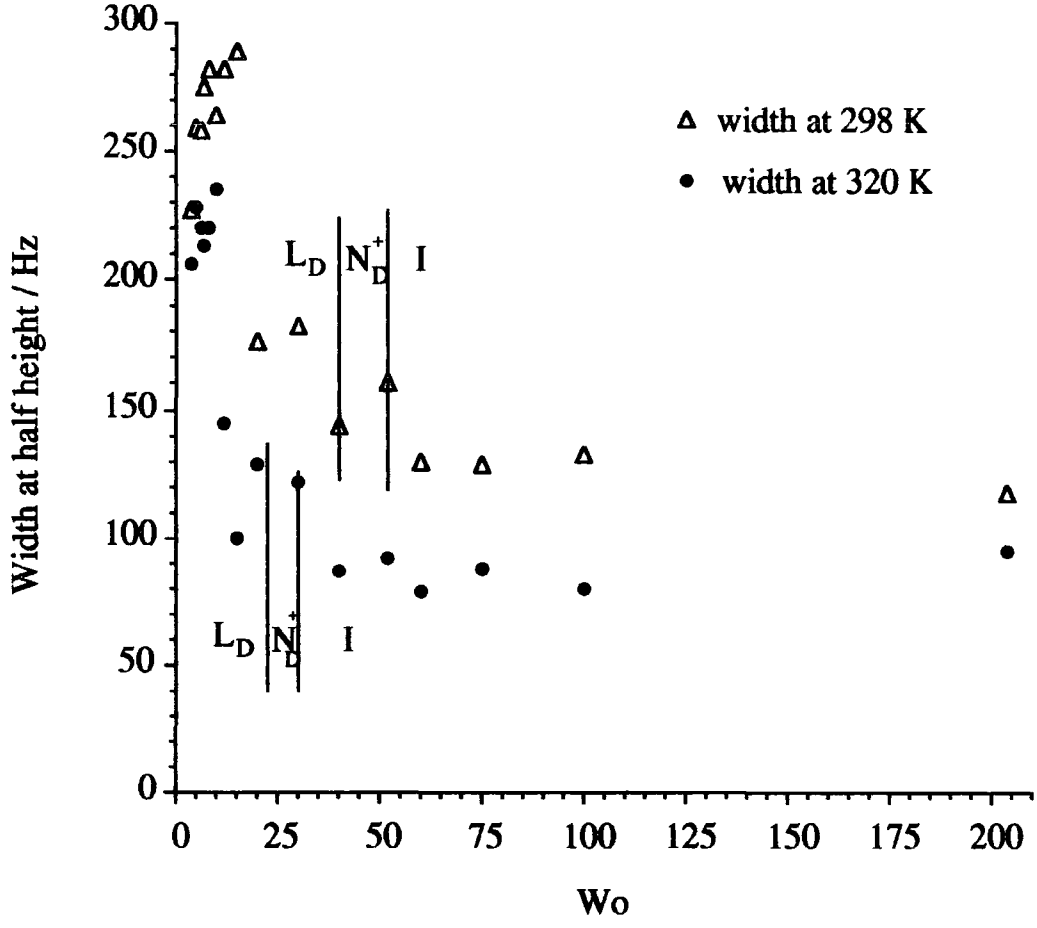

Each point on the above graph has an error of ±14 Hz in the linewidth measurement. The phase boundaries at each temperature are marked on the graph.

The linewidth, and hence T_2^*, remains constant within experimental error for the isotropic phase (high W_o) at each of the two temperatures. In the ordered phases, the linewidth increases significantly, i.e. T_2^* decreases as the ordering increases. This may be explained by the way in which T_2 relaxation is sensitive to molecular motions. In the more ordered phases at low values of W_o, the motions of the water molecules are restricted, because of the orientational preference of the water molecules at the micellar surface. Relaxation is induced by time dependent interactions, which have a characteristic time of decay. This is the correlation time and is a measure of the the time that the molecule is able to

'remember' its orientation with respect to the external magnetic field that causes the relaxation. Fast local motions of the water molecules are characterised by short correlation times. However, in an ordered sample, the orientational preference of the water molecules near to the micelle surface couples with the slow motion of the micelle which is characterised by a longer correlation time. As mentioned above, T_2 is sensitive to the non fluctuating z-component of the magnetic field. T_2 decreases as molecular mobility decreases and the effective correlation times increase[6,8]. Hence the observed increase in linewidth (decrease in T_2^*) on entering the ordered phases indicates that the mobility of the molecules in the ordered phases decreases as W_0 decreases. The data shown on the graph in figure 9.7 are consistent with increased molecular mobility at higher temperatures.

The figure 9.7 shows some scattering of the data in the ordered phases. This may be due to the inhomogeneities in the magnetic field, or incorrect adjustment of the spectrometer conditions when inserting the sample. However the field inhomogeneities are the same for samples in the isotropic phase, which show only small deviations in the line width. It may be that the scatter of the data is caused by not allowing sufficient time for the sample to align within the magnet. This would cause disorder within the sample, with different regions aligned at different angles with respect to the magnetic field, thereby having a different value of T_2^*. If this were the case, then different quadrupolar splittings would arise from each region in the sample. Instances of this were indeed observed (see figure 9.8). However, if the sample was left in the magnet for sufficient time, then a spectrum of five lines is observed (figure 9.9).

Figure 9.8 ^{17}O NMR spectrum of partly aligned sample of CsPFO /water. $W_o = 52$ T=298 K after 1 hour in the magnet.

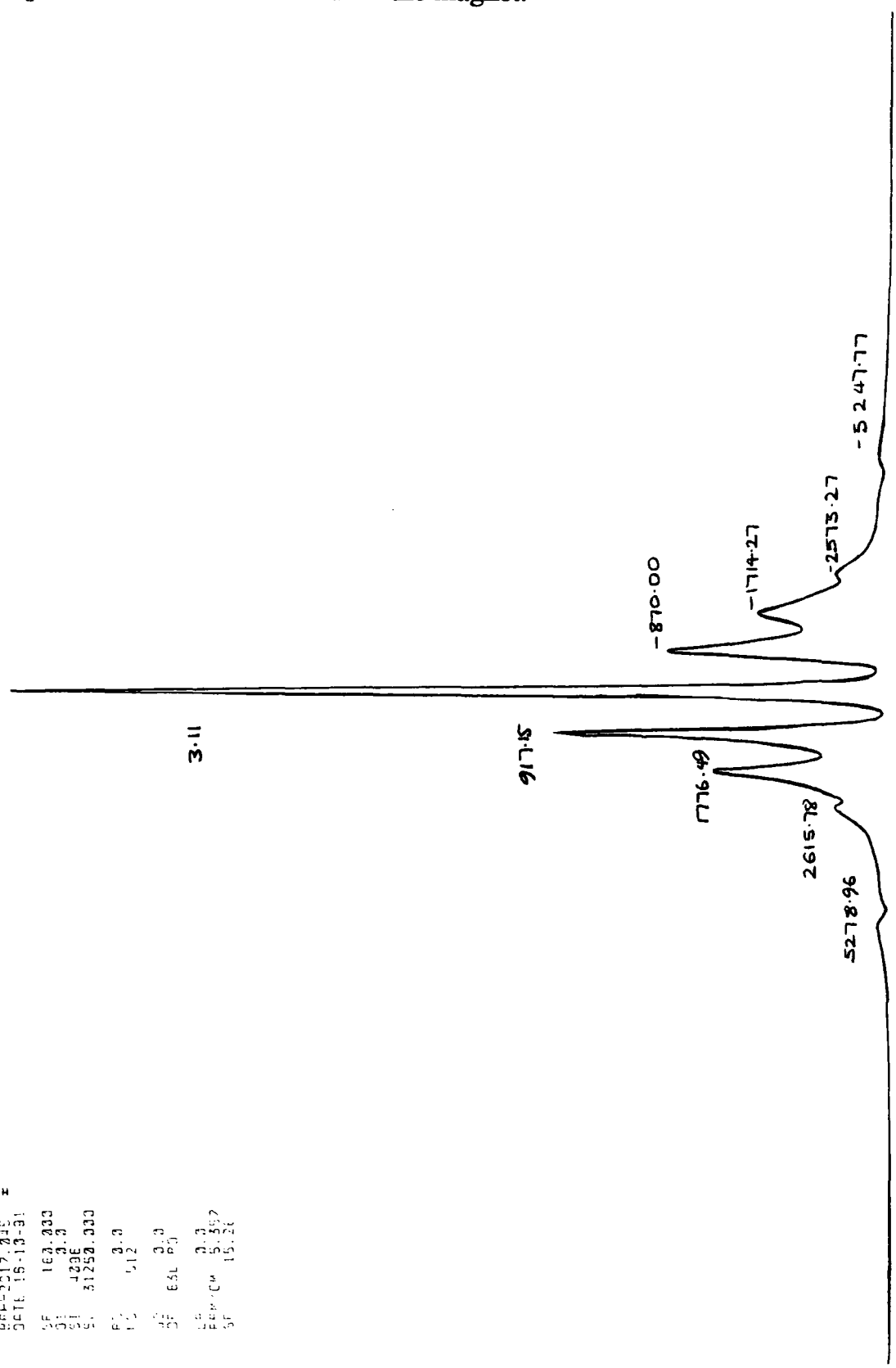

Figure 9.9 ^{17}O NMR spectrum of aligned sample of CsPFO /water. $W_o = 52$ T=298 K 72 hours in the magnet.

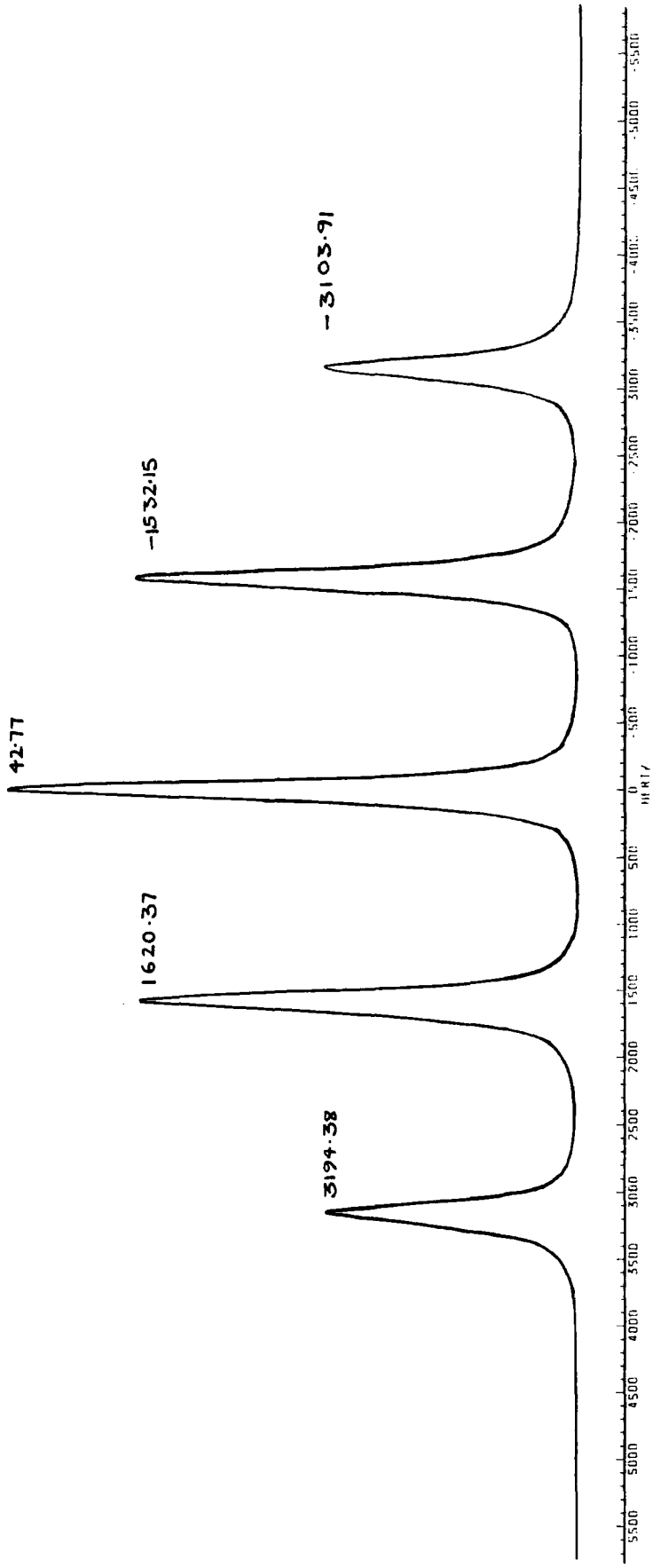

Care needed to be taken then, that all the measurements of linewidth, splitting and relaxation were made on samples whose spectra displayed only one set of lines, in order to be certain that the sample is homogeneous.

As mentioned in chapter 8, the expected intensity ratio from the five lines in the ^{17}O NMR spectrum is 5:8:9:8:5. Although this is not observed exactly for the spectrum shown in figure 9.9, the intensity ratio closely approaches the theoretically predicted ratio. Deviations from the theoretically predicted ratio will occur when the duration of the pulse is long, so that the excitation bandwidth is small, and the peaks are not all excited equally.

However, for some of the very low W_0 samples, there is a large deviation from this expected intensity ratio. The central peak has a very large intensity, which indicates that there are regions of the sample that are in the isotropic phase or contain water only (see figure 9.10). The sample whose spectrum is shown in figure 9.10 is of a very viscous sample in the lamellar phase. In order to make the nematic and lamellar phases with macroscopic ordering, it is necessary to cool the sample from the isotropic phase whilst it is in the NMR magnet[13]. For the more concentrated samples (below $W_0 \approx 15$), the isotropic phase was inaccessible (see figure 8.2 or 9.4 - the phase diagrams) with the equipment used. Although the temperature could have been raised higher, the cap of the NMR tube would probably have been displaced. Instead these macroscopically ordered samples had to be made by cooling from as high a temperature as was achievable without the danger of losing water if the tube cap were displaced. Therefore the appearance of a very large central peak indicated that there was phase separation within the sample into regions that were ordered and showed quadrupolar splitting, and regions that were isotropic. If sufficient time was allowed such that only one set of lines appeared, then the ordered regions were all aligned with the same director to the magnetic field and the measurements made are reliable.

Figure 9.10 ^{17}O NMR spectrum of CsPFO /water. W_o = 5, T=320 K. after 70 hours in the magnet

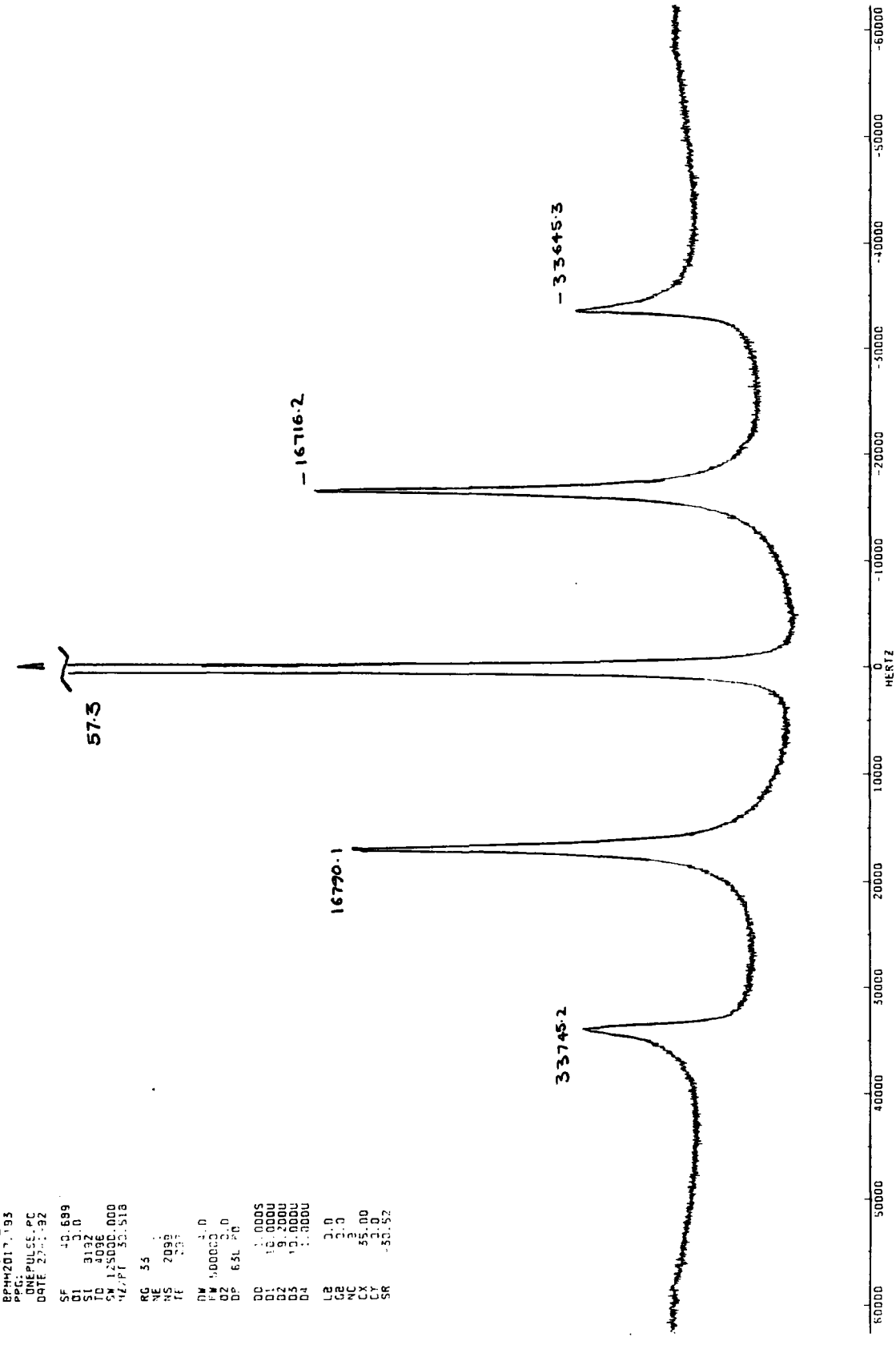

9.3.4. Spin-Lattice relaxation time measurements

The spin-lattice relaxation times were measured by the inversion recovery method as described in section 9.2.4. The results are shown in table 9.4 below. The values of T_1 are given in milliseconds. The quantity R_1 is the reciprocal of T_1.

Table 9.4 Values of spin lattice relaxation times of the ^{17}O nucleus at 298 and 320 K for the CsPFO/ water system as a function of W_o.

Wo	$\frac{1}{W_o}$	T_1 at 298K /ms	R_1 at 298K /s^{-1}	T_1 at 320K /ms	R_1 at 320K /s^{-1}
pure water	0	6.61	151	11.07	90
204	0.005	6.32	158	10.50	95
100	0.010	6.37	157	10.25	98
75	0.013	6.19	162	9.60	104
60	0.017	6.16	162	9.80	102
52	0.019	6.09	164	9.87	101
40	0.025	7.84	128	9.21	108
33	0.030	6.07	165	11.20	89
30	0.033	5.81	172	10.94	91
20	0.050	5.18	193	8.48	118
15	0.067	4.96	202	8.36	120
12	0.083	4.72	212	7.72	130
10	0.100	4.61	217	7.91	126
8	0.125	4.29	233	7.34	136
7	0.143	3.67	272	6.38	157
6	0.167	3.79	264	4.99	200
5	0.200	3.97	252	5.28	189
4	0.250	3.84	260	5.07	197

Figure 9.11 Graph of T_1 versus Wo at 298 and 320 K.

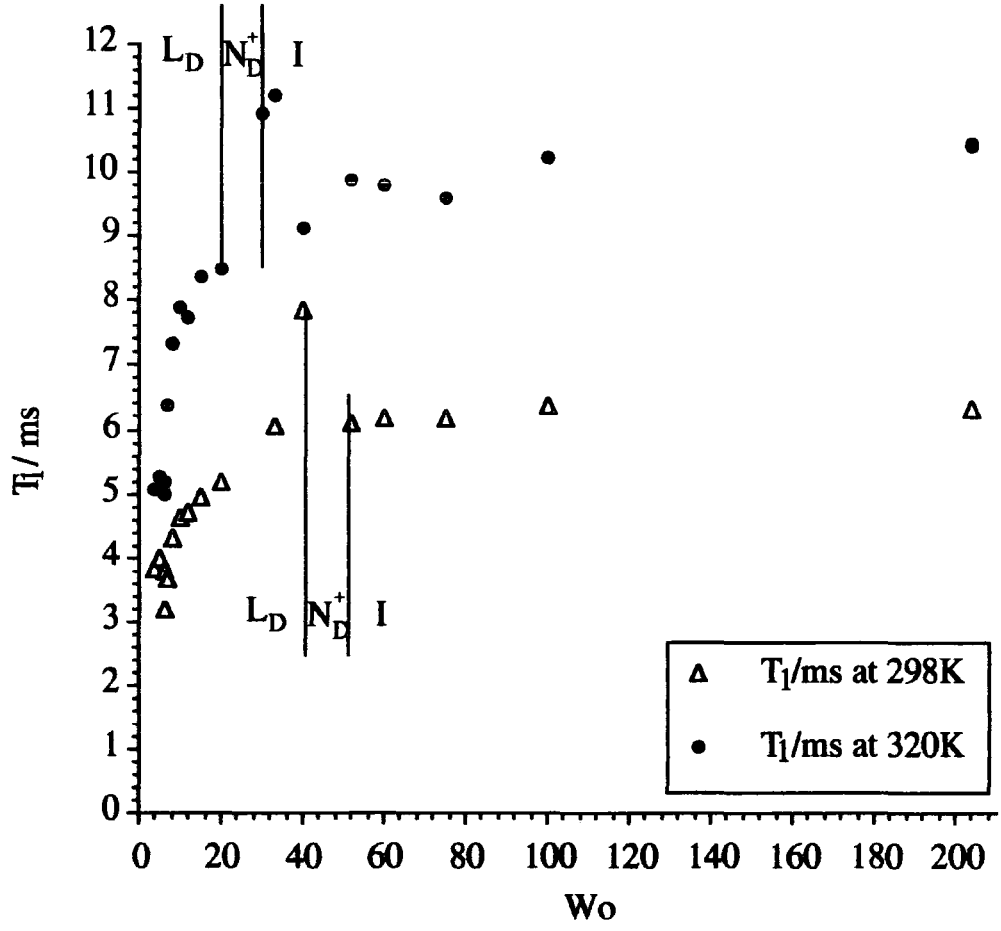

The above graph shows the relaxation times T_1 at the two temperatures used in these experiments. The error in measuring the T_1 values is estimated as being ±0.5 ms i.e. ±5%, which was found by repeated determinations of T_1. The relaxation times at high values of W_o approach those of pure water as measured and shown in table 9.4. There is some scattering of the data, which appears to coincide with the nematic phase. However, the scatter in the data is more likely to be caused by sample inhomogeneities, or the temperature of the sample being higher than assumed. The trends in the data in figure 9.11 indicate that in the isotropic phase, the relaxation time T_1 is very similar to that of pure water. This implies that in the dilute regime, the CsPFO micelles do not perturb the water very much; or that if they do, then the water at the micelle surface exchanges rapidly with the water that is not near the micelle surface. This rapid motion of the water molecules also averages the quadrupolar interaction, so that no

quadrupolar splitting is seen for the samples in the isotropic phase. In the more concentrated and ordered samples at low values of W_o, there is much less free water. Hence there will be a smaller contribution from the diffusive exchange of water between free water and the micelle surface. In this case, where there is little free water between micelles, the motion of the water molecules is restricted to be at the surface of the micelles, and the quadrupolar relaxation time of the water will have a larger contribution from the motions of the micelles themselves. The micelles, being large, will move slowly compared with a water molecule, thus T_1 will be smaller.

This also explains the difference between the two sets of data shown in figure 9.11. At the lower temperature, molecular motions are slower, i.e. the correlation times are longer. Hence T_1 is lower, providing that the motional narrowing condition applies.

9.3.5. Quantitative analysis of spin-lattice relaxation data

Further analysis of the T_1 relaxation data may be carried out using a two site model with rapid exchange between the sites. This is similar to that which was applied to the AOT data in chapter 7. The model has been previously applied to ^{17}O relaxation data[15]. If the exchange process is rapid compared with the relaxation rates at both sites then the following equation applies:

$$R_1 = R_{1f} + (R_{1b} - R_{1f}) \frac{n_b}{W_o}$$

where

$R_1 = (T_1)^{-1}$	observed relaxation rate /s^{-1}
R_{1f}	relaxation rate of water free water /s^{-1}
R_{1b}	relaxation rate of bound water /s^{-1}
n_b	number of water molecule bound per CsPFO molecule

The value of R_{1f} has been found by measuring the value of T_1 for pure water at the two temperatures used in these experiments (see table 9.4). In the graph below, the two sets of R_1 data are presented on the same axes for comparison.

Figure 9.12 Graph of R_1 versus 1/Wo at 298 and 320 K

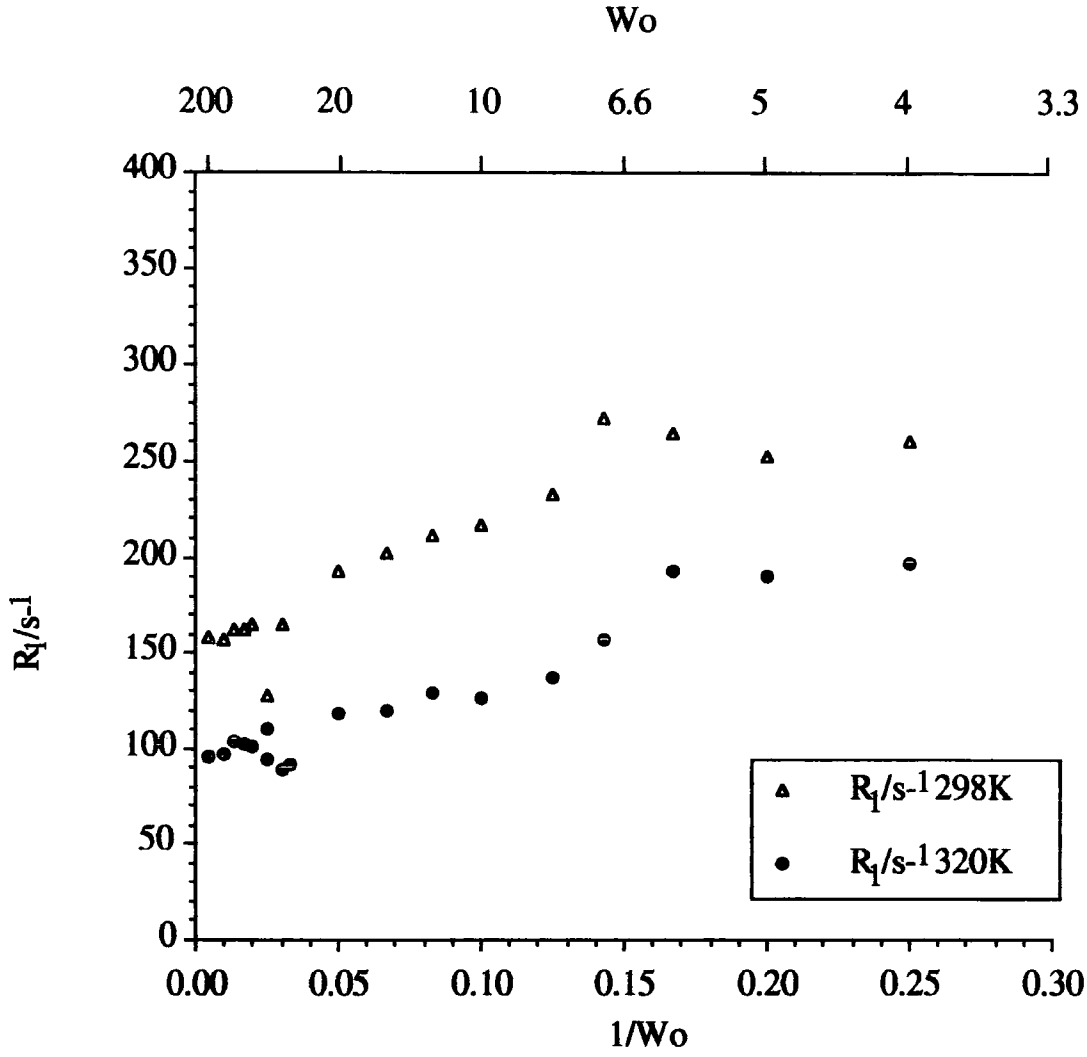

The values of W_o are also shown on the above graph for convenience. The two sets of data will have random errors of approximately ± 5% as found for the T_1 measurements shown in figure 9.11. The next two figures show each set of R_1 data at the two different temperatures plotted as a function of $1/W_o$ as before, but with a linear least squares fit according to the two site equilibrium model.

Figure 9.13 Graph of R_1 versus 1/Wo at 298 K

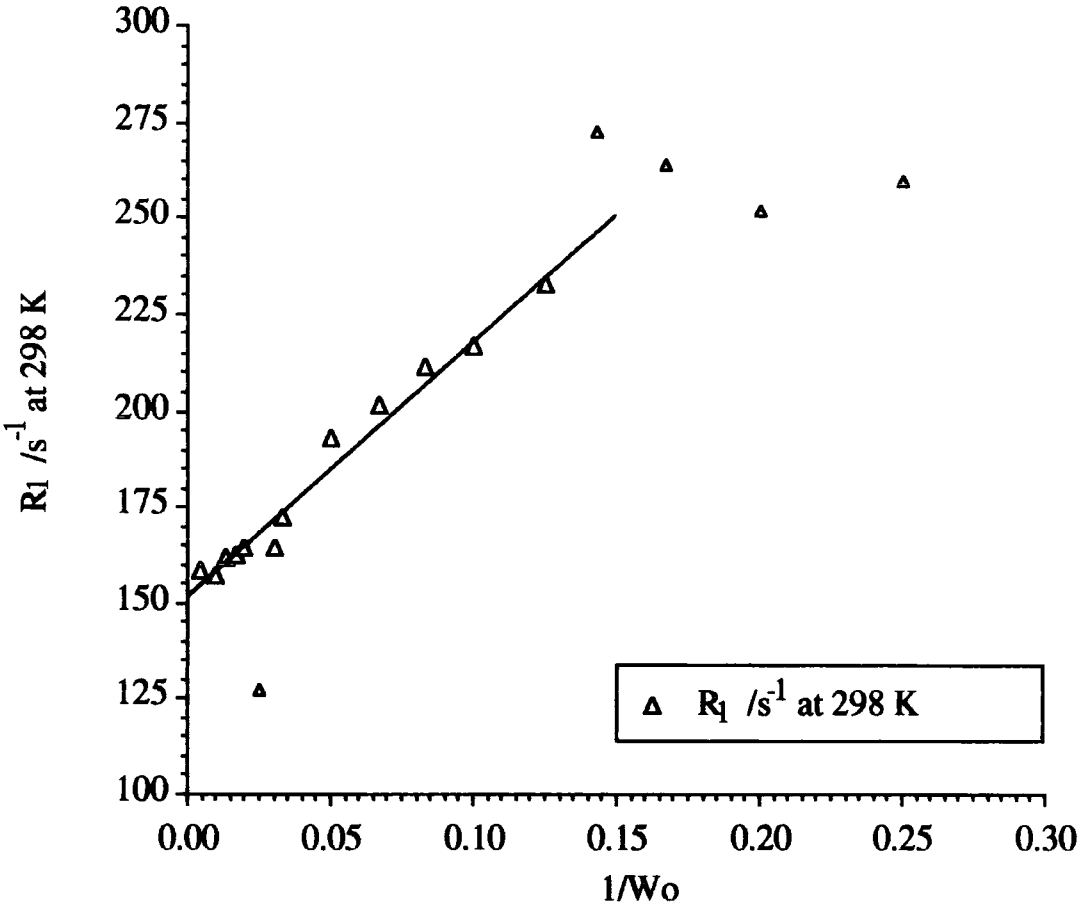

At 298 K: $R_1 = 152 + \frac{672}{W_o}$ correlation coefficient = 0.987

The smaller triangles have not been taken into account in the calculation of the gradient and intercept. The value of R_1 at $W_o = 40$, $1/W_o = 0.025$ clearly appears to have a large error. Those points at $W_o < 7$, i.e. $1/W_o > 0.15$, do not fit to the model at all; these points would not be expected to fit to the two state model as the sample is a two phase mixture of lamellar and crystalline CsPFO when W_o is less than 7 at 298 K.

A similar analysis of the T_1 data at 320 K is shown below

Figure 9.14 Graph of R_1 versus 1/Wo at 320 K

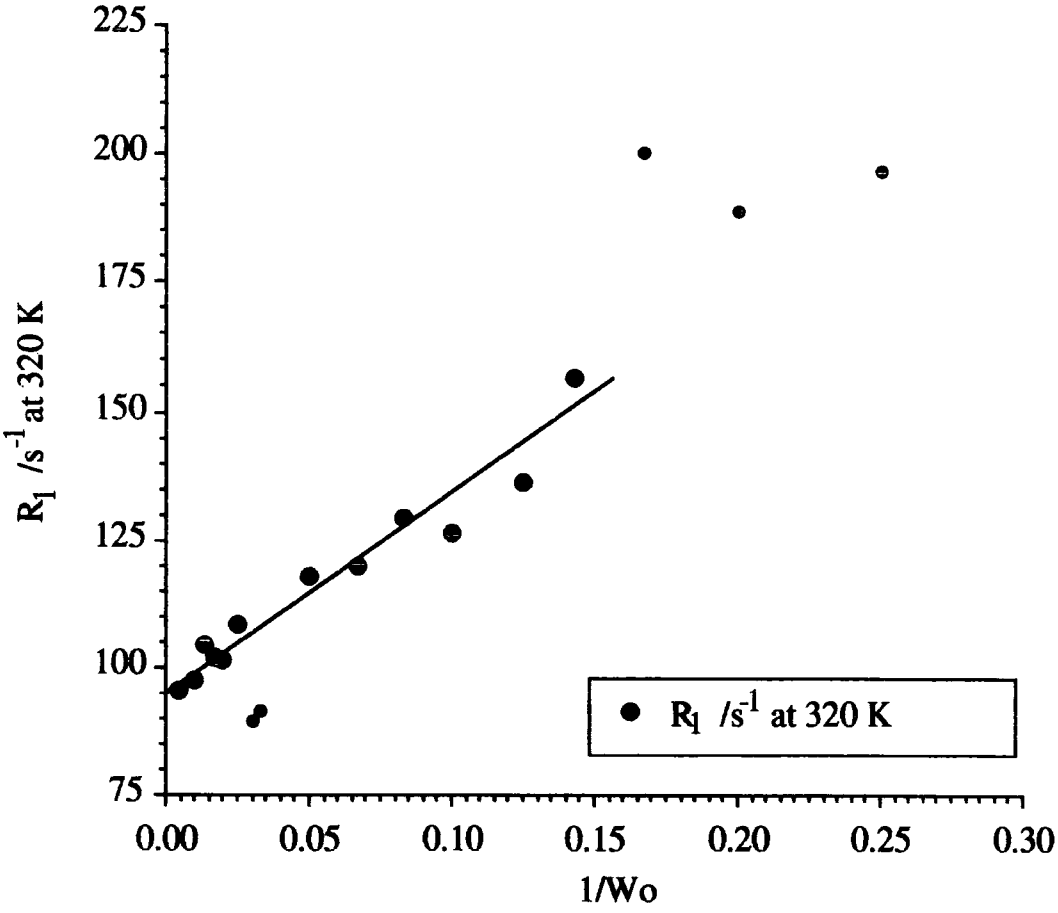

At 320 K: $R_1 = 94.797 + \frac{397.20}{W_o}$ correlation coefficient =0.977

The smaller points were not included in the calculations, but are shown for completeness. Again, there are some errors in the some of the values of T_1 as discussed above. At 320 K, two phases appear when W_o is less than about 5, but the points from $W_o < 6$ have been omitted from the calculations as the deviations are considered to arise from two phases from this point.

The intercept has a value of 94 s^{-1}, and this is similar to the experimental value of 90 s^{-1} found by experiment (see table 9.4). In this instance the gradient is 397 s^{-1}. This value of this quantity is not easily interpreted, but the gradient is nevertheless lower than the corresponding value found at 298 K. This is more easily seen in figure 9.12., where the relaxation rate at the higher temperature is lower than the rate at the higher temperature, as explained at the end of section 9.3.4. The diffusive exchange of water between the surface and the bulk-like

regions may be fast compared with the difference in the relaxation rates between these two regions, in which case that the relaxation of the bound molecules dominates.

The interesting point to note about the above graphs, figure 9.13 and 9.14, is that a straight line does exist, and that no change of slope across the single phase regions is observed. This implies that the behaviour of the water as observed is dominated by the water bound to the micelles, and that the binding does not alter much across the phase diagram.

Now according to the two site equilibrium model as used here, the intercept is equivalent to R_{1f}. At 298 K the value of the intercept is 152 s^{-1}, which compares very favourably with the value of 151 s^{-1} found by experiment (see table 9.4). The gradient has a value of 672 s^{-1}. This is the value of $(R_{1b}-R_{1f})n_b$. Although R_{1f} is known, the values of R_{1b} and n_b are both unknown. The value n_b may be estimated as being in the region of 8≈9, if it is assumed that the Cs^+ ion binds strongly to about 6 water molecules and that the carboxylate group binds somewhat more weakly to 2≈3 water molecules. This may be used to give a value of R_{1b}, and hence rotational correlation times as shown for a series of values in the table 9.5 below. The correlation time is given according to the following equation[16]:

$$R_{1b} = \frac{12\pi^2}{125}\chi^2\left\{1 + \frac{\eta^2}{3}\right\}\tau_c$$

Where $\eta = 0.93$; η is the asymmetry parameter of the electric field gradient, and has the same value as in ice. Using a value of $\chi = 6.67$ MHz, the value for ice discussed previously, the values of τ_c may be found. The results of these calculations are shown in table 9.5.

Table 9.5 Estimated values for n_b and calculated values for R_{1b}

	298 K		320 K	
n_b	R_{1b} / s^{-1}	τ_c / ps	R_{1b} / s^{-1}	τ_c / ps
6	264	4.86	160	2.95
7	248	4.57	150	2.76
8	236	4.35	143	2.63
9	227	4.18	138	2.54
10	219	4.03	134	2.47

These correlation times are of the correct order of magnitude, and there are significant differences between the two temperature. It is interesting to note that the actual value of n_b chosen seems to make little difference to the value of the rotational correlation time.

Here it is important to remember that the quadrupolar splitting observed in these experiments was of the order of 2 - 20 kHz. As the quadrupolar coupling constant for the ^{17}O nucleus is 6.67 MHz, there is therefore only a very small orientational anisotropy. This small anisotropy in the environment of the water molecule is characterised by the residual quadrupolar splitting.

9.4. Conclusions

The interaction between the water and the micelles means that there is a preferred orientation of the water with respect to the micellar surface. As the micelle is large and moves very slowly on the NMR timescale, so the water is in an anisotropic environment This is the source of the residual quadrupolar splitting. The extent of water perturbation has been shown to be small, being restricted to the counter-ions and headgroup only. The nature of that perturbation is such that the orientational anisotropy of the water with respect to the micelle surface is not large.

This seems to be in accord with the conclusions drawn from the AOT work, that the observed behaviour of the water is dominated by the water bound to the ions.

It is interesting to compare this conclusion with work on similar systems. Halle *et al* have studied the ^{17}O relaxation in non-ionic surfactants and in AOT/iso-octane[17]. They find a linear relationship between relaxation rate and $1/W_o$ down to very low water contents, and suggest that 'the surfactant induced perturbation of the water relaxation is local and short range'[18]

9.5. References

(1) Lines D., Sutcliffe H. *J. Fluorine Chem.* **1984**, *25*, 505.
(2) Boden N., Parker D., Jolley K. W. *Mol. Cryst. Liq. Cryst* **1987**, *152*, 121.
(3) Matthews R. S., 1992, Personal communication re fluorine-fluorine coupling constants and chemical shifts.
(4) Bellamy L. J. *The Infrared Spectra of Complex Molecules*; Chapman and Hall: London, **1980**Vol. 2.
(5) Weiblen D. G. In *Fluorine Chemistry*; Eds. J. H. Simons; Academic Press: New York, **1954**; Vol. 2; pp 449.
(6) Harris R. K. *Nuclear magnetic resonance spectroscopy*; Pitman: London, **1983**.
(7) Hills B. P., 1992, Personal communication.
(8) Shaw D. *Fourier Transform NMR spectroscopy*; Elsevier: Amsterdam, **1984**.
(9) Derome A. E. *Modern NMR Techniques For Chemistry Research*; Pergamon Press: Oxford, **1987**; Organic Chemistry Series; Vol. 6.
(10) Lindblom G., Wennerström H., Lindman B. In *ACS Symposium Series*; Eds. H. A. Resing and C. G. Wade; American Chemical Society: Washington D.C., **1976**; .
(11) Rendall K., Tiddy G. J. T. *J. Chem. Soc. Faraday Trans. I* **1984**, *80*, 3339.
(12) Halle B., Wennerström K. *J. Chem. Phys.* **1981**, *75*, 1928.
(13) Boden N., Corne S. A., Jolley K. W. *J. Phys. Chem.* **1987**, *91*, 4092.
(14) Chidichimo G., Coppola L., La Mesa C., Ranieri G. A., Saupe A. *Chem. Phys. Lett* **1988**, *145*, 85.
(15) Belton P. S., Wright K. M. *J. Chem. Soc. Faraday Trans. I* **1986**, *82*, 451.
(16) Halle B., Carlström G. *J. Phys. Chem.* **1981**, *85*, 2142.
(17) Carlström G., Halle B. *Langmuir* **1988**, *4*, 1346.
(18) Carlström G., Halle B. *J. Chem. Soc. Faraday Trans. I* **1989**, *85*, 1049.

CHAPTER 10

INFRARED SPECTROSCOPY OF CsPFO

10 Infrared investigation of the CsPFO/water system

An investigation of the vibrational spectra of the CsPFO/water system complements the findings from the NMR investigation. This is because vibrational spectroscopy probes environments on a much smaller scale and faster time scale than NMR owing to the difference in the wavelengths and observation times of the two techniques. The vibrational spectra are more sensitive to local dynamics than are NMR spectra, so any effects seen with infrared spectroscopy will be closely correlated to the local molecular environment. Conversely it may be expected that the infrared spectra will not be so sensitive to the high length scale ordering of the CsPFO micelles.

10.1. Sample preparation and measurement of spectra

The samples used for the infrared spectroscopic measurements were made in a similar manner to those samples used in the NMR measurements previously described in chapter 9. It was, however, possible to make all the samples at once, because the quantity of water available was not restricted, as it was with the $H_2{}^{17}O$.

D_2O with 4% v/v H_2O was used to make up the samples, since the phase diagram for the CsPFO/D_2O system is more accurately known than the H_2O system[1,2]. Using D_2O also allows the carbonyl band in the infrared spectrum to be examined more easily, as there is no overlap of the ν(CO) band by the bending mode δ(OD) of water.

Attenuated total reflection (ATR) infrared spectroscopy was attempted on the CsPFO/water samples. However, it was not possible to reproduce the spectra of the same sample. The causes of this might have been:

(1) Inadequate sample coverage of the ATR crystal. This would have been most likely to occur with the most viscous samples where $W_0 \leq 10$. The arrangement of the ATR crystal and mount is such that the sample must be injected through a narrow tube of length ≈ 15 mm, and then spread out

over the surface of the crystal. When the crystal mounting assembly was dismantled, it could be seen that the surface of the crystal was not completely covered with the sample. To circumvent this, smearing the most viscous samples onto the whole face of the crystal was attempted. This did not give any more reproducible data.

(2) A second problem was the adsorption of the CsPFO onto the surface of the ATR crystal. The ATR crystal is made from zinc selenide. Significant intensity in the ν(CF) region of the spectrum was observed after the sample had been removed from the crystal by washing with water. CsPFO is very soluble in water, but water was not able to remove all the CsPFO from the ZnSe ATR crystal. Cleaning the ATR crystal by refluxing in a still with alcohol was necessary to remove all traces of the CsPFO. ZnSe is known to be attacked by acidic species, so the reason for the non removal of CsPFO by water alone may be that the CsPFO had reacted with the surface of the ZnSe crystal, to become strongly bonded to it.

Therefore it was decided that ATR spectroscopy could not be used to study the CsPFO/water system. Instead, transmission infrared spectroscopy using CaF_2 or AgCl plates was carried out.

The advantage of using transmission spectroscopy was that the temperature could be controlled accurately with the available equipment. This was important to enable a direct comparison between the results from the vibrational spectra and the NMR spectra where temperature control of the sample was very important.

The disadvantage of the transmission arrangements is that macroscopic ordering of the sample was not available. However, this is insignificant, as any ordering effects would not be seen unless the sample were macroscopically ordered and polarized radiation were used.

The pathlength of the transmission cell may be accurately determined by interference fringes in an empty cell (see chapter 4).

Samples with W_0 values of 4,5,6,7,8,10,12,15,20,30,50 and 100 were made, to cover the spread in W_0 values used for the NMR measurements. These values extend over the phase diagram (chapter 8) from the isotropic, through the nematic and lamellar phases to the very low water content mixed lamellar/crystalline phase.

10.2. Infrared spectra - results and discussion

A typical spectrum is shown in figure 10.1. This is a sample of CsPFO/D_2O at a mole ratio of $W_0 = 20$, held between two CaF_2 plates with a pathlength of 8 μm at a controlled temperature of 298 K. The assignments for the bands are as follows:

Table 10.1 Assignments of bands in the vibrational spectrum of CsPFO/D_2O

$\frac{\bar{\nu}}{cm^{-1}}$	assignment[3,4]
≈ 3400	decoupled ν(OH)
≈ 2500	coupled ν(OD)
1675	$\nu_a(CO_2^-)$
≈1380	overtone of ν(CF) deformations
1150-1220	ν(CF)

Unfortunately is has not been possible to make a firmer assignment of the bands near 1200 cm^{-1}, other than that they are ν(CF) vibrations. Extensive literature searches did not yield any information on the assignments of bands in the spectra of fluorocarbon chains. Bellamy[4] comments that the assignment is particularly difficult. However, the general principal of symmetric vibrations having a lower energy than antisymmetric vibrations implies that the higher frequency vibrations probably correspond to antisymmetric CF_2 stretching vibrations.

Figure 10.1 Infrared transmission spectrum of CsPFO/D_2O W_0=20, T=198 K.

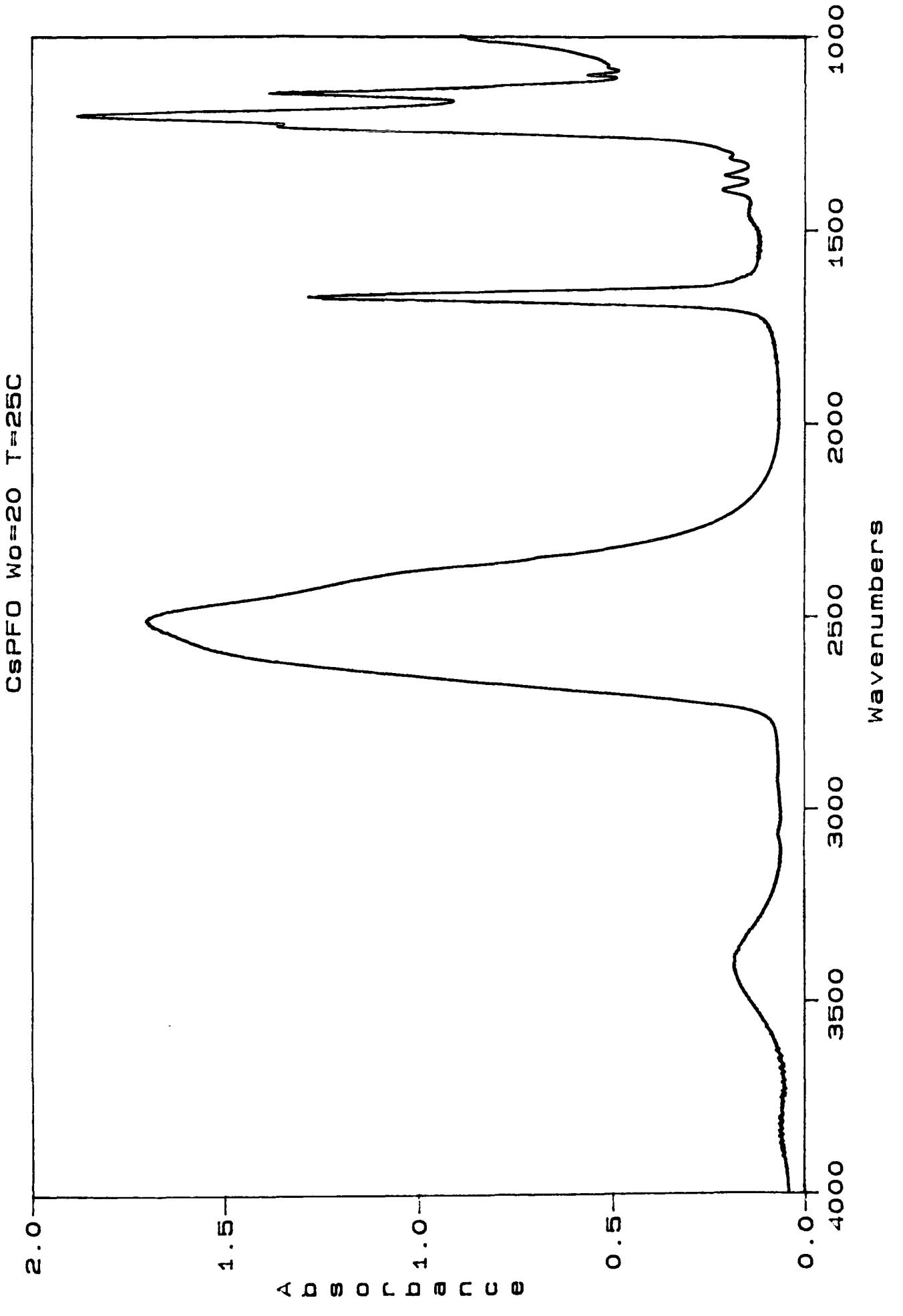

Figure 10.2 Infrared transmission spectra of decoupled ν(OH) band at 298 K. W_o = 4,5,6,7,8,10,12,15,20,30,50

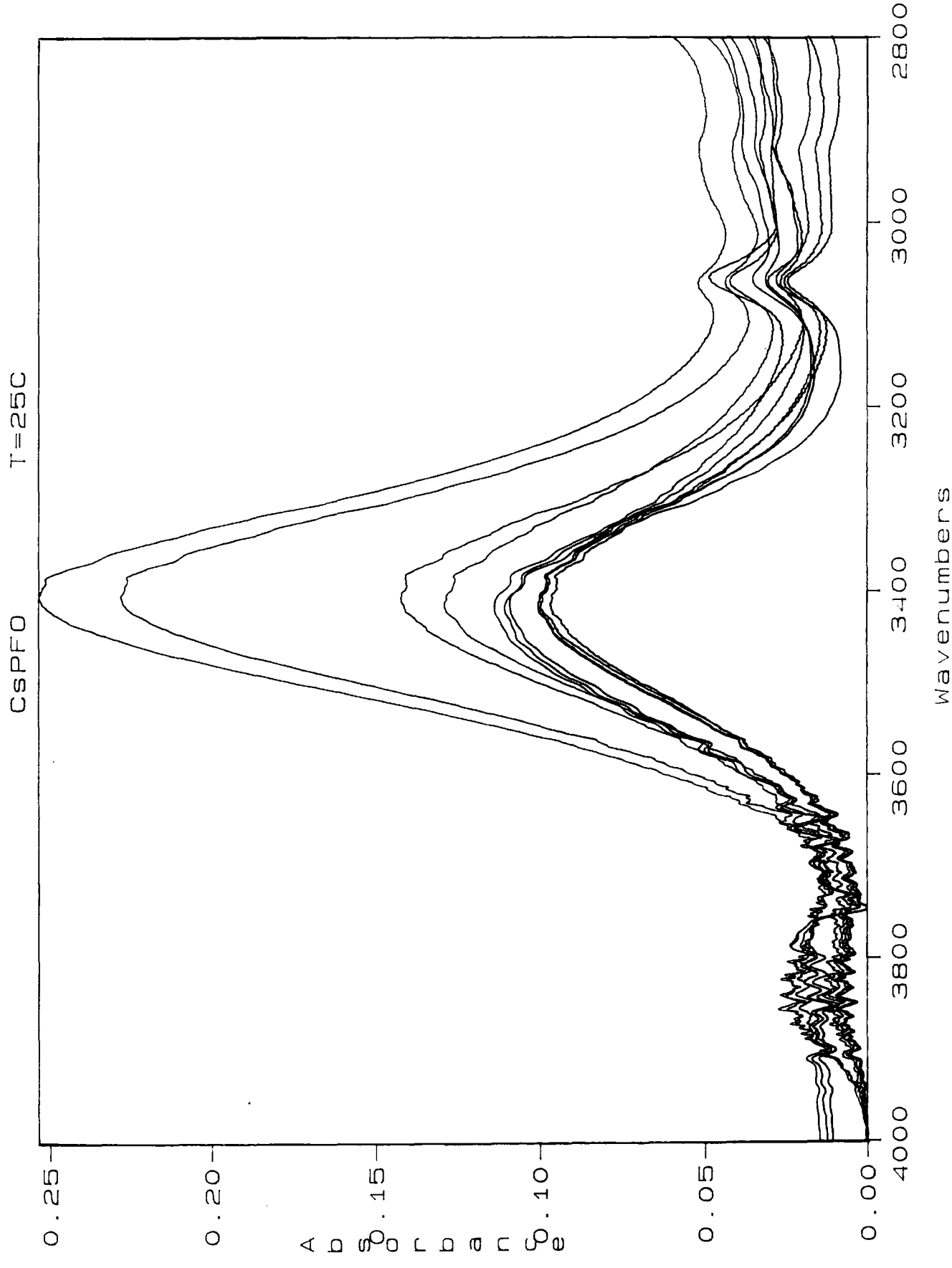

Figure 10.3 Infrared transmission spectra of decoupled ν(OH) band at 320 K. W_o = 4,5,6,8,10,12,15,20,30,50

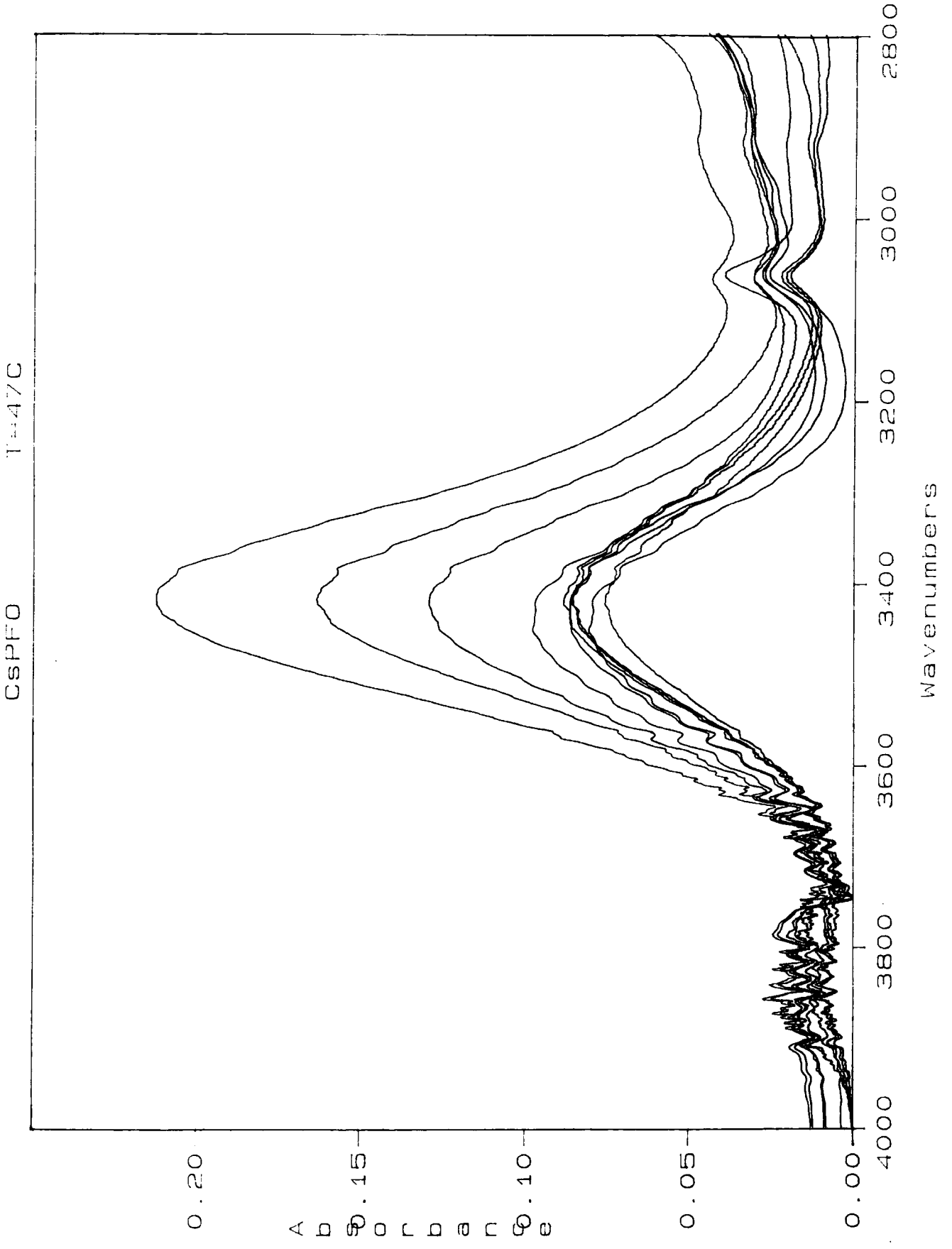

The parameters of the decoupled ν(OH) band at the various W_0 values selected are shown in table 10.2. The frequency position is taken as the position of maximum absorbance allowing for any spectral noise. The width at half height is measured by extrapolating a baseline between 4000 and 2800 cm^{-1} for each spectrum, and finding the difference in frequency position between the two points where the value of the absorbance is half the maximum value. The integrated area of the band is found relative to this same baseline, by using the software program that controls the spectrometer.

Table 10.2 showing parameters of the decoupled ν(OH) band at 298 K

Wo	frequency cm^{-1}	width cm^{-1}	Integral cm^{-1}	Pathlength μm	Integral pathlength
4	3407	248	22	8.0	2.8
5	3415	233	24	8.0	3.0
6	3411	250	25	8.0	3.1
7	3416	247	23	8.0	2.9
8	3408	244	22	8.0	2.8
10	3421	246	26	8.0	3.3
12	3419	243	23	8.0	2.9
15	3418	236	22	8.0	2.8
20	3407	239	32	8.0	4.0
30	3407	240	53	8.0	6.6
50	3405	242	60	8.0	7.5
100	3402	244	284	35	8.1

The frequency position of the ν(OH) band at 298 K is shown in figure 10.4 below. At low values of W_0 the frequency position shows some scatter. This may be due to an error in measuring the frequency position, but the spectra do show a clear band shift (figures 10.2 and 10.3). At 298 K, the CsPFO/D_2O system exists as two separate phases (L_D + K) below $W_0 = 10$. This microscopic heterogeneity means that the amount of L_D phase that is being observed is unknown. Not until $W_0 = 10$ does the system become single phase. Therefore at the very lowest W_0 values, the existence of two phases means that the water may be in a wide range of environments, some much more dilute than others. Thus

the frequency position is erratic. Above $W_0 = 10$, the frequency position drops sharply with increasing water content, especially between $W_0 = 15$ and 20.

The frequency position of the decoupled ν(OH) vibration in bulk water at 298 K is given as[3] 3402±2 cm^{-1}. Figure 10.4 below shows that this value is reached when $W_0 = 100$. The water appears to be bulk-like by $W_0 = 20$, where the frequency position is 3407 cm^{-1}, which indicates that fewer than 20 water molecules are perturbed by this system.

Figure 10.4 showing frequency position of decoupled ν(OH) band at 298 K versus W_0

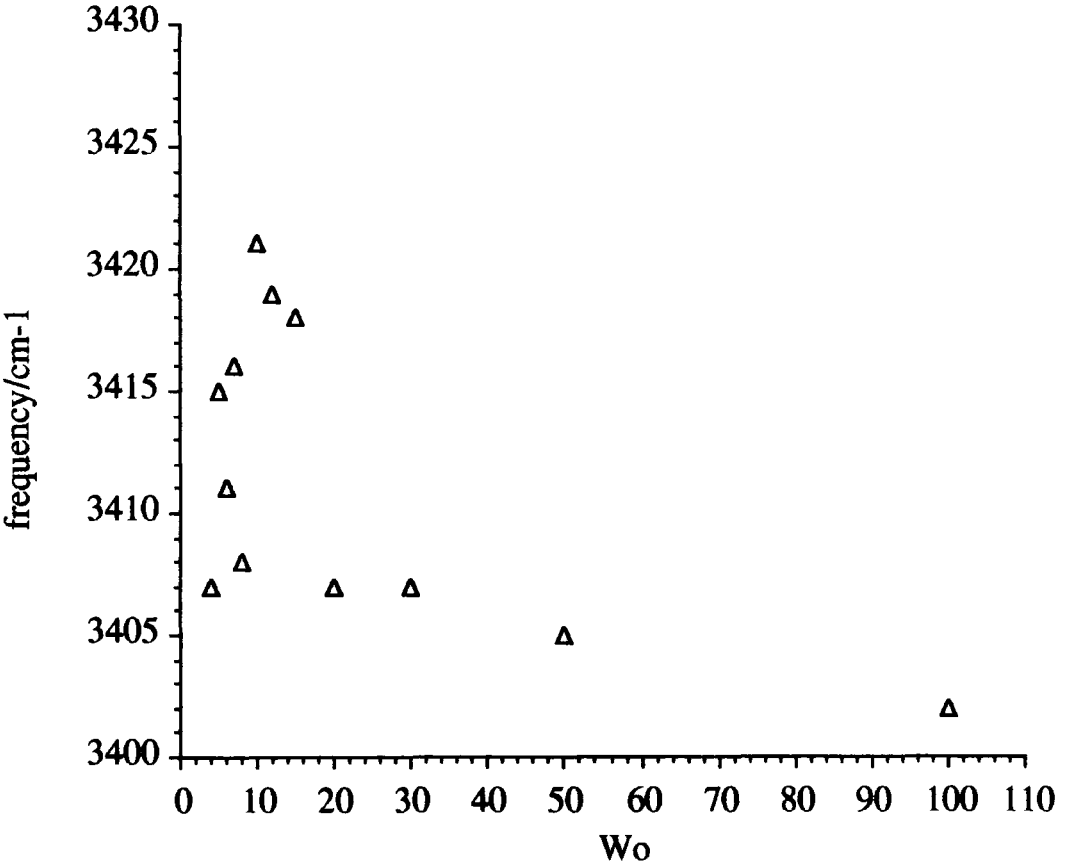

The error in the frequency position is estimated to be ±2 cm^{-1}.

Table 10.3 showing parameters of the decoupled ν(OH) band at 320 K

Wo	freqency cm^{-1}	width cm^{-1}	Integral cm^{-1}	Pathlength μm	Integral pathlength
4	3428	245	19	8.0	2.4
5	3412	246	21	8.0	2.6
6	3419	234	29	8.0	3.6
7	3419	246	18	8.0	2.4
8	3421	250	20	8.0	2.5
10	3440	252	19	8.0	2.4
12	3439	246	22	8.0	2.8
15	3432	241	18	8.0	2.3
20	3422	247	28	8.0	3.5
30	3417	249	38	8.0	4.8
50	3414	248	52	8.0	6.5
100	3419	253	248	35	7.1

When the temperature was raised to 320 K (47 °C), a similar trend in the data was observed. The results are given in table 10.3. Figure 10.5 below shows the frequency position of the ν(OH) band at 320K. In bulk water at 320 K, the frequency position of the ν(OH) band is 3417 cm^{-1}. Scattering of the values of the frequency position occurs again at low W_0 values. However this is not simply attributable to the existence of two phases L_D + K, as according to the phase diagram, this does not occur until $W_0 \leq 5$. This does not mean, however, that the sample is one phase. Microscopic phase separation may indeed occur within the sample due to effects such as temperature gradients, impurities, or crystallization induced by the surface of the cells. It seems therefore, that the reason for the scatter in frequency positions at very low W_0 values is due to microscopic phase separation. This may be confirmed by examining the bandwidths and by comparison with the NMR data.

Figure 10.5 showing frequency position of decoupled ν(OH) band at 320 K versus W_0

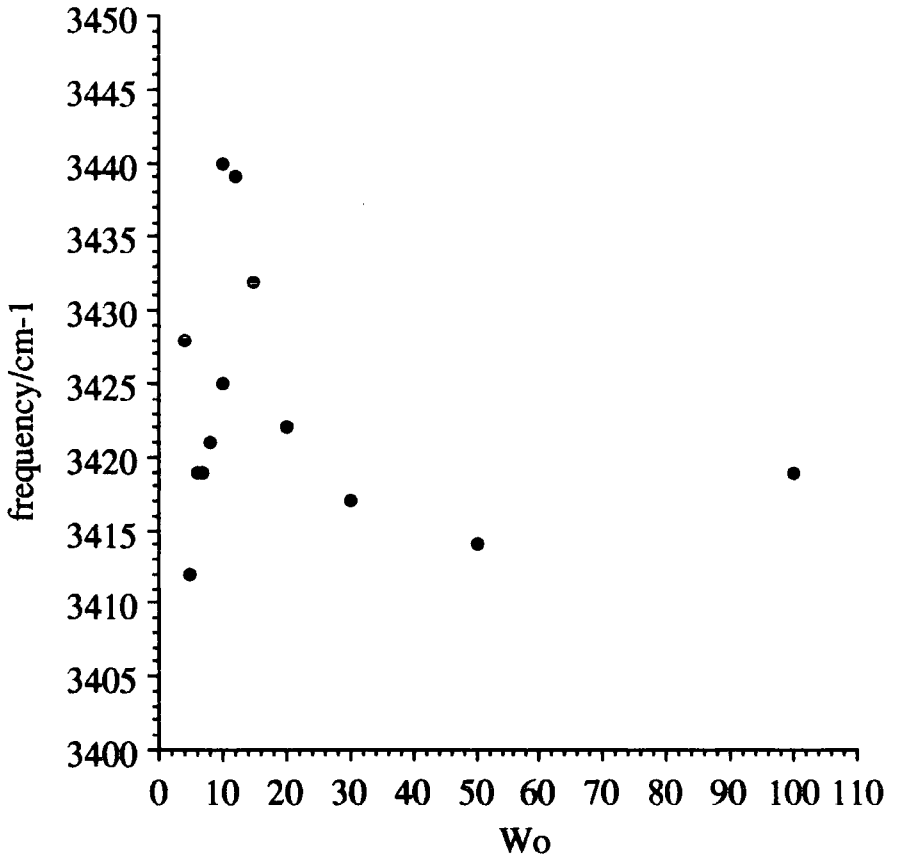

The width of the ν(OH) band at 298 K in bulk water is 255±5 cm^{-1}. At 320 K the bandwidth is 3 cm^{-1} wider[3]. Figures 10.6 and 10.7 show how the width of the decoupled ν(OH) band varies with W_0 for the CsPFO /D_2O system.

For the CsPFO/D_2O system at 298 K, the width at $W_0 = 100$ is 244 cm^{-1}, which is somewhat less than the bulk water value. Again the data is scattered at low W_0 values; compare for example the widths at $W_0 = 5$ and 6, where a large deviation is shown for only a small change in concentration. At 320 K, the bulk water value of the width is reached when $W_0 = 100$. What both figures 10.6 and 10.7 show is that the width remains constant within error above $W_0 = 15$. The reason for the scatter at low W_0 values is the microscopic phase separation that leads to large deviations in the bandwidths.

Figure 10.6 showing full width at half height of decoupled ν(OH) band at 298 K

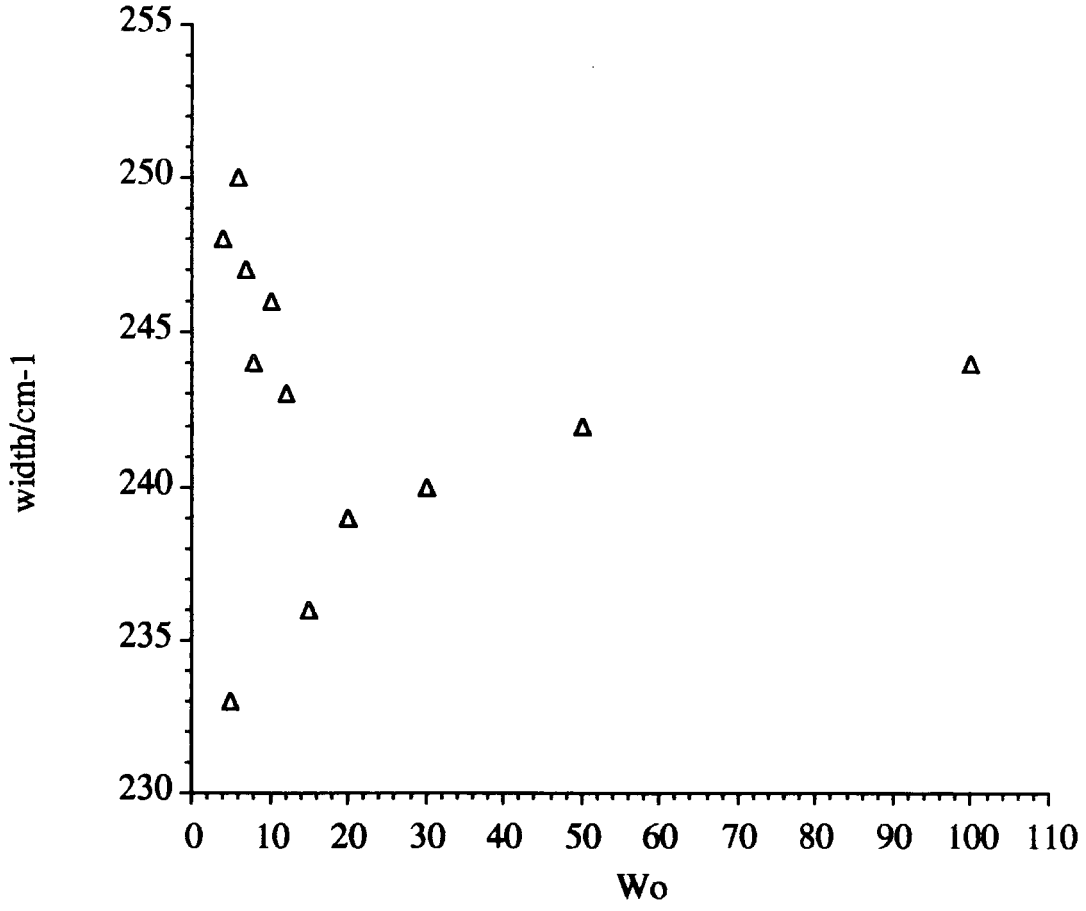

The error in the width measurement is estimated as being ±2 cm^{-1}

Figure 10.7 showing full width at half height of decoupled ν(OH) band at 320 K

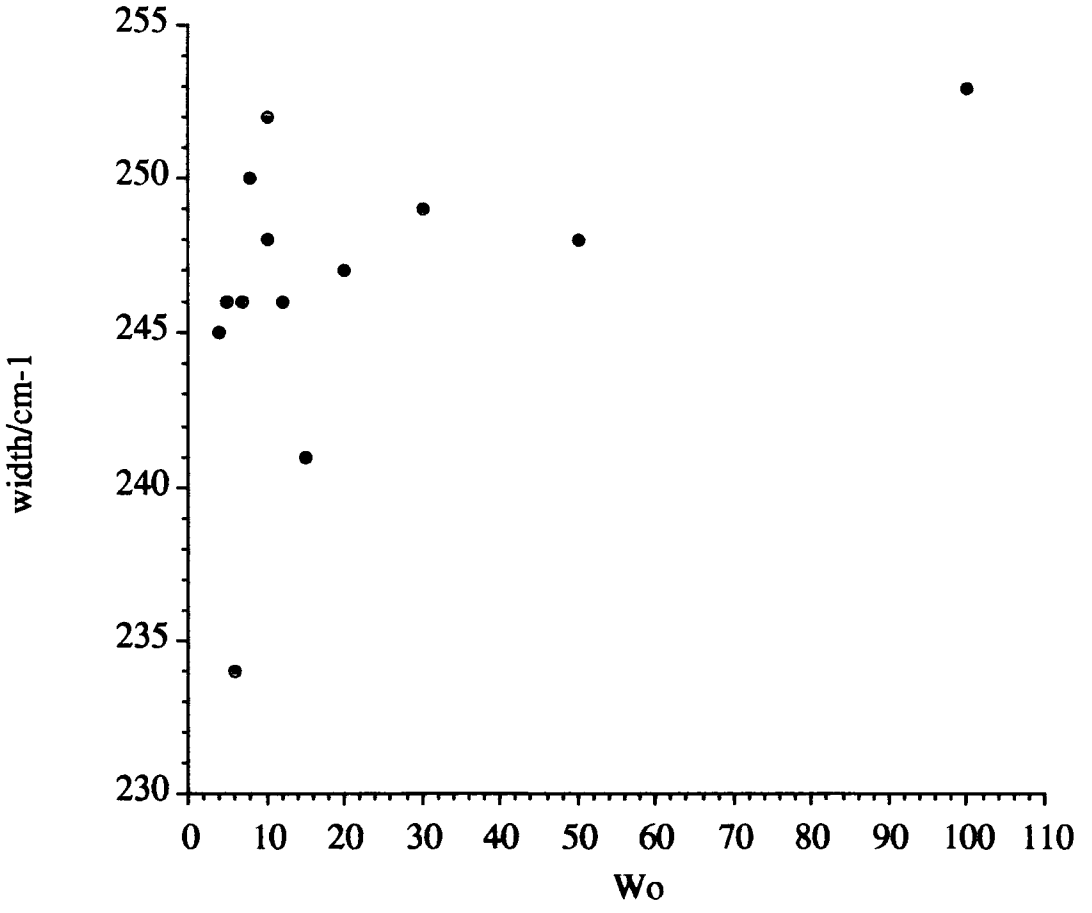

This is in agreement with the findings from the NMR investigation, where the large central peak in the quadrupolar ^{17}O NMR spectrum indicated the presence of regions of isotropic water. The time-scale of observation in the infrared experiment is much faster than the NMR experiment. This implies that the infrared spectra will be more sensitive to different molecular environments, whereas the NMR experiment will tend to observe average environments. However, only one band is seen in the decoupled ν(OH) region of the spectrum; a narrower band due to a perturbed species may exist, but is not observed beneath the band due to bulk water.

The coupled ν(OD) band is examined for shape changes, indicative of environmental changes as discussed for the AOT system in chapter 6. (See figure 10.8 and 10.9). No shape changes were observed on changing concentration

across the whole range from $W_0 = 4$ to 100. (Only the sample at $W_0 = 8$ appears to be different, which casts doubt upon its composition). However, the shape of the coupled ν(OD) band for $W_0 = 100$ is the same as for $W_0 = 4$. This indicates that the water environment is uniform across the whole composition range, which is unreasonable; or that the perturbation is only small.

There is a difference in band shape of the coupled ν(OD) bands at the two different temperatures used in these experiments. This is because different bands shift to different extents and change width with temperature, causing changes in vibrational coupling; as discussed for the AOT system (chapter 6).

As the NMR data indicated that isotropic or bulk-like water was present at very low water contents ($W_0 < 8$), it may be that this is the effect being observed with the infrared spectra. This probably explains the scattering of the width and frequency data; bulk-like values for these parameters are observed because of microscopic phase separation; but this does not explain why spectra of perturbed water are observed.

The graphs of frequency and width when examined together suggest that the perturbation of the water is greatest between $W_0 = 10$ and 20. The figures 10.4 - 10.7 show that at $W_0 = 15$, the frequency position is at its maximum in this system and the ν(OH) band is at its narrowest. Below $W_0 = 10$, the perturbation of the water is even greater as has been shown from the ^{17}O NMR quadrupolar splittings (chapter 9). However, the infrared spectra do not show this. The phenomenon of microscopic phase separation means that both bulk-like and perturbed water exist simultaneously on the infrared timescale. Since the more severely perturbed water has a higher frequency of vibration and a narrower band width, the spectrum of the perturbed water may be obscured by the spectrum of the bulk-like water. At $W_0 = 10$, all of the ionic headgroups are hydrated, and there is sufficient water available such that the system can become one phase. This explains the maximum in the frequency position (figures 10.4 - 10.5).

Figure 10.8 showing coupled ν(OD) band at 298 K. W_o = 4, 5, 6, 7, 8, 10, 12, 15, 20, 30, 50.

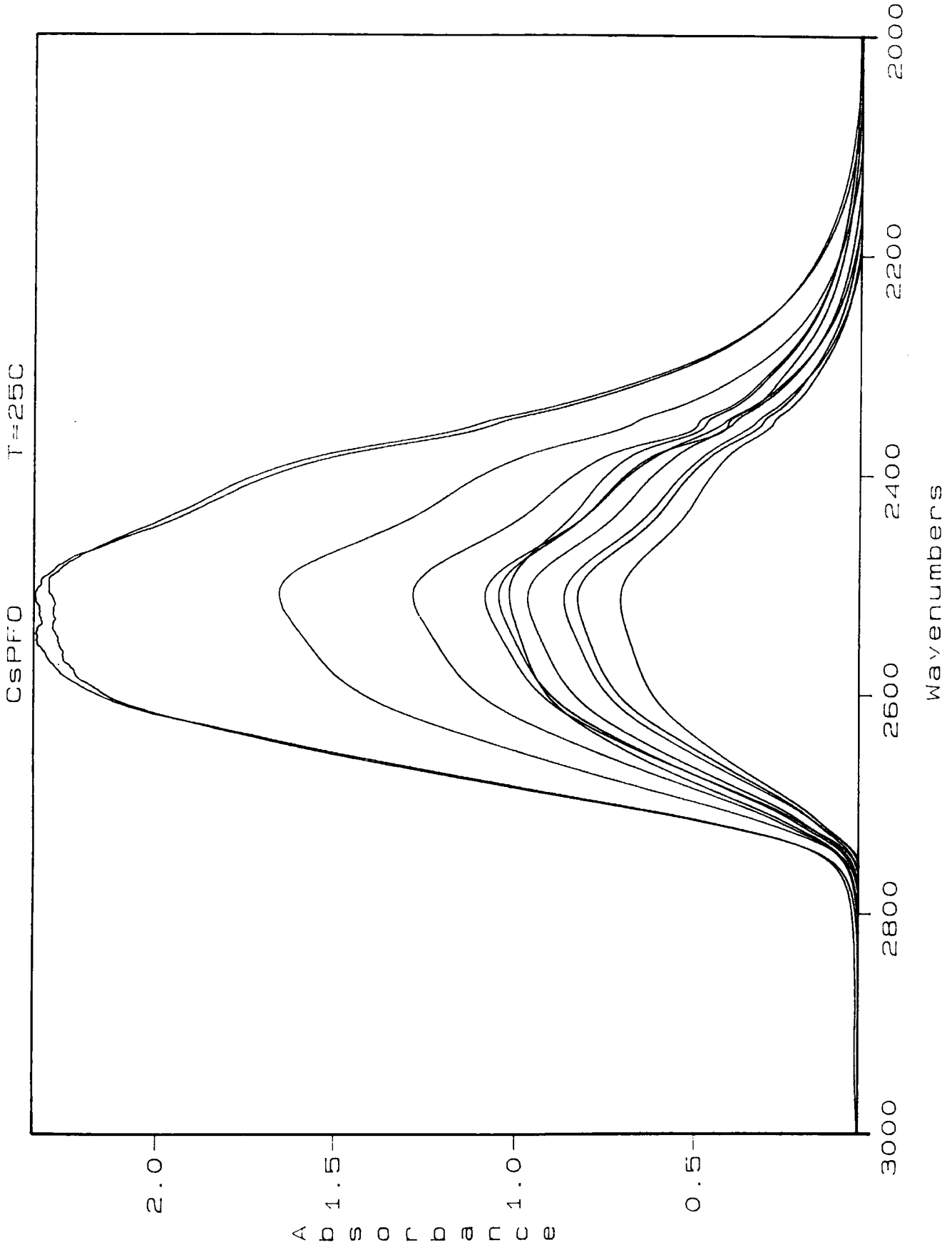

Figure 10.9 showing coupled ν(OD) band at 320 K. W_o = 4, 5, 6, 8, 10, 12, 15, 20, 30, 50.

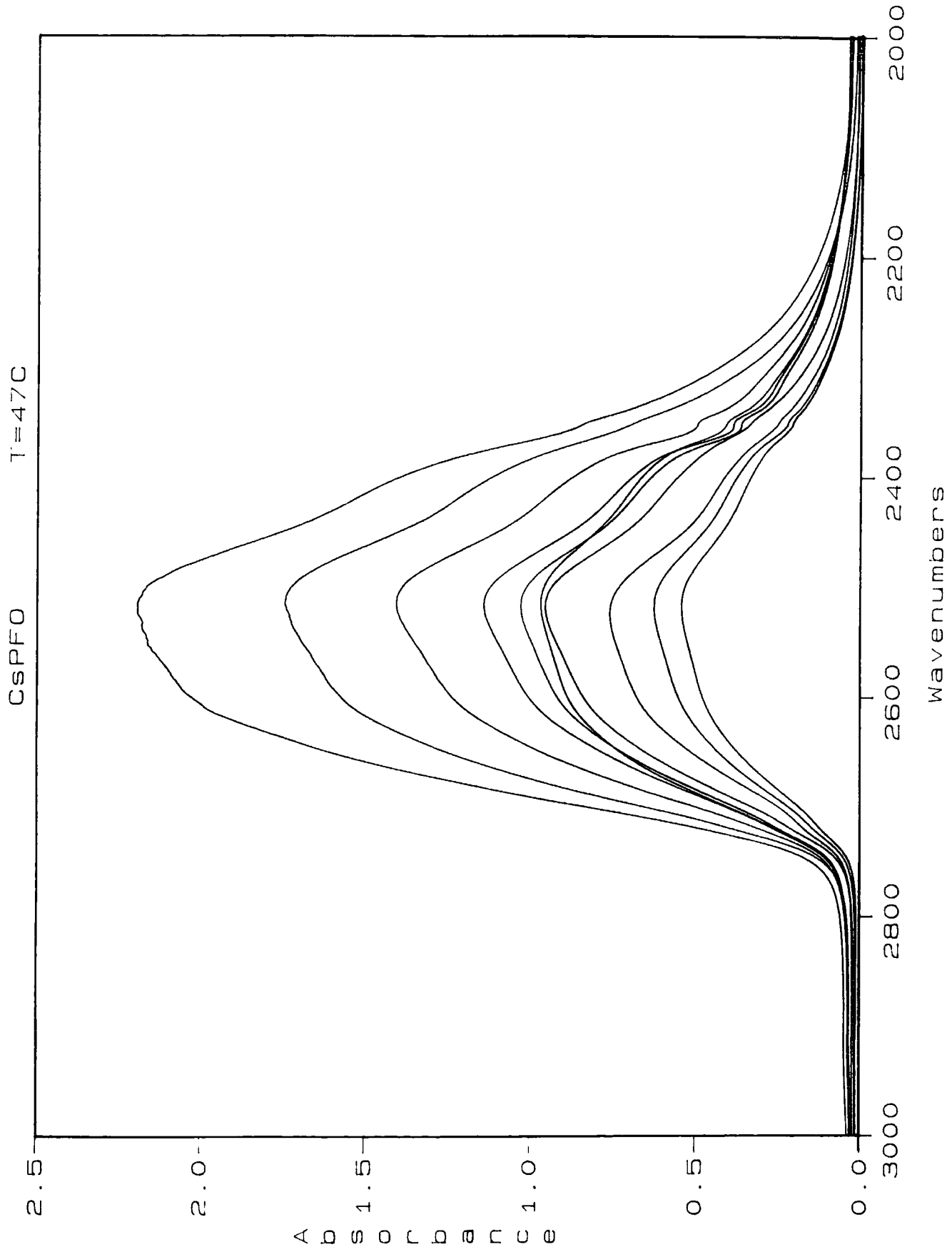

10.3. Integrated intensity of the ν(OH) band

The integrated intensity of the absorption band may also be measured. This shows the extent of the perturbation of the water in the concentration range under investigation.

In order to be able to carry out a quantitative investigation into the intensities of the absorption bands, the molar concentrations of CsPFO in water are needed - more precisely the molar concentration of the water in solution needs to be found. Data concerning the concentration of the CsPFO in water is available [2,5].

If C_S is the surfactant concentration in moles.dm^{-3}, then the molar concentration of water in the sample (C_W) is $W_O \times C_S$, as W_O is simply the mole ratio of water to surfactant. The molar concentration of CsPFO has been found for several values of the weight fraction (ϕ_W)[2]. These values have been used here to calculate an empirical relationship between weight fraction of CsPFO and molar concentration of water.

Table 10.4 Molar concentrations of CsPFO solutions

ϕ_W	W_O	C_S	$C_W = C_S \times W_O$
0.0110	2457	0.022	55.0
0.0120	2247	0.024	54.8
0.0290	1013	0.054	54.7
0.0522	550	0.098	54.1
0.100	272	0.190	51.7
0.195	124	0.401	49.7
0.221	97.09	0.510	49.5
0.225	95.24	0.520	49.5
0.287	68.97	0.691	47.7
0.530	25.19	1.522	38.3
0.626	17.30	1.946	33.7
0.632	16.89	1.975	33.4
0.648	15.82	2.054	32.5

C_S and C_W have units of moles.dm^{-3}. A graph of C_W versus ϕ_W is given in figure 10.10. A line of least squares fit is also shown on the diagram. It indicates

that the experimental determination of the concentration is slightly in error for two of the points at low weight fractions. However there is a good correspondance between ϕ_W and C_W.

Figure 10.10 Empirical relationship between molar concentration and weight fraction

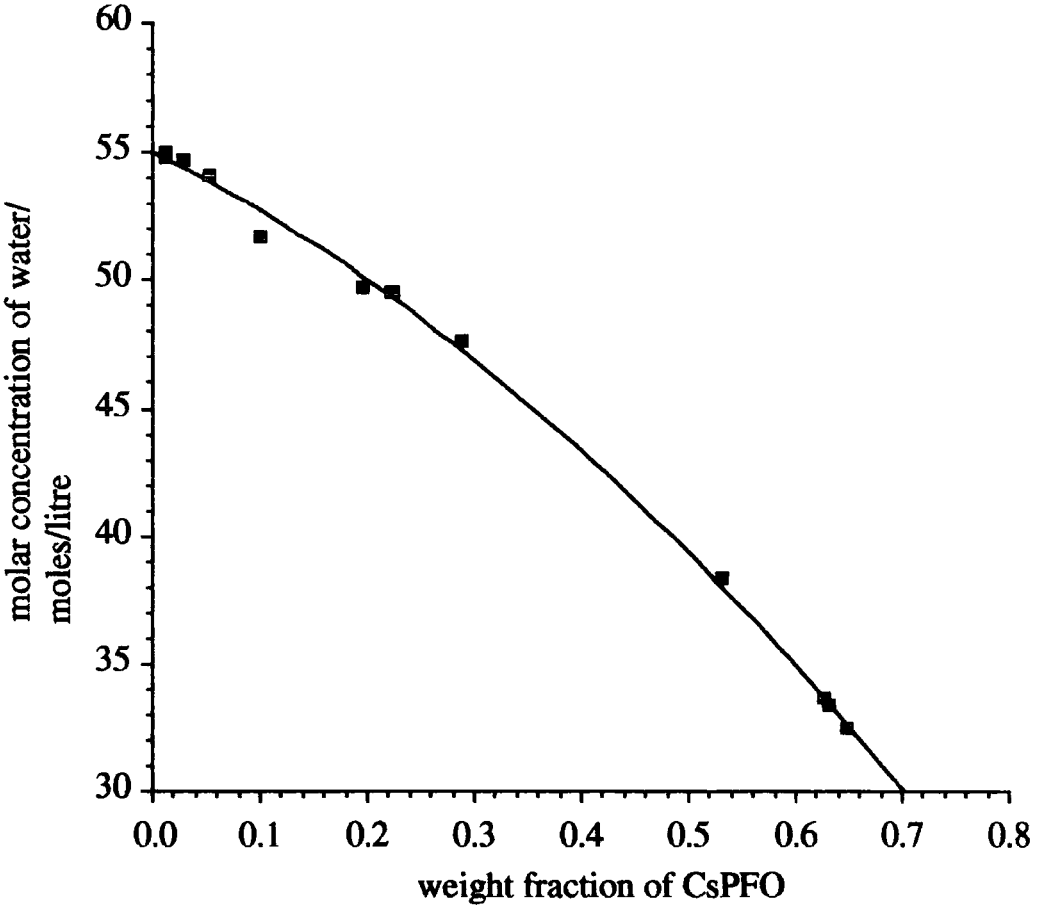

Using a least-squares fitting routine, it was found that the empirical relationship between C_W and ϕ_W is:

$$C_W = 55.052 - 20.824\,\phi_W - 21.220\,\phi_W^2 : r^2 = 0.998$$

This equation is only valid for $\phi_W < 0.7$, which corresponds to a W_O value of 12. The assumption has been made that the molar concentration does not change with temperature. This will not necessarily hold, although deviations are not likely to be large as the temperature difference in the experiments described here is not large. Other sources of error, such as measurement of the integrated

intensity and the exact concentration of the sample, are probably larger than the difference in concentrations with temperature.

Thus the values of the molar concentrations of water for the CsPFO/D_2O mixtures may be found by interpolating between these data points or using the empirical equation. In this instance the equation has been used (table 10.5). It is not possible, using the above data (table 10.4), to calculate the molar concentration for W_o values less than 12, as this would involve extrapolation of an empirical equation.

Table 10.5 Calculated values of the molar concentration of water at the W_o values used in the infrared experiments.

W_o	ϕ_w	C_w	Effective C_w	Intensity / pathlength at 298 K	intensity / pathlength at 320 K
12	0.695	30.35	1.214	2.9	2.8
15	0.645	32.78	1.311	2.8	2.3
20	0.577	35.97	1.439	4.0	3.5
30	0.476	40.32	1.613	6.6	4.8
50	0.353	45.06	1.802	7.5	6.5
100	0.214	49.61	1.984	8.1	7.1

The values of the integrated intensity and the pathlengths have been given in tables 10.2 and 10.3, but the data are repeated here with the molar concentrations (table 10.5). It must be remembered at this point that isotopically dilute water (4% H_2O in D_2O) was used in the experiments. Therefore the actual value of C_w used should only be 4% of the value calculated for the total water concentration, assuming that all the H_2O dissociates to form HDO. This is shown in the column headed effective C_w.

Figure 10.11 shows a graph of integrated area of the decoupled ν(OH) band normalized to pathlength versus the water concentration.

Figure 10.11 Integrated intensity normalized to pathlength versus water concentration

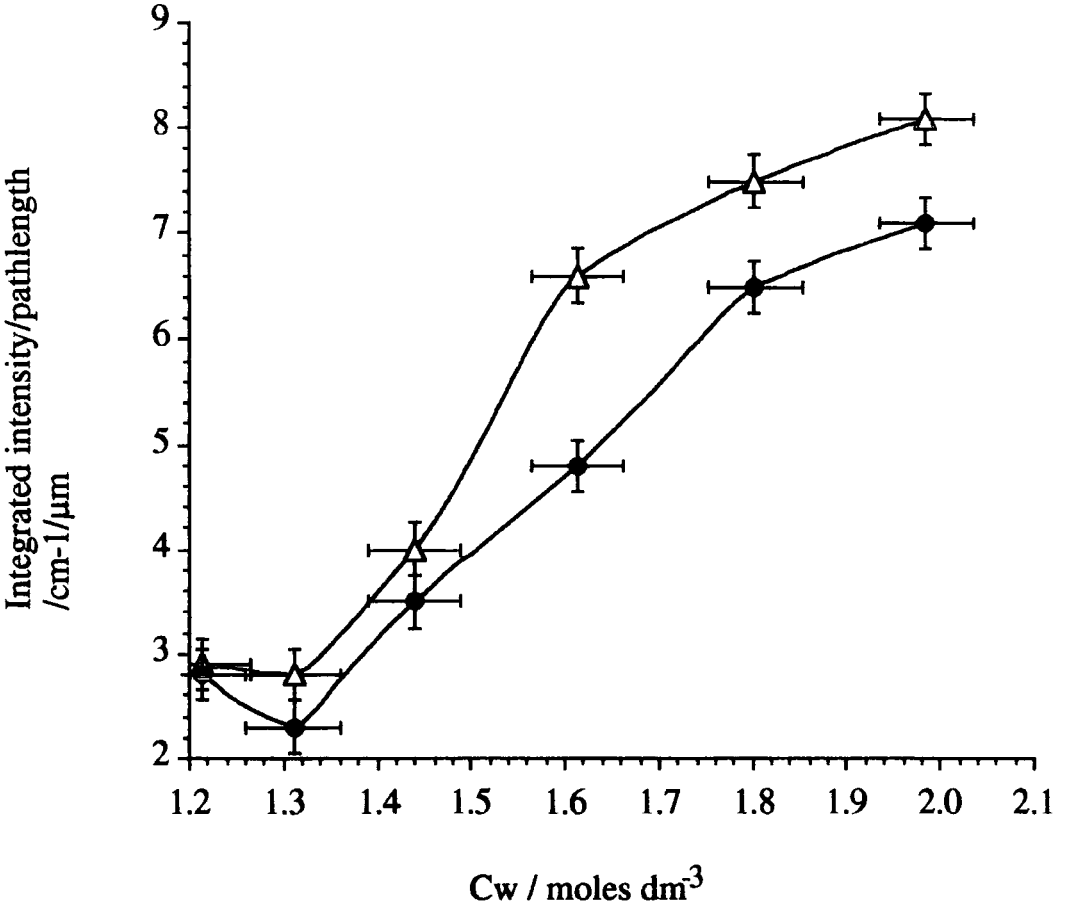

The points on the graph in figure 10.11 correspond to W_0 values of 12,15,20,30,50,100.

The lines serve as a guide to eye. The error associated with each point has been estimated as being ±0.05 mol.dm^{-3} (i.e.±5%) in C_w. This comes from the interpolation of the concentrations as described above. The error shown represents an error of ±0.03 mol.dm^{-3} in the molar concentration of water. The error in measuring the integrated area is shown as ±5%. The error in the pathlength is very small and is not included here.

The graphs do not contain many data points, and the concentrations are not available below $W_0 = 12$. However the integrated intensities do show an increase with respect to the concentrations. There is not sufficient data to show at what

point the state of water changes. A straight line may reasonably describe the data, especially at 320 K; although at 298 K, a change of gradient is apparent between $W_0 = 20$ and 30. This gradient change coincides with the onset of bulk water as concluded from the frequency and bandwidth data.

10.4. Carbonyl band

The carbonyl band has been discussed before (chapter 9) in the context of identifying whether the salt or the acid had been synthesized. Here the behaviour of the carbonyl band as a function of W_0 will be presented.

It was found that the frequency position of the carbonyl band did not vary with W_0. At 298 K the frequency position was 1673±1 cm^{-1}, and at 320 K it was 1674±1 cm^{-1}. This indicates that the carboxylate headgroup is in the same electronic environment at differing values of W_0.

However the width of the ν(CO) band was found to depend greatly on the water content. The band widths at 298 and 320 K are given in table 10.6 and displayed in figure 10.14 below. Figures 10.12 and 10.13 show the spectra of the carbonyl bands at 298 and 320 K of two representative samples at $W_0 = 4$ and $W_0 = 50$.

Table 10.6 Width at half height of carbonyl band at 298 and 320 K

Wo	Width at 298K /cm^{-1}	Width at 320K /cm^{-1}
4	43	43
5	37	38
6	38	37
7	38	37
8	35	35
10	38	37
12	35	34
15	37	35
20	32	32
30	31	30
50	29	28
100	28	27

Figure 10.12 Spectrum of carbonyl band of CsPFO/D_2O system at 298K. W_o=4 (wider band) and W_o=50 (narrower band)

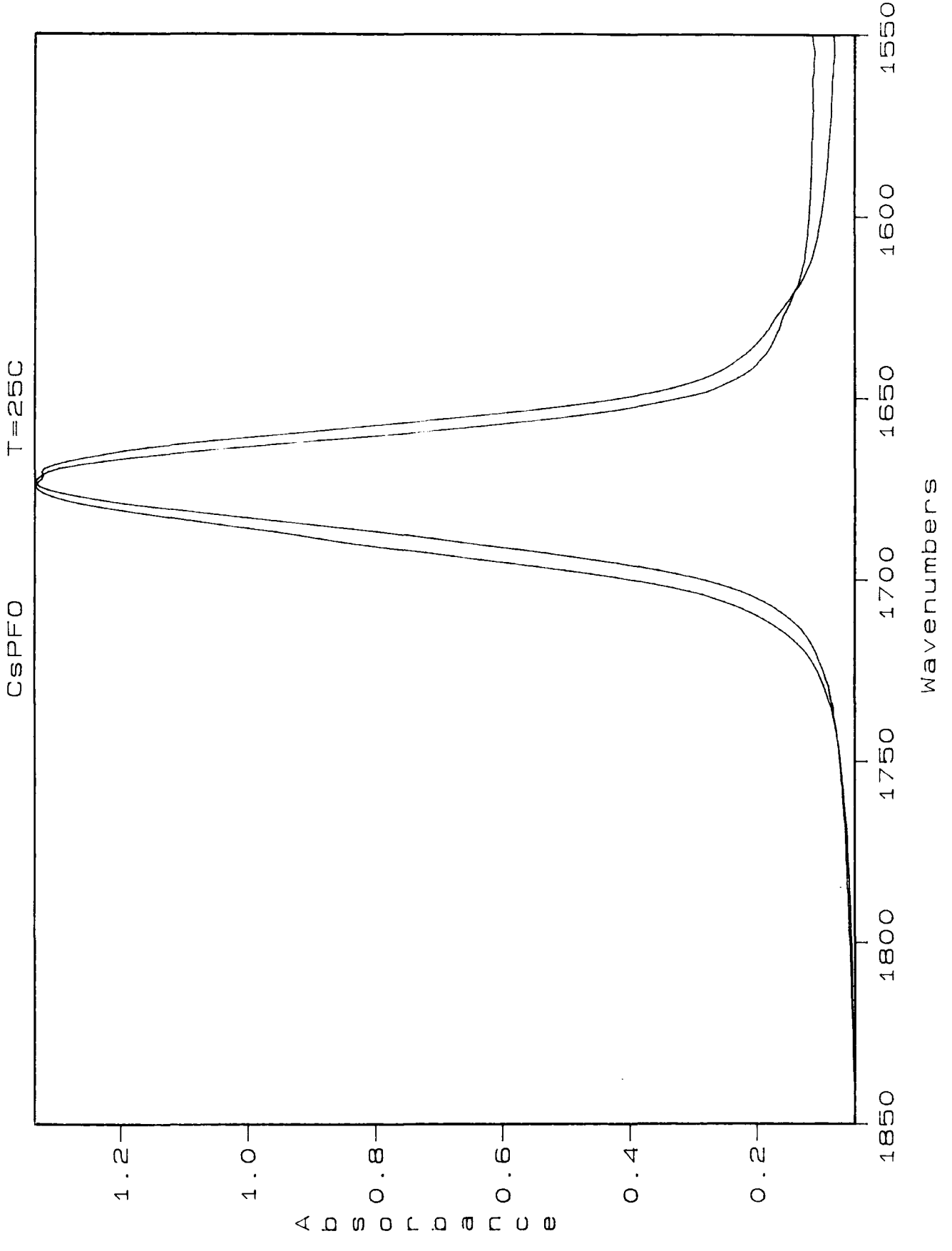

Figure 10.13 Spectrum of carbonyl band of CsPFO/D_2O system at 320K. W_o=4 (wider band) and W_o=50 (narrower band)

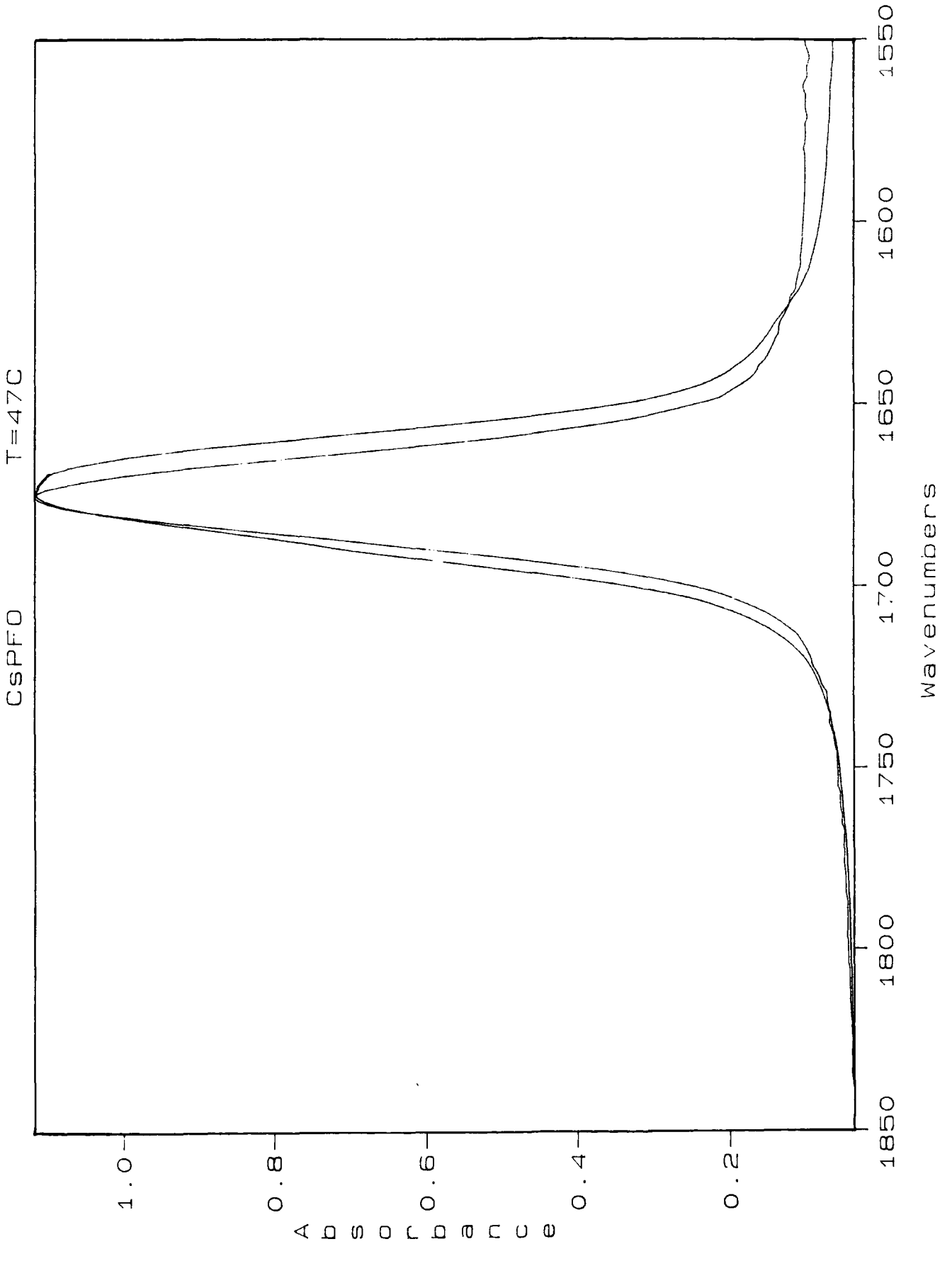

Figure 10.14 Width at half height of carbonyl band versus W_0 at 298 and 320 K.

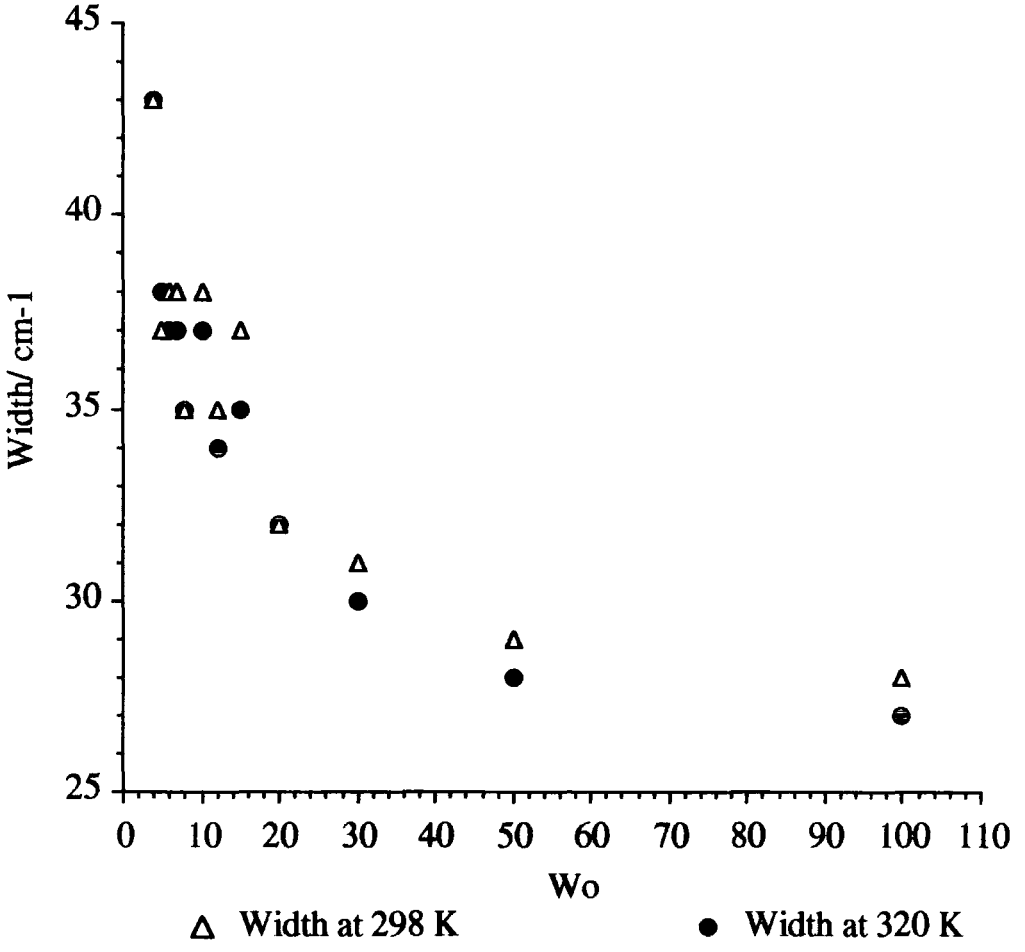

The error associated with each data point is ±2 cm^{-1}.

The data show a gradually decreasing width as W_0 increases. Within experimental error, there is no difference between the band widths at the two different temperatures; although the last three data points show a larger band-width at the lower temperature.

The changes in bandwidth may reflect a narrowing of the range of environments of the carboxylate headgroup. This is certainly the case at low W_0 values as microscopic phase separation exists. Above $W_0 \approx 15$, however, it seems more likely that such a large change in bandwidth is due to a change in the vibrational relaxation rate.

10.5. Conclusions

From the ^{17}O NMR data, the amount of water that suffers anisotropic motion has been shown to be small, and the extent of that anisotropy is small. Of the order of 10 water molecules per surfactant molecule were shown to be perturbed. The infrared data indicate that between 10≈15 water molecules are perturbed. However, for both techniques the phenomenon of microscopic phase separation was present. The ionic headgroups have a large affinity for any available water, such that the system tends to phase separate into hydrated liquid crystalline regions L_D, and crystalline regions K that are devoid of water. Once all the headgroups are hydrated ($W_0 \approx 10$), then some more water is seen to be perturbed (up to $W_0 = 20$ from the infrared integrated intensities and frequency position). However when $W_0 > 20$, then the water is seen to be bulk-like.

Microscopic phase separation also caused a large central isotropic peak in the ^{17}O NMR spectrum. So the T_1 measurements, which are sensitive to fast molecular motions, were dominated by the isotropic water, and did not show the slower motions of perturbed water molecules.

10.6 References

(1) Boden N., Corne S. A., Jolley K. W. *J. Phys. Chem.* **1987**, *91*, 4092.
(2) Boden N., Jolley K. W., Smith M. H. *Liquid Crystals* **1989**, *6*, 481.
(3) Eisenberg D., Kauzmann W. *The Structure and Properties of Water*; OUP: Oxford, **1969**.
(4) Bellamy L. J. *The Infrared Spectra of Complex Molecules*; Chapman and Hall: London, **1980**Vol. 2.
(5) Holmes M. C., Reynolds D. J., Boden N. *J. Phys. Chem.* **1987**, *91*, 5257.

Concluding Remarks

The study of two different surfactant systems, especially of the water contained within them, shows that water only suffers perturbation by ionic or very polar headgroups.

In the case of AOT, the water molecules were shown to be perturbed most by the sodium counter-ion and the sulphonate headgroup. The carbonyl groups were shown to be sensitive to the quantity of water present, but this was only a secondary effect attributed to conformational changes.

For the CsPFO system, the NMR data showed that the extent of perturbation is small, and does not extend beyond the order of 10 water molecules. The complementary infrared information confirmed this, if the effects of microscopic phase separation could be accounted for.

The caesium ion is less perturbing than the sodium ion because of its lower charge density, so sodium might be expected to perturb more water. However caesium is a larger ion than sodium, and is therefore able to bond to more water molecules. These two effects counter-balance each other to give the same hydration number of ≈ 6.

Apart from ionically bound water, distinct types were not found to exist. It is suggested that the spectroscopic data are best interpreted in terms of a continuum of water molecule interactions in rapid equilibrium with each other.

Appendix

The board of studies in chemistry requires that each postgraduate research thesis contain an appendix listing:

(a) all research conferences attended during the period when the research for the thesis was carried out;

17th – 18th December 1990, Department of physical chemistry, Oxford. Faraday Discussions of the Royal Society of Chemistry, 'The motion of molecules in confined spaces.' A poster was presented.

22nd March 1991, Unilever, Port Sunlight. NMR discussion group of the Royal Society of Chemistry.

3rd – 5th July 1991, University of Leeds, Royal Society / British Liquid Crystal Society. A poster was presented.

1st – 6th September 1991, Lübeck, Germany, 7th International Conference on Fourier Transform Spectroscopy. A poster was presented.

(b) all research colloquia, seminars and lectures arranged by the department of chemistry during the period of the author's residence as a postgraduate student. This list is appended below, those events attended by the author are marked (•).

Publication

D. J. Christopher, J. Yarwood, P.S. Belton, B. P. Hills; Journal of Colloid and Interface Science **1992**,*152*, 465.

A Fourier Transform Infrared Study of Water-Head Group interactions in Reversed Micelles Containing Sodium Bis(2-ethylhexyl) sulfosuccinate (AOT).

UNIVERSITY OF DURHAM

Board of Studies in Chemistry

COLLOQUIA, LECTURES AND SEMINARS GIVEN BY INVITED SPEAKERS 1ST AUGUST 1989 TO 31ST JULY 1990

• BADYAL, Dr. J.P.S. (Durham University) Breakthoughs in Heterogeneous Catalysis	1st November, 1989
BECHER, Dr. J. (Odense University) Synthesis of New Macrocylic Systems using Heterocyclic Building Blocks	13th November, 1989
BERCAW, Prof. J.E. (California Institute of Technology) Synthetic and Mechanistic Approaches to Ziegler–natta Polymerization of Olefins	10th November, 1989
BLEASDALE, Dr. C. (Newcastle University) The Mode of Action of some Anti–tumour Agents	21st February, 1990
BOWMAN, Prof. J.M. (Emory University) Fitting Experiment with Theory in Ar–OH	23rd March, 1990
BUTLER, Dr. A. (St. Andrews University) The Discovery of Penicillin: Facts and Fancies	7th December, 1989
CHEETHAM, Dr. A.K. (Oxford University) Chemistry of Zeolite Cages	8th March, 1990
• CLARK, Prof. D.T. (ICI Wilton) Spatially Resolved Chemistry (using Natures's Paradigm in the Advanced Materials Arena)	22nd February, 1990
COLE–HAMILTON, Prof. D.J. (St. Andrews University) New Polymers from Homogeneous Catalysis	29th November, 1989
• CROMBIE, Prof. L. (Nottingham University) The Chemistry of Cannabis and Khat	15th February, 1990
DYER, Dr. U. (Glaxo) Synthesis and Conformation of C–Glycosides	31st January, 1990
• FLORIANI, Prof. C. (University of Lausanne, Switzerland) Molecular Aggregates – A Bridge between homogeneous and Heterogeneous Systems	25th October, 1989
GERMAN, Prof. L.S. (USSR Academy of Sciences – Moscow) New Syntheses in Fluoroaliphatic Chemistry: Recent Advances in the Chemistry of Fluorinated Oxiranes	9th July, 1990
• GRAHAM, Dr. D. (B.P. Reserch Centre) How Proteins Absorb to Interfaces	4th December, 1989
GREENWOOD, Prof. N.N. (University of Leeds) Novel Cluster Geometries in Metalloborane Chemistry	9th November, 1989

HOLLOWAY, Prof. J.H. (University of Leicester) Noble Gas Chemistry	1st February, 1990
HUGHES, Dr. M.N. (King's College, London) A Bug's Eye View of the Periodic Table	30th November, 1989
HUISGEN, Prof. R. (Universität München) Recent Mechanistic Studies of [2+2] Additions	15th December, 1989
• KLINOWSKI, Dr. J. (Cambridge University) Solid State NMR Studies of Zeolite Catalysts	13th December 1989
• LANCASTER, Rev. R. (Kimbolton Fireworks) Fireworks – Principles and Practice	8th February, 1990
• LUNAZZI, Prof. L. (University of Bologna) Application of Dynamic NMR to the Study of Conformational Enantiomerism	12th February, 1990
• PALMER, Dr. F. (Nottingham University) Thunder and Lightning	17th October, 1989
• PARKER, Dr. D. (Durham University) Macrocycles, Drugs and Rock 'n' roll	16th November, 1989
PERUTZ, Dr. R.N. (York University) Plotting the Course of C–H Activations with Organometallics	24th January, 1990
PLATONOV, Prof. V.E. (USSR Academy of Sciences – Novosibirsk) Polyfluoroindanes: Synthesis and Transformation	9th July, 1990
POWELL, Dr. R.L. (ICI) The Development of CFC Replacements	6th December, 1989
• POWIS, Dr. I. (Nottingham University) Spinning off in a huff: Photodissociation of Methyl Iodide	21st March, 1990
ROZHKOV, Prof. I.N. (USSR Academy of Sciences – Moscow) Reactivity of Perfluoroalkyl Bromides	9th July, 1990
• STODDART, Dr. J.F. (Sheffield University) Molecular Lego	1st March, 1990
SUTTON, Prof. D. (Simon Fraser University, Vancouver B.C.) Synthesis and Applications of Dinitrogen and Diazo Compounds of Rhenium and Iridium	14th February, 1990
• THOMAS, Dr. R.K. (Oxford University) Neutron Reflectometry from Surfaces	28th February, 1990
THOMPSON, Dr. D.P. (Newcastle University) The role of Nitrogen in Extending Silicate Crystal Chemistry	7th February, 1990

REVISED VERSION

UNIVERSITY OF DURHAM

Board of Studies in Chemistry

COLLOQUIA, LECTURES AND SEMINARS GIVEN BY INVITED SPEAKERS 1ST AUGUST 1990 TO 31ST JULY 1991

• ALDER, Dr. B.J. (Lawrence Livermore Labs., California) — 15th January, 1991
Hydrogen in all its Glory

• BELL†, Prof. T. (SUNY, Stoney Brook, U.S.A.) — 14th November, 1990
Functional Molecular Architecture and Molecular Recognition

BOCHMANN†, Dr. M. (University of East Anglia) — 24th October, 1990
Synthesis, Reactions and Catalytic Activity of Cationic Titanium Alkyls

BRIMBLE, Dr. M.A. (Massey University, New Zealand) — 29th July, 1991
Synthetic Studies Towards the Antibiotic Griseusin-A

BROOKHART, Prof. M.S. (University of N. Carolina) — 20th June, 1991
Olefin Polymerizations, Oligomerizations and Dimerizations Using Electrophilic Late Transition Metal Catalysts

BROWN, Dr. J. (Oxford University) — 28th February, 1991
Can Chemistry Provide Catalysts Superior to Enzymes?

BUSHBY†, Dr. R. (Leeds University) — 6th February, 1991
Biradicals and Organic Magnets

COWLEY, Prof. A.H. (University of Texas) — 13th December, 1990
New Organometallic Routes to Electronic Materials

CROUT, Prof. D. (Warwick University) — 29th November, 1990
Enzymes in Organic Synthesis

• DOBSON†, Dr. C.M. (Oxford University) — 6th March, 1991
NMR Studies of Dynamics in Molecular Crystals

• GERRARD†, Dr. D. (British Petroleum) — 7th November, 1990
Raman Spectroscopy for Industrial Analysis

HUDLICKY, Prof. T. (Virginia Polytechnic Institute) — 25th April, 1991
Biocatalysis and Symmetry Based Approaches to the Efficient Synthesis of Complex Natural Products

JACKSON†, Dr. R. (Newcastle University) — 31st October, 1990
New Synthetic Methods: α-Amino Acids and Small Rings

KOCOVSKY†, Dr. P. (Uppsala University) — 6th November, 1990
Stereo-Controlled Reactions Mediated by Transition and Non-Transition Metals

• LACEY, Dr. D. (Hull University) Liquid Crystals	31st January, 1991
LOGAN, Dr. N. (Nottingham University) Rocket Propellants	1st November, 1990
• MACDONALD, Dr. W.A. (ICI Wilton) Materials for the Space Age	11th October, 1990
• MARKAM, Dr. J. (ICI Pharmaceuticals) DNA Fingerprinting	7th March, 1991
• PETTY, Dr. M.C. (Durham University) Molecular Electronics	14th February, 1991
PRINGLE†, Dr. P.G. (Bristol University) Metal Complexes with Functionalised Phosphines	5th December, 1990
• PRITCHARD, Prof. J. (Queen Mary & Westfield College, London University) Copper Surfaces and Catalysts	21st November, 1990
• SADLER, Dr. P.J. (Birkbeck College London) Design of Inorganic Drugs: Precious Metals, Hypertension + HIV	24th January, 1991
• SARRE, Dr. P. (Nottingham University) Comet Chemistry	17th January, 1991
SCHROCK, Prof. R.R. (Massachusetts Institute of Technology) Metal-ligand Multiple Bonds and Metathesis Initiators	24th April, 1991
SCOTT, Dr. S.K. (Leeds University) Clocks, Oscillations and Chaos	8th November, 1990
SHAW†, Prof. B.L. (Leeds University) Syntheses with Coordinated, Unsaturated Phosphine Ligands	20th February, 1991
• SINN†, Prof. E. (Hull University) Coupling of Little Electrons in Big Molecules. Implications for the Active Sites of (Metalloproteins and other) Macromolecules	30th January, 1991
SOULEN†, Prof. R. (South Western University, Texas) Preparation and Reactions of Bicycloalkenes	26th October, 1990
• WHITAKER†, Dr. B.J. (Leeds University) Two-Dimensional Velocity Imaging of State-Selected Reaction Products	28th November, 1990

† Invited specifically for the postgraduate training programme.

UNIVERSITY OF DURHAM

Board of Studies in Chemistry

COLLOQUIA, LECTURES AND SEMINARS FROM INVITED SPEAKERS

1991 – 1992 (August 1 – July 31)

1991

October	17	Dr. J.A. Salthouse, University of Manchester Son et Lumiere – a demonstration lecture
October	31	Dr. R. Keeley, Metropolitan Police Forensic Science Modern forensic science
• November	6	Prof. B.F.G. Johnson†, Edinburgh University Cluster–surface analogies
November	7	Dr. A.R. Butler, St. Andrews University Traditional Chinese herbal drugs: a different way of treating disease
November	13	Prof. D. Gani†, St. Andrews University The chemistry of PLP–dependent enzymes
November	20	Dr. R. More O'Ferrall†, University College, Dublin Some acid–catalysed rearrangements in organic chemistry
• November	28	Prof. I.M. Ward, IRC in Polymer Science, University of Leeds The SCI lecture: the science and technology of orientated polymers
December	4	Prof. R. Grigg†, Leeds University Palladium–catalysed cyclisation and ion–capture processes
• December	5	Prof. A.L. Smith, ex Unilever Soap, detergents and black puddings
• December	11	Dr. W.D. Cooper†, Shell Research Colloid science: theory and practice

1992

January	22	Dr. K.D.M. Harris†, St. Andrews University Understanding the properties of solid inclusion compounds
January	29	Dr. A. Holmes†, Cambridge University Cycloaddition reactions in the service of the synthesis of piperidine and indolizidine natural products

January	30	Dr. M. Anderson, Sittingbourne Research Centre, Shell Research Recent Advances in the Safe and Selective Chemical Control of Insect Pests
February	12	Prof. D.E. Fenton†, Sheffield University Polynuclear complexes of molecular clefts as models for copper biosites
• February	13	Dr. J. Saunders, Glaxo Group Research Limited Molecular Modelling in Drug Discovery
February	19	Prof. E.J. Thomas†, Manchester University Applications of organostannanes to organic synthesis
February	20	Prof. E.Vogel, University of Cologne *The Musgrave Lecture* Porphyrins: Molecules of Interdisciplinary Interest
February	25	Prof. J.F. Nixon, University of Sussex *The Tilden Lecture* Phosphaalkynes: new building blocks in inorganic and organometallic chemistry
• February	26	Prof. M.L. Hitchman†, Strathclyde University Chemical vapour deposition
• March	5	Dr. N.C. Billingham, University of Sussex Degradable Plastics – Myth or Magic?
March	11	Dr. S.E. Thomas†, Imperial College Recent advances in organoiron chemistry
• March	12	Dr. R.A. Hann, ICI Imagedata Electronic Photography – An Image of the Future
March	18	Dr. H. Maskill†, Newcastle University Concerted or stepwise fragmentation in a deamination–type reaction
April	7	Prof. D.M. Knight, Philosophy Department, University of Durham Interpreting experiments: the beginning of electrochemistry
May	13	Dr. J–C Gehret, Ciba Geigy, Basel Some aspects of industrial agrochemical research

† Invited specially for the postgraduate training programme.